

**Corso di Dottorato in Neuroscienze  
Curriculum Neuroscienze e Neurotecnologie  
Ciclo XXX**

**Title:**

**“A combined experimental and computational approach to  
investigate emergent network dynamics based on  
large-scale neuronal recordings”**

**Author: Davide Lonardoni**  
**Supervisors: Dr. Luca Berdondini (PI)**  
**Dr. Thierry Nieus**



**ISTITUTO  
ITALIANO DI  
TECNOLOGIA**





## **Acknowledgements**

---

The work that I will present in this thesis would have never been conceived and finalized without the support of many people I have encountered during these three years of my Ph.D. First and foremost, I am truly indebted to my supervisors for the scientific discussions, critical reviews, cross-disciplinary comments to my work and wise guidance that supported my research activities. I would like to thank Dr. Luca Berdondini for the privilege of recruiting me into his lab. I am truly indebted for the trust he gave me since the very beginning of the Ph.D. and for his push toward independent research. I am grateful for his endless support in pushing my targets further with thoughtful comments and wise discussions. My gratitude goes also to thank Dr. Thierry Nieuws, who has become during these years more than a simple supervisor, but rather a real friend. The support I received from him, from both the personal and scientific spheres, cannot fit within a single page of acknowledgments; specifically for the continuous remote supervision I am receiving upon he left IIT.

Furthermore, I am grateful to all past and present lab members, starting from Hayder Amin, a friend more than a colleague, who performed many of the experiments on primary neuronal cultures used in my work and who definitely helped me with our daily fruitful discussions that, I have to admit, opened my mind to the broad field of neuroscience. Alessandro Maccione and Fabio Boi, who performed the experiments on retina whole mounts included in my dissertation, for their precious and patient support, but more importantly for sharing the weight of negative results that I have sometimes obtained during the last years. I really appreciated their attitude in turning negativity into positivity. Stefano Di Marco and Silvia Bisti, who critically evaluated the results obtained during the second part of my Ph.D. and who provided me with thoughtful pieces of advice to interpret my data. Moreover, I especially thank Stefano for supported me with experimental recordings from both neuronal cultures and ex-vivo retina preparations. Stefano Zordan, with whom I always had thoughtful discussions about the technical implementation of algorithms for large-scale data analysis. Giannicola Angotzi, for his endless positive support and credits that continuously relieved me during the epochs of stress and anxiety I have been experiencing during some periods of my Ph.D. Similarly, I am grateful to Mario Malerba for the relaxing environment he created during his stay in our lab. A special thanks also go to Serena Riccitelli, Lidia Giantomasi, and Aziliz Lecomte that, even though they only recently joined the lab, have brought a friendly and supportive atmosphere and with whom I had interesting and inspiring discussions. Finally, I would like to thank Ermanno Miele. By sharing his scientific and personal experience he has shed some new light on my future career perspectives.

Beyond my lab members, I own a massive debt of gratitude to my parents, Ferdinando and Nives, that unconditionally and independently of my choices, always supported me during my entire life and especially during my Ph.D. In an occasion such as this one, I hope that all the stress and anxiety I inevitably reversed on you during the last three years will turn into proudness and joy for the achievements reached by your son. Similarly, I am grateful to all my relatives who blindly trusted me and always remotely supported my activities with their heartwarming thoughts.

My last thought goes to you, Josephine. During the last years you have been my precious belayer: the constant source of strength and inspiration that prevented me from falling during the challenges encountered during my Ph.D. Your continuous encouragement (and sometimes a good kick on my back when I was struggling for nothing) was a priceless support during this adventure.



# Table of contents

<b>AN INTRODUCTION TO THE MOTIVATIONS, IMPLEMENTATION AND ACHIEVEMENTS OF MY PHD .....</b>	<b>1</b>
<i>Motivations of this research.....</i>	<i>1</i>
<i>Roadmap of the research activities developed in this thesis.....</i>	<i>2</i>
<i>Achieved milestones .....</i>	<i>3</i>
<i>Organization of the manuscript .....</i>	<i>5</i>
<i>Bibliography.....</i>	<i>6</i>
<b>CHAPTER I - BASIC CONCEPTS OF SPONTANEOUS COORDINATED SPIKING ACTIVITY IN IN VIVO AND IN VITRO NEURONAL SYSTEMS.....</b>	<b>7</b>
<i>Spontaneous spiking activity in the early phase of brain development.....</i>	<i>7</i>
Functional relevance of coordinated spiking events during brain circuits development.....	10
Mechanisms underlying the spontaneous generation of coordinated spiking activity in developing brain circuits .....	11
<i>Spontaneous spiking activity in neuronal networks in vitro.....</i>	<i>14</i>
An overview of neuronal culture development .....	15
Cellular and synaptic properties of neuronal cultures.....	15
Hypothesis of mechanisms underlying the spontaneous generation of coordinated spiking activity in neuronal cultures .....	18
Computational modeling of the spiking regimes in neuronal networks.....	19
Network-wide recordings of neuronal activity .....	21
<i>Bibliography.....</i>	<i>25</i>
<b>CHAPTER II - COMPUTATIONAL AND EXPERIMENTAL STUDY ON THE INITIATION MECHANISMS OF SPONTANEOUS COORDINATED SPIKING EVENTS IN NEURONAL CULTURES.....</b>	<b>33</b>
<i>Aims and Rationale.....</i>	<i>33</i>
Limitations of experimental technologies motivate computational network modeling .....	35
<i>Dynamics of spontaneous spiking activity recorded in neuronal culture networks.....</i>	<i>36</i>
All or none network activations .....	36
Comparison of spontaneous activity recordings of low and high-resolution platforms .....	38
<i>A biophysical computational network model of hippocampal cultures .....</i>	<i>41</i>
Testing biologically plausible models of network connectivity.....	42
Assessment of simulated versus experimentally recorded spiking activity.....	45
<i>Manipulation of synaptic transmission: model validation and effects on network dynamics.....</i>	<i>47</i>
AMPA.....	47
GABA.....	48
NMDA .....	51
Other mechanism of neuronal interaction.....	52
<i>Investigating determinants underlying the spontaneous emergence of network bursts .....</i>	<i>54</i>

Intrinsic neuronal excitability .....	54
Border or finite size effects of the network .....	55
Functional connectivity reveals the localization of the NBs ignition sites .....	56
Functional communities give rise to NBs .....	59
The spiking activity preceding a network burst exhibits stereotyped spatial-temporal patterns .....	61
Emergence of local inhomogeneities in the network connectivity .....	64
<i>Applications and extension of the computational network model .....</i>	<i>66</i>
Modelling and interpreting the effects of PRRT2-gene deletion in neuronal cultures.....	66
From 2D networks to 3D neuronal culture computational network models.....	69
<i>Bibliography.....</i>	<i>72</i>
<b>CHAPTER III - BASIC CONCEPTS ON RETINA PHYSIOLOGY AND FUNCTION.....</b>	<b>77</b>
<i>Anatomical structure of the retina.....</i>	<i>77</i>
<i>Input/output properties of the retina.....</i>	<i>82</i>
<i>Techniques for population recordings of Retinal Ganglion Cells.....</i>	<i>84</i>
<i>Local and long-range horizontal interactions shape the response of retinal ganglion cells.....</i>	<i>86</i>
<i>Bibliography.....</i>	<i>89</i>
<b>CHAPTER IV - DEVELOPMENT AND APPLICATION OF DATA ANALYSIS TOOLS FOR LARGE-SCALE</b>	
<b>RETINAL GANGLION CELLS RECORDINGS ON CMOS-MEAS .....</b>	<b>93</b>
<i>Experimental platform.....</i>	<i>93</i>
<i>Integrated analysis chain of light-evoked retinal ganglion cells responses .....</i>	<i>97</i>
Selection and classification of retinal ganglion cells based on light-evoked responses .....	98
Fast receptive fields (RF) estimation .....	101
<i>Identification of visual stimulation artifacts through the analysis of RGCs light-evoked responses .....</i>	<i>103</i>
<i>Investigating the effects of the spatial extension of visual stimuli on local RGCs responses.....</i>	<i>104</i>
<i>Discussion .....</i>	<i>117</i>
<i>Bibliography.....</i>	<i>125</i>
<b>CHAPTER V - DISSEMINATION AND ATTENDED SCHOOLS .....</b>	<b>127</b>
<i>Peer-reviewed contributions .....</i>	<i>127</i>
<i>Oral presentations.....</i>	<i>127</i>
<i>Poster presentations.....</i>	<i>128</i>
<i>Schools attended .....</i>	<i>128</i>
<b>ANNEX I - NEURONAL CULTURES PROTOCOL, MODEL IMPLEMENTATION AND ANALYSIS.....</b>	<b>131</b>
<i>Large-scale recording of neuronal spiking activity in cultured networks.....</i>	<i>131</i>
<i>Detection and quantification of spontaneous activity in neuronal cultures .....</i>	<i>134</i>
<i>Bibliography.....</i>	<i>139</i>
<b>ANNEX II - PREPARATION OF MOUSE RETINA WHOLE-MOUNTS ON CMOS-MEAS .....</b>	<b>141</b>
<i>Retina preparation for high-resolution CMOS-MEA recordings.....</i>	<i>141</i>
<b>ANNEX III - EVALUATION REPORTS AND REVIEWS.....</b>	<b>143</b>







# ***An introduction to the motivations, implementation and achievements of my PhD***

## ***Motivations of this research***

---

Progress in neuroscience is tightly related to the available techniques used to functionally and structurally investigate neuronal systems. According to the neuron doctrine<sup>1</sup>, which started to emerge following the pioneering works of Santiago Ramón y Cajal, a single neuron represents the foundation of the nervous system. Consequently, the conceptual basis of neuroscience embraced this assumption for several decades. Nowadays, with the advent of multi-neuronal recording approaches and advances of several theoretical works have put forward the concept that assemblies and communities of neurons<sup>2</sup>, rather than individual neurons, are at the core of the implementation and execution of brain functions. In this view, these assemblies generate emergent and complex spiking patterns that regulate physiological functions<sup>3</sup>.

It is nowadays clear that brain functions emerge from complex dynamical interactions that cannot be restricted to the scale of neuronal assemblies, but rather involve an even wider range of spatial and temporal scales in the whole brain than previously thought. High-resolution microscopy, biomolecular tools, and functional imaging capabilities enabled observations at different scales, ranging from the quantification of molecules within individual cells up to characterizations of behavioral related activity changes in the whole brain. The different, yet interrelated signaling networks of genes, molecules, cells and circuits co-exist, but despite the enormous and constantly increasing amount of scale-specific self-standing information that can nowadays be acquired, bridging these multiple functional scales together remains challenging. Relating macroscopic effects, such as behaviors, to operating principles at lower scales, represents one among the major current challenges of modern neuroscience<sup>4</sup>.

In particular, by zooming in neuronal systems, one of the intriguing features that it emerges is the heterogeneous composition of their functional networks at different scales. This intrinsic large variability in function and in structure, at cellular and subcellular scales, is apparently in contradiction with the robustness of neuronal networks to execute the tasks they are devoted to. However, as it was proposed, the heterogeneity itself might be a valuable mechanism to increase the reliability and robustness of a neuronal system. For instance, cellular heterogeneity properties might be at the core of cell assemblies operating through population coding. Thus, heterogeneity is more likely not the consequence of a biology's imprecision, rather a fundamental approach adopted by nature. In line with this view, computer simulations also showed that functionally

similar networks could be obtained with many different sets of microcircuits, as long as there is an appropriate set of well-balanced network properties that are maintained. Therefore, these considerations suggest that in addition to the need of investigating the function of different neuronal types and their contribution to the outputs of different brain circuits, advancing in the study and in the comprehension of the fundamental properties of neuronal networks is a fundamental knowledge that we need to acquire in order to understand better how brain circuits operate and might dysfunction in disease.

An approach to study large neuronal assemblies and brain circuits at multiple scales enabled by the computational power available nowadays consists in combining experimental measures performed using modern high-resolution technologies and computational modeling. In my thesis, I have followed and attempted to develop this data-driven approach further. In particular, I focused my research on developing computational tools and I have applied them to specific studies aiming at *i)* contributing in disentangling how spontaneous coordinated spiking patterns in neuronal networks in-vitro are generated as a consequence of network interactions and *ii)* how horizontal pan-retinal interactions might contribute in encoding visual sensory information in the retina. To do so, I have developed computational models and analysis tools based on an emerging generation of multi-electrode arrays that provides high dimensional recordings of neuronal activity from thousands of spiking neurons in individual brain circuits and networks. As it will be described in the following paragraphs, the results obtained by focusing on the specific questions addressed in my work support the view of the important role played by network interactions and communities of neurons in these two neuronal systems, to initiate coordinated spiking activity and to process visual information, respectively.

### ***Roadmap of the research activities developed in this thesis***

---

Exploring network-wide interactions is undoubtedly a still very challenging and intriguing topic that I attempted to address during my Ph.D. using computational and mathematical methods for analysis and modeling in combination with experimental datasets acquired with my colleagues at the IIT-NetS<sup>3</sup> laboratory and by using high-resolution multi-electrode arrays based on CMOS technology (CMOS-MEAs). In particular, the overall aim of my Ph.D. was to adopt this synergic computational and experimental approach to investigate specific functional effects emerging from network interactions in two experimental models, which are hippocampal neuronal cultures and the mice retinal circuit. However, it has to be noted that given the only recent adoption of the CMOS-MEA technology to investigate the retinal circuit, my contribution to the study of this brain circuit involved an important effort on the development and validation of the data analysis tools. Thus, during this thesis, I could not implement a data-driven computational model of this circuit as I could instead do for in-vitro neuronal networks. However, the work spent on developing these tools and in analyzing experimental data was crucial to debug our experimental setup. Indeed, I found and fixed several misbehaviors of the visual stimulator that had an important impact on the results of our experiments.

Briefly, in the first part of my Ph.D. I aimed at exploiting computational modeling and experimental data to study the generation of coordinated spontaneous spiking activity in

developing neuronal networks. I have focused on primary hippocampal neuronal cultures, as a reduced model to investigate network interactions. Importantly, these networks can be recorded almost entirely at the scale of single-neurons with CMOS-MEAs and, currently, they are the only mammalian neuronal system that can be monitored with such a low percentage of single neurons undersampling. Further, neuronal cultures represent an intriguing system from the computational point of view. Primary embryonic neurons grown in culture form an intricate network of connections that can spontaneously exhibit stereotyped network-wide activations and sparse spiking activity. Although no specific physiological circuit is associated with their spontaneous network dynamic, these neuronal systems allow investigating the critical elements that sustain and trigger these emergent network events. In my research, I developed a computational network model and I extensively validated the model against experimental recordings that only a high spatial and temporal resolution recording platform could provide. The strong expertise on CMOS-MEAs and in recording activity from neuronal cell cultures available at the NetS<sup>3</sup> laboratory supported my work since its early phase and provided the necessary elements for the computational model validation and its application. Personally, given my mathematical background, I found the intrinsic complexity of these neuronal systems a fascinating and engaging topic.

Starting from the second year of my Ph.D., I implemented the second part of my work by focusing on a physiological relevant sensory brain circuit, the retina. From this point of view, the retina is an ideal input/output neuronal system to study how networks of neurons organized in different layers convert visual inputs into pre-processed spike-trains for down-stream cortical circuits. In particular, by taking advantage of the large recording area of CMOS-MEAs that allow pan-retinal recordings from several thousand of retinal ganglion cells from each individual and explanted retina, I aimed at investigating the effects of long-range interaction in the processing of visual information. In particular, I contributed to developing and validating the experimental and data analysis platform. Then, I explored the effects of spatially confined visual stimuli in modulating retinal ganglion cells responses with respect to full-field (unconfined) stimuli. This research line still leaves several open questions, but I estimate that my research has contributed in setting a solid ground for ongoing and future studies.

## ***Achieved milestones***

---

During my Ph.D., the synergic effort within the IIT-NetS<sup>3</sup> laboratory provided an excellent science and technology environment to implement my computational investigation. Specifically, former and present colleagues supported this work with high-resolution recordings of spiking activity from biological preparations that served as the basis for biophysical and realistic computational modeling and analysis. Overall, the major achievements and findings of my 3-years PhD, see Fig 1.1. research are shortly summarized here below.

1. I implemented a computational network model that mimics *in silico* the spontaneous spiking activity recorded with high-resolution CMOS-MEAs and that allows to advance our understanding of the impact of single cell interaction within *in vitro* networks of hippocampal neurons. Within this computational framework, all the biological relevant properties included in the network

model, ranging from the dynamics of network-wide spiking activity down to the concentration of neurotransmitters available in a given synapse, are synthetically available and can be integrated with experimental evidence. In this respect, the computational model provides a formal description of the biological processes observed in our experiments as well as useful predictions on the outcome of experiments that are difficult to perform. Further, I was also able to adapt and apply this model to estimate the spontaneous activity that was experimentally observed in a 3D neuronal culture model and in a genetically modified 2D culture model of Paroxysmal disorder.

2. I have found that the computational network model can provide good estimations of the quantities of interest resulting from experimental manipulations of the network, without requiring the addition of time-consuming adjustments of parameters. Indeed, it was essential to understand the limits of my model to capture and reproduce the spiking activity of a network. To demonstrate this, the model was challenged to reproduce recordings acquired with high-density CMOS-MEAs in specific cases, e.g., by using chemical compounds that selectively block specific ion channels. The achieved results demonstrate the capabilities of this *in-silico* model to study and parallel experimental observations on these neuronal cultures.

3. The computational model was successfully exploited to investigate determinants underlying the spontaneous generation of network bursting events in networks of cultured neurons. These network bursts are propagating and transient spiking activations of the network, lasting a few hundreds of milliseconds and separated by quiescent intervals of sparse spiking activity. Our results suggest that a particular, self-organized, local network organization is in charge of initiating network burst. These functional communities of neurons most likely act by amplifying the pre-burst spontaneous and sparse spiking activity of the network. Simulation and experimental results show that the amplification relies on highly clustered and recurrent circuits that are repeatedly activated by similar spiking patterns.

4. The assumptions used to implement the computational model used to investigate network bursts also suggest that a simple connectivity rule based on the relative distance among neurons might be sufficient to explain the self-organization of the functional communities of neurons responsible for the insurgence of network bursts in cultures. This connectivity rule acts by introducing inhomogeneous connectivity in the network and is plausible with experimental evidence.

5. I have successfully implemented a fully automated chain for the analysis of large-scale recordings in the retina that allowed to drastically reducing the analysis time and the need for human supervision. Differently than for the study on neuronal cultures that could already count on a well established set of data analysis algorithms, setting up and validating the experimental and analysis machinery was a required target of my work, before even considering implementing a computational model of the retina to estimate activity that is not accessible through CMOS-MEA recordings (e.g., neuronal activity in the inner layers of a retina).

6. I have validated and optimized our experimental setup through the analysis of light-evoked retinal ganglion cells responses in retina whole-mounts on planar CMOS-MEAs. . Based on the analysis of spike train responses I was able to detect artifacts introduced by the light-stimulation system and to find countermeasures.

7. I applied the automated chain of analysis to reveal the potential effects of long-range horizontal interactions in retinal processing. In this first experimental study, we found that the extension of uniform light stimuli projected onto the retina can influence the response dynamics of retinal ganglion cells and their receptive fields. This suggests that the encoding of visual stimuli in the retina is not only restricted to canonical local vertical circuits, but it occurs with the contribution of the entire retina, through modulatory effects that might be introduced by long-range lateral connections that remain to be better understood.

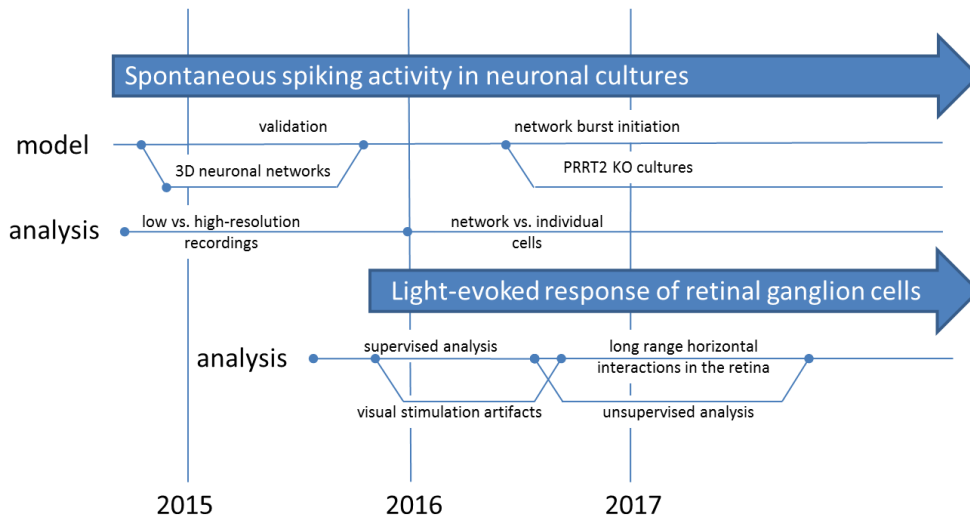


**Fig 1.1: Overview of the research activities implemented in my Ph.D., namely, to investigate network interactions involved in the generation of spontaneous spiking activity in neuronal cultures and, upon analyzing and validating large-scale experimental recordings in the retina, in shaping light-evoked retinal ganglion cells responses. Concerning my study on neuronal cultures, the major effort was allocated to the computational network modeling and to use it to disentangle mechanisms involved in the generation of coordinated spiking activity (or network bursts). On the retina, I focused my effort on implementing and applying to our study unsupervised analysis tools that allowed revealing the effects of spatially restricted visual stimuli in shaping retinal ganglion cells responses that are most likely involving long-range horizontal interactions in the entire circuit.**

## ***Organization of the manuscript***

This thesis is organized in five chapters. In Chapter I and Chapter II, I will present the relevant literature and my work dedicated to the investigation of mechanisms of initiation of coordinated spiking events in neuronal cultures. I used a biophysical computational network model that I have developed to reproduce experimental recordings from neuronal cultures. Additional extensions of the computational model were developed to support the interpretation of experimental findings obtained through collaborations established during my Ph.D. These contributions are also included at the end of Chapter II and consisted in using computational model simulations to investigate spontaneous spiking activity in 3D neuronal cultures with Prof. L. Ballerini (SISSA, Trieste, Italy) and the spontaneous spiking activity in a genetically modified culture model of Paroxysmal disorder, in collaboration with Prof. F. Benfenati (NSYN Dept. of IIT, Genova, Italy).

In Chapter III I will introduce anatomical and functional notions of the retinal circuit that will be instrumental for my study reported in Chapter IV. In the later chapter, I will describe the development of an unsupervised data analysis framework for large-scale recordings of light-evoked retinal ganglion cells responses and its application for the study of the effects of spatially restricted visual stimuli. These stimulation protocols were developed to reveal possible modulatory effects of long-range horizontal interactions. In particular, I have implemented and applied an unsupervised data analysis chain that includes the improvement of data analysis tools previously used in the lab and developed within the RENVISION EC-funded project.

The Chapter V summarizes my dissemination activities, including peer-reviewed journal contributions, oral and poster presentations. This chapter also reports the schools that I have attended during my three years of Ph.D.

In Annexes I-II I report additional information concerning the experimental protocols and computational methods used for my studies described in Chapter II and in Chapter IV. Finally, in Annex III I report the evaluation report of this dissertation of both Dr. Michele Giugliano and Dr. Tim Gollisch, that kindly agreed on reviewing and suggesting improvements to my work. Consequently, in the same section, I have included the changes apported to the dissertation as a result of the comments received.

## ***Bibliography***

---

1. Bullock, T. H. NEUROSCIENCE: The Neuron Doctrine, Redux. *Science (80-. )*. **310**, 791–793 (2005).
2. Buzsáki, G. Large-scale recording of neuronal ensembles. *Nat. Neurosci.* **7**, 446–451 (2004).
3. Kirkby, L. A., Sack, G. S., Firl, A. & Feller, M. B. A role for correlated spontaneous activity in the assembly of neural circuits. *Neuron* **80**, 1129–1144 (2013).
4. Dehghani, N. Theoretical principles of multiscale spatiotemporal control of neuronal network : a complex systems perspective. *bioRxiv* 1–13 (2016). doi:10.1101/097618

# ***Chapter I - Basic concepts of spontaneous coordinated spiking activity in in vivo and in vitro neuronal systems***

In this chapter, at first, I will summarize the major literature describing coordinated spontaneous spiking activity in different developing brain circuits, hypothesis of their functional role and the potential mechanisms that were suggested to underline the initiation of these propagating events. Then, I will introduce the state-of-the-art on the study of spontaneous spiking activity in neuronal cultures, hypothesis of mechanisms underlying the spontaneous generation of coordinated spiking activity and computational models proposed so far to reproduce the spiking dynamics of these neuronal systems. Finally, I will give an overview of the recording techniques suitable for monitoring at large-scale these networks of neurons. In all these sections, I will focus on aspects that will be instrumental for my study developed in Chapter II that is focused on the study of the initiation of coordinated spiking activity in neuronal networks *in vitro*.

## ***Spontaneous spiking activity in the early phase of brain development***

---

In the early phase of brain circuits development, even before that newborn neurons established chemical or electrical synaptic contacts and form networks, neurons exhibit spontaneous electrical activity that is usually uncorrelated among cells<sup>1</sup>. As soon as neurons start forming networks and establish synaptic communication, their spontaneous activity starts including coordinated spiking activity patterns<sup>2</sup>. The spontaneous generation and propagation of such patterns of spikes (bursts of action potentials) are the results of cellular interactions occurring in these forming networks<sup>3</sup>, while changes in the dynamics of these coordinated events were shown to be driven by the effects of neuromodulation<sup>4</sup>, GABA switch<sup>5</sup> or, integration of inputs from upstream circuits or sensory inputs<sup>6</sup>. Interestingly, as I will shortly review here below and as summarized in Table 1.1, so far coordinated spiking activity was observed in the early stage of development of different brain circuits, including the retina<sup>6</sup>, cochlea<sup>9</sup>, spinal cord<sup>10</sup>, hippocampus<sup>11</sup>, neocortex<sup>12</sup> and cerebellum<sup>13</sup>. However, it has to be noted that one of the circuits that was so far the mostly investigated is the retina, during the development of the visual system<sup>8,14</sup>. Therefore, several cited references will be referring to this brain circuit.

### *Coordinated spiking activity in the developing retina*

In the developing retina<sup>7,15</sup>, retinal ganglion cells exhibit transient bursts of action potentials that propagate at first (before birth in mice) as waves of depolarization<sup>16</sup> and later (after birth and before eye-opening in mice) across the retinal ganglion cell layer<sup>17</sup>. Importantly, changes in the dynamics were found to be concomitant with the development and wiring of the retinal circuit and with the formation of the visual system<sup>18</sup>. These propagations of coordinated spiking activity events earned the name of retinal waves<sup>19</sup> and characterized the spontaneous activity in the retina during a transitory period ending at eye-opening (post-natal day 12, P12 in mice). After this period they completely disappear and the final refinement of the retinal circuit is successively driven by the integration of visual inputs<sup>15,16</sup>. Retinal waves are classified into three major classes that are sequentially expressed at different developmental stages. The first class (stage I, P0-P9 in mice) is mainly mediated by gap junctions<sup>20</sup>. The second (stage II, P9-P10 in mice) depends on cholinergic transmission<sup>15</sup> and the third class (stage III, P10-P13 in mice) depends on the glutamatergic transmission between bipolar cells<sup>21</sup>. A recent study on retinal waves of my laboratory in collaboration with the group of E. Sernagor (University of Newcastle) used high-resolution CMOS-MEAs in P1-P12 mice retinas<sup>17</sup> to characterize the ontogenesis and the spatiotemporal properties of retinal waves over the whole retina. It was shown that early cholinergic waves exhibited random trajectories of propagation exploring a large area of the retina but involving a few ganglion cells. Next, the inhibition provided by GABAergic transmission upon maturation (occurring around P6) significantly decreased the speed of propagation. At P10, the glutamatergic signaling induced relevant modulation of the retinal waves, determining repetitive trajectories originating from a few and well-segregated regions of the retina. At this stage, the number of sites originating retinal waves decreased as the circuit further developed until eye-opening where retinal waves disappeared. With respect to the work of this thesis on neural cultures, it is interesting to remark that regardless of the developmental stage, after a retinal wave the retinal ganglion cell layer remained in a quiescent state of sparse and asynchronous firing that could last for a few tens of seconds up to minutes.

### *Coordinated spiking activity in the developing cochlea*

Similarly to the developing retina, also the auditory system gives rise to the spontaneous propagation of bursts of action potentials<sup>9</sup>. On the timescale of several tens of seconds, the transient and periodic emergence of bursts of action potentials characterizes the network activity of the developing cochlea, several weeks before onset of hearing<sup>21,22</sup>. During this period, inner hair cells drive the spiral ganglion cell spiking activity with a burst of  $\text{Ca}^{2+}$  spikes. In turns, the excited ganglion spiral cells generate a transient burst of action potentials that are transmitted to the auditory centers of the brain<sup>24</sup>. Whether hair cells are intrinsically capable of orchestrating this phenomenon or whether their firing is supported by other cell types is still matter of debate. However, recent evidence indicates that the Kolliker's organ supports the insurgence of this spontaneous activity by releasing ATP in a well-defined time interval coincident with the spontaneous spiking activity period<sup>25</sup>. Importantly, at hearing onset<sup>24</sup>, this coordinated activity completely disappears, similarly as it occurs at eye-opening in the retina.



### *Coordinated spiking activity in the developing spinal cord*

Motor neurons in the spinal cord exhibit a similar spiking regime that disappears upon the fully functional development of central pattern generation circuits<sup>27</sup>. Indeed, motor neurons coordinate among themselves to generate spontaneous and recurrent bursts of oscillatory activity separated by a few minutes of silence<sup>28</sup> prior to muscle fiber innervation<sup>29</sup>. Similarly to changes in dynamics of retinal waves also spiking pattern elicited by motor neurons evolve during development<sup>29,30</sup>.

### *Coordinated spiking activity in the developing hippocampus*

A few days before birth and until a few days after birth also pyramidal cells in the hippocampus exhibit bursts of spikes that are correlated among a few neurons<sup>31</sup>. These recurrent local activations later evolve in massively coordinated spiking patterns entraining large populations of hippocampal neurons. These coordinated patterns are referred as Giant Depolarizing Potentials<sup>11</sup>. Depolarizing GABAergic transmission underlies and supports the generation of these rhythms<sup>5</sup> with the additional help of a peculiar hub-like network structure<sup>32</sup>.

### *Coordinated spiking activity in the developing cerebellum*

Purkinje cells in the developing cerebellum exhibit spontaneous coordinated bursts of action potentials that propagate to the base of the cerebellar lobules before establishing the connectivity to receive primary inputs<sup>13</sup>. Purkinje cells, in the absence of any input, exhibit pacemaker features of spiking activity<sup>33</sup>. Differently from the previously mentioned examples, the quiescent periods separating the discharges of spiking activity are interleaved by a short time interval of hundreds of milliseconds<sup>3</sup>. As reported in Table 1.1, although each one of these developing brain circuits differs in its final network wiring, neuronal cell-types and ultimately biological function, all these brain circuits need to self-organize to develop spontaneous coordinated spiking activity by sharing the following common properties:

- (i) the coordinated spiking activity events propagate in the developing neuronal network after formation of synaptic contacts;
- (ii) the coordinated spiking activity is intrinsically generated in the network without the need of external natural (or artificial) inputs;
- (iii) the coordinated spiking activity expressed in different brain circuits shares grossly similar time-scales of activation;
- (iv) external stimuli can dramatically disrupt these coordinated events;
- (v) the time course of the spiking activity in the network after a coordinated spontaneous event is characterized by a quiescent interval of sparse (or asynchronous) spiking activity.

Overall, the properties of these developmental spiking regimes are also highly conserved across species<sup>3</sup> and are remarkably robust to small alterations of the neuronal physiology, thus suggesting that redundant mechanisms of generation are embedded in newly formed networks<sup>1</sup>. As it will be summarized in the next section, a relevant subject of investigation<sup>6,18</sup> regards the questions of why neuronal systems do require this stereotyped spiking regime at the early stage of their development and how neuronal networks give rise to complex spatio-temporal patterns of activity without external inputs.

	Time interval of appearance	Spiking activity regime	Frequency of occurrence
Retina	E17-P1	Localized propagation of burst in the ganglion cell layer	30s
	P1-P14	Extended propagation of burst in the ganglion cell layer	1-2min
Spinal Cord	E12-18	Oscillatory propagation of burst within and between spinal cord segments	1-3min
Hippocampus	E18-15	Correlation of spikes among a few pyramidal cells	8s
	P3-P10	Correlated burst of action potential between CA3 and CA1 subnetworks	3-10s
Cochlea	P7-P10	Burst of action potentials with features similar to retinal waves	5-60s
Cerebellum	P4-P6	Travelling waves of spikes propagating towards the cerebellar lobule base	100ms

**Table 1.1. Summary of the spontaneous spiking patterns and of their frequency of occurrence observed during the early stage of development of different brain circuits (adapted from <sup>1</sup>).**

### ***Functional relevance of coordinated spiking events during brain circuits development***

The initiation and propagation of coordinated spiking events across several thousands of neurons in a network require the consumption of a not negligible amount of energy <sup>34</sup>. Since coordinated spiking events were observed during the development of different brain circuits and across different species, it is reasonable to consider that this energy is not wasted<sup>35</sup> and, as already suggested, this type of activity is rather required for the circuit development, for its formation, wiring and refinement. Understanding how these endogenous coordinated spiking patterns are relevant for circuit development is the subject of several studies<sup>36</sup>. However, this remains an open question in neuroscience.

A very plausible hypothesis to explain the emergence of bursts of action potentials states that the recurrent spiking activity plays a role in driving the strengthening of synaptic contacts and in refining neuronal connectivity<sup>6</sup>. It was also suggested<sup>37</sup> that the propagating nature of these events can play a role in inducing spatial boundaries that map the spatial organization within the circuit to target downstream regions or upstream input circuits. Several studies on retinal waves in the development of the visual system support this hypothesis<sup>17</sup>. Indeed, recent evidence indicates that retinal waves can effectively coordinate downstream visual areas by generating correlated

waves of spiking activity and, vice-versa<sup>38</sup>. Hence, coordinated waves of spikes conveyed by RGCs to their axonal targets are sufficient for the establishment of eye-specific segregation of the axons of retinal ganglion cells<sup>8</sup> and are capable of driving activity-dependent wiring of visual circuits before vision onset<sup>38</sup>. Furthermore, the spatial correlations of retinal waves can eventually provide a cue to map the activity of retinal ganglion cells onto downstream areas to form a topographic map of the visual input in the visual cortex<sup>39,40</sup>. Similar arguments have been proposed for propagating bursts in the early stage of development of the auditory system<sup>9</sup>. Following what was reported for the retina, it was suggested that specifically repeated coordinated spiking pattern might help in the formation and refinement of a tonotopy map and frequency tuning in primary auditory areas<sup>41</sup>. Instead, the motor systems are not spatially organized as the visual and auditory sensory systems<sup>42</sup>. Consequently, whether the coordinated spiking activity can contribute in mapping spinal circuits onto the peripheral afferents is still a matter of debate<sup>6</sup>. However, the fact that the motor neuron axon pathfinding depends on specific patterns of activity supports the hypothesis of a role played by episodic coordinated events in the network wiring also in this system<sup>43</sup>.

Overall, these examples provide considerable evidence suggesting that spontaneous coordinated activity might functionally act as an effective mechanism used to establish and map connections among circuits in the developing brain<sup>6</sup>.

### ***Mechanisms underlying the spontaneous generation of coordinated spiking activity in developing brain circuits***

As previously introduced, parallel to questions on the functional role of coordinated spiking activity during the development of brain circuits, another important question regards how these events might be intrinsically generated in a neuronal systems<sup>36</sup>. The observation of this type of activity in different brain circuits suggests that the mechanisms underlying the generation of coordinated spiking activity should be independent of the intrinsic properties of neurons as well as of the architecture of specific brain circuits<sup>3</sup>. Here, I summarize the most plausible hypotheses that were formulated to explain the generation of these events. As it will be developed later some of these hypotheses were explored in our study to explain the generation of network bursts in neuronal cultures.

#### ***Transient network connections***

Fault tolerance and insensitiveness to unreliable neurons may strikingly be achieved through redundant network architectures that can be transiently established by neurons in developing circuits<sup>44</sup>. The spread of spiking activity in the retinal ganglion cell layer (RGCL) supports this hypothesis because, in immature retinas before birth, the recurrent excitatory network established by starburst amacrine cells<sup>45</sup> can regulate the generation of coordinated spiking activity in the retinal ganglion cell layer through the formation of cholinergic and GABAergic synapses. Conversely, at a mature stage, the retinal circuit prevents the spread of action potentials along the RGCL layer as it is needed to obtain a fine representation of the visual space<sup>46</sup>. Similarly, motor neurons in the developing spinal cord form a network of excitatory connections locally

modulated by interneurons<sup>47</sup> that become functionally silent upon circuit maturation<sup>48</sup>. Before hearing onset and with comparable mechanisms, hair cells in the developing cochlea exhibit coordinated activity driven by a supporting circuit (Kolliker's organ) that transiently release ATP<sup>23</sup>. The latter circuit, as well as the purinergic receptors activated by ATP, are present only in a defined time window during development that corresponds to an interval between a few days after birth and hearing onset<sup>9,25</sup>.

#### *Role of gap-junctions in regulating network activity*

A network of gap junctions represents another interesting mechanism that might induce correlation among the spiking activity of several neurons. Gap junctions can electrically couple different neurons and can consequently intrinsically correlate their spiking activity, but they can also desynchronize the spiking activity depending on the firing rate<sup>49</sup>. Although most of the electrical connections are removed as chemical synapses appear<sup>50,51</sup>, some gap junctions between specific neuron types persist and can contribute to the generation of spontaneous network activity during later stages of development. Further, gap junctions are proved to be involved in coordinating the spiking activity of pyramidal cells in the hippocampus at their very early stage of development<sup>20</sup>. Moreover, other mechanisms such as the transient excitatory network formation can benefit from the presence of electrical coupling among neighboring cells. For instance, electrical coupling contributes to regulate and spread the spiking activity during a retinal wave<sup>52</sup>.

#### *Depolarizing effect of GABAergic transmission before switch*

Another characteristic feature of developing brain circuits is given by the crucial excitatory contribution of canonically inhibitory GABA and glycinergic synaptic transmission<sup>2</sup>. As also investigated by other teams at IIT-NBT, at an early stage of development the high intracellular concentration of  $\text{Cl}^-$  induces a depolarizing effect on the membrane potential upon activation of GABA receptors. Conversely, at a mature stage, the  $\text{Cl}^-$  ions diffuse out of the cell thanks to the activation of  $\text{Cl}^-$  transporters that reduce the intracellular concentration of  $\text{Cl}^-$  and switch the functional role of GABA receptors from depolarization to hyperpolarization<sup>5</sup>. Hence, during the early stage of development, the excitatory contribution of precursors GABAergic hyperpolarizing synapses can represent an intriguing mechanism for the onset of coordinated spiking activity in a forming network<sup>1</sup>. Nevertheless, it is not clear yet whether GABA signaling has the same functional role in all developing neural systems<sup>3</sup>. For instance, while in the turtle retina cholinergic retinal waves can be disrupted upon GABA<sub>A</sub> antagonist administration<sup>15</sup>, in other animal models, such as ferrets or mice, the blockage of GABA<sub>A</sub> receptors induce the modulation of the retinal waves without impairing their generation<sup>53</sup>. Similar results hold true for the developing cochlea<sup>9</sup>. Instead, motor neurons in the spinal cord might benefit from the excitation provided by GABA signaling. It was shown that the administration of an antagonist of GABA<sub>A</sub> greatly reduced, but did not disrupt, the onset of coordinated spiking patterns<sup>54</sup>. On the other hand, it is worth to mention that GABA signaling is essential for generating coordinated and patterned activity in the hippocampus, and specifically giant depolarizing potentials (GDP)<sup>11</sup>. In this circuit, the switch from excitation to inhibition of GABA receptors is tightly correlated with the disappearance of GDPs<sup>55</sup>. On the other hand, GABA depolarization is the sole excitatory driving force in the developing cerebellum<sup>13</sup>.

GABAergic Purkinje cells are autonomously firing at all stages of development and the blockage of GABAergic transmission disrupts the generation of coordinated events<sup>11</sup>. Thus, the local GABAergic connectivity established between these neurons induces correlations among nearby neurons that eventually might lead to the propagation of bursting waves towards the base of the cerebellar lobule. As the cerebellar network matures, the local connectivity between Purkinje cells greatly diminishes and prevents the generation of other coordinated events<sup>3</sup>.

#### *Extrasynaptic signaling*

Extrasynaptic transmission is an additional mechanism that can be involved in the generation of correlated activity in developing neuronal networks<sup>36</sup>. Cumulative evidence suggests a considerable contribution of this peculiar signaling pathway. Spillover of neurotransmitters from the synaptic cleft can be sensed by extrasynaptic receptors of neighboring neurons and glia and can thus provide inputs for coordinating spiking activity among neurons. Recent evidence shows that retinal waves before eye-opening are anticipated by an increase of extrasynaptic glutamate that can facilitate the depolarization of retinal ganglion cells and that is not limited to the directed target of bipolar cells<sup>21</sup>. Indeed, at this stage of development retinal waves are not anymore mediated by starburst amacrine cells, but rather by bipolar cells<sup>56</sup>. On the other side, in the hippocampus, it was shown that the frequency of endogenous correlated spiking patterns is enhanced by transient increases of extrasynaptic glutamate<sup>57</sup>.

#### *Homeostatic regulation of networks*

The above-mentioned strategies for establishing coordinated spiking patterns might coexist with a different level of contributions and at different phases of circuits development<sup>36</sup>. Importantly, the presence of a set of mechanisms, rather than one, can ensure robustness for the generation of coordinated spiking activity in case of failure of a crucial component<sup>3,58</sup>. For instance, in mice models in which the production of acetylcholine was blocked by a transgenic modification, cholinergic retinal waves were replaced after a few days by compensatory propagations of spiking activity<sup>59</sup>. Importantly, although the mechanism of compensation is still poorly understood, the delayed appearance of such propagations suggests that the retinal network needs to compensate the lack of cholinergic waves<sup>52</sup> during development. Similarly, in mice lacking of the NKCC1 transporter, Giant Depolarizing Potentials in the developing hippocampus were still observed, although with fewer neurons were observed to participate in these coordinated spiking activity events compared to wild-type conditions<sup>60</sup>. In this knockout mice, GABAergic transmission is never depolarizing and consequently, even though the major drive for GDPs entrainment is absent, backup mechanisms such as an increased excitability of CA3 pyramidal cells, were suggested to most likely be involved in compensating and supporting the generation of GDPs<sup>61</sup>. This evidence opens fascinating biological questions on the rescue mechanisms that brain circuits can adopt during brain development and to the need of better understanding whether the compensated or endogenous spiking activity lead to equally performing brain circuit's implementations. With respect to the work developed in this thesis, these observations further confirm the need of brain circuits to express coordinated spiking events during brain development and reinforce our motivation in studying how these events might be generated in developing neural systems.

## ***Spontaneous spiking activity in neuronal networks in vitro***

---

The expression of spontaneous coordinated spiking activity with a changing dynamics during development is not only a prerogative of *in vivo* forming brain circuits, but it is also expressed by *in vitro* grown neuronal networks<sup>62</sup>. Thus, either *in vivo* or *in vitro* neuronal systems seem to be committed to a remarkably similar fate consisting in the need of expressing a changing spontaneous activity during their development<sup>1,63</sup>.

Neurons plated on multi-electrode arrays<sup>64,65</sup>, regardless of their origin, tend to form networks that all converge to a relatively stable and stationary spiking regime in which neurons are transiently bursting at high rate and in a coordinated fashion<sup>65</sup>. These transient events, here referred as network burst (NB), last a few hundreds of milliseconds, after which neurons enter in a recovery period of asynchronous and sparse firing regime lasting several tens of seconds<sup>62</sup>.

Somehow similarly as observed in brain circuits, neuronal networks cultured *in vitro* (either 2D or 3D) express a rich range of dynamical changes in their spontaneous activity<sup>66</sup>. On top of this, experimental observations suggest similarities with *in vivo* developing brain circuits. First, the emergence of NBs in primary neuronal cultures is ubiquitous across different cellular preparations<sup>65</sup>, which can include hippocampal<sup>67</sup>, cortical<sup>68</sup> and spinal cord<sup>69</sup> neurons, from different animal models such as rat<sup>63</sup>, mouse<sup>70</sup> and even human IPSCs derived neurons<sup>71</sup>. Importantly, neurons *in vitro* form networks that retain their tissue specificity<sup>65</sup> and intrinsic cellular heterogeneity<sup>72</sup> that are also reflected when expressing spontaneous spiking activity and network responses to pharmacological treatments. This suggests that the emergence of NBs more likely relies on network interactions rather than on single-neuron properties<sup>65</sup>. In support of this, NBs appear in cultures only upon synaptic contact formation<sup>64</sup>. Blockage of excitatory synaptic transmission disrupts the emergence of NBs<sup>73</sup>. Second, neuronal cultures do not require external inputs to exhibit NBs. These events are intrinsically generated and modulated during network development<sup>74</sup>. Conversely, a distributed external stimulation of the network can greatly reduce NBs occurrence<sup>75,76</sup>. This might suggest a similarity with *in vivo* brain circuits where the disappearance of coordinated spiking patterns occurs upon the onset of sensory inputs or integration of upstream circuit's inputs<sup>1</sup>. Third, the spiking regime expressed by neuronal cultures at mature stage is characterized by distinct spatio-temporal patterns of action potentials<sup>77</sup>. This spatio-temporal and propagating dynamics, revealed with the advent of high-resolution recording technologies<sup>78,79</sup>, resemble the spontaneous spiking patterns observed in developing brain circuits.

Importantly, it has to be remembered that even though *in vitro* and *in vivo* spiking regimes likely share grossly similar features and dynamics, the direct relation of network bursting events of neuronal cultures to the spontaneous coordinated spiking patterns observed *in vivo* has not to be overestimated. Obviously, this is due to the radical differences existing among these neuronal systems<sup>65,80</sup>. Indeed, *in vitro* neuronal cultures represent a reduced and isolated system with respect to *in vivo* developing brain circuits. Among the many differences, gap junctions between neurons grown *in vitro* are not directly involved in regulating the spiking activity because either they are not present<sup>81</sup> or do not have an evident functional role<sup>73</sup>.

## ***An overview of neuronal culture development***

Dissociated embryonic neurons from mice or rat plated in cultures form networks that continuously evolve during the first weeks of culture and establish a spontaneously active network<sup>62,70</sup>. As a consequence of this development, the spiking activity of these newly formed neuronal networks exhibits a considerably large set of qualitatively different spiking patterns<sup>66</sup>. In the case of rat cortical cultures, the extracellular trace of action potentials can be recorded after 4-5 DIVs. The spiking regime at this early stage is characterized by a sparse and asynchronous firing among neurons. Upon synaptic contact formation, NBs start to emerge and persist along the lifetime of the culture and tend to regularize their periodicity as the culture ages<sup>66</sup>. The depolarizing effect of GABA, which switch to hyperpolarization after 12 DIVs<sup>68</sup>, has been proven to sustain and coordinate neurons in the network<sup>82</sup>. The developmental stage of the culture is also reflected in its spontaneously expressed spiking activity. Although gradual and significant changes in spatio-temporal patterns<sup>63</sup> and interneuronal correlations<sup>62</sup>, the spiking activity converges after roughly 21 DIVs to a stable regime characterized by NBs interleaved with quiescent periods of sparse spiking activity. At this stage, neuronal cultures are commonly considered as “mature”<sup>74</sup>. Interestingly, the network bursting regime has been proven to support neuronal growth during the lifetime of the culture and neurons that are not recruited in NBs tend to be eliminated from the network<sup>83</sup>.

## ***Cellular and synaptic properties of neuronal cultures***

Although some intrinsic cellular properties are inherited from the original brain circuit from which neurons have been dissociated, neuronal cultures also express spontaneously forming cellular and synaptic features that are observed in different preparations. The next two sections summarize the key elements preserved in cortical and hippocampal cultures based on experimental works reported in the literature. Given the ubiquitous appearance of NBs in neuronal cultures, this review will focus in particular on those general features that are not tissue specific or dependent on the animal model.

### ***Neuronal composition of *in vitro* networks***

Neurons in networks cultured *in vitro* can be divided into two major populations of excitatory and inhibitory neurons (approximately 80%-20%, respectively). Alterations in the excitatory to inhibitory balance was proven to modify the emerging network firing dynamics. For instance, in networks where the number of inhibitory neurons was pairing the number of the excitatory ones, the spontaneous network activity was observed to become more patterned and with long sequences of NBs that resemble superbursts<sup>84</sup>. The heterogeneity of the cellular properties within a neuronal network is another key intrinsic feature of these dynamical systems. Such neuronal heterogeneity originates at different scales. First, the input/output transfer function of each neuron strictly depends on the single-cell intrinsic properties. Second, the amount and type of synaptic contacts established by each neuron can vary considerably. Finally, the biophysical features of individual neurons, such as their excitability, was also proven to significantly differ within a population<sup>85,86</sup> and was it shown to change over long-time-scales<sup>70</sup>. Despite such

heterogeneous neuronal properties, networks of neurons express stable spiking regimes and firing distributions with low inter-culture variability<sup>70</sup>. This apparent contradiction (the unreliability of single cells vs. robust and stable network spiking activities) might be explained by the interaction of several distinct units through a suitable architecture of connections in the network. Whether this heterogeneity is functional for the implementation of stable and reliable network functions is still a debated question.

#### *Synaptic transmission in neuronal cultures at mature stage*

As previously introduced, network bursts in cultures arise upon wiring of the network and regardless of the animal model or brain circuit used for the preparation. Consequently, it is reasonable to consider that network interactions and neuronal connectivity, both mediated by synaptic transmission, are fundamentals of network bursts generation.

In cultures, the main synaptic interactions are given by three major types of synaptic contacts, namely AMPA, GABA, and NMDA. Several works investigated the effects of antagonists of AMPA, GABA and NMDA in modulating the network spiking activity. Here, I shortly summarize this literature. Importantly, note that in a virtually uncoupled network, as it could be obtained by blocking all the mentioned receptors, the network bursting regime disappears<sup>87</sup>, thus stressing the importance of synaptic communication for coordinated spiking activity.

Since network bursts require neurons to fire sequences of densely packed action potentials, an essential condition for neuronal depolarization is the presence of excitatory synaptic contacts. At mature stage, the only synaptic source of excitation is provided by AMPA and NMDA receptors<sup>88</sup>. The blockage of these two receptors through CNQX and APV<sup>87</sup> or by  $Ca^{2+}$  removal<sup>89</sup> determines the disappearance of network bursts. Notably, the blockage of AMPA transmission (as obtained by using CNQX either with the presence<sup>67</sup> or not<sup>90</sup> of glycine to avoid interaction of CNQX with NMDA) while leaving GABA and NMDA receptors unaltered, has the effect of blocking the network bursting regime. On the other hand, the same pharmacological treatment in  $Mg^{2+}$ -free medium does not block the generation of network bursts<sup>88</sup>. In the latter experimental condition, NMDA receptors do not require the effect of AMPA to depolarize the membrane potential (removal of magnesium block) and, consequently, they can be activated independently from AMPA activity. However, in normal conditions the activation of NMDA receptors strictly requires a sustained depolarization to remove the  $Mg^{2+}$  block and, consequently, to generate a depolarizing effect<sup>91</sup>. This evidence suggests a primary role for AMPA in triggering NBs in normal conditions, but also that NMDA receptors can provide an additional excitatory drive depending on AMPA receptor's activity. Interestingly, the blockage of NMDA receptors when leaving functional the AMPA and GABA transmission, for instance upon APV administration, greatly reduces the bursting period of neurons<sup>27</sup> and minimizes the reverberatory spiking activity after the onset of a network burst<sup>92,93</sup>. Moreover, neurons in AMPA driven networks (i.e., with GABA and NMDA blocked) exhibit short and brief burst compared to those observed in purely NMDA driven networks (i.e., with GABA and AMPA blocked). This indicates a potential role of NMDA receptors in supporting persistent and long lasting bursts<sup>87</sup>. Finally, the blockage of GABAergic transmission increases the spiking rate of the culture and induce epileptiform spiking activity<sup>94</sup> with intense bursting<sup>95</sup>. Furthermore, local



blockage of GABAergic transmission determines the insurgence of new complex spatio-temporal patterns of spiking activity with respect to baseline<sup>96</sup>.

### *Network Bursting Regimes in neuronal cultures*

The occurrence of quasi-periodic periods of tonic spiking (>100Hz) lasting a few hundreds of milliseconds and separated by a quiescent period of sparse firing (<5 Hz) was already observed in neuronal cultures by Robinsons et. al.<sup>97</sup> in the early 1990s. Very early works that recorded the activity of neuronal cultures using planar multi-electrode arrays (MEAs) suggested that these periods of tonic firing (or network bursts) could be propagating events<sup>65</sup>, while successive investigations considered these events more as precise network-wide synchronization events rather than propagations<sup>68,89,98,99</sup>. Recently, large-scale recording techniques such as calcium imaging<sup>79</sup> and high-resolution CMOS multi-electrode arrays<sup>78</sup> confirmed the propagating nature of network bursts.

Among the different studies on the spontaneous activity expressed by neuronal cultures, the most comprehensive classification of the network bursting dynamics along with *in vitro* development was reported by Wagenaar et al.<sup>66</sup> It was shown that these networks develop a range of different spiking activity regimes. The range of bursts is remarkably large and it includes tiny, variable, bimodal, fixed size, long-tailed bursts or superbursts. Overall, this range of coordinated spiking events can be reduced into two main categories of either single network bursts or superbursts. While a superburst consists of a chain of network activation separated by less than 500ms, a single network burst is a unique sharply defined network-wide depolarization. The classification of network bursts with respect to their spatiotemporal spiking pattern<sup>77</sup> also revealed the expression of only a few classes of events (i.e., sharing similar spatio-temporal patterns) in each culture (typically <10). These events are repeated over time but in an aperiodic fashion<sup>72</sup>. Additionally, as it will be more deeply addressed in Chapter II, the presence of only a few classes of these network-wide events<sup>77</sup> also implies the presence of only a few sites in the network that initiate these events and their propagation in the network<sup>78</sup>.

Overall, the spontaneous coordinated spiking activity expressed by neuronal cultures at a mature stage roughly splits equally between network bursts and superbursts events<sup>66</sup>. The expression of these two major classes of spiking regimes suggests the presence of two mechanisms of ignition for an NB depending on whether the NB is the first elicited after a quiescent period or if it is initiated right after another NB, as part of a superburst<sup>84,100</sup>. Indeed, at the end of a single NB, synaptic phenomena such as short-term depression, or cellular features such as spike triggered hyperpolarizing currents<sup>64</sup>, prevent the generation of successive NBs at short delays from previous network-wide events and tend to drive the network into a quiescent period. Although the mechanisms underlying the generation of superbursts are still debated, several hypotheses deriving in particular from computational studies have been proposed<sup>92,100–103</sup>. Among these hypotheses, it has been suggested that a potential drive to initiate NBs just after another event might be due to bundles of connection along the boundary of the *in vitro* network<sup>103</sup>. Indeed, at the end of an NB, these bundles of neurites can provide an excitatory feedback signal that might depolarize neurons at the end of their recovery phase<sup>103</sup>. Another potential candidate revealed by computational simulations relies on synaptic features. The

interplay between short-term synaptic facilitation and depression might induce a chain of NB, specifically with a network interacting with strong facilitating synapses<sup>104</sup>. On the other hand, the asynchronous release of neurotransmitters has also been shown to be able to induce a superbursting regime in the network<sup>102</sup>. Finally, the long-lasting depolarization determined by NMDA receptors might support persistent activities such as superburst<sup>105</sup>. In parallel, experimental evidence suggested that the asynchronous release induced by calcium accumulation during bursts<sup>92</sup> and the activation of NMDA receptors<sup>87</sup>, rather than strong facilitating synapses or ad-hoc properties of the network connectivity, are potential mechanisms supporting the generation of persistent activity as superburst in neuronal cultures<sup>92</sup>.

### ***Hypothesis of mechanisms underlying the spontaneous generation of coordinated spiking activity in neuronal cultures***

As for *in vivo* brain circuits, the capability of cultured neurons to form networks that generate spontaneous network bursts has also raised the interest of several studies<sup>65,79,89,106</sup>. Different potential mechanisms were proposed to explain the emergence of these events in these *in vitro* models. From the theoretical point of view, a formal and elegant mathematical theorem (Kuramoto model<sup>107</sup>) states that network synchronization can be achieved if a system of identical, or nearly identical, oscillators are coupled in an all-to-all fashion, with interactions that depend from the sinusoidal phase differences among oscillators. Extensions of this theorem to local dense network connectivity instead of all-to-all connections results in a richer dynamic comprising uniform synchrony or spatiotemporal waves and spirals propagating patterns. Although it is tempting to adopt the Kuramoto model for a formal explanation of the emergence of spontaneous coordinated spiking activities in a network, this model has several limitations once applied to biological systems. First, it requires nearly similar intrinsically oscillating neurons. Second, although a dense local connectivity might be a first approximation of the connectivity in a neuronal culture, the assumption of a diffusive coupling holds true only during the early phase of network formation<sup>68,81</sup>. Third, the dynamics resulting from the adoption of the Kuramoto model is intrinsically periodic, while network bursts occur in an aperiodic fashion<sup>72</sup>.

Despite these limitations, this theoretical model provides some hints on how neuronal cultures might establish network-wide coordinated activity. An intriguing hypothesis derived from the Kuramoto model considers the presence of intrinsically oscillating neurons, or pacemakers, that can effectively entrain the entire network into the network bursting regime. However, while the presence of pacemaker neurons has been observed in young cultures, there is no clear evidence of the presence of intrinsically oscillating neurons in these networks at a mature stage. Several pieces of evidence indicate that the membrane potential of neurons is stable between bursts<sup>108</sup>, no changes in the excitability between bursts occur<sup>68</sup> and pacemaker potentials have never been recorded in hippocampal cultures<sup>67,68</sup>. Further evidence<sup>75</sup> also indicates that intrinsically bursting neurons were found only in neuronal cultures younger than 21 DIVs, while cultures older than three weeks are mostly composed of random spiking neurons.

Alternatively, several works<sup>98,109–111</sup> reported the presence of individual or groups of neurons, referred as “burst leaders”, that can statistically lead to the generation of NBs by firing at the

onset of these events<sup>109</sup>. The overall mechanism proposed in these works suggests that a “primary circuit”<sup>109</sup> of burst leaders activates surrounding neurons with a percolation process and can thus drive the spiking regime of the entire network. Under this scenario, burst leaders fire in advance presumably because of a higher input connectivity and excitability than other neurons in the network. However, although a considerable high firing rate is a characteristic feature of burst leaders, this is not a necessary property of these neurons<sup>109</sup>. Another possible scenario considered a direct interaction among burst leaders to coordinate among themselves the initiation of an NB<sup>112</sup>.

Studies suggesting the presence of burst leaders highlight that specific cellular structures of the network might drive the generation spontaneous network-wide spiking activities. On the other hand, to overcome the need of the presence of neurons with specific properties in the network, another hypothesis for NB generation considers that these events are the result of the interaction of large populations of neurons. These interactions might involve different neuronal cell-types<sup>113</sup> and different network-wide architectures<sup>98</sup>. However, the experimental observation that spontaneous coordinated spiking activity also emerges in small networks of a few tens of neurons<sup>67</sup> is in contrast with this hypothesis.

More recently, a hypothesis that recapitulates the salient features of the different previous explanations suggested that NBs might be originated by the interplay between the individual dynamics of single-neurons and local network interactions<sup>65</sup>. By considering this hypothesis, the work of Orlandi et al.<sup>79</sup> provided the computational evidence that the particular regions of the network that are devoted to the enucleation of NBs from the uncoordinated spiking activity act as noise amplifiers. As it will be developed later in this work, our results confirm and extend this hypothesis both through computational and experimental results. Our study revealed that complex network behavior could simply arise with a simple rule of connectivity and spontaneously active, non-oscillating neurons, thus indicating a promising strategy used by biology to induce spontaneous activity at the early stage of development without needing to rely on task-specific neurons or network architectures.

### ***Computational modeling of the spiking regimes in neuronal networks***

The investigation of the spiking regimes that a neuronal network can express can benefit from several biophysical computational models that can be used to test hypothesis and support experimental evidence. However, it has to be highlighted that each one of the proposed models is based on specific assumptions. Although some modeling choices are relatively simple and supported by experimental evidence, such as the excitatory to inhibitory ratio, some other choices are derived, in the best case scenario, from educated guesses and thus represent a-priori assumptions.

An important theoretical work of Brunel<sup>114</sup> has demonstrated that sparsely connected excitatory and inhibitory integrate and fire neuron models<sup>115</sup> can exhibit a rich repertoire of spiking regimes depending on the strength of the coupling among neurons and their intrinsic spiking activity. Although a neuronal culture represents a much more complex dynamical system compared to the network configuration that was analytically studied in Brunel’s work, this formal

result provides an interesting indication on how to implement and numerically solve biophysical models of neuronal networks. Parallel to this study, the computational model of Markram et al.<sup>116</sup> has provided one of the first attempts to replicate complex network spiking activity *in silico*. In this pioneering work, authors have shown that networks of neurons with randomly connected excitatory and inhibitory synapses equipped with short-term plasticity mechanisms can exhibit spontaneous, network-wide synchronization of the spiking activity. Specifically, network synchronization occurred and ended as a consequence of the short-term depression of excitatory synapses. Indeed, in this model it was observed that the network synchronization disappeared whenever the firing rate distribution of neurons shifted to high firing rates, thus preventing the recovery of synaptic neurotransmitters. Despite the general weaknesses of this work resulting from the adoption of a random connectivity and from the intrinsically oscillatory behavior of neurons, this model has set the ground for further and more detailed biophysical models of neuronal networks. Next, I will shortly summarize some of these works.

Integrate and fire neurons exhibit only two possible firing regimes, either periodic firing or no spiking activity, depending on the steady input current that is provided. Consequently, to relax the assumption of a network of coupled oscillators, Segev et al.<sup>99</sup> proposed to use a dynamic threshold that depends on the membrane potential to make neurons to fire. Although the authors implemented an all-to-all connectivity rule reminiscent of Kuramoto oscillators, with these settings and by including depressing synapses, the simulated network exhibited aperiodic network synchronizations. Importantly, while precise synchronous oscillation was derived from an all-to-all network connectivity, imprecise and approximately synchronous network events could be obtained with a sparse random connectivity<sup>117</sup>. The desynchronization effect induced by sparse connections was also a function of the coupling strength among neurons. Surprisingly, while an increased synchrony could be easily obtained by increasing the strength of excitatory-to-inhibitory synapses, a strengthening of inhibitory-to-excitatory synapses did not decrease the synchrony, thus indicating that the interplay among excitatory and inhibitory neurons could effectively modulate the spiking activity in an unexpected manner.

All works that have followed this approach<sup>85,116,118,119</sup>, however, did not truly attempt to mimic the biophysical properties of a specific neuronal system but rather investigated under which conditions a network of oscillatory-like entities could precisely synchronize. Instead, to reduce the gap between simulation and biology, Persi et al.<sup>118</sup> upgraded and further developed the network model of Markram by driving the individual neuron spiking activity through random input currents and by mimicking the neuronal heterogeneity in terms of input resistance. With these settings, it has been possible to match the experimentally observed features of the interspike interval distribution as well as the internetwork burst distribution of mature cortical cultures<sup>106</sup>. However, the inclusion of the neuronal heterogeneity had a cost on the applicability and goodness of the model. Indeed, different virtually indistinguishable network behaviors can arise from different combinations of synaptic settings or other parameters<sup>120</sup>, thus suggesting that it can be easy to force simulations to the desired output and thus limiting the biological plausibility of the model. On the other hand, the similar behaviors that can arise from large and variegated sets of parameters in this model also suggest that biology might exploit a large number of configurations to generate reliable and robust behaviors at the network scale. For instance, it may be sufficient to

have an appropriate set of network properties to produce the desired circuit behavior without fine-tuning of any given synaptic or cellular characteristic. Hence, based on this consideration the computational investigation in this field shifted to studies on the network connectivity features that could efficiently generate reliable network bursting regimes.

Small-world networks<sup>121</sup> represent a good abstract candidate for the generation of network-wide synchronizations since they combine regular local connections with long-range. Roxin et. al.<sup>122</sup> reported that while regular unidimensional networks of purely excitatory neurons did not show network synchronization phenomena, the presence of a few shortcutting connections could entrain the network in the self-sustained generation of network burst. With all the limits of this simple network model, this work demonstrated that the network architecture could have an impact on the generation of the collective spiking activity. An additional feature of small-world networks is that the transition from a sparse spiking regime to an almost synchronous regime occurs abruptly and requires only a few of shortcutting connections<sup>123</sup>.

Scale-free network was also proven to be successful in the generation of network synchronization compared to random graphs network topologies. In these network models constructed based on Hopfield-type rules, a small subset of nodes, or hub neurons, is connected to a large fraction of the remaining neurons. Consequently, these hub neurons are in a favorable position to regulate the spiking activity of the whole network<sup>124</sup>. In these studies, it has also suggested that a potential mechanism for the generation of NBs relies on the self-organization of developing networks into a hub-like architecture<sup>125</sup>. Interestingly, the presence of a hub-like network structure was observed in the early phase of the developing hippocampus, where the excitatory drive of interneurons that extend their range of connection over a wide set of neurons could dictate the initiation of coordinated spiking activity<sup>32</sup>.

### ***Network-wide recordings of neuronal activity***

During the last decades, the number of simultaneously recorded neurons *in vivo* doubles every seven years<sup>126</sup> mimicking to some extent Moore's law for transistor density. In this respect, the largest contribution that allowed this exponential sampling increase is largely due to the advent of multi-electrode arrays (MEAs) and of optical recording methods.

The usage of extracellular electrodes dates back to the Galvani's experiments on frog's legs published in 1791 and represented one the earliest approaches to record and investigate bioelectrical activity generated by neurons<sup>127</sup>. Later technological developments lead to glass micropipette electrodes that allowed single-cell intracellular measures of the resting membrane potential<sup>128</sup>. The evolution of this approach gave rise to the introduction of the patch clamp technique<sup>129</sup>, which allows the recording of the membrane potential variation induced as a consequence of neuronal activity. The patch clamp technique is a good approach for monitoring single neurons and it provides a remarkable signal to noise ratio due to the direct access to the intracellular environment. However, its major limitations are the intrinsic invasiveness of the approach, which impedes long-term recordings, and the need of fine positioning individual pipettes, which limits the number of simultaneously recorded units. The latter drawback constituted the primary motivation to develop techniques capable of satisfying the increasing

need of sampling large neuronal populations to investigate neuronal interactions. Historically, this goal was achieved by realizing bundles of single extracellular electrodes<sup>130</sup> as well as by realizing with microelectronic fabrication processes multi-site measuring devices by embedding a few tens of electrodes over a plastic substrate<sup>131,132</sup>. The latter approach allowed the first monitoring of the extracellular activity of cultured dorsal root ganglions in 1972<sup>133</sup>.

G. Gross and J. Pine<sup>134,135</sup> introduced in different pioneering works the concept of microelectrode arrays (MEAs) by designing a planar multi-site device on which cultures could be grown and extracellular activity recorded. The device of G. Gross was used to record single spikes of over 3mV peak-to-peak in amplitude from isolated snail ganglions. J. Pine was the first demonstrating the use of multi-electrode array (MEAs) devices to record from mammalian neurons. Further developments were applied to several experimental models<sup>136</sup> such as dissociated neuronal culture<sup>135</sup>, murine spinal neuronal networks<sup>137,138</sup>, retina<sup>139</sup>, spinal cord<sup>140</sup> and cardiac myocyte cells<sup>141</sup> and allowed long-term recordings<sup>142</sup>. These first devices were designed and constructed within the laboratory and consequently lacked of standardized shapes, arrangements or electrochemical properties of the electrodes<sup>143</sup>. However, the general properties and key concepts of these first devices do not differ much; they are all based on the individual connection of electrodes with a contact pad through a metal wire. These devices use individual microelectrodes to sense the small amplitude (typically a few tens to hundreds of microvolts) voltage variations (compared a reference electrode) occurring in the surrounding extracellular space that can be induced by nearby neurons. Due to the extracellular neuron-electrode coupling, these microelectrodes do not break the cellular membrane and can monitor the neuronal activity for long-time (up to months) without harming neurons. Hence, contact pads represent nothing more than simple wires; they passively connect the region of interest to the outside world, where external electronics can condition and process the bioelectrical signals. Thanks to their simple design, these passive devices have been proven to be extremely robust in terms of accessibility and ease usage in a broad range of research and clinical applications<sup>136</sup>. However, the hard-wired signal transmission in this device determines considerable constraints on the number of the electrode to provide a more accurate sampling for the space required by the tracks within the chip, the number of the contact pad and a potential cross-talk among many closed by lines. The spatial arrangement, the number of electrodes, their morphology and electrochemical properties all influence the sensing performances (i.e., signal-to-noise ratio, sensing field, stability, etc.). Despite the sub-millisecond temporal resolution of these devices, the limited number of electrodes integrated into conventional microfabricated MEAs provides a spatially down-sampled description of the overall network activity. In this regard, two different technologies found a successful application to significantly reduce such down-sampling.

Specifically, live-imaging techniques based on fluorescent dyes, such as calcium-imaging, have been demonstrated for multiple single-neuron recordings. Although these approaches provide single-cell resolution, they typically compromise on the temporal resolution and are sensitive to slow varying signals as the calcium concentration inside the cells<sup>144</sup>. Nevertheless, with this approach, hundreds of single neurons can be simultaneously monitored both *in vitro*<sup>145</sup> and *in vivo*<sup>146</sup> (up to few hundreds of micrometers in depth using 2P microscopy techniques). Improvements of optical systems through CCD cameras and DLP mirrors in combination with 3P

systems might provide in the incoming future 3D recordings of deeper brain regions. In parallel, advances in biomolecular optical probes lead to a new generation of GCaMP indicators with a superior temporal resolution compared to conventional one. Current developments of the fluorescent reporters provided a promising generation of indicators that are sensitive to voltage variation rather than calcium concentration, allowing the membrane potential monitoring dynamic of a single cell within a network.

With a different approach, the advent of low-power microelectronic technology based on Complementary Metal-Oxide Semiconductor (CMOS) circuits provided a mean to tackle these limitations by combining the passive acquisition of MEA with an integrated CMOS circuit capable of signal processing as signal amplification and multiplexing<sup>147</sup>. Further application of the CMOS technology in multi-electrode array designs lead to new generations of monolithic microelectronic devices (CMOS-MEAs) with dense and large-area electrode arrays. In this case, to increase the density of electrodes, the required circuits for amplification, filtering, addressing and time division multiplexing of the electrode signals can be integrated right below the electrode surface. These active devices integrate all the electronic components within the electrode matrix itself and this approach allowed to drastically diminishing the inter-electrode pitch while preserving a large recording area of several square millimeters. The advantages of these devices<sup>148,149</sup> are (i) the limited number of output contact pads, as most of the signal processing is performed on-chip, (ii) the quality of the signal that is immediately processed and digitized directly underneath the sensing electrode, minimizing cross-talk among adjacent electrodes, and (iii) the capability of monitoring neuronal networks over large fields-of-view (several square millimetres), down to single cell-resolution and at high temporal resolution (sub-millisecond).

Although the potential of the CMOS miniaturizing technology, the number of recordable electrodes still represent a limit for MEAs. Nowadays, the electrode densification achieved with CMOS bioelectronics lead to devices with 11'016 microelectrodes (electrode size of 7  $\mu\text{m}$  and 17  $\mu\text{m}$  pitch size) over a total recording area of 2 x 1.75  $\text{mm}^2$ , and thus a density of 3150 electrodes/ $\text{mm}^2$ . This platform, originally devised by the group of A. Hierlemann provided a spatial sampling accuracy of a few tens of micrometers, but only from a small and selectable subset of the available recording electrode channels<sup>149</sup>. Beside the latter constrain yielding to a simultaneous recording of a few hundred of electrodes, this technology has been used to monitor with unprecedented details, the interactions among a few neurons by tracking the signal propagation within their axonal and dendritic arborisation<sup>150</sup>. The recent development of this technology resulted in a novel CMOS-MEA featuring 59'760 electrodes with 2048 actively recording channels for *in vitro* investigations<sup>151</sup>.

Differently than targeting the acquisition of highly accurate electrical images from a subset of on-chip electrodes, devices providing a large number of recording electrodes and capable of whole-array sub-millisecond recordings were developed in CMOS technology based on the concept of active-pixel-sensor (APS), i.e., platforms that enable direct signal conditioning, processing, multiplexing and digital conversion for each electrode-pixel. This approach has been declined in a commercially available platform<sup>152</sup> that provides a coarser and homogeneous spatial sampling (42  $\mu\text{m}$  electrode to electrode pitch yielding a 580 electrodes/ $\text{mm}^2$  density) and a full-frame stream of electrical images of the neuronal network in contact with the chip<sup>95</sup>. Specifically,

the chip features 4096 squared electrodes of 21  $\mu\text{m}$  side arranged in a 64x64 matrix that covers an area of 7.11  $\text{mm}^2$ . Differently than Hierlemann's devices, in this platform each electrode is an active-pixel-sensor and, consequently, it is readily accessible individually. Hence, the selection of a sub-region of interest yield to an increase of the sampling rate proportional to the amount of discarded electrodes.

My work deals with recordings based on this later CMOS-MEA device developed in our laboratory and that was proven to accurately quantify network spiking activity<sup>153,154</sup> and resolve with greater details network-wide phenomena such as the propagation of network burst in cultures<sup>77</sup> or retinal waves in retinal whole mounts<sup>155</sup>.



## Bibliography

---

1. Wenner, P. Spontaneous Patterned Activity in Developing Neural Circuits. *Encycl. Neurosci.* **11**, 357–363 (2009).
2. Ben-Ari, Y. Developing networks play a similar melody. *Trends Neurosci.* **24**, 353–360 (2001).
3. Blankenship, A. G. & Feller, M. B. Mechanisms underlying spontaneous patterned activity in developing neural circuits. *Nat. Rev. Neurosci.* **11**, 18–29 (2010).
4. Luhmann, H. J. *et al.* Spontaneous Neuronal Activity in Developing Neocortical Networks: From Single Cells to Large-Scale Interactions. *Front. Neural Circuits* **10**, 40 (2016).
5. Ben-Ari, Y. Excitatory actions of GABA during development: The nature of the nurture. *Nat. Rev. Neurosci.* **3**, 728–739 (2002).
6. Kirkby, L. A., Sack, G. S., Firl, A. & Feller, M. B. A role for correlated spontaneous activity in the assembly of neural circuits. *Neuron* **80**, 1129–1144 (2013).
7. Meister, M., Wong, R. L., Baylor, D. a & Shatz, C. J. Synchronous Bursts of Action Potentials in Ganglion Cells of the Developing Mammalian Retina. *Science (80- )*. **252**, 939–943 (1991).
8. Torborg, C. L., Hansen, K. A. & Feller, M. B. High frequency, synchronized bursting drives eye-specific segregation of retinogeniculate projections. *Nat. Neurosci.* **8**, 72–78 (2005).
9. Tritsch, N. X., Yi, E., Gale, J. E., Glowatzki, E. & Bergles, D. E. The origin of spontaneous activity in the developing auditory system. *Nature* **450**, 50–55 (2007).
10. Landmesser, L. T. & O'Donovan, M. J. Activation patterns of embryonic chick hind limb muscles recorded in ovo and in an isolated spinal cord preparation. *J. Physiol.* **347**, 189–204 (1984).
11. Garaschuk, O., Hanse, E. & Konnerth, A. Developmental profile and synaptic origin of early network oscillations in the CA1 region of rat neonatal hippocampus. *J. Physiol.* **507**, 219–236 (1998).
12. Garaschuk, O., Linn, J., Eilers, J. & Konnerth, A. Large-scale oscillatory calcium waves in the immature cortex. *Nat. Neurosci.* **3**, 452–459 (2000).
13. Watt, A. J. *et al.* Traveling waves in developing cerebellar cortex mediated by asymmetrical Purkinje cell connectivity. *Nat. Neurosci.* **12**, 463–473 (2009).
14. Wong, R. O. L. & Oakley, D. M. Changing patterns of spontaneous bursting activity of on and off retinal ganglion cells during development. *Neuron* **16**, 1087–1095 (1996).
15. Sernagor, E., Eglon, S. J. & Wong, R. O. L. Development of retinal ganglion cell structure and function. *Prog. Retin. Eye Res.* **20**, 139–174 (2001).
16. Wong, R. O. L., Meister, M. & Shatz, C. J. Transient period of correlated bursting activity during development of the mammalian retina. *Neuron* **11**, 923–938 (1993).
17. Maccione, A. *et al.* Following the ontogeny of retinal waves: pan-retinal recordings of population dynamics in the neonatal mouse. *J. Physiol.* **592**, 1545–1563 (2014).
18. Leighton, A. H. & Lohmann, C. The Wiring of Developing Sensory Circuits—From Patterned Spontaneous Activity to Synaptic Plasticity Mechanisms. *Front. Neural Circuits* **10**, 71 (2016).
19. Meister, M., Wong, R., Baylor, D. & Shatz, C. Synchronous bursts of action potentials in ganglion cells of the developing mammalian retina. *Science (80- )*. **252**, 939–943 (1991).
20. Catsicas, M., Bonness, V., Becker, D. & Mobbs, P. Spontaneous Ca<sup>2+</sup> transients and their transmission in the developing chick retina. *Curr Biol* **8**, 283–286 (1998).
21. Blankenship, A. G. *et al.* Synaptic and Extrasynaptic Factors Governing Glutamatergic Retinal Waves. *Neuron* **62**, 230–241 (2009).
22. Jones, T. a, Jones, S. M. & Paggett, K. C. Primordial rhythmic bursting in embryonic cochlear ganglion cells. *J. Neurosci.* **21**, 8129–8135 (2001).
23. Wang, H. C. & Bergles, D. E. Spontaneous activity in the developing auditory system. *Cell Tissue Res.* **361**, 65–75 (2015).
24. Jones, T. A., Leake, P. A., Snyder, R. L., Stakhovskaya, O. & Bonham, B. Spontaneous discharge patterns in cochlear spiral ganglion cells before the onset of hearing in cats. *J. Neurophysiol.* **98**, 1898–908 (2007).
25. Forsythe, I. D. Hearing: A fantasia on Kölliker's organ. *Nature* **450**, 43–44 (2007).
26. Lippe, W. R. Rhythmic spontaneous activity in the developing avian auditory system. *J. Neurosci.* **14**,

- 1486–1495 (1994).
27. Corner, M. A., Van Pelt, J., Wolters, P. S., Baker, R. E. & Nuytinck, R. H. Physiological effects of sustained blockade of excitatory synaptic transmission on spontaneously active developing neuronal networks - An inquiry into the reciprocal linkage between intrinsic biorhythms and neuroplasticity in early ontogeny. *Neurosci. Biobehav. Rev.* **26**, 127–185 (2002).
  28. Markram, H., Wang, Y. & Tsodyks, M. Differential signaling via the same axon of neocortical pyramidal neurons. *Proc. Natl. Acad. Sci.* **95**, 5323–5328 (1998).
  29. Milner, L. D. & Landmesser, L. T. Cholinergic and GABAergic inputs drive patterned spontaneous motoneuron activity before target contact. *J. Neurosci.* **19**, 3007–3022 (1999).
  30. Bekoff, A. Ontogeny of leg motor output in the chick embryo: A neural analysis. *Brain Res.* **106**, 271–291 (1976).
  31. Crépel, V. *et al.* A Parturition-Associated Nonsynaptic Coherent Activity Pattern in the Developing Hippocampus. *Neuron* **54**, 105–120 (2007).
  32. Bonifazi, P. *et al.* GABAergic Hub Neurons Orchestrate Synchrony in Developing Hippocampal Networks. *Science (80-. )*. **326**, 1419–1424 (2009).
  33. Raman, I. M. & Bean, B. P. Inactivation and recovery of sodium currents in cerebellar Purkinje neurons: Evidence for two mechanisms. *Biophys. J.* **80**, 729–737 (2001).
  34. Tozzi, A., Zare, M. & Benasich, A. A. New Perspectives on Spontaneous Brain Activity: Dynamic Networks and Energy Matter. *Front. Hum. Neurosci.* **10**, 247 (2016).
  35. Raichle, M. E. The Brain's Dark Energy. *Science (80-. )*. **314**, (2006).
  36. Kerschensteiner, D. Spontaneous Network Activity and Synaptic Development. *Neurosci.* **20**, 272–290 (2014).
  37. Huberman, A. D., Feller, M. B. & Chapman, B. Mechanisms Underlying Development of Visual Maps and Receptive Fields. *Annu. Rev. Neurosci.* **31**, 479–509 (2008).
  38. Ackman, J. B., Burbridge, T. J. & Crair, M. C. Retinal waves coordinate patterned activity throughout the developing visual system. *Nature* **490**, 219–225 (2012).
  39. Dhande, O. S. *et al.* Development of Single Retinofugal Axon Arbors in Normal and 2 Knock-Out Mice. *J. Neurosci.* **31**, 3384–3399 (2011).
  40. Xu, H. ping *et al.* An Instructive Role for Patterned Spontaneous Retinal Activity in Mouse Visual Map Development. *Neuron* **70**, 1115–1127 (2011).
  41. Johnson, S. L. *et al.* Presynaptic maturation in auditory hair cells requires a critical period of sensory-independent spiking activity. *Proc. Natl. Acad. Sci. U. S. A.* **110**, 8720–8725 (2013).
  42. Kandel, E. R., James H. Schwartz & Thomas M. Jessell. *Principles of Neural Science. Neurology* **3**, (2000).
  43. Hanson, M. G., Milner, L. D. & Landmesser, L. T. Spontaneous rhythmic activity in early chick spinal cord influences distinct motor axon pathfinding decisions. *Brain Res. Rev.* **57**, 77–85 (2008).
  44. Dehghani, N. Theoretical principles of multiscale spatiotemporal control of neuronal network : a complex systems perspective. *bioRxiv* 1–13 (2016). doi:10.1101/097618
  45. Zhou, Z. J. The function of the cholinergic system in the developing mammalian retina. *Prog. Brain Res.* **131**, 599–613 (2001).
  46. Zheng, J. J., Lee, S. & Zhou, Z. J. A developmental switch in the excitability and function of the starburst network in the mammalian retina. *Neuron* **44**, 851–864 (2004).
  47. Nishimaru, H., Restrepo, C. E., Ryge, J., Yanagawa, Y. & Kiehn, O. Mammalian motor neurons corelease glutamate and acetylcholine at central synapses. *Proc. Natl. Acad. Sci.* **102**, 5245–5249 (2005).
  48. Mentis, G. Z., Siembab, V. C., Zerda, R., O'Donovan, M. J. & Alvarez, F. J. Primary afferent synapses on developing and adult Renshaw cells. *J. Neurosci.* **26**, 13297–310 (2006).
  49. Russo, G., Nieus, T. R., Maggi, S. & Taverna, S. Dynamics of action potential firing in electrically connected striatal fast-spiking interneurons. *Front. Cell. Neurosci.* **7**, 209 (2013).
  50. Maxeiner, S. *et al.* Spatiotemporal transcription of connexin45 during brain development results in neuronal expression in adult mice. *Neuroscience* **119**, 689–700 (2003).
  51. Yu, Y. C. *et al.* Preferential electrical coupling regulates neocortical lineage-dependent microcircuit

- assembly. *Nature* **486**, 113–117 (2012).
52. Akrouh, A. & Kerschensteiner, D. Intersecting circuits generate precisely patterned retinal waves. *Neuron* **79**, 322–334 (2013).
  53. Wang, C. T. *et al.* GABA(A) receptor-mediated signaling alters the structure of spontaneous activity in the developing retina. *J Neurosci* **27**, 9130–9140 (2007).
  54. O'Donovan, M. J., Chub, N. & Wenner, P. Mechanisms of spontaneous activity in developing spinal networks. *J. Neurobiol.* **37**, 131–145 (1998).
  55. Leinekugel, X., Medina, I., Khalilov, I., Ben-Ari, Y. & Khazipov, R. Ca<sup>2+</sup> oscillations mediated by the synergistic excitatory actions of GABA(A) and NMDA receptors in the neonatal hippocampus. *Neuron* **18**, 243–255 (1997).
  56. Torborg, C. L. & Feller, M. B. Spontaneous patterned retinal activity and the refinement of retinal projections. *Prog. Neurobiol.* **76**, 213–235 (2005).
  57. Cattani, A. A., Bonfardin, V. D., Represa, A., Ben-Ari, Y. & Aniksztejn, L. Generation of slow network oscillations in the developing rat hippocampus after blockade of glutamate uptake. *J. Neurophysiol.* **98**, 2324–36 (2007).
  58. Turrigiano, G. Maintaining your youthful spontaneity: Microcircuit homeostasis in the embryonic spinal cord. *Neuron* **49**, 481–483 (2006).
  59. Stacy, R. C. Disruption and Recovery of Patterned Retinal Activity in the Absence of Acetylcholine. *J. Neurosci.* **25**, 9347–9357 (2005).
  60. Pfeffer, C. K. *et al.* NKCC1-Dependent GABAergic Excitation Drives Synaptic Network Maturation during Early Hippocampal Development. *J. Neurosci.* **29**, 3419–3430 (2009).
  61. Sipila, S. T. *et al.* Compensatory Enhancement of Intrinsic Spiking upon NKCC1 Disruption in Neonatal Hippocampus. *J. Neurosci.* **29**, 6982–6988 (2009).
  62. Chiappalone, M., Bove, M., Vato, A., Tedesco, M. & Martinoia, S. Dissociated cortical networks show spontaneously correlated activity patterns during in vitro development. *Brain Res.* **1093**, 41–53 (2006).
  63. Van Pelt, J., Wolters, P. S., Corner, M. A., Rutten, W. L. C. & Ramakers, G. J. A. Long-term characterization of firing dynamics of spontaneous bursts in cultured neural networks. *IEEE Trans. Biomed. Eng.* **51**, 2051–2062 (2004).
  64. Maeda, E., Robinson, H. P. & Kawana, A. The mechanisms of generation and propagation of synchronized bursting in developing networks of cortical neurons. *J. Neurosci.* **15**, 6834–45 (1995).
  65. Gross, G. W. & Kowalski, J. M. Origins of Activity Patterns in Self-Organizing Neuronal Networks in Vitro. *J. Intell. Mater. Syst. Struct.* **10**, 558–564 (1999).
  66. Wagenaar, D. A., Pine, J. & Potter, S. M. An extremely rich repertoire of bursting patterns during the development of cortical cultures. *BMC Neurosci.* **7**, 11 (2006).
  67. Bacci, A. Synaptic and intrinsic mechanisms shape synchronous oscillations in hippocampal neurons in culture. *Eur. J. Neurosci.* **11**, 389–397 (1999).
  68. Opitz, T. Spontaneous Development of Synchronous Oscillatory Activity During Maturation of Cortical Networks In Vitro. *J. Neurophysiol.* **88**, 2196–2206 (2002).
  69. Keefer, E. W., Gramowski, A. & Gross, G. W. NMDA Receptor-Dependent Periodic Oscillations in Cultured Spinal Cord Networks. *J Neurophysiol* **86**, 3030–3042 (2001).
  70. Slomowitz, E. *et al.* Interplay between population firing stability and single neuron dynamics in hippocampal networks. *Elife* **2015**, (2015).
  71. Amin, H. *et al.* Electrical responses and spontaneous activity of human iPS-derived neuronal networks characterized for 3-month culture with 4096-electrode arrays. *Front. Neurosci.* **10**, 121 (2016).
  72. Thivierge, J.-P. & Cisek, P. Nonperiodic Synchronization in Heterogeneous Networks of Spiking Neurons. *J. Neurosci.* **28**, 7968–7978 (2008).
  73. Nakanishi, K. & Kukita, F. Functional synapses in synchronized bursting of neocortical neurons in culture. *Brain Res.* **795**, 137–146 (1998).
  74. Pasquale, V., Massobrio, P., Bologna, L. L., Chiappalone, M. & Martinoia, S. Self-organization and neuronal avalanches in networks of dissociated cortical neurons. *Neuroscience* **153**, 1354–1369

(2008).

75. Baltz, T., Herzog, A. & Voigt, T. Slow oscillating population activity in developing cortical networks: models and experimental results. *J. Neurophysiol.* **106**, 1500–1514 (2011).
76. Wagenaar, D. A. Controlling Bursting in Cortical Cultures with Closed-Loop Multi-Electrode Stimulation. *J. Neurosci.* **25**, 680–688 (2005).
77. Raichman, N. & Ben-Jacob, E. Identifying repeating motifs in the activation of synchronized bursts in cultured neuronal networks. *J. Neurosci. Methods* **170**, 96–110 (2008).
78. Gandolfo, M., Maccione, A., Tedesco, M., Martinoia, S. & Berdondini, L. Tracking burst patterns in hippocampal cultures with high-density CMOS-MEAs. *J. Neural Eng.* **7**, 56001 (2010).
79. Orlandi, J. G., Soriano, J., Alvarez-Lacalle, E., Teller, S. & Casademunt, J. Noise focusing and the emergence of coherent activity in neuronal cultures. *Nat. Phys.* **9**, 582–590 (2013).
80. Potter, S. M. Neuronal Dynamics and Plasticity How Should We Think About Bursts? *th Int. Meet. Substrate-Integrated Microelectrodes* (2008).
81. Rouach, N., Segal, M., Koulakoff, A., Giaume, C. & Avignone, E. Carbenoxolone Blockade of Neuronal Network Activity in Culture is not Mediated by an Action on Gap Junctions. *J. Physiol.* **553**, 729–745 (2003).
82. Voigt, T., Opitz, T. & de Lima, A. D. Synchronous oscillatory activity in immature cortical network is driven by GABAergic preplate neurons. *J. Neurosci.* **21**, 8895–905 (2001).
83. Voigt, T., Baier, H. & de Lima, A. D. Synchronization of Neuronal Activity Promotes Survival of Individual Rat Neocortical Neurons in Early Development. *Eur. J. Neurosci.* **9**, 990–999 (1997).
84. Chen, X. & Dzakpasu, R. Observed network dynamics from altering the balance between excitatory and inhibitory neurons in cultured networks. *Phys. Rev. E - Stat. Nonlinear, Soft Matter Phys.* **82**, 1–8 (2010).
85. Persi, E., Horn, D., Volman, V., Segev, R. & Ben-Jacob, E. Modeling of Synchronized Bursting Events: The Importance of Inhomogeneity. *Neural Comput.* **16**, 2577–2595 (2004).
86. Benson, D. L., Watkins, F. H., Steward, O. & Banker, G. Characterization of GABAergic neurons in hippocampal cell cultures. *J. Neurocytol.* **23**, 279–295 (1994).
87. Suresh, J. *et al.* Network burst activity in hippocampal neuronal cultures: the role of synaptic and intrinsic currents. *J. Neurophysiol.* **115**, 3073–3089 (2016).
88. Lin, Y. C. *et al.* Development of excitatory synapses in cultured neurons dissociated from the cortices of rat embryos and rat pups at birth. *J. Neurosci. Res.* **67**, 484–493 (2002).
89. Penn, Y., Segal, M. & Moses, E. Network synchronization in hippocampal neurons. *Proc. Natl. Acad. Sci.* **113**, 3341–3346 (2016).
90. Martinoia, S., Bonzano, L., Chiappalone, M. & Tedesco, M. Electrophysiological activity modulation by chemical stimulation in networks of cortical neurons coupled to microelectrode arrays: A biosensor for neuropharmacological applications. *Sensors Actuators, B Chem.* **108**, 589–596 (2005).
91. Maheswaranathan, N. Emergent bursting and synchrony in computer simulations of neuronal cultures. *Front. Comput. Neurosci.* **6**, 15 (2012).
92. Lau, P.-M. & Bi, G.-Q. Synaptic mechanisms of persistent reverberatory activity in neuronal networks. *Proc. Natl. Acad. Sci.* **102**, 10333–10338 (2005).
93. Pasquale, V., Martinoia, S. & Chiappalone, M. A self-adapting approach for the detection of bursts and network bursts in neuronal cultures. *J. Comput. Neurosci.* **29**, 213–229 (2010).
94. Colombi, I., Mahajani, S., Frega, M., Gasparini, L. & Chiappalone, M. Effects of antiepileptic drugs on hippocampal neurons coupled to micro-electrode arrays. *Front. Neuroeng.* **6**, 10 (2013).
95. Berdondini, L. *et al.* Active pixel sensor array for high spatio-temporal resolution electrophysiological recordings from single cell to large scale neuronal networks. *Lab Chip* **9**, 2644 (2009).
96. Baruchi, I. & Ben-Jacob, E. Towards neuro-memory-chip: Imprinting multiple memories in cultured neural networks. *Phys. Rev. E - Stat. Nonlinear, Soft Matter Phys.* **75**, 50901 (2007).
97. Robinson, H. P. C. Periodic synchronized bursting and intracellular calcium transients elicited by low magnesium in cultured cortical neurons Periodic Synchronized Bursting and Intracellular Calcium Transients Elicited by Low Magnesium in Cultured Cortical Neurons. *J. Neurophysiol.* **70**, 1606–1616 (2012).

98. Baruchi, I., Volman, V., Raichman, N., Shein, M. & Ben-Jacob, E. The emergence and properties of mutual synchronization in in vitro coupled cortical networks. *Eur. J. Neurosci.* **28**, 1825–1835 (2008).
99. Segev, R., Shapira, Y., Benveniste, M. & Ben-Jacob, E. Observations and modeling of synchronized bursting in two-dimensional neural networks. *Phys. Rev. E. Stat. Nonlin. Soft Matter Phys.* **64**, 9 (2001).
100. Vedunova, M. *et al.* Seizure-like activity in hyaluronidase-treated dissociated hippocampal cultures. *Front. Cell. Neurosci.* **7**, 149 (2013).
101. Volman, V., Gerkin, R. C., Lau, P. M., Ben-Jacob, E. & Bi, G. Q. Calcium and synaptic dynamics underlying reverberatory activity in neuronal networks. *Phys. Biol.* **4**, 91–103 (2007).
102. Huang, C. H., Huang, Y. T., Chen, C. C. & Chan, C. K. Propagation and synchronization of reverberatory bursts in developing cultured networks. *J. Comput. Neurosci.* **42**, 177–185 (2017).
103. Gritsun, T. A., le Feber, J. & Rutten, W. L. C. Growth Dynamics Explain the Development of Spatiotemporal Burst Activity of Young Cultured Neuronal Networks in Detail. *PLoS One* **7**, e43352 (2012).
104. Masquelier, T. & Deco, G. Network Bursting Dynamics in Excitatory Cortical Neuron Cultures Results from the Combination of Different Adaptive Mechanism. *PLoS One* **8**, e75824 (2013).
105. Wang, X. J. Synaptic reverberation underlying mnemonic persistent activity. *Trends Neurosci.* **24**, 455–463 (2001).
106. Segev, R. & Ben-Jacob, E. Spontaneous synchronized bursting in 2D neural networks. *Phys. A Stat. Mech. its Appl.* **302**, 64–69 (2001).
107. Acebrón, J. A., Bonilla, L. L., Vicente, C. J. P., Ritort, F. & Spigler, R. The Kuramoto model: A simple paradigm for synchronization phenomena. *Rev. Mod. Phys.* **77**, 137–185 (2005).
108. Murphy, T. H., Blatter, L. a, Wier, W. G. & Baraban, J. M. Spontaneous synchronous synaptic calcium transients in cultured cortical neurons. *J. Neurosci.* **12**, 4834–4845 (1992).
109. Ham, M. I., Bettencourt, L. M., McDaniel, F. D. & Gross, G. W. Spontaneous coordinated activity in cultured networks: Analysis of multiple ignition sites, primary circuits, and burst phase delay distributions. *J. Comput. Neurosci.* **24**, 346–357 (2008).
110. Eckmann, J. P., Jacobi, S., Marom, S., Moses, E. & Zbinden, C. Leader neurons in population bursts of 2D living neural networks. *New J. Phys.* **10**, 15011 (2008).
111. Eytan, D. & Marom, S. Dynamics and Effective Topology Underlying Synchronization in Networks of Cortical Neurons. *J. Neurosci.* **26**, 8465–8476 (2006).
112. Schroeter, M. S., Charlesworth, P., Kitzbichler, M. G., Paulsen, O. & Bullmore, E. T. Emergence of Rich-Club Topology and Coordinated Dynamics in Development of Hippocampal Functional Networks In Vitro. *J. Neurosci.* **35**, 5459–5470 (2015).
113. Segev, R., Baruchi, I., Hulata, E. & Ben-Jacob, E. Hidden Neuronal Correlations in Cultured Networks. *Phys. Rev. Lett.* **92**, 118102–1 (2004).
114. Brunel, N. Phase diagrams of sparsely connected networks of excitatory and inhibitory spiking neurons. *Neurocomputing* **32–33**, 307–312 (2000).
115. Andrew, A. M. Spiking Neuron Models: Single Neurons, Populations, Plasticity. *Kybernetes* **32**, k.2003.06732gae.003 (2003).
116. Tsodyks, M., Uziel, a & Markram, H. Synchrony generation in recurrent networks with frequency-dependent synapses. *J. Neurosci.* **20**, RC50 (2000).
117. Börgers, C. & Kopell, N. Synchronization in Networks of Excitatory and Inhibitory Neurons with Sparse, Random Connectivity. *Neural Comput.* **15**, 509–538 (2003).
118. Persi, E., Horn, D., Segev, R., Ben-Jacob, E. & Volman, V. Neural modeling of synchronized bursting events. *Neurocomputing* **58–60**, 179–184 (2004).
119. Krishnamoorthy, V., Weick, M. & Gollisch, T. Sensitivity to image recurrence across eye-movement-like image transitions through local serial inhibition in the retina. *Elife* **6**, E2391-2398 (2017).
120. Prinz, A. A., Bucher, D. & Marder, E. Similar network activity from disparate circuit parameters. *Nat. Neurosci.* **7**, 1345–1352 (2004).
121. Watts, D. J. & Strogatz, S. H. Collective dynamics of ‘small-world’ networks. *Nature* **393**, 440–442 (1998).

122. Roxin, A., Riecke, H. & Solla, S. A. Self-sustained activity in a small-world network of excitable neurons. *Phys. Rev. Lett.* **92**, 198101–1 (2004).
123. Percha, B., Dzakpasu, R., Zochowski, M. & Parent, J. Transition from local to global phase synchrony in small world neural network and its possible implications for epilepsy. *Phys. Rev. E - Stat. Nonlinear, Soft Matter Phys.* **72**, (2005).
124. Grinstein, G. & Linsker, R. Synchronous neural activity in scale-free network models versus random network models. *Proc. Natl. Acad. Sci.* **102**, 9948–9953 (2005).
125. Downes, J. H. *et al.* Emergence of a small-world functional network in cultured neurons. *PLoS Comput. Biol.* **8**, e1002522 (2012).
126. Stevenson, I. H. & Kording, K. P. How advances in neural recording affect data analysis. *Nat. Neurosci.* **14**, 139–142 (2011).
127. Renshaw, B. Central effects of centripetal impulses in axons of spinal ventral roots. *Journal of neurophysiology* **9**, 191–204 (1946).
128. Ling, G. & Gerard, R. W. The normal membrane potential of frog sartorius fibers. *J. Cell. Physiol.* **34**, 383–396 (1949).
129. Neher, E. & Sakmann, B. Single-channel currents recorded from membrane of denervated frog muscle fibres. *Nature* **260**, 799–802 (1976).
130. VERZEANO, M. Activity of Cerebral Neurons in the Transition from Wakefulness to Sleep. *Science (80-. )*. **124**, 366–367 (1956).
131. Hanna, G. . & Johnson, R. . A rapid and simple method for the fabrication of arrays of recording electrodes. *Electroencephalogr. Clin. Neurophysiol.* **25**, 284–286 (1968).
132. Jobling, D. T., Smith, J. G. & Wheal, H. V. Active microelectrode array to record from the mammalian central nervous system in vitro. *Med. Biol. Eng. Comput.* **19**, 553–560 (1981).
133. Thomas C.A., S. P. A. L. G. E. B.-N. Y. A. O. L. . A Miniature Electrode Array to Monitor the Bioelectric Activity of Cultured Cells. *Experimental Cell Research* **74**, 61–66 (1972).
134. Gross, G. W., Rhoades, B. K., Azzazy, H. M. E. & Ming-Chi Wu. The use of neuronal networks on multielectrode arrays as biosensors. *Biosens. Bioelectron.* **10**, 553–567 (1995).
135. Pine, J. Recording action potentials from cultured neurons with extracellular microcircuit electrodes. *Journal of Neuroscience Methods* **2**, 19–31 (1980).
136. Stett, A. *et al.* Biological application of microelectrode arrays in drug discovery and basic research. *Anal. Bioanal. Chem.* **377**, 486–495 (2003).
137. Gross GW, L. J. Long-term monitoring of spontaneous single unit activity from neuronal monolayer networks cultured on photoetched multielectrode surfaces. *J. Electrophys. Tech.* 55–69 (1982). Available at: <https://neurolab.gatech.edu/labs/potter/meas/references>.
138. Kamioka, H., Maeda, E., Jimbo, Y., Robinson, H. P. C. & Kawana, A. Spontaneous periodic synchronized bursting during formation of mature patterns of connections in cortical cultures. *Neurosci. Lett.* **206**, 109–112 (1996).
139. Cunningham, W. *et al.* Fabrication of microelectrode arrays for neural measurements from retinal tissue. *J. Phys. D. Appl. Phys.* **34**, 2804–2809 (2001).
140. Jánosy, V. *et al.* Multielectrode culture chamber: a device for long-term recording of bioelectric activities in vitro. *Acta Biol. Hung.* **41**, 309–20 (1990).
141. Israel, D. a, Barry, W. H., Edell, D. J. & Mark, R. G. An array of microelectrodes to stimulate and record from cardiac cells in culture. *Am. J. Physiol.* **247**, H669-74 (1984).
142. Regehr, W. G., Pine, J., Cohan, C. S., Mischke, M. D. & Tank, D. W. Sealing cultured invertebrate neurons to embedded dish electrodes facilitates long-term stimulation and recording. *Journal of Neuroscience Methods* **30**, 91–106 (1989).
143. Thiébaud, P., De Rooij, N. F., Koudelka-Hep, M. & Stoppini, L. Microelectrode arrays for electrophysiological monitoring of hippocampal organotypic slice cultures. *IEEE Trans. Biomed. Eng.* **44**, 1159–1163 (1997).
144. Grewe, B. F., Langer, D., Kasper, H., Kampa, B. M. & Helmchen, F. High-speed in vivo calcium imaging reveals neuronal network activity with near-millisecond precision. *Nat. Methods* **7**, 399–405 (2010).
145. Palazzolo, G. *et al.* Fast wide-volume functional imaging of engineered in vitro brain tissues. *Sci. Rep.*

- 7**, 8499 (2017).
146. Bovetti, S., Moretti, C. & Fellin, T. Mapping brain circuit function in vivo using two-photon fluorescence microscopy. *Microsc. Res. Tech.* **77**, 492–501 (2014).
  147. Jochum, T., Denison, T. & Wolf, P. Integrated circuit amplifiers for multi-electrode intracortical recording. *J. Neural Eng.* **6**, 12001 (2009).
  148. Berdondini, L. *et al.* High-density electrode array for imaging in vitro electrophysiological activity. *Biosens. Bioelectron.* **21**, 167–174 (2005).
  149. Frey, U. *et al.* Cell recordings with a CMOS high-density microelectrode array. *Annu. Int. Conf. IEEE Eng. Med. Biol. - Proc.* **2007**, 167–170 (2007).
  150. Bakkum, D. J. *et al.* Tracking axonal action potential propagation on a high-density microelectrode array across hundreds of sites. *Nat. Commun.* **4**, 2181 (2013).
  151. Dragas, J. *et al.* In Vitro Multi-Functional Microelectrode Array Featuring 59 760 Electrodes, 2048 Electrophysiology Channels, Stimulation, Impedance Measurement, and Neurotransmitter Detection Channels. *IEEE J. Solid-State Circuits* **52**, 1576–1590 (2017).
  152. 3Brain - high resolution technology. (2015). Available at: <http://www.3brain.com/>.
  153. Maccione. Experimental investigation on spontaneously active hippocampal cultures recorded by means of high-density MEAs: analysis of the spatial resolution effects. *Front. Neuroeng.* **3**, 4 (2010).
  154. Amin, H., Maccione, A., Zordan, S., Nieus, T. & Berdondini, L. High-density MEAs reveal lognormal firing patterns in neuronal networks for short and long term recordings. *2015 7th Int. IEEE/EMBS Conf. Neural Eng.* 1000–1003 (2015). doi:10.1109/NER.2015.7146795
  155. Maccione, A. *et al.* Toward Pan-Retinal Characterization of Ganglion Cells Responses To Finely Controlled Spatio-Temporal Light Stimuli on 4096 Cmos-Meas. 2014 (2014).





# ***Chapter II - Computational and experimental study on the initiation mechanisms of spontaneous coordinated spiking events in neuronal cultures***

In this chapter, I report and discuss results obtained from my experimental-computational study on the mechanisms of initiation of coordinated spiking events in neuronal networks *in vitro*. This study integrates the analysis of the spontaneous spiking activity recorded with my colleagues using CMOS-MEAs and hippocampal neuronal cultures and the analysis of synthetic data generated by the computational network model that I have developed. While experimental evidence provided assumptions and necessary evidence enabling to develop and validate the computational model, the computational model enabled to exploit its complete parametric description to investigate different hypothesis of burst initiation.

At first, I will summarize the aims and rationale of this study. Then, I will report the characterization of the spontaneous spiking activity that we recorded in these networks using CMOS-MEAs and, successively, the development and validation of a computational network model mimicking such spiking dynamics. The validation also included a series of studies using the model to investigate experimentally observed effects of pharmacologically manipulated synaptic transmission. This is followed by a section in which I report results obtained in my experimental-computational study on the initiation of coordinated events (or network bursts, NBs). Finally, I describe applications and extensions of my computational network model that I had the opportunity to explore through collaborations.

## ***Aims and Rationale***

---

As described in Chapter I, spontaneous network-wide synchronization (or coordinated spiking activity) interleaved with periods of sparse spiking characterize the spontaneous activity of neuronal cultures<sup>1</sup> after network formation. Neurons in cultures mature and self-organize to form complex neuronal networks<sup>2</sup> that show the spontaneous generation of biological electrical activity in the form of trains of action potentials<sup>3,4</sup>. Differently than organoids<sup>5,6</sup> or 3D cortical cultures<sup>7</sup>, that are 3D *in vitro* preparations whose network connectivity and cellular properties develop from undifferentiated cells following similarities with brain circuit development, these 2D networks lack of evident physiological network structures. However, such lack of organization is just apparent. Indeed, despite the variable network connectivity and cellular composition, different neuronal cultures remarkably share common features. First, even though cultures are prepared with

variable compositions of primary cells, the excitatory to inhibitory neuron ratio is conserved across different mature neuronal cultures. Second, although neuronal cultures are isolated systems, they are spontaneously active and exhibit a steady spiking activity without any external stimulation. Third, different preparations express similar spiking regimes and the self-generation of highly reproducible complex spatiotemporal firing patterns. Additionally, at mature stage, the firing rate distributions exhibit a log-normal like profile which is reliably preserved across different neuronal cultures.

Finally, it is plausible to consider that neurons grown *in vitro* inherit the genetic features and cellular properties of the stage of *in vivo* development reached at the time of their dissection. In addition to these biological properties, the experimental use of high-resolution CMOS-MEAs<sup>8</sup> electrophysiological recordings allowed to access a large number of spiking neurons in these networks, thus providing a unique experimental opportunity to investigate their spontaneously firing regimes at a very low undersampling of cellular activity. Consequently, with respect to the aim of my study *in vitro* systems on CMOS-MEAs are an interesting model to investigate mechanisms and biological functions underlying the spontaneous generation of coordinated spiking activity.

Investigating the mechanisms underlying the spontaneous generation of coordinated spontaneous spiking activity in these isolated and self-forming neuronal networks might reveal basic and robust mechanisms exploited by neurons to set the basis for their subsequent integration in functional neuronal circuits. However, even though the initiation of spontaneous bursts of spikes and their subsequent propagation in a neuronal network represent a hallmark of developing circuits, the network mechanisms behind the initiation of these burst events are not fully understood yet.

As discussed in Chapter I, two major classes of mechanisms were proposed to contribute to the autonomous generation of network bursting events<sup>9</sup>. First, from the neuronal doctrine, the focus is on individual neurons that regulate the network spiking activity and trigger network-wide patterned activity through a burst of action potentials. Consequently, these neurons require a peculiar set of features in order to act as pacemakers of the network, including a high number of connections, a favorable position in the network in which they are embedded, peculiar intrinsic properties as excitability or periodic bursting. On the other hand, the new large-scale techniques of investigation<sup>10</sup> put forward the hypothesis that the patterned spontaneous activity might result from the interaction of single neurons rather than from the functional role of individual neurons<sup>11,12</sup>. In this respect, the ubiquitous emergence of coordinated spiking patterns in the early stage of brain circuits with different wirings suggests a highly preserved mechanism of initiation and an appealing contribution of the local network connectivity<sup>13</sup>.

As described in this chapter, in my work I aimed at investigating the possible mechanism of initiation of spontaneous network bursts in neuronal networks *in vitro* using large-scale experimental recordings and by exploiting a data-driven computational network model to test different hypothesis.

## ***Limitations of experimental technologies motivate computational network modeling***

Despite the remarkable improvements in large-scale recording technologies and the emerging opportunities offered by micro-/nano-electrodes for intra-cellular like signals recordings<sup>14,15</sup>, current methods do not allow to simultaneously acquire the intracellular membrane potential of each neuron in large networks even in cultured 2D networks. Additionally, it is currently not possible to experimentally acquire a full-detail information about the actual structural and functional connectivity of a network or details on additional players (e.g., receptors, synapses) that can contribute in shaping the network dynamics. This information is essential in order to understand which are the necessary elements exploited by neuronal networks to give rise to the complex spatiotemporal patterns and to correlate every single dynamical unit with the overall network activity. Indeed, minimal perturbations of the units can lead to unpredictable outcomes in a complex network. On the other hand, the robust behavior of neuronal cultures also indicates the presence of an invariant and persistent mechanism of generation that is not sensitive to the activity of all possible players. Hence, understanding which is the set of features that are essential and those that are negligible requires the full characterization and monitoring of the neuronal system. Although such detailed and multi-scale description still represents an enormous challenge for current neurotechnologies, the use of *in silico* simulations through computational biophysical modeling of neuronal networks might be exploited in parallel with the nowadays available experimental recording technologies. Within this framework, experimental evidence provides the ground truth to generate assumptions and hypothesis that can be then tested and supported via computational investigations.

In this work, I exploited high-resolution experimental datasets in combination with simulations to disentangle determinants underlying the initiation and the dynamics of collective bursting activity in cultured neuronal networks. Importantly, the high spatial and temporal resolution of the experimental electrophysiological recordings acquired with CMOS multi-electrode arrays (CMOS-MEAs)<sup>8,16–18</sup> provided the basis for a faithful implementation and validation of a biophysical network model. The extracellular potential variations induced by spiking activity in neuronal cultures was recorded at a sub-millisecond resolution with 4096 closely spaced microelectrodes (i.e., 42  $\mu\text{m}$  inter-electrode separation). Such a comprehensive access to the spiking activity of several thousands of neurons composing the network allowed to quantify mean activity parameters finely, to precisely localize the sites of the network where NBs originate and to track and classify these spatiotemporal propagations<sup>19</sup>, thus providing the ground truth for my computational model validation.

## ***Dynamics of spontaneous spiking activity recorded in neuronal culture networks***

---

As previously introduced, neuronal cultures represent a versatile reduced model for the investigation of complex network dynamics based on the current recording capabilities, see Fig 2.1A. An intriguing aspect is the capability of these networks to self-organize and to generate a rich repertoire of spontaneous network-wide propagations of spikes interleaved with periods of sparse spiking (or “all or none network activations”), see Fig 2.1B. Briefly, embryonic rat hippocampal neurons were seeded on high-density CMOS-MEAs at a density of  $\approx 1600$  cell/mm<sup>2</sup>. After 20 – 24 Days In Vitro (DIVs), extracellular voltage traces of the spontaneous activity in the network were recorded for periods of 10 minutes. Once acquired, these raw traces were analyzed off-line upon a first step aimed at detecting and extracting the timings of the action potentials. To do so, we used algorithms implemented in the BrainWave software (3Brain AG, Switzerland) and custom Python scripts that I developed to visualize and to quantify different features of the spiking activity of these networks. In the next sections, I will shortly summarize the main properties of the spontaneous spiking activity unveiled by high-density multi-electrode array recordings in *in vitro* neuronal networks of hippocampal neurons.

### ***All or none network activations***

In Fig 2.1B I report two illustrative raster plots of network bursts showing the typical “all or none activity” that is observed after  $\approx 20$  DIVs. As shown, either neurons fire a few and uncoordinated spikes, or they are in large majority collectively active for a few hundreds of milliseconds. Coordinated network-wide activations are here referred as Network Burst (NB), whereas with “quiescent periods” I define those intervals of asynchronous firing observed in between two consecutive NBs. On the timescale of 100 ms, almost all neurons in the network fire sequences of a few spikes at a high rate ( $\approx 100$  Hz), making these events easy to detect by setting a hard threshold on the mean firing rate of the entire population. During quiescent epochs, neurons fire action potentials at a significantly low rate ( $\approx 0.1$  Hz). It is important to highlight that previously published works have shown that NBs are not simple, coherent synchronizations of neurons, but are rather characterized by a much richer dynamics. In particular, by reordering the electrode channels in the raster plots (see Annex I – Large-Scale Recordings) it is possible to observe a significant delay among the spikes recorded at different sites during an NB, see Fig 2.1C. Importantly, such delay correlates with the position of the recording electrode in the array, thus already indicating the presence of a propagation of spiking activity (see next section). Even though, this network bursting dynamic slightly changes as the cultured neurons grow, it remains stable for several hours, that is much more than the observation period of a recording (10 min). Furthermore, although the wiring in cultured neurons varies from one to another cell culture, after maturation they always exhibit a network bursting regime.

## Tracking and classifying network bursts propagations

High-resolution recordings revealed that these propagations of spikes during NBs follow precise and stereotyped spatio-temporal patterns that can be easily classified and grouped in a few classes. The first-step approach that was proposed reduces the dimensionality of each NB propagation by computing the weighted mean position of the spiking activity over time. This method is referred as the Center of Activity Trajectory (CAT)<sup>20</sup> and allows to visually represent the propagation patterns of the NBs (an example is shown in Fig 2.1D).

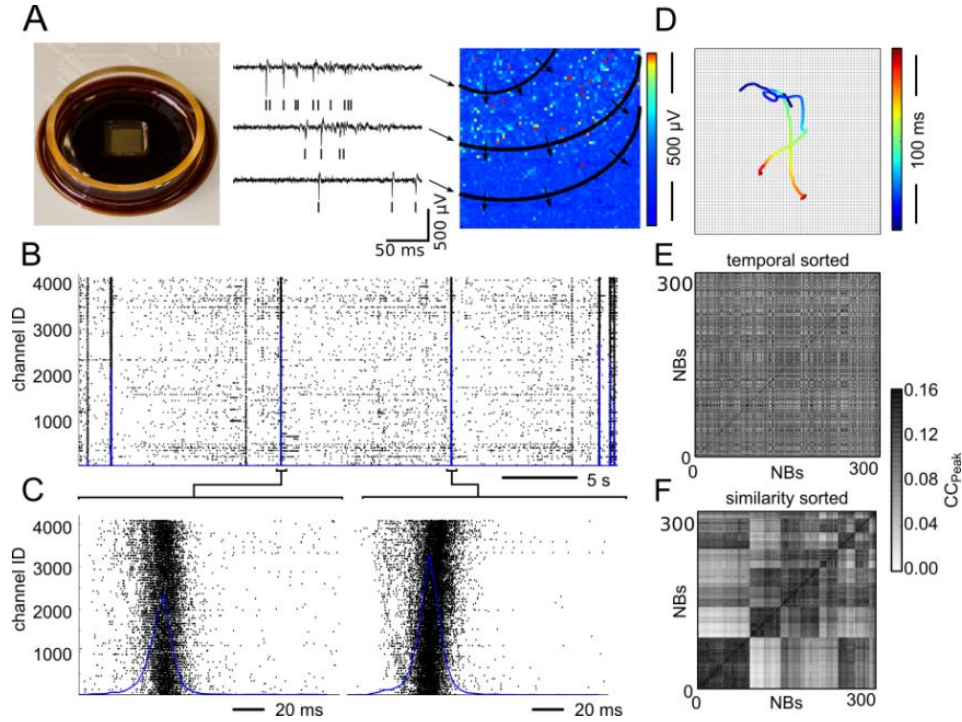


**Fig 2.1: High-resolution recordings of the spontaneous activity of hippocampal cultures at mature stage (19-21 DIVs).** (A) View of the CMOS-MEA cell culture well, with a matrix of 64x64 electrodes that collects extracellular signals from neuronal cultures grown on-chip. Three illustrative recorded traces displaying a transient variation of the extracellular voltage, or action potentials (spikes). Black bars mark all the detected spikes that, in this case, are part of a network burst (NB). As shown on the activity map (i.e., color-coded representation of the extracellular voltage for the 64x64 recording electrodes) the different timing of neuronal activations depends on the position of the electrodes in the matrix. (B) Raster plot depicting the spontaneous spiking activity of hippocampal cultures in a 40s snapshot. NBs consist of giant network depolarization lasting few hundreds of milliseconds. The blue line (array-wide spike count over 5ms time windows) highlights the simultaneous activation of neurons during one of these events. (C) A closer look at two NBs reveals different propagations of the spiking activity for the two events, as it can be better appreciated (D, time of the propagation is color-coded) by the analysis of their Center-of-Activity Trajectory, CAT. The two consecutive NBs depicted in (C) exhibit different propagations as also indicated by (E) the cross-correlation matrix of NBs. (F) NBs can be clustered in a few classes of similar NBs upon their reordering with a hierarchical clustering method.

The analysis of CATs shows that once cultured networks are formed, they give rise to a limited set (less than 10) of NB propagation classes (i.e., an “alphabet of a few letters”<sup>19</sup>) as highlighted by the cross-correlation matrices in Fig 2.1E,F. The persistence and recurrence of the same pathways

of propagation along time suggested us that the circuitry underlying the initiation and propagation of NBs rely on built-in properties of the formed network. In particular, only a few areas (or “hot spots”) of the network, specific to each class of NBs, contribute to the ignition of these events and the network endows reliable and robust pathways for their propagation throughout the network. Importantly, as shown in Fig 2.1F, NBs of a given class of propagation repeat several times during the recording, without a particular temporal structure of repetition, see Fig 2.1E.

### ***Comparison of spontaneous activity recordings of low and high-resolution platforms***

Conventional passive low-resolution MEAs and active high-resolution CMOS-MEAs are radically different devices. They integrate electrodes with different sensitivities to extracellular signals. Further, they feature different surface topologies that might impact on the network formation and thus on the expressed activity. Therefore, as a first step, I was interested in comparing the statistics of the spiking activity recorded with electrodes from neuronal cultures grown on these two different types of devices, while maintaining the same and well-controlled cell culture conditions. Although high-resolution MEAs are available since a few years<sup>8,18</sup>, a quantitative comparison of the spiking activity acquired with passive and active platforms was still missing. Moreover, this first part of my study allowed evaluating the pros and cons of the metrics computed on the experimental data that were then successively used to develop my data-driven computational network model.

To perform this study, we recorded neuronal activity from cultures grown on 60 electrode array passive MEAs (from Multichannel Systems, Germany) and on 4096 electrode array CMOS-MEAs (from 3Brain AG, Switzerland). Briefly, the passive MEAs used in this study consisted of arrays of round recording electrodes of 30  $\mu\text{m}$  in diameter and arranged in an equispaced grid covering a recording area of approximately 2.6  $\text{mm}^2$ . Further, the electrode material was TiN. This electrode material provides a rough electrode surface that contributes to increasing the real electrode area, thus reducing the electrode impedance and increasing the electrode sensitivity. For these devices, the electrical activity of several neurons positioned in the neighborhood of each electrode can contribute to the extracellular potential recorded by every single electrode.

On the other side, high-resolution CMOS-MEAs provided a recording area of 2.7  $\text{mm}^2$  and 4096 square electrodes of 21  $\mu\text{m}$  x 21  $\mu\text{m}$  in sizes with an electrode pitch of 42  $\mu\text{m}$ . Unlike passive devices, the squared electrodes of our CMOS-MEAs are embedded by 2  $\mu\text{m}$  into the top insulator. This different electrode morphology of CMOS-MEAs is supposed to confine the sensing area of each electrode to a smaller sensing region than passive devices although the rough platinum electrode coating increases the electrode sensitivity.

#### ***Analysis of low and high-resolution recordings***

At the time-scale of seconds, the spontaneous network spiking recorded from cultures at a similar age (19-21 DIVs) looks qualitatively similar in both recordings acquired using the two MEA devices, see Fig 2.2. Indeed, both conventional (Fig 2.2A) and high-resolution recordings (Fig 2.2B) exhibit network-wide synchronizations interleaved with quiescent recovery epochs characterized

by sparse and asynchronous spiking. However, the quantification of first-order spiking statistics revealed some discrepancies and in particular in the burst activity parameters, see Fig 2.2C. To detect a burst of action potentials within the spike trains recorded by a single electrode, I used a conventional definition of bursts, that is a sequence of at least  $N_{\text{spk}}=5$  whose interspike interval smaller than  $IS_{\text{Imax}}=100$  ms.

Specifically, in high-density CMOS-MEA recordings, a smaller set of electrode channels (30-40%) recorded bursts of action potentials and, consistently with the latter quantification, the number of spikes that were not belonging to a burst (or Random Spikes) was close to the whole amount of detected action potentials, see Fig 2.2D.

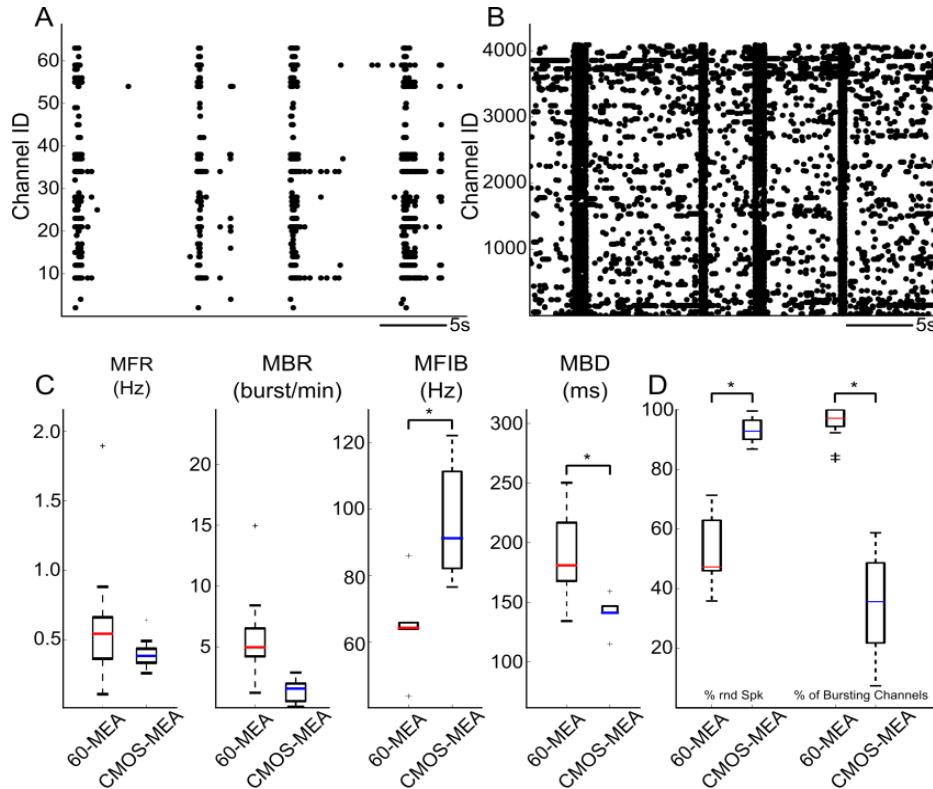


**Fig 2.2 Qualitative and quantitative comparison of the spontaneous activity in low (60 electrodes MEAs, 60-MEA) and high resolution (4096 electrodes CMOS-MEA) recordings.** (A) Raster plots of a 60-MEA recording and of (B) a 4096 CMOS-MEA recording, both of 30 s showing several NBs. (C) First-order statistics of the analyzed parameters, i.e., Mean Firing Rate (MFR), Mean Bursting Rate (MBR), Mean Frequency Inter-Bursts (MFIB), Mean Burst Duration (MBD) for n=6 cultures CMOS-MEA and n=5 cultures 60-MEA. (D) Percentage of random spikes and electrode channels detecting at least one burst for the two devices. \*p=0.01, t-test.

#### Single electrode channel bursts during network bursts

As reported in the previous paragraph, the higher percentage of random spikes detected in high-resolution CMOS-MEA recordings indicates that a smaller fraction of electrodes detects long sequences of densely packed spikes. Consequently, to identify NBs in high-resolution CMOS-MEA recordings, one cannot rely solely on the spike trains of individual electrodes. Given this observation, a deeper comparative analysis of datasets acquired with the two devices was performed by looking at single electrode spike-trains on the two devices. In an illustrative

snapshot (Fig 2.3A-B), I highlight with red dots the burst detected during two NBs and recorded from different cultures grown on low and high-density devices.

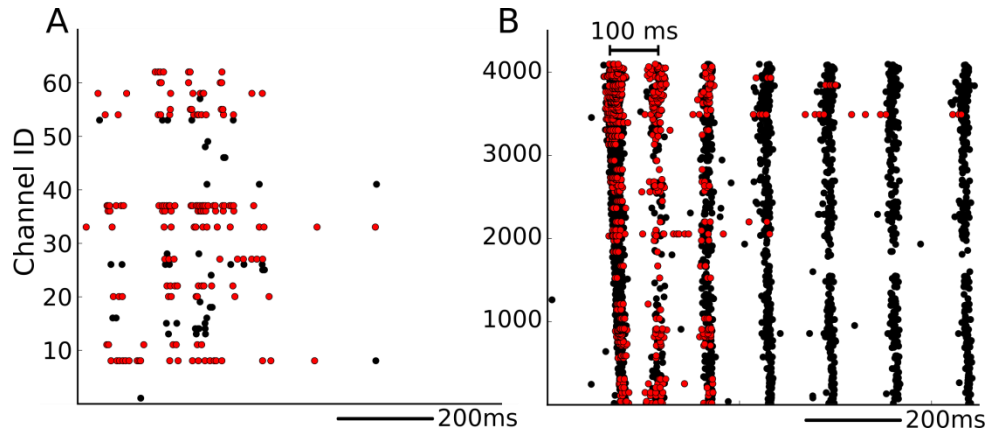


**Fig 2.3: A closer look at network bursts and single-channel bursts for low and high-resolution recordings. (A) Raster plot of 1s of activity displaying a single NB a 60-MEA recording and (B) multiple NBs for a CMOS-MEA recording. The red dots indicate those spikes accounted for a burst using classical definition. Note that spikes accounted as a burst in the CMOS-MEA recording are not clustered into a single NB.**

Interestingly, the spikes belonging to a burst recorded with the CMOS-MEA belongs to different NBs tightly packed together (named superbust<sup>1</sup>). Hence, by decomposing superbusts into single NBs, the comparative analysis revealed that the number of spikes recorded during a single NB is remarkably smaller for high-density MEAs compared to conventional MEAs, as quantified in Fig 2.4A. Specifically, the distribution of spikes belonging to NBs in 60-MEA recordings revealed a much flatter profile and included a significant fraction of long sequences of consecutive spikes (up to 17 per single electrode channel). Consequently, single network events recorded with high-resolution CMOS-MEAs are composed of a small fraction of electrodes that are in a bursting state, see Fig 2.4B.

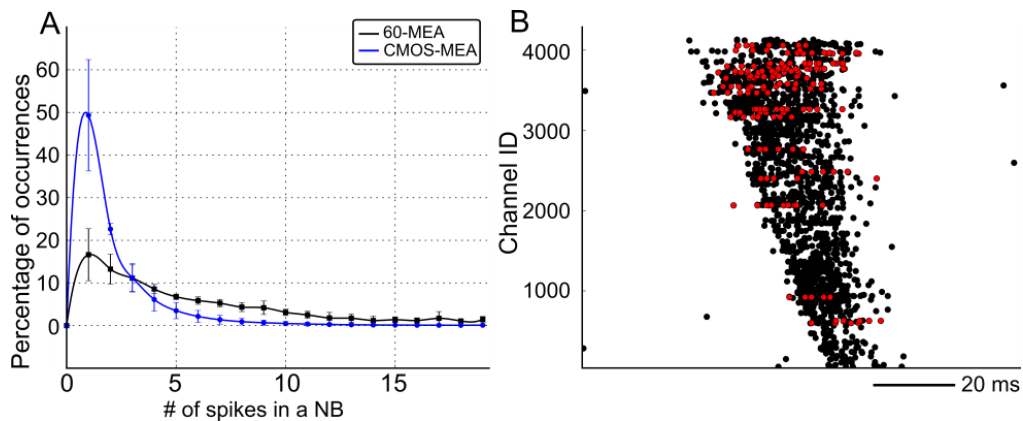


**Fig 2.4: Spike count per electrode channel composition of network bursts. (A) The occurrence of the number of recorded spikes during NBs for passive and active devices. (B) Single network burst recorded with CMOS-MEA reveal a few electrodes recording burst (red dots) while the more substantial part of electrode record less than five spikes (black dots). Note that an NB consists of the subsequent activation of neurons in time that contributes to a few spikes.**



## Discussion

Our analysis shows that NBs recorded with the CMOS-MEA are composed mainly of a few spikes (less than three). Importantly, while network bursts characterize a network phenomena consisting in the sequential activation of neurons, the MBR is a quantity defined on a single electrode basis and then averaged over the active electrodes in the recording. As the MBR is affected by electrode sensitivity, the down-sampling of the electrode grid used to decrease the spatial resolution of CMOS-MEAs resulted, as shown in another published experimental work<sup>21</sup>, in a higher variability of the MBR, which can potentially be explained by the fact that only a few electrodes are actually recording single-channel bursts.

Importantly, although single electrode channels participate to a network burst with a few spikes, the propagation of these action potentials determines an up-state of the network lasting much longer than the activation of a single electrode channel. Specifically, the subsequent temporal occurrence of a few spikes fired by neurons in different spatial locations of the network is coherent with the interpretation of NBs as a propagation of action potentials across the culture, rather than a synchronous phenomenon.

Several aspects might explain the different outputs of the two platforms. First, different sensing properties characterize the electrodes of these devices, from the dimension up to the shape. Specifically, round and planar electrodes characterize conventional passive MEA whereas the electrode in CMOS-MEA the electrodes are squared and below the plane of the chip. These different configurations influence the portion of the extracellular space sensed by the electrode. Given the result of this exploration, squared and below-plane electrodes seem to provide a more confined region of sensing than circular ones. Besides geometric considerations about the shape of the electrodes, also the reduced electrode area of CMOS-MEA ( $21\ \mu\text{m} \times 21\ \mu\text{m}$ ) in respect to the conventional MEA ( $30\ \mu\text{m}$  diameter) used can favor the sensing confinement to the dimension of a single soma. Second, the definition of a burst with the same threshold on  $\text{ISImax}$  for all electrode channels might be too restrictive<sup>22</sup>. However, the parameter exploration by varying the  $\text{ISImax}$  shows that this difference persists even for the lowest  $\text{ISImax}$ <sup>23</sup>.

## ***A biophysical computational network model of hippocampal cultures***

---

High-resolution electrical recordings provide a detailed picture of the spiking activity in entire networks of cultured neurons<sup>19</sup>. This technology can be combined with optical microscopy and biomolecular tools to acquire structural and functional information to gain insights on network development, its organization and to study responses induced by a wide range of stimuli, pharmacological manipulations or toxic insults<sup>24</sup>. However, even though the constantly increased experimental resolution of the technologies used to acquire structural and functional data in neuronal systems, a full detail description of networks at the cellular and sub-cellular scales remains inaccessible also in the case of these reduced experimental models.

As previously introduced, a possible approach to overcome current limitations to estimate experimentally hidden variables consists in combining biophysical data-driven computational network modeling with experimental research. The computational model developed in my work is based on a set of 4096 adaptive exponential integrate and fire neurons<sup>25</sup>, including both excitatory

and inhibitory neurons (see Annex I – Computational network model for an extended description). In the model, each neuron receives independent Poisson inputs that generate subthreshold fluctuations of the membrane potential and lead to asynchronous spiking activity in an uncoupled network. The three most important chemical synapses, equipped with short-term plasticity mechanism<sup>26</sup>, specifically AMPA, GABA and NMDA, mediate the interaction among neurons. The central assumption in this biophysical model regards the neuronal connectivity within the network. Consequently, as described in the next section, I first had to explore several biologically plausible models of connectivity to assess which one best fitted experimental observations obtained from networks.

### ***Testing biologically plausible models of network connectivity***

Each neuronal culture grows and forms a new network with an unpredictable connectivity among the neurons. To overcome this source of heterogeneity, several groups attempted to drive the network connectivity towards predefined patterns as grid<sup>27</sup> or compartmentalized<sup>28</sup> networks or favoring the growth of local clusters<sup>29</sup>. However, irrespective of the different conditions, cell cultures always express similar dynamics and changes in the activity along their development.

While the study of these neurodevelopmental rules giving rise to such a reproducible development of ongoing activity in neuronal networks is very intriguing, my work aimed to identify assumptions on the network connectivity useful to implement a network model of formed networks capable of reproducing the statistical properties of the spiking activity recorded in our experiments. In this regard, to assess which assumption on network connectivity can truly mimic experimental recordings, several models of network topology were challenged to reproduce the salient qualitative characteristics of the spontaneous activity of a neuronal culture, see Fig 2.1. This was an essential step in our biophysical computational model development because different network topologies lead to significant differences in the simulated network spiking activity that could also be radically different from the experimental one.

In order to define the connectivity graph of our network model, the neurons were placed on a unitary square area, corresponding to the active area of the CMOS-MEA, with a uniform spatial distribution. In Fig 2.5A, I report illustrative representations of different network topologies considered in this study. To simplify the visualization, I considered small networks of 40 neurons at fixed positions, while the connectivity was modified according to the rules defining each tested network topology. The directionality of the synaptic connections between pairs of neurons was assigned with equal probability. Although bidirectional connections are quite common in the brain, computer simulations have shown that networks with only depressing synapses (as assumed in this work) tend to evolve unidirectional connections<sup>26</sup>. For the different connectivities we considered the following theoretical network models:

***Random Graphs (RANDOM)***: the connection probability is predefined a priori. Links among all possible pairs of neurons are sampled uniformly with a predefined probability<sup>30</sup>. Consequently, the network connectivity is independent of the spatial arrangement of neurons.

**Preferential Attachment-node degree Graphs (PAnd):** an iterative procedure constructs the network: at each step, the algorithm inserts a new node into the network (i.e., a neuron) with a predefined amount of  $M$  edges (i.e., synapses). This neuron attaches preferentially to the nodes with the highest degree available in the network at that specific step<sup>31</sup>.

**Preferential Attachment-position Graph (PAP):** As in the preferential attachment model, at each step, a new node is added to the network and attached to the  $M$ -closer nodes<sup>32</sup>.

**Preferential Attachment-position-node Graph (PAndp):** In this preferential attachment graph model, the preference of link attachment is balanced equally<sup>33</sup> between the distance (PAP graphs) and node degree (PAnd).

**Gaussian Graphs (GAUSS):** the connection probability depends only on the Euclidean distance between pairs of neurons and decays as a radial Gaussian function<sup>34</sup>.

**Radius Graph (RADIUS):** each pair of neurons lying within a predefined radius of interaction connects to each other<sup>35</sup>.

The outcome of this preliminary computational study on the effects of the different tested network topologies revealed that the spontaneous spiking activity is strictly related to the organization of the network connections. These connections affect not only the propagation of the coordinated spiking activity in the network (Fig 2.5C), but also the distribution of the firing rates in the network (Fig 2.5B).

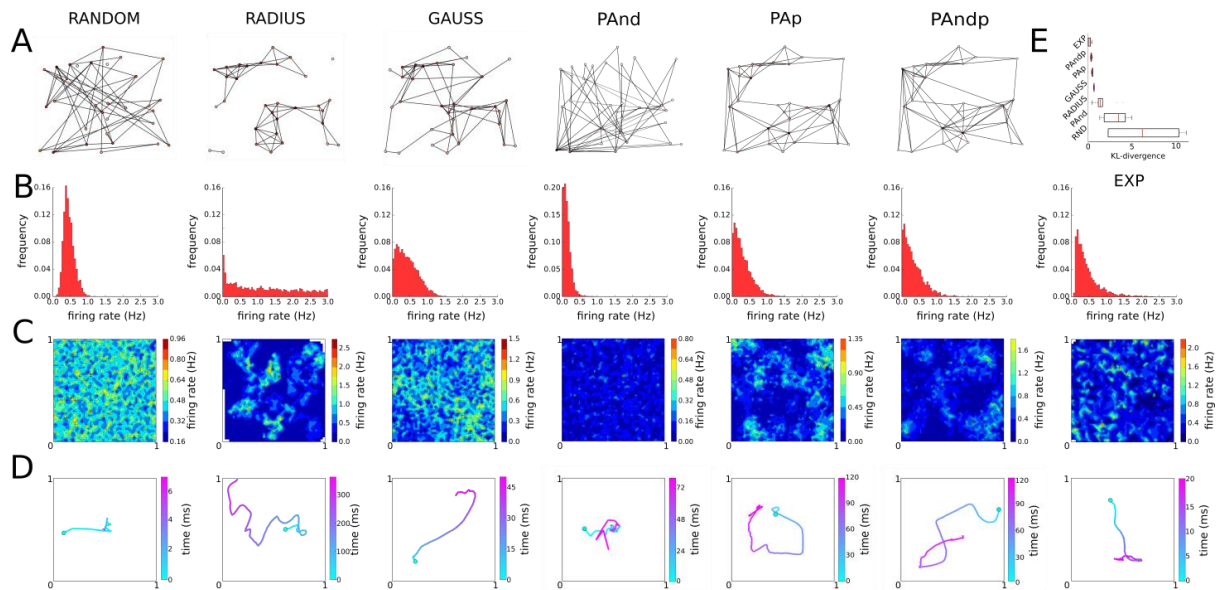


**Fig 2.5: Network activities for different topologies compared to experimental recordings (EXP).** (A) Different network models induce different topologies over the same arrangement of neurons in a unit square as indicated by the small representative networks (40 neurons). (B) Firing rate distributions, (C) spatial distribution of the firing rates and (D) representative CATs. In the random graph, the activity spreads homogeneously and quickly across the whole network (first column). In the radius graph, the CAT propagates slowly across the network compared to the experimental data (bottom column). Finally, in the Gauss graph (third column) the CAT compares well with the corresponding experimental ones. The better matching of the CATs is also reflected in the firing rate distributions when compared to experimental ones (E).

In particular, **RANDOM** networks elicit short-ending network burst (NB) with no clear spatial propagation of spiking activity since their topology does not take into account the position of the neurons in the network. This observation derives from the fact that the center activity trajectory (CAT) of each NB rapidly converges to the center of the network. Moreover, the firing rate distribution of these networks has a binomial shape profile and is spatially uniform. A similar argument holds for the trajectories of NBs elicited by **PAnd** network models. Indeed, in **PAnd** the CATs converge also rapidly to the center of the network since, similarly to the random graphs, the connectivity disregards the spatial arrangement of the neurons. Consequently, to simulate natural-like propagations, the connectivity should depend on the distance among neurons. Position-based PA networks (**PAP** and **PAndp**), indeed, can express propagations of spiking activities in our simulations. However, the presence of active hub neurons characterizing these models induces too many turning points in the propagation (suggesting a hub by hub propagation of spiking activity) that differ from experimentally observed propagations. Additionally, the distribution of the simulated firing rate at these “turning” locations exhibits bumps of high firing activity in only a few spatially segregated regions of the network while a significant fraction of the neurons remains silent (dark blue regions) and, thus, do not participate to NBs. Conversely, **RADIUS** networks give rise to prolonged propagations of spiking activity due to the lack of shortcutting connections. According to the network architecture, the spatial distribution of the firing rate density in regions where neurons are more connected due to spatial density inhomogeneities of synaptic contacts while, regardless of the spatial position, the firing rate distribution has a flat profile.

The network burst propagation and the spatial firing rate maps (Fig 2.5B-C) induced by **GAUSS** graphs, instead, exhibited a good match with the experimental data (Fig 2.5, last column), albeit position based PA networks approximate slightly better the experimental firing rate distribution than Gaussian graphs, as quantified by the Kullback-Leibler divergence, see Fig 2.5E ( $0.62 \pm 0.12$  vs.  $0.84 \pm 0.23$  respectively). Beyond these qualitative assessments, **GAUSS** graphs can also quantitative reproduce the time scales of NBs and the firing rate distributions observed in our experimental data, as reported in the next section.

## Discussion

The comparative analysis of the performance of different theoretical network models indicated that position-based graphs mimicked the spontaneous spiking activity significantly better than networks whose connectivity was unrelated to the spatial arrangement of the neurons. However, by restricting the field of interest to position-based graphs, the lack of long-range connections in radius graphs determined slower spatial propagations ( $\approx 38$  mm/s) of spiking activity than the ones observed in experimental recordings ( $\approx 146$  mm/s) and, consequently, gave rise to longer duration of NBs (Mean Bursting Duration of  $572.32 \pm 32.76$  ms vs.  $126.27 \pm 45.84$  ms).

Instead, both preferential attachment position based models and Gaussian graphs provided the best match to the experimental data. However, while these preferential attachment models imposed an hub-like structure, Gaussian graphs replicated experimental observations without the implicit need for a hub architecture. In this regard, previously published works<sup>36,37</sup> already reported a major network connectivity contribution in favoring the emergence of network

synchronizations. Specifically, the features characterizing small-world<sup>38</sup> and scale-free<sup>31</sup> network models could provide a posteriori functional explanation for the spontaneous synchronization of spiking activity<sup>39</sup> and several computational works set the network connectivity based on these assumptions<sup>40</sup>. However, as suggested in<sup>41,42</sup> the small-world properties are inherited by the fact that neuronal connectivity depends on the distance between neurons rather than imposed as a priori model<sup>40,43,44</sup>.

Furthermore, experimental data obtained with optical microscopy and immunostaining on low-density neuronal cultures suggest that neuronal connectivity in formed networks depends on the reciprocal distance among neurons<sup>45</sup>. On the other hand, to keep a minimal network connectivity model, complex approaches as growing networks<sup>46</sup> or detailed neuronal arborisation<sup>47</sup>, although tempting, were not taken into consideration due to their intrinsic computational complexity.

Therefore, network models with Gauss graph connectivity provide the best compromise to reproduce our experimental observations and were used to develop our computational model.

### ***Assessment of simulated versus experimentally recorded spiking activity***

In the previous section, I have shown that network models with Gauss graph connectivity provide the best compromise to reproduce qualitatively the experimental observations. Here, I further investigated the statistics of the spiking activity expressed by this computational network model and compared the outcomes of the analysis with our experimental recordings. Indeed, for experimental recordings in neuronal cultures, the spike-sorting analysis performed in our laboratory has shown that we can consider that the majority of each electrode records spike trains from a single unit.

The visual inspection of simulated raster plots reveals a similar network-wide spiking activity (Fig 2.1B vs. Fig 2.6A) and a comparable timescale of NBs propagations ( $72 \pm 28$  ms, Fig 2.6B) to the experimental data ( $65 \pm 33$  ms, Fig 2.1C). Interestingly, the results show that in the simulations, as in the experiments, each class of NB consists of a sequential activation of neurons depending on their spatial position, see Fig 2.6B, with a propagation speed estimated in  $\approx 146$  mm/s and  $\approx 128$  mm/s for experimentally recorded and simulated NBs respectively.

Moreover, CATs computed on simulated data display smooth trajectories similar to the experimental ones<sup>19</sup> (Fig 2.1D vs. Fig 2.6C), and, notably, the classification of these spatiotemporal patterns (Fig 2.6D-E) reveals only a few clusters of trajectories (Fig 2.6F), with no evident periodic sequence, as depicted in Fig 2.6D. As shown previously, the same analysis performed on experimental data revealed the presence of a few clusters of trajectories, see Fig 2.1F-G. Additionally, the quantitative comparison between experimentally ( $n=15$ ) and simulated ( $n=20$ ) network statistics, i.e., mean firing rate (MFR,  $0.51 \pm 0.34$  vs.  $0.42 \pm 0.28$  Hz, respectively, **p-value 0.27**), mean bursting rate (MBR,  $2.03 \pm 1.29$  vs.  $1.89 \pm 0.93$  burst/min, respectively, **p-value 0.97**), mean firing intra-burst (MFIB,  $122.53 \pm 35.84$  vs.  $106.89 \pm 51.93$  Hz, respectively, **p-value 0.35**) and mean burst duration (MBD,  $126.27 \pm 45.84$  vs.  $112.42 \pm 32.93$  ms, respectively, **p-value 0.95**) further confirms these qualitative observations, see Fig 2.6G. Importantly, different simulations obtained by little perturbations of the cellular properties (i.e., the parameters defining the behavior of the

simulated neurons) and different anatomical networks based on the Gauss graph lead to variability in the network descriptors similar to the one resulting from different experimental recordings. All in all, the simulated spike trains recapitulate most of the salient properties of hippocampal cultures observed in our recordings and already reported in some previous studies<sup>1,48,49</sup>.

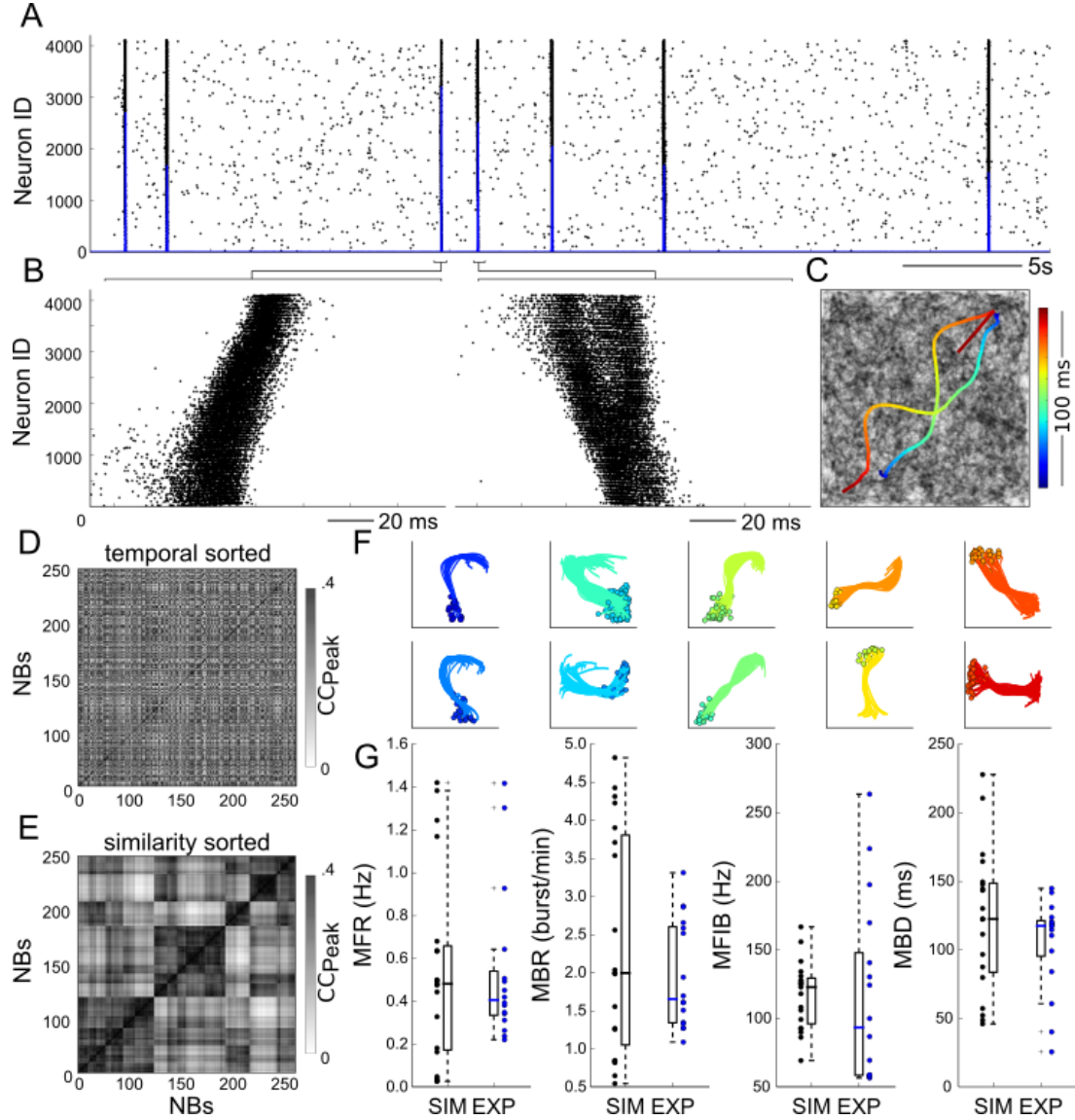


**Fig 2.6: Spontaneous spiking activity of simulated and experimental neuronal culture networks.** (A) Raster plot of the simulated spontaneous spiking activity showing sporadic NBs interleaved by sparse spiking as occurs in experimental recordings Fig 2.1B. (B) Magnification on the first two simulated NBs in A reveals specific spatio-temporal patterns of neuronal activation, c.f. Fig 2.1C. By applying the same tools of analysis designed for experimental recordings, the cross-correlation matrix of simulated NBs (D) reveals similar a-periodic sequences of similar trajectories (c.f. Fig 2.1E,F). The classification of CATs (F) according to the reordered cross-correlation matrix (E) indicate the presence of common ignition sites (circles) of propagation and preferential pathways of propagation through the network. (G) Mean quantitative statistics, i.e., firing rate (MFR), bursting rate (MBR), firing intraburst (MFIB) and burst duration (MBD), recapitulate the value and the variability of the experimental ones (n=15 experimental recordings, n=20 simulations, p-values 0.27, 0.97, 0.35, and 0.95, respectively).

## ***Manipulation of synaptic transmission: model validation and effects on network dynamics***

---

Although I have shown that the computational network model can generate synthetic network-wide spiking activity with properties that are both qualitatively and quantitatively comparable to neuronal culture recordings, we further validated its responses to pharmacological manipulations that are known to alter the network firing regime. Hence, to explore the capability of reproducing different network spiking regimes, the network model was challenged to mimic the firing activity of neuronal cultures subjected to pharmacological manipulations of the three synaptic receptors endowed in the model, namely AMPA, GABA, and NMDA.

The contribution of AMPA, GABA, and NMDA to the network spontaneous activity was explored through simulations and by cross-validating our simulated data with experimental recordings that were either acquired in our laboratory or that were reported in the literature.

### ***AMPA***

Previous computational modeling works<sup>44,50</sup> on networks endowed with AMPA and GABA synapses (or AG-networks) reported that AMPA and GABA conductances are sufficient to reproduce the essential features of the spontaneous spiking activity expressed by neuronal cultures. This includes the sporadic initiation of NBs. As previously shown, our network model, that includes both AMPA and GABA synapses, also reproduces these dynamics.

Importantly, experimental works<sup>51,52</sup> indicated that a decrease in AMPA efficacy upon pharmacological treatments with CNQX (a selective blocker of AMPA receptors), induced a diminished network bursting activity and eventually the complete silencing of the bursting activity. Here, to elucidate the effects of the AMPA conductance on the generation of NBs, a similar experiment was performed *in silico*. To do so, the magnitude of the AMPA conductance was linearly decreased, and changes in the spiking activity were evaluated by computing the firing rate and the percentage of random spikes, i.e., those spikes not belonging to a burst. To ensure a fair comparison among networks with different AMPA conductances, GABA inhibition in these simulations was unaltered. The simulations revealed that reducing the AMPA excitations pairs with a diminished spiking activity of the network, see Fig 2.7A. Specifically, we found that a reduction higher than 25% decreased the mean firing rate of the network from  $0.92 \pm 0.23$  Hz to  $0.12 \pm 0.06$  Hz and prevented the network from exhibiting NBs (Fig 2.7B, black dashed lines,  $n=10$ ). Indeed, for more significant reductions of the AMPA conductance, the percentage of random spikes approached  $94.45 \pm 5.34$  %, i.e., the totality of the spikes expressed by the network (Fig 2.7B, red dashed lines,  $n=10$ ). The inclusion of NMDA excitatory conductance in the model (or AGN-network, Fig 2.7B, black lines,  $n=10$ ) was found not to alter the overall qualitative trends observed by changing the AMPA conductance in AG-networks. However, we concluded that under low-AMPA conditions (<20% respect to basal condition), the addition of NMDA currents could partially compensate for the reduction in AMPA excitation (Fig 2.7A, B, solid lines). Indeed, for a 30% decrease in AMPA conductance, the spiking activity of the AGN-networks became very sparse, with rare single-channel burst  $4.45 \pm 1.43$ % and interspike intervals (ISIs) of several seconds, on

average  $7.23 \pm 1.23$  s (Fig 2.7C, red distribution). Conversely, in AGN-networks under control condition (i.e., 0% decrease in AMPA conductance), the ISI distribution (Fig 2.7C, blue line) showed both short ( $<100$  ms) and long ( $>500$  ms) ISIs, thus indicating the presence of NBs interleaved with periods of asynchronous spikes. Importantly, the shift from uncoordinated to coordinated firing regimes in neuronal networks requires homeostatic changes in AMPA conductances<sup>53</sup> that are comparable to the one identified through our simulations.

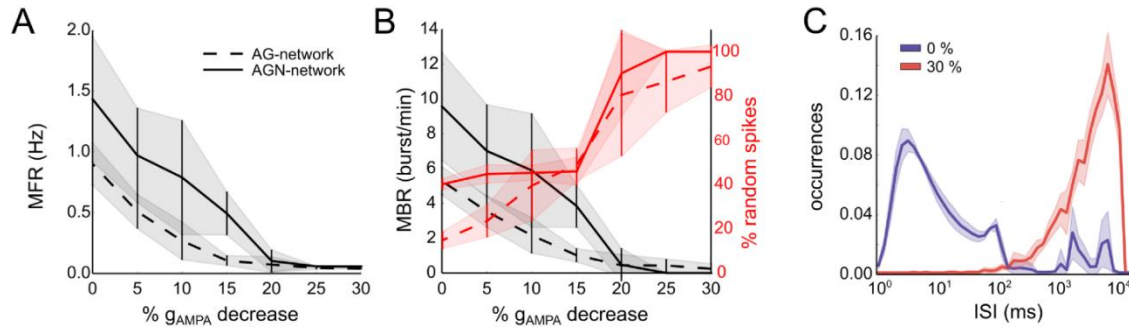


**Fig 2.7: A computational exploration of AMPA synaptic transmission in modulating the spiking activity of neuronal cultures.** (A) Mean firing rate (MFR) for decreasing values of AMPA conductances in networks endowed with AMPA and GABA conductances only (solid line, AG-networks), and with the additional contribution of NMDA conductance (dashed lines, AGN-networks). (B) A decreased efficacy of AMPA synapses determines a diminished mean bursting rate (MBR) together with an increased percentage of random spikes. (C) The ISI distribution in a low AMPA conductance scenario exhibits a single peak centered on intervals lasting several hundreds of milliseconds, while in control condition the envelope of the ISI distribution reduction displays an additional peak centered on a few millisecond timescale. The missing peak indicates that single neuron bursts do not occur along the simulation and consequently neither network bursts.

## GABA

Our recordings<sup>8</sup> and other reported experimental works<sup>54,55</sup> show that the blockage of inhibitory transmission mediated by GABA unalters network bursting regime in neuronal cultures, but rather modulates the dynamic. We have verified this condition in our computational network model by setting the conductance of all inhibitory connections to zero, (GABA-OFF,  $n=5$ ). The lack of the regulatory function of inhibition causes epileptic-like spiking activities characterized by more frequent ( $+88 \pm 5\%$  increase of MBR), densely packed, ( $+56 \pm 4\%$  increase of MFIB) and fast propagating NB ( $-29 \pm 4\%$  decrease of MBD) compared to control condition when the GABA conductances are active, see Fig 2.8A. Moreover, upon blockage of inhibition, single neurons participate in an NB with a consistently higher number of spikes ( $8.23 \pm 1.78$  spikes, Fig 2.8A, inset) than observed under control conditions ( $3.97 \pm 1.03$  spikes, GABA-ON). The predictions of the model agree with experimental observations ( $+110 \pm 9\%$  increase of MBR,  $+50 \pm 1\%$  increase of MFIB,  $-18 \pm 2\%$  decrease of MBD) obtained with pharmacological manipulations of the cultures (under  $30 \mu M$  Bicuculline, a competitive antagonist of  $GABA_A$  receptors), thus confirming the reliability of the model, see Fig 2.8B. Note, though, that our computational exploration exhibited a much richer dynamic than previously observed<sup>56</sup>. Indeed, an analysis of the NB clusters (based on



their trajectories) in the GABA-ON/OFF conditions, revealed that by blocking GABA we could distinguish NB clusters with trajectories that appeared predominantly in control condition, in the GABA-OFF condition or that were insensitive to the removal of inhibition and consequently appeared along all the simulated experiment, see Fig 2.8B-C. Finally, it is also possible to note that upon blockage of inhibition, the trajectories within a given cluster exhibited a reduction of  $\approx 20\%$  in the mean path variance and less convoluted pathways, as a consequence of the higher intraburst firing rate and of the shorter NB duration that contributes to better define the NB trajectory, see Fig 2.8D. Importantly, the appearance of new ignition sites and a new cluster of trajectories under the GABA-OFF condition is also consistent with previous experimental investigations<sup>56</sup>.

By exploiting the model, we could investigate the underlying mechanisms of these variations in the network dynamics. Indeed, the model under GABA-OFF condition indicates that an increased and almost simultaneous excitation due to the lack of an inhibitory counterpart determines a higher integration of synaptic inputs and an increased neuronal firing during NBs. As consequence of the increased firing, both neurons, and synapses are more strongly depressed during an NB, thus shortening the time-window in which the membrane potential is sufficiently depolarized to induce firing.

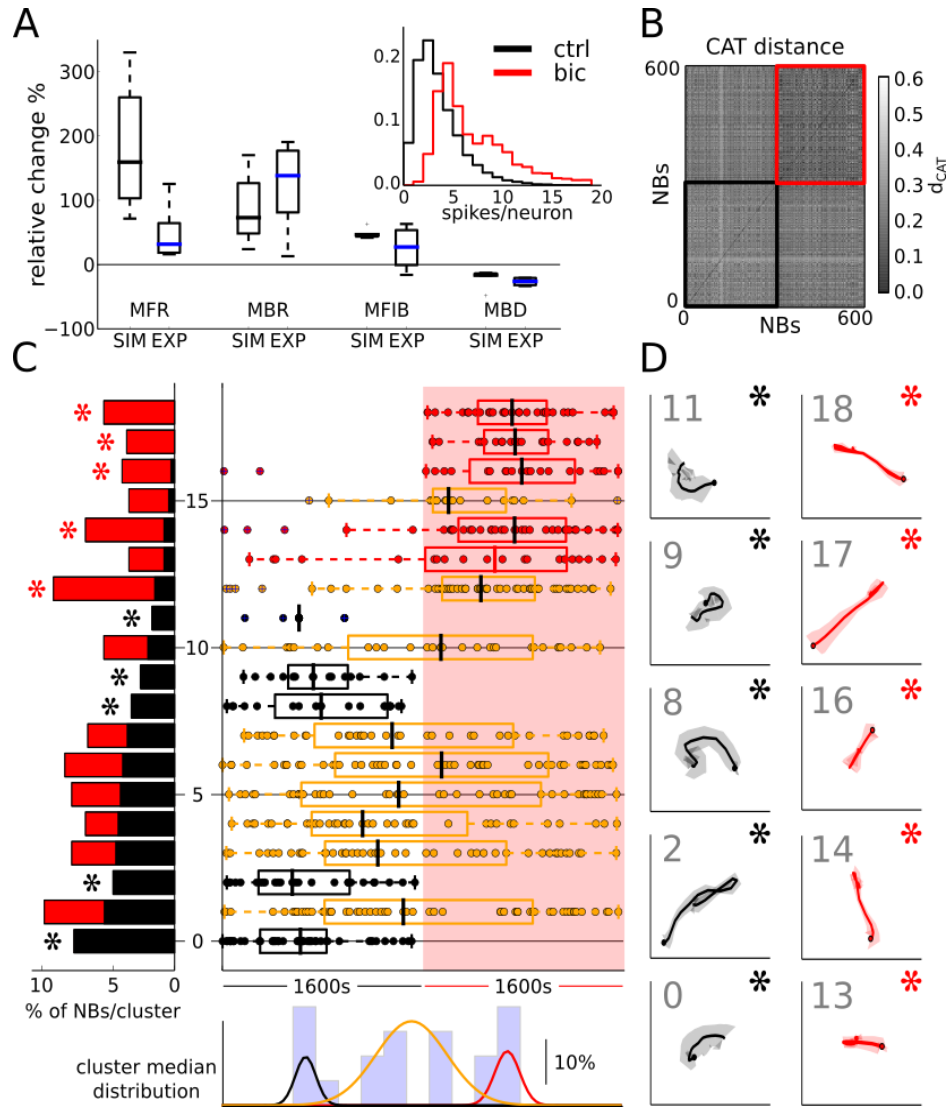


**Fig 2.8: The role of GABA inhibition on network bursting dynamic and propagation.** Inhibition-ON (black, control) and inhibition-OFF (red, blockade of inhibition  $g_{\text{GABA}} = 0$ ). (A) The model predicts the changes in spiking statistics observed in experiments (P-values: 0.052, 0.473, 0.189, 0.449, t-test independent,  $n=4$  experimental recordings,  $n=5$  simulations). By blocking the inhibition, the spike count per neuron during NBs displays a shift toward higher values (inset). (B) The matrix of CATs does not show abrupt changes across the GABA-ON (black square) and GABA-OFF condition. (C) Clustering analysis of the CATs in GABA-ON/OFF phases. Most of the CAT clusters are populated by NBs of the two phases while some clusters are representative of the GABA-ON phase (e.g., cluster IDs 0, 2) and others of the GABA-OFF phase (e.g., cluster IDs 16, 17). The Gaussian curves are determined by fitting Gaussian Mixture Models and minimizing the Akaike criterion. (D) The CATs clusters that appear exclusively during the GABA-ON or GABA-OFF phase (mean: thick line; standard deviation: shaded area). In GABA-OFF condition, the trajectories are more regular (mostly straight lines) and stereotyped (lower variance).

## NMDA

Finally, we investigated also the effects induced by modifying NMDA synaptic currents in mediating the entire network spiking activity of our computational model. As shown in this section, the addition of NMDA receptors in the model supports long-lasting depolarizations of the membrane potentials that can eventually lead to sequences of NBs separated by a few hundreds of milliseconds, also referred as superbursts, see Fig 2.9A. This latter evidence was also supported by experimental data that showed a significant increase of single NBs from  $\approx 8\%$  to  $\approx 80\%$  upon APV (a NMDA antagonist) administration, i.e., a disappearance of superbursts (Fig 2.9A, middle and bottom panel).

The characteristic longer time-scale of the NMDA excitation<sup>57</sup> respect to other dynamics taking place in the modeled synapses and neurons suggests it could be a good candidate to trigger a chain of sequences of NBs named superburst<sup>1</sup>. This consideration is confirmed by a few observations. First, in previous investigations, the time interval separating two NBs in a superburst, lasting a couple of hundreds of milliseconds, was found comparable to the additional excitation provided by the integration of NMDA currents. Second, the contribution of the NMDA current depends on the relative value of the magnesium block potential ( $V_{Mg}$ ) respect to membrane potential ( $V_m$ ) of the impinged neuron. Whenever  $V_m < V_{Mg}$ , the contribution of the NMDA current is negligible (shunted), and it becomes quite relevant once  $V_m > V_{Mg}$ . Consequently, these observations indicate that a proper balance between the adaptation of the membrane potential and the activation of NMDA currents can faithfully trigger a sequence of NBs, right after the end of another one.

In our simulations, incorporating the NMDA synapses (AGN-network), the model replicated qualitatively (i.e., respect to experiments) the suberbusting patterns without any parameter adjustment, see Fig 2.9B. Specifically, we found that the additional excitation provided by NMDA currents provide the driving force to trigger chains of consecutive NBs and the magnesium block ensures the closure of the chain of NBs once the spike-triggered adaptation current overcomes the contribution of synaptic currents.

Similar to experimental recordings, in our simulations, the blockade of the NMDA (mimicking APV application) causes the disappearance of superburst, i.e., sequences of NBs separated by less than  $\approx 500$  ms as quantified in Fig 2.9C. The disruption of the suberbusting regime is also highlighted by the disappearance of the peak (solid arrow) at 200 ms (left) and 1000 ms (right) in the ISI distribution and in the difference of ISI distribution, see Fig 2.9D. The mentioned peaks, indeed, represents the firing between consecutive NBs in the superbursts and between superburst, respectively. It is important to note that the excitatory drive of NMDA receptors can also work synergically with other mechanisms that include, but are not limited to, the asynchronous release of neurotransmitters<sup>58</sup>, actively facilitating synapses<sup>59</sup> but also reverberating spiking activities on the boundary of the cultured neuronal network<sup>60</sup>. Thus, there could be other potential mechanisms contributing to the sustainment of the superburst regime, but our work suggests that the NMDA conductance is fundamental to sustain the latter firing regime.

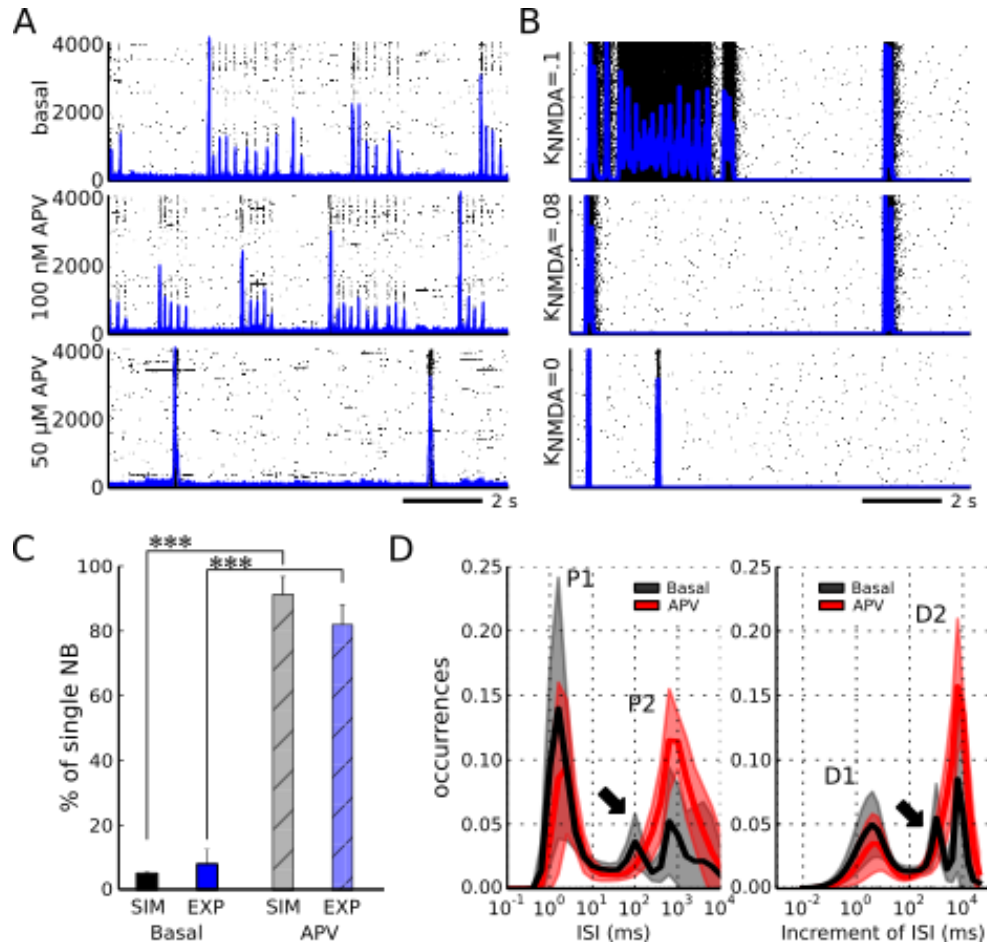


**Fig 2.9: The NMDA receptor is involved in the generation of superbusts.** (A) Consecutive NBs are clearly visible in some experiments (blue line is the spike count over 10 ms time windows) and disappear gradually as the concentration of AP5 (a NMDA receptor blocker) provided to the culture increases (bottom panel). (B) By varying the efficacy of NMDA receptors ( $K_{NMDA}$ ) the model mimics the different concentrations of APV (i.e., the raster plots of the simulations are in good matching with experiments). (C) In a NMDA-free condition (under APV), the network is characterized by single NBs both in experiments (n=3) and AG-networks (n=10). (D) The firing pattern of the superbust regime (black distribution, n=10 simulations) is characterized by three peaks in the ISI and dISI distributions.

### Other mechanism of neuronal interaction

In addition to chemical synaptic signal transduction, gap-junctions can also potentially mediate the initiation and the propagation of spiking activity within a neuronal network<sup>61</sup>, as it occurs in the proliferative ventricular zone of a developing neocortex<sup>9</sup>. However, neuron gap-junction hippocampal neuronal play a minor role in modulating the spiking activity at mature stage<sup>62</sup> and further evidence also suggest that neuron to astrocytes intracellular communication is not essential for eliciting spontaneous network bursts<sup>63</sup>. These results were of particular interest in the design phase of the network model because they allowed reducing the elements to simulate.

### *Extrasynaptic signaling*

Alternative mechanisms that might impact on the network spiking activity regard the activation of extrasynaptic receptors. For instance, previous works observed neuroprotective benefits induced by the activation of extrasynaptic NMDA receptors upon administration of low concentrations of NMDA (less than 200 nM)<sup>64,65</sup>. Despite the pros of the network model reported so far and the interesting topic of investigation, the notion of the extrasynaptic receptor is somehow undefined in point process neurons that lack any spatially extensive dendritic arborization. At the current stage, testing this type of hypothesis is far beyond the capability of the network model, and it consequently represents a limitation of this work. However, a first exploration about the effect of extrasynaptic NMDA receptors can faithfully be implemented by including a phenomenological model of the currents regulated by extrasynaptic NMDA receptors and by scaling the strength of synaptic input to compensate for the lack of compartments.

### *Dendritic computation*

Cumulating evidence<sup>66</sup> shows that neuronal computation benefits of dendritic processing of incoming inputs. The dendritic computation is not solely limited to the spatiotemporal integration of distinct afferents<sup>67</sup>, but it also includes the cross-talk among adjacent synapses<sup>68,69</sup>, thus increasing the potential non-linear interactions between different inputs in a neuron. The dendritic computation could outperform the processing capability of single cells and represent an appealing subject of investigation. Hence, a future direction we envisage is to upgrade the current implementation of the network model to spatially extended interacting neurons.

### *Summary*

The computational investigation of the effects of three major synaptic players included in our model (AMPA, GABA, NMDA) to the spiking activity and dynamics expressed in neuronal networks revealed that while AMPA receptors are required for the spontaneous expression of NBs, NMDA and GABA mainly regulate the dynamics of the network bursting regime. Specifically, in line with experimental results and previous modeling works, the blockage of inhibition through GABA modulates NBs, but without disrupting their initiation. Indeed, we observed that inhibition regulates the duration, the strength, the occurrence of NBs (i.e., the frequency) and the stability of the NBs propagation paths. On the other hand, NMDA can support the insurgence of a superbursting regime by providing an excitation lasting hundreds of milliseconds that prevents single neuronal hyperpolarization at the end of each NBs. Finally, this part of my work allowed also to support the value of the implemented model further and to develop knowledge on possible mechanisms that might affect experimentally observed changes in the network spiking activity and dynamics. The presented network model might be directly applicable to the interpretation of experimental recordings of spontaneous activity changes induced by neuroactive compounds or may provide complementary information on the integration at the cellular scale of electrical<sup>70</sup> or optogenetic<sup>71</sup> external stimuli.

## ***Investigating determinants underlying the spontaneous emergence of network bursts***

---

In this section, following the validation of the computational network model, I report results obtained by exploiting this model to unveil the potential mechanisms underlying the ignition of spontaneous NBs in *in vitro* neuronal networks.

Previous published works suggested different potential sources for NB ignition, including local network effect induced by single neuronal excitability or intrinsic neuronal properties as intrinsic periodic bursting<sup>72</sup> of pacemaker neurons<sup>46</sup>, hub-like network structures in which hub-neurons regulate and coordinate the activity of the entire network<sup>73,74</sup>, and assemblies of neurons in which spatially localized sets of neurons initiate the NBs as a consequence of their internal wiring structure<sup>75,76</sup>. My study considered different and potential sources of the spontaneous ignition of NBs that were investigated through simulations. In particular, we investigated a set of potential mechanisms generating NBs. In particular, we considered:

- (I) The intrinsic excitability of individual excitatory neurons
- (II) Border or finite size effects of the network
- (III) The local network interactions established by neurons

In the following, we will provide a step-by-step analysis of these factors, and we will show that although they can contribute to the generation of NBs, they cannot fully explain the emergent network activities.

### ***Intrinsic neuronal excitability***

A first hypothesis is that NBs might be initiated in areas characterized by a higher concentration of more excitable neurons than the rest of the network. To dissect a potential role of this intrinsic excitability I modified the spatial distribution of more excitable neurons in our simulated networks while maintaining unaltered the rest of the network parameters. I quantified the heterogeneity of neuronal excitability in the simulated networks by quantifying the single-neurons input resistances ( $R_{in}$ ), i.e., the expected membrane potential depolarization from the resting state of the neuron as a consequence of the injection of a current step, according to Ohm's first law, see Fig 2.10A-B. The input resistances of all neurons in the network were computed and a control simulation provided the ground truth of trajectories elicited by the control network, see Fig 2.10C. Next, in order to test the possibility that the excitable neurons could determine spontaneous NBs, we populated one area of the network with the excitatory neurons having the highest  $R_{in}$  and placing those with the lower input resistance outside of the area. This operation occurs by exchanging the parameters of the neuronal models in a one to one correspondence, see Fig 2.10D.

Consequently, the overall distribution of excitability, i.e.,  $R_{in}$ , was preserved, conversely the spatial distribution of excitability exhibited peaks in the targeted area instead of a uniform profile. With this setting, a replication of the control simulation by applying the same initial condition, and background noise provided a fair comparison of the spiking activity. Thus, a comparison of the CATs, associated with NBs, between the two simulations allowed to inspect whether a new cluster

of trajectories could originate from the high excitability area by leaving (almost) unaltered the rest of the network. Simulation results show that, while maintaining unaltered the network connectivity in the different configurations, the additional spatial clustering of excitable neurons gives rise to a different spatial distribution of the spiking activity in the simulated networks. Specifically, bumps of higher firing rate were visible by computing 2D-spatial histograms of the network firing rate, thus indicating a potential contribution of the localization of more excitable neurons in initiating NBs. However, only a few (2 out of 86) new trajectories were elicited by altering the neuronal excitability in the network.

This test leaves open the possibility that either the changes in excitability included in the model was not sufficient to induce new NBs, or the number of replaced neurons was too small. However, to have a relevant impact on the number of trajectories (10%) consider that we had to move at least 25% neurons (not shown).

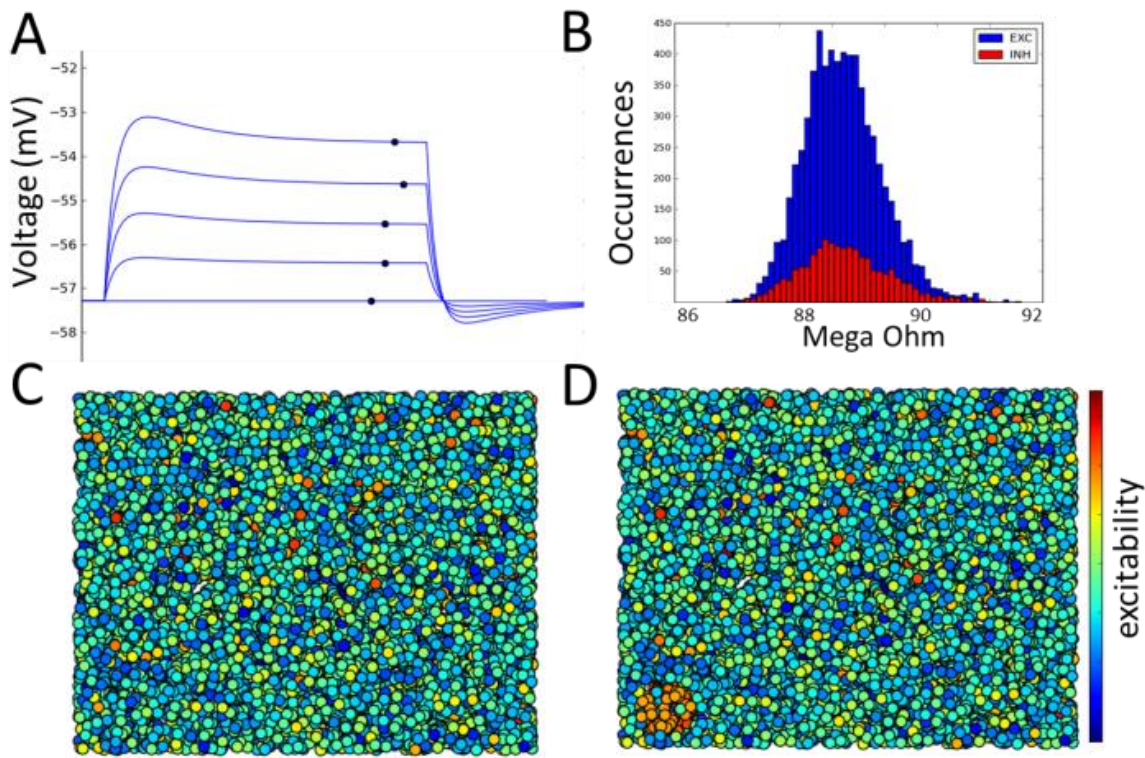


**Fig 2.10: Assessing the role of intrinsic heterogeneity in simulated neuronal networks.** (A) The input resistance is quantified by fitting the steady depolarizations reached (black dot) respect to the injected currents. (B) Input resistance distribution for excitatory and inhibitory neurons. (C) Control network, in which the excitability is uniformly distributed in the network. (D) New configuration of the network in which the most excitable excitatory neurons were spatially clustered in the corner of the network while preserving the properties of all the other neurons.

### ***Border or finite size effects of the network***

To understand to what extent the finite-size effect influences the propagation of activities in the network, we performed simulations with a virtually infinite topology by embedding the network on a torus obtained by setting periodic boundary conditions among the up/down and



left/right borders of the network, see Fig 2.11A. In this setting, a neuron lying close to the left/right border can connect to a neuron lying close to the right/left border (Fig 2.11A, red line). Similarly, a neuron placed at the bottom/top can connect to a neuron lying close to the top/bottom border of the network. With this setting, the model displayed similar dynamics to the one observed in the standard network model on the unit square with borders (spontaneous propagations characterized by few ignition sites). Similarly to the conventional 2D network, we could also perform a cluster analysis on the CATs of the propagating events, see Fig 2.11B. As shown in Fig 2.11C these events propagated on the entire torus indicating that these activities leave and re-enter the unit-square network multiple times, see Fig 2.11D. Noticeably, these events last a bit longer than in the 2D network, but they systematically ended after a few hundreds of milliseconds. Therefore, these results indicate that the finite size of our networks seem not altering the initiation of NBs observed in our experiments and simulations with 2D networks.

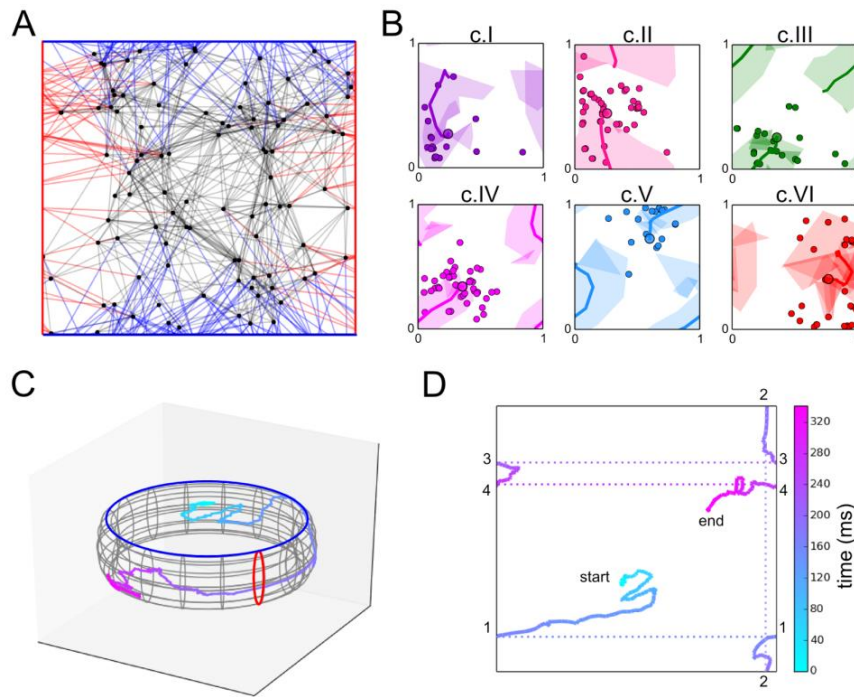


**Fig 2.11: Spontaneous network bursts emerge in infinite-like networks.** (A) An illustrative toroidal network constructed by introducing periodic boundary conditions to a 2D network. The neurons placed close to the matching borders (red-red, blue-blue) connect according to the same rule used for the standard 2D network. The links crossing the borders are in blue (top-bottom) and red (left-right). (B) Different clusters of network bursts depicted on a unit square area (dots = initiation sites, solid lines = average trajectory, shaded area = standard deviation). (C) An exemplary trajectory of cluster c.IV (see panel B) is depicted on the torus and (D) on the unit square for illustrative purposes.

### ***Functional connectivity reveals the localization of the NBs ignition sites***

The analysis of the functional links, i.e., relations among neurons that exhibit similar spiking activity across the entire experimental ( $n=15$ ) and simulated ( $n=20$ ) dataset, revealed considerable inhomogeneities in their spatial distribution. The functional graph obtained by retaining the most significant functional links according to the method described in Annex I – Detection of ignition sites, showed a confinement of its links within four to thirteen well-segregated regions of the



network. In those regions (black delimited areas in Fig 2.12A-B), the density of links per unit square exceeded more than three folds the average level of the network ( $5.12 \pm 1.44$  vs.  $0.89 \pm 0.53$  functional links per neuron respectively, averaging over both simulations and experiments). Consequently, we investigated the possible relation between these regions of high density of functional links and the network areas initiating NBs obtained by the CAT analysis or Ignition Sites (ISs).

Specifically, the application of a post-processing filter to highlight segregated components within the functional graph (see Annex I – Detection of ignition sites for further details) of our simulated network revealed a few (<10) clusters of neurons in distinct and spatially localized regions of the network, here referred as fCOMs. By construction, the neurons in the different fCOMs share similar firing patterns along the entire recordings (cross-correlation peak  $0.52 \pm 0.06$  for simulated networks and  $0.19 \pm 0.04$  for recordings) with the exception of a time shift in the order of a few milliseconds (less than 1ms, i.e., neurons belonging to an fCOM fire almost synchronously). A possible explanation for such a tight coordinated spiking activities among pairs of neurons could be the presence of direct structural connections among them. However, in all simulated networks (n=20) the overlap between the functional links and the underlying anatomical connections structural connectivity was below 4.9%, thus excluding the presence of direct structural connections.

These properties of the functional graph were also verified in experimentally recorded neuronal networks. Interestingly, this allowed to reveal a similar organization of the functional graphs as obtained from simulated networks also in our high-resolution experimental recordings, see Fig 2.12B. Notably, as quantified in Fig 2.12C-D, the superimposition of the fCOMs regions with the NBs initiation sites, determined from the CAT analysis, revealed their co-localization ( $96 \pm 4\%$  and  $84 \pm 7\%$  for simulation and experiments respectively). Yet, the fCOMs covered a marginal area of the entire network, i.e.,  $18 \pm 6\%$  and  $36 \pm 9\%$  for experimental recordings and simulations respectively, see Fig 2.12E.

Interestingly, a first outcome of this result is the possibility to take advantage from the analysis of functional connectivity to design a new algorithm for detecting NB ignition sites, both in experimental and synthetic data. The advantage compared to the CAT analysis is to enable determining with the required accuracy the set of neurons that are involved in NBs initiation. We thus evaluated the detection accuracy of the ignition sites based on the functional connectivity analysis by using a bootstrapping approach (see Annex I – Detection of ignition sites for the description). This showed a significant co-localization between fCOMs and CAT origins in both simulated data (18 out of 20 simulations) and experimental recordings (10 out of 15 experimental recordings). We also noticed that this analysis sometimes detected more fCOMs than clusters of trajectories and thus NB ignition sites. For instance, in the exemplary case reported in Fig 2.12B (bottom-right), the fCOMs did not give rise to any NB propagation. However, on the other hand, all the detected NB trajectories (and thus classes) could be associated to a specific fCOM. Consequently, the fCOM analysis proposed here provides an upper bound for the detection of the NB ignition sites. Importantly, this is obtained just by analyzing the overall spiking activity expressed by the network, or in other words, without any prior knowledge of the spatio-temporal patterns of NBs.

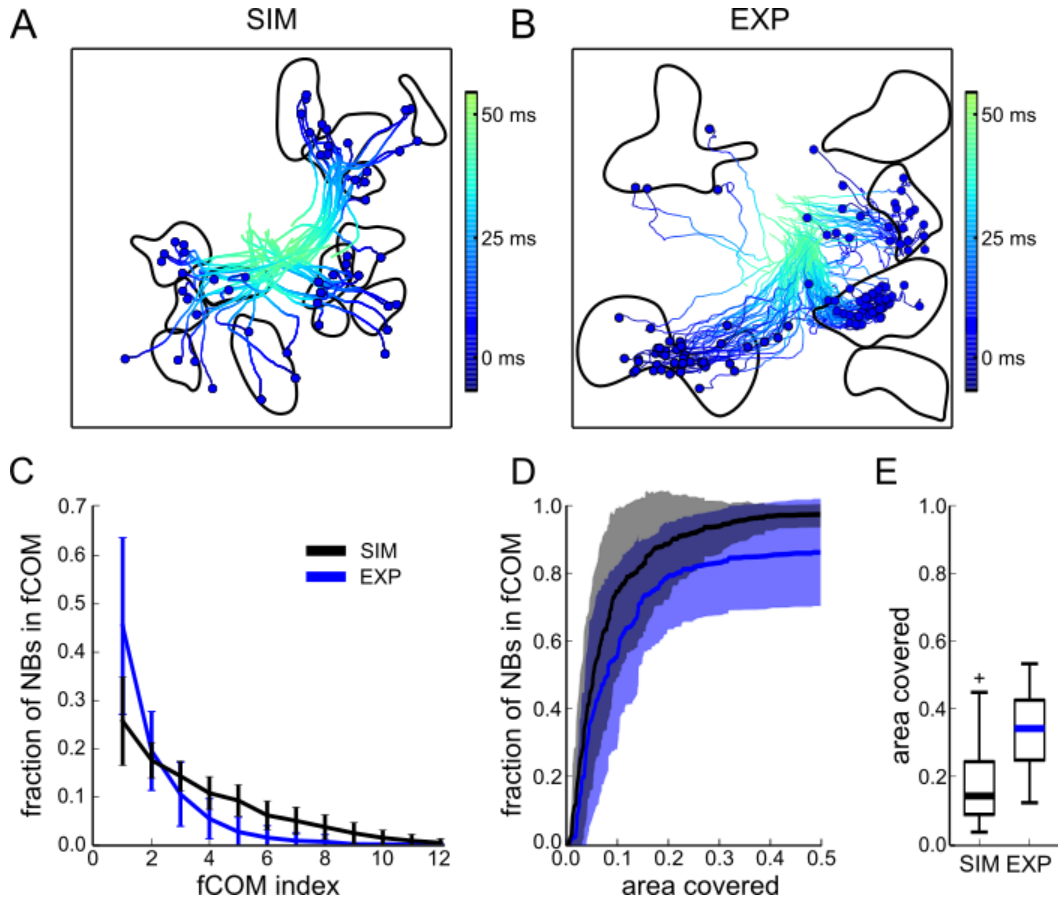


**Fig 2.12: Network regions initiating spontaneous NBs correspond to functional communities (fCOMs).** Spatial map of the functional communities (fCOMs) and CATs computed for NBs in (A) simulations (B) and recordings (for clarity, CATs are only depicted up to 50 ms after NB initiation). (C) The fraction of NBs with ignition sites (ISs) corresponding to a specific fCOM over the total number of NBs, for simulated (black) and experimental (blue) data. (D) Fraction of NBs whose IS colocalize with regions delimited by an increasing number of fCOMs ('area covered') with respect to the total amount of NBs. Solid lines mark the average values whereas shaded areas refer to standard deviations (black:  $n=20$  simulations, blue:  $n=15$  recordings). (E) Even though the number of fCOMs can exceed the ISs, the total area covered by the fCOMs on average is below 40% of the total area of the network in both experiments and simulations.

Given the colocalization that I have found between fCOMs and NB ignition sites, I investigated which features might characterize the structural and, consequently, functional properties of the local neuronal sub-networks in the fCOMs. To assess the presence of a particular structural connectivity that similarly connects neurons in each fCOM, I designed an algorithm allowing to quantify the occurrence of a set of structural connectivity motifs<sup>77</sup> (all non-isomorphic graphs up to six nodes) among fCOMs.

Notably, we found that distinctive structural motifs characterized the fCOMs with respect to other regions of the network. In particular, the comparison between fCOMs and the null models (sCOM, rCOM, rndCOM, see Annex I - Quantification of structural connectivity motifs for definition) revealed that while simple path connections are more likely in regions not associated with NB ignitions sites (Fig 2.13A-C), the fCOMs overexpress structural motifs characterized by

high clustering and degree of recurrent connections (clustering coefficient of  $0.56 \pm 0.30$  respect to  $0.19 \pm 0.27$ , Fig 2.13D). The statistical analysis performed in all network simulations ( $n = 20$ ), robustly supported this result, thus suggesting that the presence of highly recurrent local circuits represent an essential property of the network to initiate spontaneous NBs.

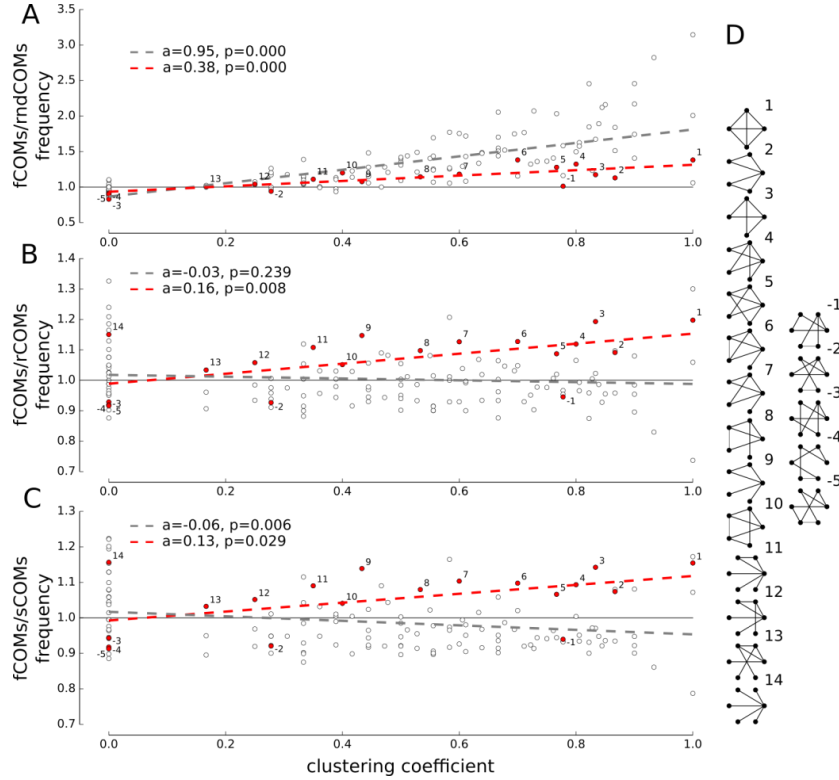


**Fig 2.13: Analysis of the structural connectivity motifs in the functional communities of the network.** Clustering coefficient of structural motifs tested (up to six nodes and isomorphic subgraphs) against the relative abundance of structural motifs in fCOMs and the null-models tested: rndCOMs (A), rCOMs (B) and sCOMs (C), see Annex I - Quantification of structural connectivity motifs. Red dots mark the structural motifs occurring with a significant frequency difference ( $p$ -value  $< 0.05$ , t-test) for all null-models. Regression lines visualize the trend among all the tested motifs (gray) and the statistically different ones (red). (D) Illustration of overabundant (positive index) and under-represented (negative indexes) structural motifs found in fCOMs with respect to the null models depicted in A-C. As highlighted by the red lines, a high clustering coefficient characterizes the structural motifs that are significantly over-expressed in fCOMs; conversely, significantly under-represented structural motifs resulted in low clustering coefficients ( $0.56 \pm 0.30$  vs.  $0.19 \pm 0.27$ , respectively).

### **Functional communities give rise to NBs**

The recurrence and the high clustering coefficient of the structural motifs underlying the fCOMs suggest a possible explanation of the mechanism underlying the triggering of spontaneous NBs. We hypothesized that the fCOMs could amplify asynchronous spontaneous spiking activities in the network that would eventually lead to the initiation of NBs. We tested this hypothesis in the model simulations by probing the network with mild sub-threshold stimulations delivered to fCOMs and non-fCOMs regions (areas not being part of any fCOM) and quantified the probability

of evoking NBs in these two different types of network regions: ISs and reference regions, see Fig 2.14A. It is important to highlight that the goal is to identify the sensitivity of these different regions to coordinate fluctuations of the spiking activities of the local neurons. Thus, the stimulation used in our simulations could either not evoke an NB (Fig 2.14B.1) or efficiently evoke an NB after few tenths of milliseconds (Fig 2.14B.2). Whenever the stimulation does not evoke an NB, the effect on the overall network dynamic is assumed to be negligible as it activates at most a few of the target neurons (<25% in the worst case scenario, which represents less than 1% of the neurons in the entire network), see Fig 2.14B.3.

The stimulation protocol, indeed, was designed to sense the responsiveness of the simulated network to spatially confined stimuli. Therefore, sub-threshold stimuli were delivered to target subregions of the network (e.g.,  $R_I$  Fig 2.14C) to provide a transient artificial activations of the AMPA conductance. All the probed regions consisted of  $\approx 40$  neurons with an intensity that decays quadratically from the centre of the site of stimulation. Specifically, for  $d \leq 0.08$ , the magnitude of AMPA conductance was provided by the equation

$$g_{STIM} = \left(1 - \left(\frac{d^2}{0.08}\right)\right) g_{ST} \text{ with } g_{ST} = 45nS$$

For distances  $d > 0.08$  from the stimulation point the conductance was arbitrary set to zero ( $g_{STIM} = 0 nS$ ). The seven probed regions in our simulations correspond to four fCOMs (*I*, *II*, *III*, and *IV*, Fig 2.14C) and three additional reference points ( $R_I$ ,  $R_{II}$ ,  $P_{III}$ , Fig 2.14C) in the network. Note that reference regions ( $R_I$ ,  $R_{II}$ ,  $P_{III}$ ) did not give rise to any NB in the spontaneous spiking activity of the associated control simulation (c.f. Fig 2.14C with Fig 2.12A). Importantly,  $P_{II}$  has been chosen to test the spatial sensitiveness of region *II* in amplifying sub-threshold fluctuations.

Interestingly, all fCOMs displayed an almost two-fold higher probability of evoking an NB ( $39.07 \pm 3.74\%$ ) respect to reference regions ( $23.35 \pm 4.08\%$ ), see Fig 2.14D. Additionally, a focused stimulation is required to efficiently ignite NBs since the probability of evoking events of  $P_{III}$  is significantly lower than the one of *II* ( $12.93 \pm 5.43\%$  decrease of efficiency).

Hence, our simulations show that fCOMs are also spatially selective to subthreshold stimulations and require the simultaneous depolarization of their neurons to give rise to an NB. All in all, fCOMs are indeed capable of initiating NB events by amplifying through their recurrent connections the fluctuations of the membrane potential of neurons due to the intrinsic spontaneous activity or of fading and sparse activity coming from the remaining part of the network.

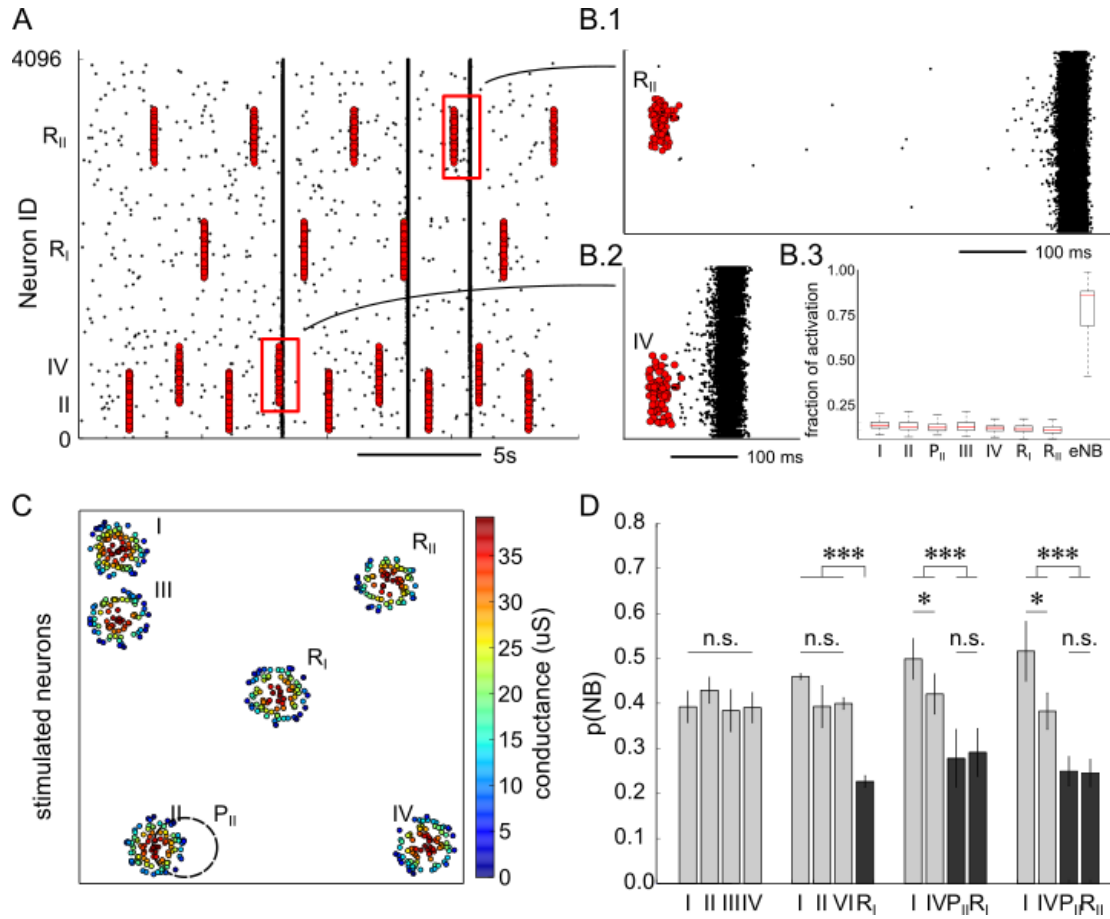


**Fig 2.14: Functional communities amplify sub-threshold stimulation of the membrane potential.** A mild depolarization of the membrane potential of neurons composing fCOMs and reference regions highlight functional differences in the simulated network ( $n=10$ ). (A) Raster plot of an illustrative protocol of stimulation. Red dots mark the timing of stimuli delivered to single neurons of four distinct fCOMs, while black dots represent the spontaneous spiking activity of the network. The stimulation delivered can be ineffective (B1) or efficient (B2) in evoking network events. While an effective stimulation activates all the neurons in fCOMs, an ineffective stimulation determines the activation of a few neurons, ensuring a negligible effect on the network dynamics (B3). (C) The location tested were four fCOMs (I, II, III and IV c.f. Fig 2.12A) and three reference regions as depicted in ( $R_I$ ,  $R_{II}$ ,  $P_{II}$  c.f. Fig 2.12A). The strength of stimulation delivered to the considered neurons is color-coded. (D) The probability of evoking NBs depend significantly on the probed region. The probability of evoking NBs by stimulating the fCOMs doubles respect to the stimulation delivered to the non-fCOM areas. Note that the probability of evoking NBs by stimulating the out of focus region II (c.f.  $R_{II}$ ) is comparable to that of stimulating random regions in the network. \* $p<0.05$ , \*\* $p<0.01$ , \*\*\* $p<0.001$ .

### ***The spiking activity preceding a network burst exhibits stereotyped spatial-temporal patterns***

A plausible hypothesis on the initiation of NBs supported by our findings on fCOMs is to consider that the amplification induced by the recurrent connectivity underlying the fCOMs might influence the local spiking activity and generates stereotyped pre-NB patterns of activation that induce these network-wide events. This hypothesis is also partially supported by the presence of

burst leader, i.e., individual channels that statistically lead the initiation phase of a network burst<sup>78</sup>, observed in low-resolution recordings. The full-knowledge of network activity and the high-resolution recordings provide the suitable framework to verify this hypothesis and to extend the notion of burst leader to neuronal assemblies eventually. Hence, I have analyzed the spiking activity for a time-window of 100 ms preceding the onset of an NB (pre-NB, see Annex I – Detection and clustering of pre-NB spiking activity for further details). With a novel approach, the spike trains of the pre-NB are interpreted as graphs (NB-graph), where each spike is seen as a node of a graph, and it is connected to a nearby node (i.e., spikes) when a criterion of the vicinity in time and space is satisfied.

Once the pre-NB activity is converted to a graph, we can exploit the tools derived from the graph theory to identify similar sub-graphs between distinct NBs, here referred to as temporal motifs. Consequently, we defined as measure of similarity the presence or not of sub-graphs that appears in two different pre-NBs. This measure of similarity, based on the relationships among nodes in the graph architecture of the pre-NB activities, preserves the network properties, i.e., the temporal order of spike timing as well as their spatial sequence of activation, without involving the absolute timing of the spikes directly. Importantly, this similarity measure quantifies the vicinity of spikes patterns, and it is robust to the noise (Fig 2.15A, shared spikes  $M=12$ ).

By considering similar two spiking patterns that shared at least a subgraph of six nodes (temporal motif), we found an interesting behavior concerning the initiation phase of NBs. Indeed, this analysis revealed that NBs belonging to the same cluster of propagation (or NB class) shared at least a spatio-temporal pattern of more than six spikes during the very beginning of the initiation phase of the NB, see Fig 2.15B. In our simulations ( $n=10$ ), this similarity among pre-NB spiking patterns for NBs of the same cluster (i.e., detected by CAT analysis) was significantly higher with respect to pre-NBs spiking patterns associated to any other NB ( $66.7 \pm 8.1\%$  vs.  $4.2 \pm 0.8\%$  respectively), see Fig 2.15C. To test the consistency of this result, the maximum threshold for similarity, i.e., the number of spikes composing the common temporal motif, was varied for sequences of spikes of different length, from 6 to 60 spikes, see Fig 2.15D. This revealed a plateau reaching 67% of similarity between pre-NB belonging to the same class at approximately 50 spikes indicating that the pre-NBs spike trains can share very complex patterns.

Given such similarity observed in the pre-NB spiking activity, we then clustered the NBs using the novel similarity measure instead of considering the CATs. As for the CAT analysis (Fig 2.6E), the reordered similarity matrix of the pre-NBs spiking activity displayed a clear block structure. This result further confirms that the initiation phase of NBs strongly characterizes these events, see Fig 2.15E. Notably, the very same analysis applied to experimental recordings ( $n=5$ ) also lead to a block structure (Fig 2.15F) that is also similar to the one obtained with the CATs analysis (Fig 2.1F), although the comparison of the results obtained with both analyses is not as strong as obtained from synthetic data. Altogether, these results support the hypothesis of a dedicated local circuitry (or functional community of neurons) that gives rise to network-wide propagation through a stereotyped amplification of the sparse and asynchronous spontaneous spiking activity of the neuronal culture.

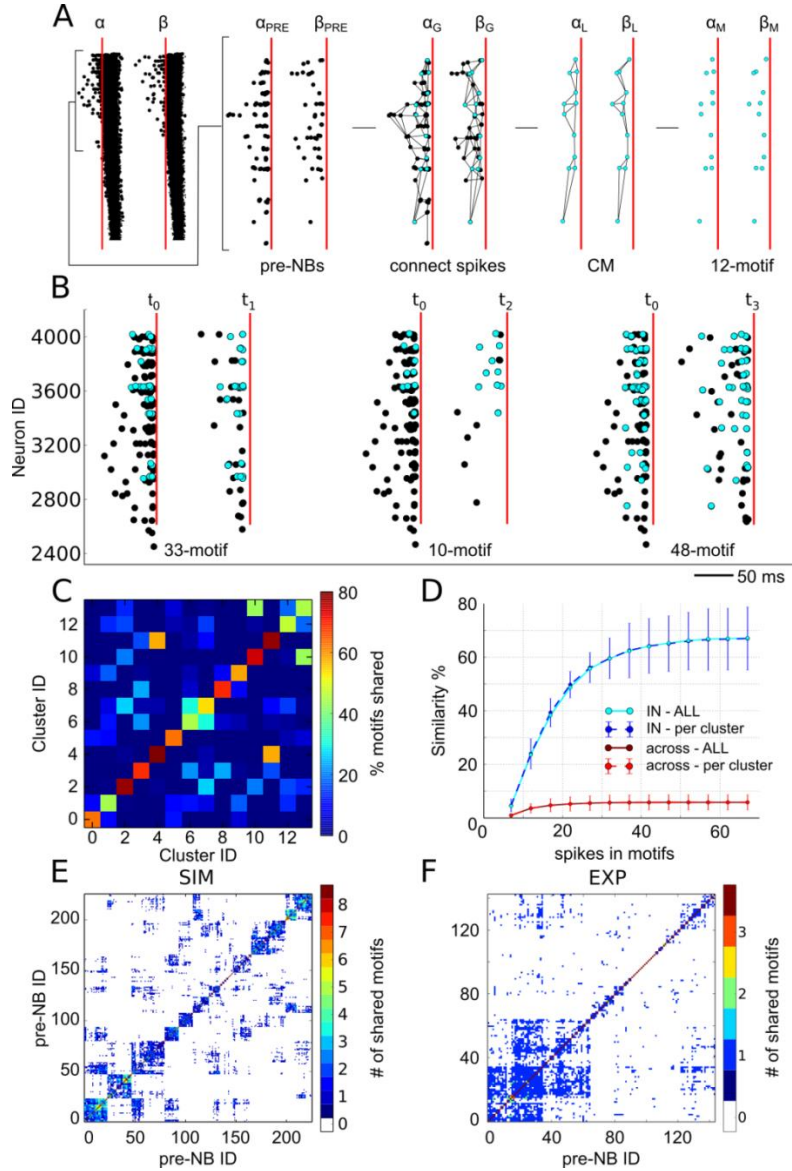


**Fig 2.15: Stereotyped spiking patterns associated with ignition sites characterize the initiation phase of NBs.** (A) Detection of similar temporal motifs within the pre-NBs activities: starting from two NBs ( $\alpha$ ,  $\beta$ ), the pre-NB activity ( $\alpha_{PRE}$ ,  $\beta_{PRE}$ ) is considered to construct the NB-graphs ( $\alpha_G$ ,  $\beta_G$ ). Next, isomorphic sub-graphs were detected in the two largest connected components ( $\alpha_L$ ,  $\beta_L$ ) and the number of spikes within the shared sub-graph (temporal motifs ( $\alpha_M$ ,  $\beta_M$ ) defined the strength of similarity ( $M=12$  spikes). (B) All NBs of the same cluster (e.g., cluster ID 0) share common pre-NB temporal motifs (cyan spikes). For instance, the NB occurring at the time  $t_0$  shares a temporal motif with the event at the time  $t_1$  but differs from the temporal motif shared between NBs occurring at the time  $t_2$  and  $t_3$ . (C) Normalized similarity matrix of clustered NBs with  $M > 5$ . The clustered NBs share the highest number of motifs (i.e., higher values on the diagonal), indicating that the pre-NB activity is informative of the following NB. (D) Cumulative similarity plot corresponding to the data in panel C but normalized with respect to the cluster size (per-cluster, dashed line) or to the total number of NBs (solid lines). The similarity is consistently higher for the pre-NB activity of NBs belonging to the same cluster (IN) than for the NBs of other clusters (ACROSS). (E) Reordered similarity matrix of pre-NB activity of a simulated network, showing a block structure. Each block is relative to an NB cluster characterized by similar pre-NB spiking patterns. (F) Reordered similarity matrix of recorded pre-NB activity in a cultured network, still allowing for a block structure.

### ***Emergence of local inhomogeneities in the network connectivity***

Our results suggest that the initiation of NBs in a neuronal network is associated to the fCOMs and to their particular local neuronal connectivity properties that differ from the rest of the network. Here, I performed additional simulations to understand better how these local inhomogeneities in the network connectivity might arise in the computational network model.

To do so, I applied the Gaussian connectivity algorithm to six distinct spatial arrangements of neurons, ranging from a regular grid (Fig 2.16A) to a fully random distribution (Fig 2.16F). In regular grids (Fig 2.16A-B) the node degree remains constant at the center of the network, and it decreases when approaching the border of the network because of a finite size effect (i.e., lack of nearby neurons to connect with). Interestingly, in the random arrangements, clusters of densely interconnected nodes emerged (Fig 2.16E-F) without requiring any external mechanism of guidance, but instead arise from a distributed mechanism of connections.

We further investigated the impact of the neuron disposal with respect to the node degree and the clustering coefficient of graphs preserving the Gaussian rule of connectivity. Interestingly, the node degree and the clustering coefficient increase when increasing randomness of the neuronal disposal (Fig 2.17A-B,  $n=10$  graphs for each node arrangement). Furthermore, we also found that the spatial distribution of node degrees is not uniform over the entire network. Indeed, the variability of the average node degree computed over 3x3 subdivisions of the original network (Fig 2.17C) increases with the random disposal of the neurons (Fig 2.17D).

All in all, our computational exploration revealed that the denser interconnected communities, emerge naturally from a combination of factors, including the random arrangement of neurons, the distance-dependent connectivity rule and the sparsity of the neuronal connections. The factors above determine how the network autonomously expresses network bursts, suggesting a potential robust mechanism that biology might exploit to ensure persistent spiking activities considering the intrinsic spatial variability, heterogeneity and the initial wiring of a developing neuronal network that will further evolve (e.g., sculpted by activity).



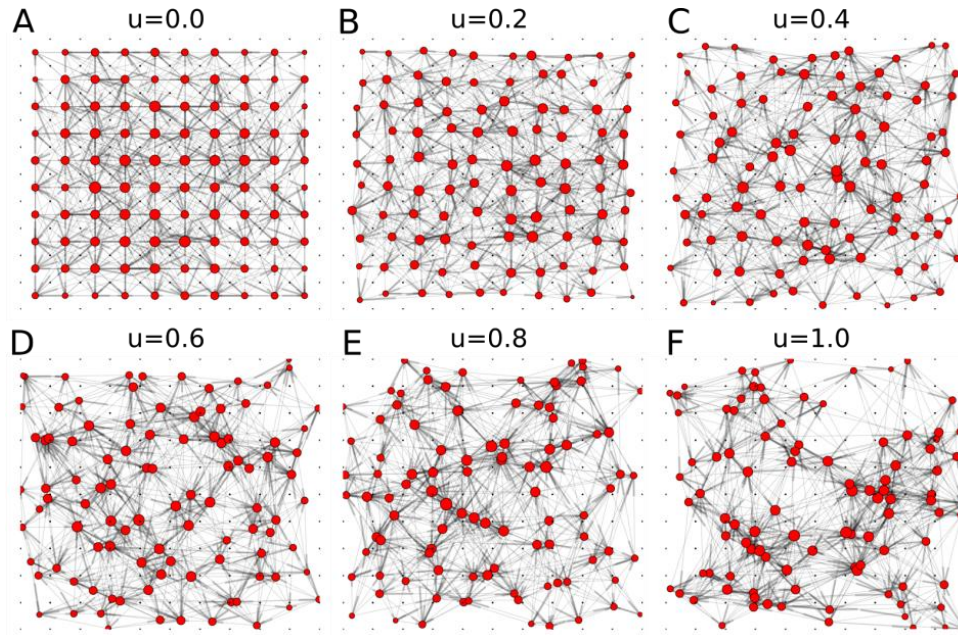


**Fig 2.16: Emergence of densely connected micro-circuits.** Microcircuits with a denser connectivity pattern (the size of each node is proportional to its degree) emerge moving from a regular grid network (A,  $u=0$ ) to a fully randomized network (F,  $u=1$ ). All networks consisted of  $N=100$  neurons.

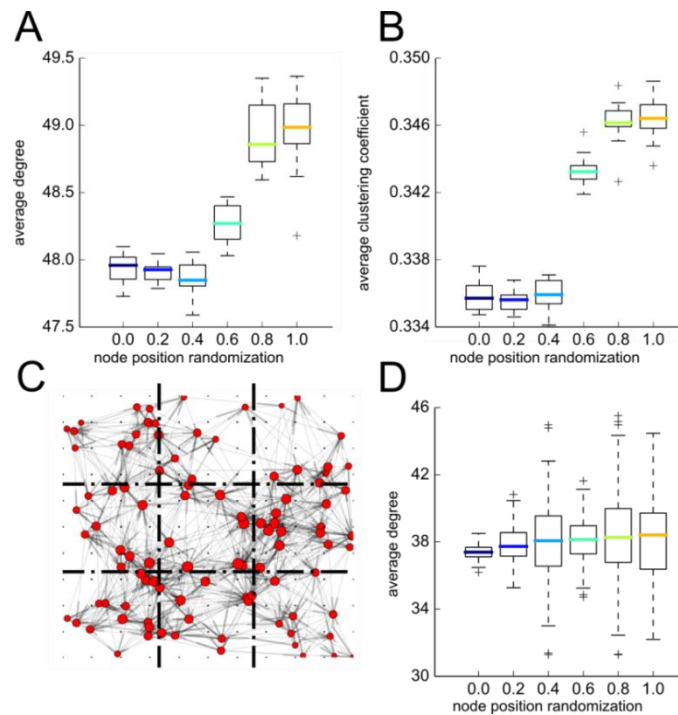


**Fig 2.17: Graph theory parameters for different randomization levels of neuron arrangements.** The average degree (A) and the average clustering coefficient (B) increase with the increasing random disposition. (C) An illustrative example of a small network ( $N=100$  neurons) shows that the different  $3 \times 3$  sub-regions can have quite variable node degrees. (D) The variability of the node degree is a function of at the randomness of the neuronal arrangement. For each node position randomization, we generated  $n=5$  networks each with 4096 neurons.

## ***Applications and extension of the computational network model***

---

Given the versatility and the goodness of our biophysical computational network model in predicting and replicating a vast number of spontaneous spiking regimes, I also explored its extension to explain biological principles underlying changes in the spiking activity observed in different experimental conditions compared to those studied so far on a 2D network of wild-type neurons. In particular, I have applied the model to two experimental conditions i) to interpret experimental data obtained from a transgenic neuronal culture in which the PRRT2 gene was deleted, and ii) to interpret the spontaneous activity recorded from 3D neuronal cultures by extending the model from 2D to 3D.

### ***Modelling and interpreting the effects of PRRT2-gene deletion in neuronal cultures***

In humans, mutation of the PRRT2 protein determines paroxysmal disorders such as epilepsy, kinesigenic dyskinesia, migraine or episodic ataxia<sup>79</sup>. As reported by our collaborators, the deletion of PRRT2 determined several changes at a synaptic and cellular level also in neuronal cultures. Specifically, at the cellular level, a misbalance between GABAergic and glutamatergic transmission characterized KO cultures respect to control ones in favor of a global increase in excitation. Indeed, the population of excitatory neurons increased by 10% while the inhibitory population decreased more than 30%, respect to conventional cultures. The reported misbalance might itself explain the hyperactive spiking activity of KO networks, which exhibit a 30% increase in firing rate together with a 10% increase of the parameters associated with network burst activity. However, the explanation is not straightforward given the information acquired at the synaptic level. Patch-clamp experiments revealed a 25% reduction in the peak magnitude of evoked Excitatory Post Synaptic Currents (eEPSCs) with a consequent increase in the paired-pulse response (PPR) and a lower release probability (Pr). Conversely, evoked Inhibitory Post Synaptic Currents (eIPSCs) display a symmetric behavior: the peak current increased by 25%, the paired-pulse response diminished, and the release probability increased. Additionally, compared to control hippocampal cultures, mutant cultures exhibit a 20% decrease in the number of excitatory synapses while inhibitory contacts were unchanged.

This latter evidence indicates that although the mutant network exhibits a higher excitation due to the presence of more excitatory neurons, their synaptic efficacy is severely impaired compared to control cultures and this reduction in efficacy and number of excitatory connections is further amplified by an increased contribution of GABAergic synapses. Moreover, upon treatment with bicuculline, the spontaneous spiking activity of both WT and KO cultures displayed similar changes in the spiking activity. Consequently, changes in the GABAergic transmission alters similarly the PRRT2 KO and control cultures, suggesting that the impaired maturation of the GABAergic transmission (e.g., a late GABA switch) does not occur in KO cultures in these recordings. Additionally, this experiment further indicates that the hyperactivity of KO cultures cannot be attributed to a lack of functional GABAergic neurons.

*Changes in short-term plasticity are necessary, but not sufficient, to explain the hyperexcitability of PRRT2-KO networks*

Given the counterintuitive experimental picture characterized by a decreased strength of excitation in favor of inhibition at the synaptic level, a set of simulations were designed to assess whether the altered excitatory to inhibitory neuron ratio, could explain the increased spontaneous spiking activity of KO cultures in simulated networks. To target the question related to cellular and synaptic properties, rather than a different network connectivity contribute, control and KO simulated network shared the same structural graphs. Importantly, an additional fitting of neuronal and network parameters to the synaptic and cellular evidence ensured a fair comparison between computational and experimental exploration. Here, the advantage of computational investigation concerned the capability of pairing each simulated control culture to a corresponding KO with a few modifications induced by the working hypothesis. Specifically, to preserve the cellular and synaptic features of control network as close as possible, KO network construction starts from a control simulation as follows:

- Converting a random set of inhibitory neurons into excitatory ones in order to match the Excitatory to Inhibitory (E/I) ratio of KO cultures, see Fig 2.18A.
- Setting the excitatory synaptic facilitation to the experimentally reported values, see Fig 2.18B
- Randomly removing the 20% of excitatory synapses

Concerning KO cultures modeling, additional sets of simulations assessed the hypothesis of an enhanced excitability of excitatory neurons, through a decreased spike-triggered adaptation, in contributing to KO hyperactivity (+IE condition) respect to KO condition (-IE). Specifically, the update of the self-inhibition provided by the spike-triggered adaptation at each action potential elicited by the neuron was set to half of the control value ( $b = 20$  vs.  $b = 40$  for +IE vs. -IE condition). The outcome of this change determined a slower adaptation in firing rate induced by the injection of a current step, see Fig 2.18C.

Remarkably, despite the significantly lower number of synaptic contacts and their reduced strength, the PRRT2 KO simulated spiking activity is still characterized by the appearance of NBs. However, the experimental findings simulated, could not fully explain the hyperactivity of KO networks. Specifically, although changes in the excitatory facilitation are required for simulated networks to exhibit network-wide activation, they were not sufficient to reproduce the experimental trends in the average network parameters.

Consequently, by taking a closer look at the dynamics of NBs in KO-culture, a possible mechanism that could recapitulate the difference observed experimentally was an enhanced spike-triggered adaptation. Indeed, NBs of KO cultures were characterized by longer durations and a higher number of spikes compared to control cultures. Thus, a new set of simulations for which excitatory neurons displayed less adaptation in response to a current step (Fig 2.18C-D), well-captured the experimental evidence (KO+IE). In particular, the simulated spiking activity exhibited an increased firing and bursting rates that was missing without a different intrinsic excitability, see Fig 2.18E-H.

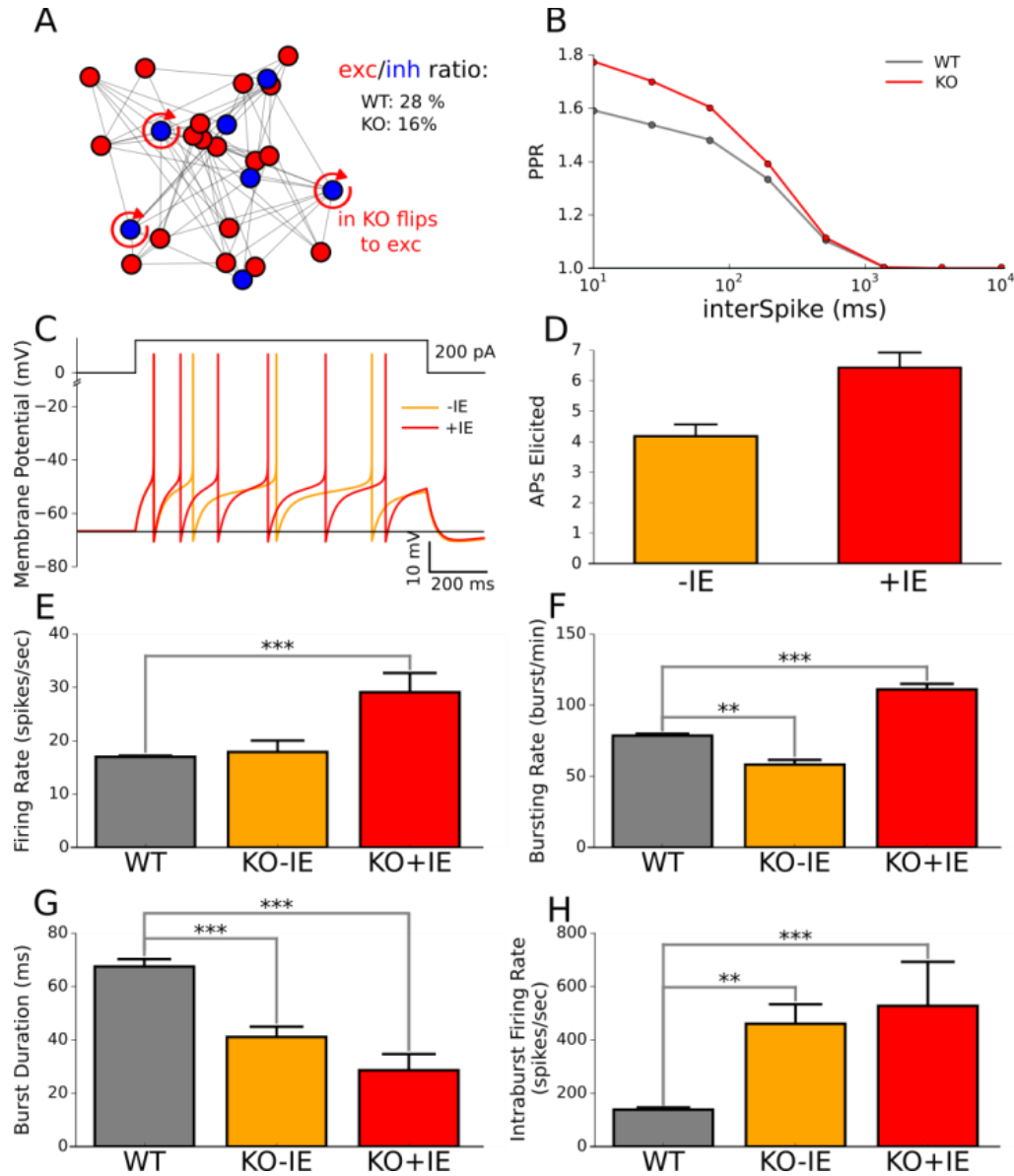


**Fig 2.18: Modeling of the PRRT2-KO synaptic phenotype at the network level.** (A) Representative close-up of a simulated network. In order to maintain the proper inhibitory to excitatory ratio, randomly chosen inhibitory neurons (40% of the WT inhibitory population, blue) were turned into excitatory (red) neurons in the PRRT2-KO simulations. (B) Paired-pulse ratio of excitatory synapses as a function of ISIs. (C) Representative membrane potential traces of excitatory neurons for two conditions of Intrinsic Excitability (IE): -IE used in WT and KO (-IE) samples and the more excitable neurons +IE implemented in KO networks (+IE). (D) Quantitative analysis of action potentials generated by (-IE) and (+IE) neurons in response to 1-s step injection of 200 pA current. (E-H) Network statistics are reported for WT (gray), KO-IE (orange) and KO+IE (red) networks (N=10/experimental group). The increased facilitation of KO networks cannot fully explain the evidence observed in the experiments (KO-IE, orange). However, by integrating an enhanced Intrinsic Excitability (KO+IE, red), the simulations reproduced the experimental data qualitatively. Paired t-test \* $p < 0.05$ , \*\* $p < 0.01$ , \*\*\* $p < 0.001$ .

This observation, deriving from the computational exploration of the parameter space, indicate that the KO networks require an increase intrinsic excitability to balance the lower network connectivity and excitatory transmission. Indeed, with this setting, the simulations fully reproduce all the phenotypes characterizing the increased PRRT2-KO spiking activity, although other unexplored mechanisms can work synergically with the one suggested by the computational exploration. Consequently, our collaborators assessed the computational hypothesis through ad-hoc patch-clamp experiments. These new experiments indeed showed that the excitability of the excitatory neurons is also altered in the KO.

Altogether the insights gained through the computational exploration suggested a set of new experiments that further validated the combination of experimental and computational approaches to advance with the characterization of the PRRT2 KO data.

### ***From 2D networks to 3D neuronal culture computational network models***

Brain circuits fully exploit a 3D environment to develop and grow, leading to complex functional circuit structurally organized in a tridimensional space. However, although neurites and neurons in culture can overlap one on top of the others, the overall network can be assumed as bi-dimensional rather than a 3D organization. A natural question arises on how the different and more natural 3D spatial arrangement<sup>80</sup> can affect the spontaneous activity of a neuronal network. To address this question, a fruitful collaboration with Laura Ballerini (SISSA) allowed us to compare 2D to 3D cell cultures network activities recorded by calcium imaging. Our collaborators developed biocompatible scaffolds of porous materials to grow neurons in a 3D environment<sup>81</sup>. Hippocampal cultures were grown in the conventional 2D environment and 3D configuration for 21 DIVs and monitored through calcium imaging approach, and a few hundreds of micrometers in the 3D cultures were scanned. Notably, our colleagues in Trieste observed different patterns of activity in 3D geometries compared to the classical 2D ones. Specifically, in 3D cultures, the InterEvent Interval (the time between synchronous calcium events, IEI) was significantly lower than the one recorded in the 2D networks, thus suggesting a crucial role of the network wiring in regulating the occurrence of such population events (Fig 2.19B, black bars). To this end, we extended the 2D model that we developed to support experimental findings and to investigate how the connectivity can alter the spontaneous neuronal spiking activity. In order to effectively compare the simulation results to the experiments, we made the reasonable assumption that synchronous calcium events correspond to the network bursts generated by the computational model.

The working hypothesis was that the 3D wiring could itself explain the higher frequency of NBs observed in 3D cultures respect to 2D ones. In order to build the 3D network, we assumed that the neurons connected with the same radial-basis rule used in the 2D network (see Annex I – Network topology). To obtain the same number of synaptic contacts per neuron in both 2D/3D topologies the number of connections in the 2D network was decreased by randomly removing synaptic contacts. The latter assumption is crucial to assess whether the 3D wiring is the main determinant of the observed differences. Importantly, a similar percentage of active cells in 2D and 3D networks supports the hypothesis that a comparable number of synaptic contacts exist in the two

networks. Hence, by keeping most of the number of parameters of the 3D network as in the 2D one, we can test whether a genuine change in the connectivity of the 3D networks (respect to the 2D ones) can itself explain the increased synchronous calcium events.

Consequently, to perform the simulations, first, a 3D network was built by using a 3D symmetric radial basis function with variance set to  $\sigma^2=0.0035$ . Second a 2D network associated with the 3D one was constructed with the same link-length distribution (i.e., by setting the same variance  $\sigma^2=0.0035$  in a 2D standard network). Then, for each neuron in the 2D network, a random subset of connections was removed to get the same number of synaptic contacts of the 3D network. The latter step is needed to balance the increased density of neurons in 2D respect to 3D configuration while keeping the degree distribution between the two conditions as close as possible. Notably, multiple runs ( $n = 10$ ) of each tested 2D/3D topology determined differences in the spiking activity of 2D/3D simulated networks comparable to the one observed experimentally. Indeed, the IEI of simulated networks significantly diminished in 3D networks quantitatively pairing the experimental observation both in control condition and even upon mimicking the effects of bicuculline. (i.e., by setting GABA conductance to zero; Fig 2.19B).

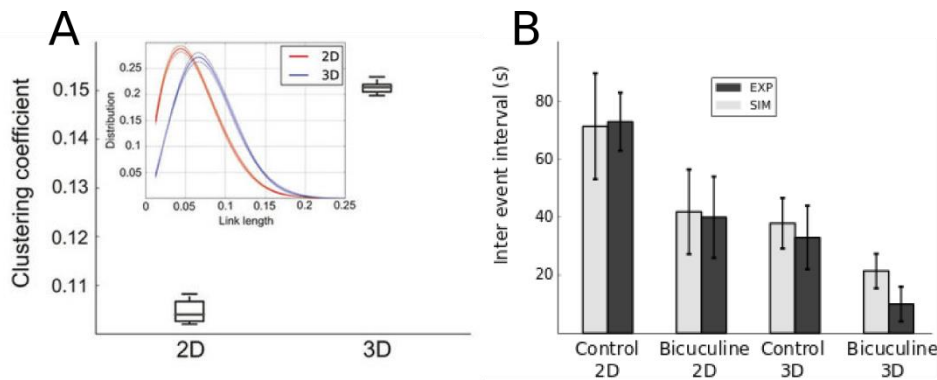


**Fig 2.19: Comparison between 2D and 3D-topologies respect to graph theory parameters. (A) 3D networks significantly differ for their clustering coefficient. (B) The Inter-event intervals for control, and bicuculline conditions observed in the 2D and 3D environments. The model (white bars) mimics correctly the experimentally observed dynamics (black bars) and support the idea of a different wiring as a key player in the observed differences.**

Given the accordance between the simulations and the experiments, the focus of the investigation pointed towards the differences in network connectivity between 2D and 3D simulated cultures since it represented the only difference between the two simulated configurations. Classical graph theory quantification performed onto the two candidate networks revealed that while in the 2D/3D networks the mean path length was unchanged, the clustering coefficient of 2D networks was significantly lower respect to 3D ones, see Fig 2.19A. Additionally, the link length distribution (i.e., the length of the connections, inset Fig 2.19A) of the 3D networks displayed a shift to the longer distances with a longer right-tail compared to the 2D networks. Consequently, the previous assumptions induce an increased clustering coefficient and the more extended links in 3D networks respect to 2D ones. Importantly, this evidence can suggest a possible mechanism that underlies the higher efficiency (i.e., excitability) of 3D neuronal cultures. In fact, the clustering

coefficient indicates that the simulated 3D network exhibit more recurrent and clustered connections than the 2D one, which as outlined in the previous sections, represent a suitable condition for NBs initiation sites. Conversely, the shift to longer links suggests that the spiking activity can spread much faster throughout the network but also that ignition sites can receive and amplify the sparse activity of a broader region of the network, thus explaining the higher amount of NBs per unit of time of 3D neuronal networks.

Altogether, the computational exploration supported the experimental evidence and provided insights into the mechanisms underlying the higher excitability of 3D neuronal networks, and it could be useful for further experimental and modeling investigations<sup>82</sup>.

## Bibliography

---

1. Wagenaar, D. A., Pine, J. & Potter, S. M. An extremely rich repertoire of bursting patterns during the development of cortical cultures. *BMC Neurosci.* **7**, 11 (2006).
2. Hesse, J. & Gross, T. Self-organized criticality as a fundamental property of neural systems. *Front. Syst. Neurosci.* **8**, (2014).
3. Pasquale, V., Massobrio, P., Bologna, L. L., Chiappalone, M. & Martinoia, S. Self-organization and neuronal avalanches in networks of dissociated cortical neurons. *Neuroscience* **153**, 1354–1369 (2008).
4. Maeda, E., Robinson, H. P. & Kawana, A. The mechanisms of generation and propagation of synchronized bursting in developing networks of cortical neurons. *J. Neurosci.* **15**, 6834–45 (1995).
5. Quadrato, G., Brown, J. & Arlotta, P. The promises and challenges of human brain organoids as models of neuropsychiatric disease. *Nat. Med.* **22**, 1220–1228 (2016).
6. Foley, K. E. Organoids: A better in vitro model. *Nat. Methods* **14**, 559–562 (2017).
7. Palazzolo, G. *et al.* Fast wide-volume functional imaging of engineered in vitro brain tissues. *Sci. Rep.* **7**, 8499 (2017).
8. Berdondini, L. *et al.* Active pixel sensor array for high spatio-temporal resolution electrophysiological recordings from single cell to large scale neuronal networks. *Lab Chip* **9**, 2644 (2009).
9. Kerschensteiner, D. Spontaneous Network Activity and Synaptic Development. *Neurosci.* **20**, 272–290 (2014).
10. Buzsáki, G. Large-scale recording of neuronal ensembles. *Nat. Neurosci.* **7**, 446–451 (2004).
11. Feldt, S., Bonifazi, P. & Cossart, R. Dissecting functional connectivity of neuronal microcircuits: Experimental and theoretical insights. *Trends Neurosci.* **34**, 225–236 (2011).
12. Yuste, R. From the neuron doctrine to neural networks. *Nat. Rev. Neurosci.* **16**, 487–497 (2015).
13. Menendez De La Prida, L., Bolea, S. & Sanchez-Andres, J. V. Origin of the synchronized network activity in the rabbit developing hippocampus. *Eur. J. Neurosci.* **10**, 899–906 (1998).
14. Ojovan, S. M. *et al.* A feasibility study of multi-site, intracellular recordings from mammalian neurons by extracellular gold mushroom-shaped microelectrodes. *Sci. Rep.* **5**, 14100 (2015).
15. Dipalo, M. *et al.* Intracellular and Extracellular Recording of Spontaneous Action Potentials in Mammalian Neurons and Cardiac Cells with 3D Plasmonic Nanoelectrodes. *Nano Lett.* **17**, 3932–3939 (2017).
16. Imfeld, K. *et al.* High-resolution MEA platform for in-vitro electrogenic cell networks imaging. *Annu. Int. Conf. IEEE Eng. Med. Biol. - Proc.* **2007**, 6085–6088 (2007).
17. Franks, W. *et al.* CMOS monolithic microelectrode array for stimulation and recording of natural neural networks. in *TRANSDUCERS 2003 - 12th International Conference on Solid-State Sensors, Actuators and Microsystems, Digest of Technical Papers* **2**, 963–966 (Institute of Electrical and Electronics Engineers ({IEEE}), 2003).
18. Frey, U. *et al.* Cell Recording with a CMOS High-Density Microelectrode Array. *Proc 29th Ann Intern. Conf IEEE EMBS* 4 pages- (2007).
19. Gandolfo, M., Maccione, A., Tedesco, M., Martinoia, S. & Berdondini, L. Tracking burst patterns in hippocampal cultures with high-density CMOS-MEAs. *J. Neural Eng.* **7**, 56001 (2010).
20. Chao, Z. C., Bakkum, D. J. & Potter, S. M. Region-specific network plasticity in simulated and living cortical networks: comparison of the center of activity trajectory (CAT) with other statistics. *J. Neural Eng.* **4**, 294–308 (2007).
21. Maccione, A. *et al.* A novel algorithm for precise identification of spikes in extracellularly recorded neuronal signals. *J. Neurosci. Methods* **177**, 241–249 (2009).
22. Pasquale, V., Martinoia, S. & Chiappalone, M. A self-adapting approach for the detection of bursts and network bursts in neuronal cultures. *J. Comput. Neurosci.* **29**, 213–229 (2010).
23. Lonardoni, D. *et al.* High-density MEA recordings unveil the dynamics of bursting events in Cell Cultures. in *Proceedings of the Annual International Conference of the IEEE Engineering in Medicine and Biology Society, EMBS 2015–Novem*, 3763–3766 (IEEE, 2015).
24. Amin, H., Nieuws, T., Lonardoni, D., Maccione, A. & Berdondini, L. High-resolution bioelectrical imaging



- of A $\beta$ -induced network dysfunction on CMOS-MEAs for neurotoxicity and rescue studies. *Sci. Rep.* **7**, 2460 (2017).
25. Brette, R. Adaptive Exponential Integrate-and-Fire Model as an Effective Description of Neuronal Activity. *J. Neurophysiol.* **94**, 3637–3642 (2005).
  26. Vasilaki, E. & Giugliano, M. Emergence of connectivity motifs in networks of model neurons with short- and long-term plastic synapses. *PLoS One* **9**, e84626 (2014).
  27. Marconi, E. *et al.* Emergent functional properties of neuronal networks with controlled topology. *PLoS One* **7**, e34648 (2012).
  28. Bisio, M., Bosca, A., Pasquale, V., Berdondini, L. & Chiappalone, M. Emergence of bursting activity in connected neuronal sub-populations. *PLoS One* **9**, e107400 (2014).
  29. Okujeni, S., Kandler, S. & Egert, U. Mesoscale Architecture Shapes Initiation and Richness of Spontaneous Network Activity. *J. Neurosci.* **37**, 3972–3987 (2017).
  30. Bollobás, B., Kozma, R., Miklós, D. & Tóth, B. *Handbook of Large-Scale Random Networks. Book 18*, (2008).
  31. Barabasi, A.-L. & Albert, R. Emergence of scaling in random networks. *Science (80-. )*. **286**, 509–512 (1999).
  32. Franklin, W. R. Computational Geometry: An Introduction (Franco P. Preparata and Michael Ian Shamos). *SIAM Review* **30**, 669–670 (1988).
  33. Amico, M. D. & Genova, U. Highly-Clustered Networks with Preferential Attachment to Close Nodes 2 Related Work. in *Sciences-New York* 1–6 (2006).
  34. Van Mieghem, P. Paths in the Simple Random Graph and the Waxman Graph. *Probab. Eng. Information Sci.* 535–555 (2001).
  35. Barthélemy, M. Spatial networks. *Phys. Rep.* **499**, 1–101 (2011).
  36. Grinstein, G. & Linsker, R. Synchronous neural activity in scale-free network models versus random network models. *Proc. Natl. Acad. Sci.* **102**, 9948–9953 (2005).
  37. Kitano, K. & Fukai, T. Variability v.s. synchronicity of neuronal activity in local cortical network models with different wiring topologies. *J. Comput. Neurosci.* **23**, 237–250 (2007).
  38. Watt, A. J. *et al.* Traveling waves in developing cerebellar cortex mediated by asymmetrical Purkinje cell connectivity. *Nat. Neurosci.* **12**, 463–473 (2009).
  39. Downes, J. H. *et al.* Emergence of a small-world functional network in cultured neurons. *PLoS Comput. Biol.* **8**, e1002522 (2012).
  40. Massobrio, P., Pasquale, V. & Martinoia, S. Self-organized criticality in cortical assemblies occurs in concurrent scale-free and small-world networks. *Sci. Rep.* **5**, 10578 (2015).
  41. Bialonski, S., Horstmann, M. T. & Lehnertz, K. From brain to earth and climate systems: Small-world interaction networks or not? *Chaos* **20**, 13134 (2010).
  42. Gerhard, F., Pipa, G., Lima, B., Neuenschwander, S. & Gerstner, W. Extraction of Network Topology From Multi-Electrode Recordings: Is there a Small-World Effect? *Front. Comput. Neurosci.* **5**, 4 (2011).
  43. Marinaro, G. *et al.* Networks of neuroblastoma cells on porous silicon substrates reveal a small world topology. *Integr. Biol.* **7**, 184–197 (2015).
  44. Maheswaranathan, N. Emergent bursting and synchrony in computer simulations of neuronal cultures. *Front. Comput. Neurosci.* **6**, 15 (2012).
  45. Ullo, S. *et al.* Functional connectivity estimation over large networks at cellular resolution based on electrophysiological recordings and structural prior. *Front. Neuroanat.* **8**, 137 (2014).
  46. Gritsun, T. A., le Feber, J. & Rutten, W. L. C. Growth Dynamics Explain the Development of Spatiotemporal Burst Activity of Young Cultured Neuronal Networks in Detail. *PLoS One* **7**, e43352 (2012).
  47. Jarsky, T., Roxin, A., Kath, W. L. & Spruston, N. Conditional dendritic spike propagation following distal synaptic activation of hippocampal CA1 pyramidal neurons. *Nat. Neurosci.* **8**, 1667–1676 (2005).
  48. Van Pelt, J., Wolters, P. S., Corner, M. A., Rutten, W. L. C. & Ramakers, G. J. A. Long-term characterization of firing dynamics of spontaneous bursts in cultured neural networks. *IEEE Trans. Biomed. Eng.* **51**, 2051–2062 (2004).

49. Segev, R., Shapira, Y., Benveniste, M. & Ben-Jacob, E. Observations and modeling of synchronized bursting in two-dimensional neural networks. *Phys. Rev. E. Stat. Nonlin. Soft Matter Phys.* **64**, 9 (2001).
50. Garofalo, M., Nieuw, T., Massobrio, P. & Martinoia, S. Evaluation of the performance of information theory-based methods and cross-correlation to estimate the functional connectivity in cortical networks. *PLoS One* **4**, e6482 (2009).
51. Chiappalone, M., Bove, M., Vato, A., Tedesco, M. & Martinoia, S. Dissociated cortical networks show spontaneously correlated activity patterns during in vitro development. *Brain Res.* **1093**, 41–53 (2006).
52. Bonzano, L., Bove, M. & Martinoia, S. Effects of NMDA and non-NMDA receptors antagonists on the dynamic behavior of cultured cortical networks. *Neurocomputing* **69**, 1897–1903 (2006).
53. Arnold, F. J. L. *et al.* Microelectrode array recordings of cultured hippocampal networks reveal a simple model for transcription and protein synthesis-dependent plasticity. *J. Physiol.* **564**, 3–19 (2005).
54. Mack, C. M. *et al.* Burst and principal components analyses of MEA data for 16 chemicals describe at least three effects classes. *Neurotoxicology* **40**, 75–85 (2014).
55. Suresh, J. *et al.* Network burst activity in hippocampal neuronal cultures: the role of synaptic and intrinsic currents. *J. Neurophysiol.* **115**, 3073–3089 (2016).
56. Baruchi, I. & Ben-Jacob, E. Towards neuro-memory-chip: Imprinting multiple memories in cultured neural networks. *Phys. Rev. E - Stat. Nonlinear, Soft Matter Phys.* **75**, 50901 (2007).
57. Wang, X. J. Synaptic reverberation underlying mnemonic persistent activity. *Trends Neurosci.* **24**, 455–463 (2001).
58. Volman, V., Gerkin, R. C., Lau, P. M., Ben-Jacob, E. & Bi, G. Q. Calcium and synaptic dynamics underlying reverberatory activity in neuronal networks. *Phys. Biol.* **4**, 91–103 (2007).
59. Masquelier, T. & Deco, G. Network Bursting Dynamics in Excitatory Cortical Neuron Cultures Results from the Combination of Different Adaptive Mechanism. *PLoS One* **8**, e75824 (2013).
60. Huang, C. H., Huang, Y. T., Chen, C. C. & Chan, C. K. Propagation and synchronization of reverberatory bursts in developing cultured networks. *J. Comput. Neurosci.* **42**, 177–185 (2017).
61. Perez Velazquez, J. L. & Carlen, P. L. Gap junctions, synchrony and seizures. *Trends Neurosci.* **23**, 68–74 (2000).
62. Blanc, E. M., Bruce-Keller, A. J. & Mattson, M. P. Astrocytic Gap Junctional Communication Decreases Neuronal Vulnerability to Oxidative Stress-Induced Disruption of Ca<sup>2+</sup> Homeostasis and Cell Death. *J. Neurochem.* **70**, 958–970 (2002).
63. Rouach, N., Segal, M., Koulakoff, A., Giaume, C. & Avignone, E. Carbenoxolone Blockade of Neuronal Network Activity in Culture is not Mediated by an Action on Gap Junctions. *J. Physiol.* **553**, 729–745 (2003).
64. Frega, M. *et al.* Cortical cultures coupled to Micro-Electrode Arrays: A novel approach to perform in vitro excitotoxicity testing. *Neurotoxicol. Teratol.* **34**, 116–127 (2012).
65. Choi, D. W., Koh, J. Y. & Peters, S. Pharmacology of glutamate neurotoxicity in cortical cell culture: attenuation by NMDA antagonists. *J. Neurosci.* **8**, 185–196 (1988).
66. Stuart, G. J. & Spruston, N. Dendritic integration: 60 years of progress. *Nat. Neurosci.* **18**, 1713–1721 (2015).
67. Euler, T. & Denk, W. Dendritic processing. *Current Opinion in Neurobiology* **11**, 415–422 (2001).
68. de Luca, E. *et al.* Inter-Synaptic Lateral Diffusion of GABA<sub>A</sub> Receptors Shapes Inhibitory Synaptic Currents. *Neuron* **95**, (2017).
69. Nieuw, T. LTP Regulates Burst Initiation and Frequency at Mossy Fiber-Granule Cell Synapses of Rat Cerebellum: Experimental Observations and Theoretical Predictions. *J. Neurophysiol.* **95**, 686–699 (2005).
70. Bologna, L. L. *et al.* Low-frequency stimulation enhances burst activity in cortical cultures during development. *Neuroscience* **165**, 692–704 (2010).
71. Pulizzi, R. *et al.* Brief wide-field photostimuli evoke and modulate oscillatory reverberating activity in cortical networks. *Sci. Rep.* **6**, 24701 (2016).

72. Penn, Y., Segal, M. & Moses, E. Network synchronization in hippocampal neurons. *Proc. Natl. Acad. Sci.* **113**, 3341–3346 (2016).
73. Shimon, M. & Beggs, J. M. Functional clusters, hubs, and communities in the cortical microconnectome. *Cereb. Cortex* **25**, 3743–3757 (2015).
74. Roxin, A., Rieke, H. & Solla, S. A. Self-sustained activity in a small-world network of excitable neurons. *Phys. Rev. Lett.* **92**, 198101–1 (2004).
75. Orlandi, J. G., Soriano, J., Alvarez-Lacalle, E., Teller, S. & Casademunt, J. Noise focusing and the emergence of coherent activity in neuronal cultures. *Nat. Phys.* **9**, 582–590 (2013).
76. Gross, G. W. & Kowalski, J. M. Origins of Activity Patterns in Self-Organizing Neuronal Networks in Vitro. *J. Intell. Mater. Syst. Struct.* **10**, 558–564 (1999).
77. Bullmore, E. & Sporns, O. Complex brain networks: Graph theoretical analysis of structural and functional systems. *Nat. Rev. Neurosci.* **10**, 186–198 (2009).
78. Eckmann, J. P., Jacobi, S., Marom, S., Moses, E. & Zbinden, C. Leader neurons in population bursts of 2D living neural networks. *New J. Phys.* **10**, 15011 (2008).
79. Michetti, C. *et al.* The PRRT2 knockout mouse recapitulates the neurological diseases associated with PRRT2 mutations. *Neurobiol. Dis.* **99**, 66–83 (2017).
80. Kunze, A., Giugliano, M., Valero, A. & Renaud, P. Micropatterning neural cell cultures in 3D with a multi-layered scaffold. *Biomaterials* **32**, 2088–2098 (2011).
81. Bosi, S. *et al.* From 2D to 3D: Novel nanostructured scaffolds to investigate signalling in reconstructed neuronal networks. *Sci. Rep.* **5**, 9562 (2015).
82. Severino, F. P. U. *et al.* The role of dimensionality in neuronal network dynamics. *Sci. Rep.* **6**, 29640 (2016).



# ***Chapter III - Basic concepts on retina physiology and function***

The aim of this chapter is to introduce some basic concepts on the physiological properties of the retinal circuit. In the first section the structure<sup>1</sup>, the cellular composition<sup>2</sup> and the functional wiring of retinal cells<sup>3,4</sup> are introduced to provide an anatomical overview of this sensory circuit. The second section focuses on the input-output capabilities of the retina by introducing the concepts of vertical and horizontal information processing<sup>5,6</sup> in this circuit. In the third section, I will shortly review the technological approaches<sup>7,8</sup> used to study the output spiking activity of the retina upon visual stimulation. Finally, in the last section, I will review the relevant literature on the study of horizontal interaction in modulating the response of retinal ganglion cells that I have explored in the second part of my Ph.D.

## ***Anatomical structure of the retina***

---

Visual perception starts from the eyes, where the retina transduces variation of light intensities into electrical signals, i.e., spike trains, which the brain processes to form a meaningful representation of the world<sup>1</sup>. The signal transduction that culminates in the spiking patterns conveyed by retinal ganglion cells (RGCs) to the brain represents the outcome of an early, yet complex, processing of information occurring at the network level<sup>35</sup> of the retinal circuit. To investigate how this process occurs several animal models have been used, such as primates, rabbits, cats, salamanders, turtles and mice. Each one of these animal models recapitulates some of the features of the human retinas. A first notable difference is the presence or not of the fovea, a small specialized structure located in the center of the retina that allows resolving fine details in the central part of the visual scene in day-light conditions<sup>9</sup>. Among mammals, the fovea is found only in primates retinas, while several species of birds have a double fovea to locate their preys with high accuracy. Indeed, as a result of a gain of function during evolution, the fovea is a region of the retina dedicated to high acuity tasks such as reading or detecting small remote targets. Conversely, the peripheral vision, i.e., the remaining part of the retina, is involved in the detection of large objects at distance or small objects but at a very close distance. Hence, the vision in animal models lacking fovea resembles the peripheral vision of primates. Specifically, in this study, we investigated the visual processing occurring in the mouse retina. Similarly to nonprimate mammal animals, the mouse retina does not have a fovea, however, its anatomical organization pairs the peripheral retina organization of primates<sup>10</sup>. Consequently, the results of our investigation can be faithfully interpreted in the context of peripheral vision of primates. Moreover, the mouse retina is tailored for vision in dim and low light condition<sup>10</sup> as a result of the

evolution in a dim environment. Hence, the stimulation protocol has to take into account this feature to probe the mouse retinal circuit with stimuli that, although artificial, have similar characteristics to the natural visual environment of a mouse. Importantly, also the internal organization of the mouse retina matches the primate retina as all of the principal primate retina interneurons are present also in mouse retinas<sup>11</sup>. In search of general principles underlying the encoding of visual scenes, in the next section, I report the anatomical characterization and general features of the retinal circuit shared among non-foveal mammals.

### *Layered structure of the retina*

The retina, despite its decentralized location, is part of the Central Nervous System (CNS)<sup>1</sup> and exhibits a well-organized network structure consisting of several layers of cells<sup>5,12</sup>, namely the photoreceptor, outer nuclear, outer plexiform, inner nuclear, inner-plexiform layers, that stratify one on top of another across the vertical spatial extension of the retina<sup>13</sup>. Each layer is readily detectable since it is composed of distinct constitutive cells<sup>14</sup> and wiring features<sup>14</sup>. Specifically, the plexiform layers are mostly innervated with neuronal processes whereas the remaining three layers contain cell bodies<sup>12</sup>. As shown in Fig 3.1, the constituent cellular elements of these layers<sup>10</sup> are:

- **Rods and cones**

Rods and cones populate the photoreceptor layer of the retina, with rods outnumbering the cones approximately more than twenty folds<sup>15</sup>. Rod and cones convert light stimuli into an electrical activity that is signaled downstream as a reduction of neurotransmitter release<sup>13</sup>. On the contrary, in the absence of light (e.g., in dark conditions) they spontaneously release neurotransmitters<sup>16</sup>. Specifically, the activation of photopigments as a consequence of light stimulation hyperpolarize these cells and prevent the release of neurotransmitters<sup>16</sup>. Rods and cones not only differ in their morphologies but also in functions: while rods primarily assist the vision in low luminance condition (scotopic regime), cones primarily assist with day-light vision (photopic regime)<sup>17</sup>. Rods are reported to be approximately 100 fold more sensitive than cones to single photons<sup>18,19</sup>. On the other hand, the temporal response of cones is significantly faster than the one of the rods<sup>13</sup>.

- **Horizontal cells**

These cells, whose soma is located in the inner nuclear layer<sup>20</sup>, mainly integrate the output of multiple photoreceptors horizontally and provide negative feedbacks to the photoreceptors and bipolar cells in the outer plexiform layer<sup>4</sup> (see below). Consequently, they are considered part of the outer retina from their functional role. Horizontal cells depolarize as a result of photoreceptors glutamate release, which occurs in the absence of light, and, in turn, induce hyperpolarization in the neighboring photoreceptors. Conversely, in light condition, the reduced neurotransmitter release of photoreceptors hyperpolarizes horizontal cells, resulting in photoreceptor depolarization<sup>12</sup>. Importantly, this continuous feedback determines a dynamical regulation of the photoreceptor activity that can support signal adjustments in the bright and dim environments<sup>21</sup>. Horizontal cells represent a minor fraction of the retinal interneurons (less than 5% in the inner retina)<sup>10</sup>.

- **Bipolar cells**

Bipolar cells transmit the signal of photoreceptors and horizontal cells to ganglion cells either directly or indirectly via the amacrine cells, and they provide the sole way to transmit the signal received from photoreceptors to downstream layers<sup>13</sup>. This population consists of two major types of bipolar cells: ON and OFF<sup>3</sup> that can have a transient or a sustained response<sup>20</sup>. During darkness, the release of neurotransmitters by photoreceptors determines an inhibitory effect on ON bipolar cells while it excites OFF bipolar cells. Differently, in light condition, the lack of neurotransmitter release suppresses the inhibition on ON bipolar cells and determines the firing of ON bipolar cells. At the same time, OFF bipolar cells become silent as a consequence of the removal of their excitatory drive<sup>22</sup>. Importantly, the ON/OFF pathway starts at the level of bipolar cells (cones form synaptic contacts with bipolar cells regardless of their type ON or OFF) and propagates downstream to the entire retina<sup>23</sup>. ON and OFF bipolar cells form synaptic contacts with retinal ganglion cells in specific locations of the inner plexiform layer: ON bipolar cells form synapses in the inner part of the inner plexiform layer whereas OFF bipolar cells in the outer one<sup>3</sup>. Furthermore, while the communication with photoreceptor is mediated by ionotropic receptors in OFF bipolar cells, ON bipolar cells integrate the signal through metabotropic receptors<sup>12</sup>. Importantly, although there are more than ten distinct bipolar cells connecting cones, it exists only a single type of bipolar cell receiving signals from the rod pathway<sup>24</sup>. Bipolar cells activity reflect a center-surround organization resulting from the direct innervation of the photoreceptors located on top of them<sup>3</sup>. The sustained or transient response of bipolar cells is ultimately determined by the desensitization recovery timescale of their receptors<sup>25</sup>.

- **Amacrine cells**

The population of amacrine cells includes a considerable number of different subtypes as a consequence of their dendritic morphology and stratification<sup>26</sup>. In general, these cells modulate the interaction of bipolar and ganglion cells through an inhibitory network extending horizontally<sup>27</sup>. Importantly, the functional role of this class of cells remains relatively poorly understood compared to the other mentioned populations of cells<sup>26</sup>. The extent of their dendritic arborizations defines the three primary populations of amacrine cells<sup>28</sup>, namely, narrow-field (about 70  $\mu\text{m}$  diameter), medium field (about 170  $\mu\text{m}$ ) and wide-field amacrine cells (350  $\mu\text{m}$ ). The different morphological structure indicates different potential functional roles<sup>27</sup>. The conformation of narrow-field amacrine cells mostly modulates the signal transmission locally and across distinct retinal layers<sup>29</sup>. These cells also form functional subunits within the receptive field of ganglion cells, thus suggesting a potential contribution in increasing visual acuity<sup>30</sup>. Conversely, wide-field amacrine cells span the entire retina, indicating a potential role of interaction within layers, rather than between layers<sup>26</sup>. Finally, medium-field amacrine cells have been shown to support the vertical communication pathway, even though their functional role is still largely unknown<sup>27</sup>. GABA and glycine neurotransmitters mediate the inhibitory effect of amacrine cells<sup>20</sup>. Additionally, a subclass of GABAergic amacrine cells modulates light adaptation and circadian rhythms through a diffuse release of dopamine<sup>26</sup>. Moreover, most

of the synaptic inputs integrated by ganglion cells are not direct connections from bipolar cells, rather indirect pathways having amacrine cells as signal regulators, i.e., bipolar – amacrine - ganglion cells<sup>3</sup>. Additionally, amacrine cells outnumber retinal ganglion cells more than ten folds<sup>22</sup>.

- **Retinal Ganglion Cells**

These cells end the signal processing of light in the retina and, consequently, represent the output neurons of the visual information from this circuit<sup>12</sup>. Importantly, they convert signals of bipolar and amacrine cells (which are for the most part graded potentials<sup>22</sup>) into a spike train representation. Like bipolar cells, also retinal ganglion cells are divided into several categories and subtypes<sup>12</sup>. The most extensive classification performed reported more than 30 distinct groups of these cells and was performed based on functional responses, morphological structures, and genetic signatures<sup>31</sup>. The top level of this hierarchical classification, however, reveals three major types of ganglion cells: ON, OFF and ON-OFF, as most of the other different subtypes descend from these three major classes. Each retinal ganglion cell is supposed to convey a distinct feature of the visual input as an output of the upstream circuit processing<sup>5</sup>. Retinal ganglion cells are arranged within the layer in a mosaic structure, with a different overlap of their receptive fields<sup>23</sup>.

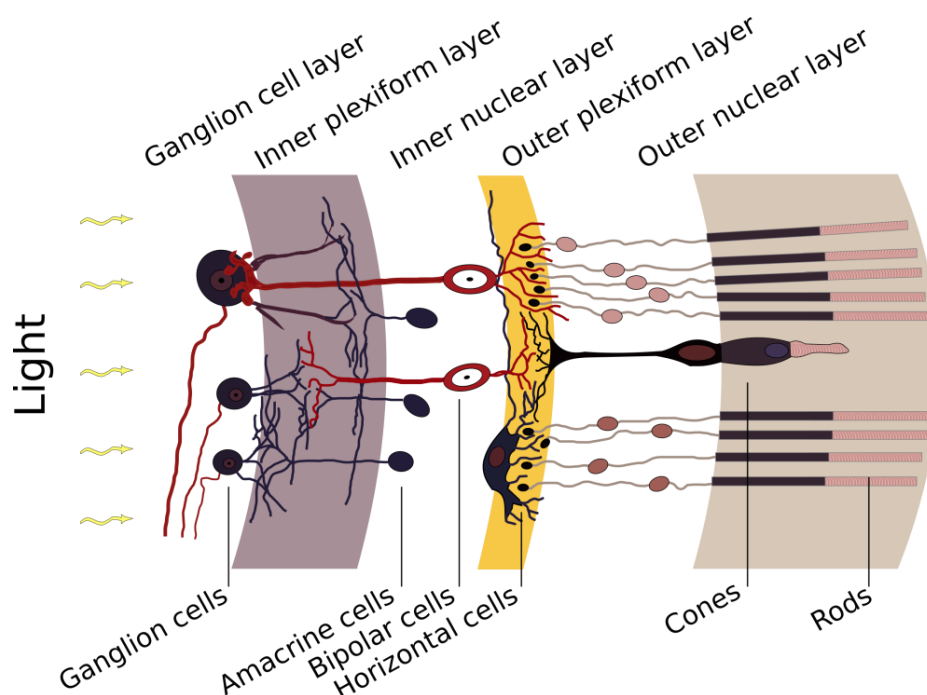


**Fig 3.1: Layered organization of the retinal circuit.** The retina has a well-defined laminar structure organized into layers: plexiform layers (inner and outer are dedicated to synaptic contacts while nuclear layers (inner and outer and ganglion cell layer contains cell bodies. Ganglion cells populate the ganglion cell layer, amacrine, bipolar and horizontal cell somas populate the inner nuclear layer while rods and cones are located into the outer nuclear layer. Image adapted from <https://commons.wikimedia.org/wiki/File:Retina-diagram.svg>, CC-BY-SA-3.0.



### *Phototransduction: from photoreceptors to ganglion cells*

As a consequence of absorption of photons that have traveled across the entire thickness of the retina (Fig 3.1), the photopigments in the outer part of the photoreceptors triggers a complex cascade of molecular reactions (phototransduction) that result in the light-modulation of the membrane potential of photoreceptors<sup>17</sup>. This electrical signal is then transferred to horizontal cells, providing feedback inhibition onto the photoreceptors and bipolar cells<sup>10</sup>. Bipolar cells receive two distinct antagonist inputs: while the photoreceptors excite (or inhibit) directly the bipolar cells, horizontal cells provide an averaged photoreceptor input that inhibits (or excite, respectively) the target bipolar cell<sup>32</sup>. Next, bipolar cells signal to ganglion and amacrine cells. In an oversimplified picture, the amacrine cell functionally regulates the signal transduction between bipolar and ganglion cells similarly to the one of the horizontal cells onto photoreceptors and bipolar cells<sup>1</sup>. Finally, ganglion cells terminate the signal transduction cascade by producing action potentials that are conveyed to the brain along with their axons<sup>7</sup>.

### *Synaptic communication among retinal cells*

Differently from other brain circuits, whose neurons predominantly generate digital-like spiking signals to convey information to post-synaptic neurons, only a few retinal cell types can fire action potentials. These cells are retinal ganglion cells and some subtypes of amacrine cells<sup>23,30</sup>. Most of the retinal neurons lack of well-defined and extended axonal processes except for retinal ganglion cells whose elongated axons, forming the optic nerve, ultimately convey the output of the retina to the dedicated brain areas<sup>12,20</sup>. Consequently, while the spike trains represent the neuronal code of the brain, locally graded and continuous signals mediate the coding and the interactions among retinal cells<sup>33</sup>. Retinal cells contact each other with either gap junctions or chemical synapses that reflect the layered structure<sup>23</sup>. Neighbouring retinal cells belonging to the same layer preferentially form gap junctions that allow bi-directional electrical couplings through direct contact with the cytosol of the cells<sup>4</sup>. Although this local interaction can exhibit different coupling strength in distinct layers, their ultimate function is to locally distribute the information in the layer as a result of the electrical correlation among contacted cells<sup>3</sup>. Depending on the layer, the outcome of this horizontal spatial integration of the visual information results in different processing mechanism as highlighted in the next section.

Conversely, cells of different layers mainly communicate through chemical synapses<sup>12</sup>. The canonical excitatory pathway transfers the signal from the photoreceptor to bipolar cells to ganglion cells in a feedforward manner<sup>32</sup>. Conversely, the inhibitory retinal neurons, i.e., horizontally and amacrine cells, indirectly transmit signals in a feedback fashion: horizontal cells onto photoreceptors<sup>21</sup> and amacrine on bipolar cells<sup>30</sup>.

## ***Input/output properties of the retina***

---

The retina is a self-standing brain circuit in the sense that the early processing of visual information occurs in the circuit itself, with minimal external modulations from other brain areas<sup>34</sup>.

The retina represents one of the most widely studied systems since the origins of neuroscience and this is because of several reasons. The first, and most obvious one concerns the functional importance of this circuit as a sensory transducer of external stimuli into meaningful spike trains for the brain<sup>5,35</sup>. Second, the ganglion cell spiking activity, i.e., the information received by the brain, can be easily recorded either intracellularly or extracellularly<sup>7</sup> thanks to their significantly higher size respect to the other retinal cells and their favorable position in the retinal circuit (a boundary layer)<sup>10</sup>. Third, the retina can be promptly stimulated with natural sensory inputs allowing direct correlation between its spiking activity and the visual stimulation<sup>1</sup>. This paradigm of investigation provided valuable knowledge concerning the correlation between the visual stimulus and the spiking activity of individual ganglion cells that are reported in this section.

It is nowadays clear that the task of the retina goes beyond a mere pre-filtering of the visual information from the world<sup>5</sup> as it is equipped with several circuits devoted to distinct tasks, including, but not limited to, motion detection<sup>36</sup>, contrast adaptation<sup>37</sup> and extrapolation and anticipation of the trajectory of a moving object<sup>38</sup>. Even in the absence of light, retinal cells are never silent as a consequence of the continuous release of neurotransmitters by photoreceptors. Hence, in steady light condition, a significant fraction of retinal ganglion cells is spontaneously active as a consequence of the intrinsic properties and the dynamical balance occurring upstream, even if no stimulus is presented. However, upon visual stimulation, patterns of spikes elicited by each ganglion cell can change significantly, even if remaining influenced by the state of the upstream network.

In general, retinal ganglion cells are most sensitive to light intensity variation occurring in a specific portion of the entire visual field, termed receptive field. On the other hand, extra-classical receptive field characterizes cells that upon stimulation onto their own receptive field are also sensitive to the distant features of the stimulus.

### ***Spatial feature extraction***

The response to light increments (or decrement) represents one of the most straightforward, yet intriguing, paradigms to understand the encoding process of visual information performed by the retina. Indeed, based on this paradigm it is straightforward to provide a first classification of the functional properties of retinal cells. Indeed, some cells respond preferentially to light increments (ON cells), while others to light decrements (OFF cells), thus defining two canonical pathways of processing. Additionally, ON and OFF retinal cells experience a considerable reduction or even suppression of the spiking activity upon application of the anti-preferred stimulus. Retinal cells that mostly exhibit these features are bipolar and ganglion cells. Importantly ON and OFF responses at the level of retinal ganglion cells are not symmetric: the ON pathway is more sensitive to increments and decrements of light (signaled as increments or decrements of spiking activity) than the OFF pathways<sup>39</sup>.

### *Centre-surround organization*

The internal organization of the receptive field further evidences the interplay between the ON and OFF pathways. Indeed, a small spot of light shined within the receptive field of a cell induces distinct types of activity depending on the position of the spot in the receptive field. Indeed, the receptive field exhibits a center-surround structure<sup>40</sup>: if the spot of light (dark) is placed in the center, it excites the target ON cell (OFF cell), whereas the stimulation in the periphery of the receptive field induces inhibition. Nevertheless, full-field stimulation induces a non-negligible response even though the surrounding part of the receptive field tends to inhibit the cell. All in all, the spatial organization of the receptive field indicates a preferred size, shape, and position of the stimulus to maximize the response of the cell<sup>41</sup>. However, the spatial tuning properties of these cells go beyond the simple sub-division of ON (OFF) center, and OFF (ON) surround: receptive fields can have a nonconcentric structure or cells can both respond to increments or decrements of light but still exhibiting a spatially defined receptive field. An essential consequence of the center-surround organization of the receptive fields is the capability of cells to detect edges separating strongly different contrasts. Indeed, the cells whose receptive field partially overlap with an edge of the image are significantly influenced by the image compared to the ones whose receptive field is entirely covered by a plain stimulus. In the best case scenario, i.e., an edge that separates the center and the surround, the preferred (anti-preferred) and anti-preferred (preferred) stimulus stimulate the center and the surround of the cell, thus enhancing the excitation (inhibition) respect to a full-field stimulus (depending on its polarity). Functionally, this spatial organization determines a higher accuracy to details since the cell is always comparing the center of the stimulus to the average information acquired by the surround.

### *Data compression*

Although the retinal circuit is constantly active even without the presence of visual stimulation, such as in dark conditions, ganglion cells very often do not respond to their preferred stimulus for its entire duration, but instead, they robustly respond at its onset. This behavior correlates with the intrinsic nature of the retina as a sensory transducer of the changing visual inputs. Indeed, as long as the stimulus is kept constant, the conveyed information is redundant and the circuit has already encoded the stimulus at its onset. In other words, it is generally considered that retinal ganglion cell transmit information about changing visual inputs, thus performing a temporal processing<sup>42</sup>. Although the fine time-scales of retinal ganglion cells responses are not uniform across the population, two major classes of temporal processing ganglion cells can be distinguished. These are transient and sustained ganglion cells. Transient ganglion cells fire in response to the preferred stimulus for less than 200ms, whereas sustained cells maintain a high firing rate for seconds after stimulus onset. This mimicking of this temporal processing occurring in the retina has been proven to be useful also for engineered video cameras. Specifically, by conveying information about changes rather than the stimulus itself, the speed of acquisition could be significantly increased as a result of the reduced amount of information to be transmitted<sup>43</sup>. Retinal ganglion cells produce highly reproducible spike trains in response to visual stimulation with low inter-trial variability<sup>44</sup>. This reliability and precision are functional for

temporal coding as latency related statistics are shown to convey significantly more visual information than spike counts in simple stimuli (flickering full-field contrasts<sup>44</sup> or square-wave gratings<sup>45</sup>). These considerations are even more relevant if one considers that all the transmission of visual information is intrinsically limited by the transmission capacity (or bandwidth) of the optic nerve<sup>13</sup>. However, in contrast to the idea of an optimal code, the receptive field of retinal ganglion cells often overlaps significantly across neighboring cells, thus resulting in redundant and correlated spike trains<sup>46</sup>. This spatially redundant information, largely resulting from electrical couplings in the inner retina<sup>47</sup>, however, is interestingly less redundant than the original image. This is because nonlinear interactions within the retina reduce spatial correlations<sup>48</sup>. Nevertheless, spatial correlations seem to be essential at the population level to correctly decoding natural scenes rather than the collective latency of response<sup>49</sup>. Hence, latency coding supports the rapid and efficient transmission of the information at the level of individual ganglion cells<sup>50,51</sup>, whereas decoding of complex visual stimuli benefits of the redundant information encoded at the population level<sup>52</sup>. It is also recognized that the retina processes visual information as a whole, in a highly distributed manner, by involving several task-specific circuits. For example, beyond the simple classification of ON-OFF cells, a considerable fraction of cells is devoted to the detection of specific features, such as motion<sup>53</sup>. The direction of a moving object (or of a global shift in the image) is reported by distinct classes of ON-OFF (four classes), ON (three classes) and OFF (one class) retinal ganglion cells. Other cells respond accurately to the differential motion respect to the background motion, to approaching objects and, finally, to rapid shifts of the image (saccade) through the suppression of the spiking activity in a few ganglion cells. Similar to the center-surround organization, each one of these cells responds vigorously to their preferred stimulus and are strongly inhibited by their anti-preferred stimulus. For instance, for a direction-selective cell, the preferred stimulus is motion in one direction, whereas the anti-preferred stimulus is motion in the opposite direction. Consequently, each retinal ganglion cells can encode two information at once, on the preferred and anti-preferred visual stimuli. For instance, motion sensitive retinal ganglion cells transmit the information of an object moving in the preferred direction by increasing their firing rate while the motion in the opposite direction is encoded as a significant decrease or total suppression of their firing rate.

### ***Techniques for population recordings of Retinal Ganglion Cells***

---

The process of formation of a meaningful image in the retina benefits of the correlations and timing-difference within spike-trains<sup>33</sup> of distinct retinal ganglion cell belonging to a given population, rather than from individual cells independently<sup>54</sup>. As for a digital picture on a screen, although each pixel is carrying information, the image is meaningful only if it observed in its entirety. Consequently, the desirable tool to study the encoding of visual information in the retina should allow simultaneous recordings of a significant fraction, ideally all, of the retinal ganglion cells spiking activity, knowing the input light stimuli. Among the different neuroethologies that were used to this aim, retina whole-mounts on multi-electrode arrays recordings are a fundamental methodology. Here, I will review these devices and I will report some of the major findings obtained so far by recording retinal ganglion cells on these devices.

### *Retina whole-mount recordings on Multi-Electrode Arrays (MEAs)*

Passive multi-electrode arrays coupled with a visual stimulator provide a suitable technology for recording visually-evoked retinal ganglion cell responses<sup>36</sup> although these conventional devices with a low-number of electrodes partially fulfill the requirements. These devices represented the turning point<sup>7</sup> for investigating visual information processing occurring in the retina as they provide simultaneously spatial and temporal details of the spiking activity of a considerable number of retinal ganglion cells in a fully functional, yet explanted, living tissue<sup>7</sup>. Indeed, the layered structure of the retina is particularly suitable for generating a good coupling with planar multi-electrode arrays<sup>55</sup> and consequently to record the extracellular potential of retinal ganglion cell contacting the electrode sites. Importantly, multi-electrode arrays can sense relatively high variations of the extracellular potential, ensuring the selectivity to signals coming from retinal ganglion cells<sup>56</sup>.

The information acquired with this approach combined with visual stimulation also allows the functional classification of cells<sup>57</sup>, the evaluation of their receptive fields<sup>55</sup> and of course the simultaneous monitoring of the spiking activity of different cell types<sup>58</sup>. Closed-loop stimulation further revealed nonlinear interactions among the subunits within the receptive field of retinal ganglion cells that can give rise to an increased sensitivity to small high-contrast details and, in a small population of ganglion cells, in an enhanced sensitivity to homogeneous visual scene<sup>59</sup>.

Importantly, the approach of using iso-response stimuli, i.e., the application of different stimuli that result in a similar response of an individual ganglion cell and defined as spike count or latency to first spike<sup>59</sup>, revealed that distinct visual inputs generate virtually indistinguishable statistics at the single neuronal level, which might be encoded by neighboring cells. This finding strongly supports the need for large-scale recording techniques to investigate the interplay between single responses and population coding.

The opportunity of monitoring at the same time the spiking activity of retinal ganglion cells has significantly advanced the knowledge of retinal processing: extensive classification of functional properties<sup>60</sup> and characterization of receptive fields<sup>61</sup> of retinal ganglion cells, sub-population of ganglion cells responding to periodic stimuli<sup>62</sup>, the anticipatory effect of motion<sup>38</sup>, the characterization of retinal waves<sup>63</sup>, the selectivity to differential motion between the center and the background<sup>64</sup>, the presence of ganglion cells that selectively respond to the reappearance of the same stimulus<sup>65</sup>. However, passive multi-electrode arrays have also drawbacks as the acquisition of an extracellular signal combined with the poor spatial sampling compared to the density of retinal ganglion cells. The dense electrode matrix provided a promising strategy to record nearly all retinal ganglion cells over a small patch of retina<sup>66,67</sup>. While passive devices are nowadays widely used, active multi-electrode arrays represent still a novelty in the field, with a few groups exploiting high-density technology that allows to cover up the retinal ganglion cell layer with a dense grid of electrodes<sup>68,69</sup> to significantly improve the spatial sampling of the retinal output<sup>8,57,68</sup> or the available recording area<sup>69</sup>. From the computational point of view, the increased spatial and temporal sampling required new sorting techniques to extrapolate the redundant information captured by neighboring electrodes<sup>66</sup> and to refine the individual ganglion cell detection<sup>70-72</sup>. High-content movies of a large fraction of retinal ganglion cells pose other

computational limitations such as handling a high volume of data and extracting relevant information out of the recordings in a reasonable amount of time (less than a working day).

### ***Local and long-range horizontal interactions shape the response of retinal ganglion cells***

---

An individual ganglion cell collects up to hundreds of inputs from bipolar cells<sup>73</sup> that themselves receive inputs from a large pool of photoreceptors<sup>3</sup>. This converging pathway of information was largely investigated to understand the specific cascade of processing that gives rise to the extraction of complex features of the visual stimulus.

The first evident consequence of this funnel-like wiring architecture is the concept of receptive field, i.e., the area of the visual space that directly influences the activity of cell upon stimulus presentation. Bipolar cells have a receptive field as a result of the connections to photoreceptors and, similarly, the convergence of multiple bipolar inputs onto a ganglion cell determine a receptive field that also inherits the features of the receptive field of bipolar cells. Historically, early quantification of the spiking activity recorded from the optic nerve revealed a correlation between the size and the intensity of a stimulus presented in the ganglion cell receptive field in triggering a response. Larger stimuli required less luminance intensity to elicit a response suggesting that encoding of visual information resulting from the integration of a pool of inputs coming from different locations<sup>41,85</sup>. However, the linear converging processing that is here described is an extremely oversimplification of the spatial integration of visual stimuli within the receptive field center. Indeed, the convergent processing is also modulated by inhibitory connections that mediate the interaction between photoreceptors and bipolar cells and bipolar cells and ganglion cells through horizontal and amacrine cells respectively. These cells provide both local and global inhibition. Locally, they regulate the activity of bipolar cells. Globally, they allow lateral transfer of information across the retina.

A seminal work<sup>76</sup> revealed signs of these non-linear transformations in the response of different cat retinal ganglion cells upon presentation of white/black reversing gratings of different spatial phases. The recorded retinal ganglion cells could be divided into two macroscopic classes based on their responses to the grating reversal. Linear cells, termed X cells, transiently increased their firing rate upon application of their preferred contrast in their receptive field, while the anti-preferred stimulus determined a significant decrease in their firing rate. Importantly, excitation can balance inhibition for some spatial phases of the gratings, resulting in a negligible effect on the spiking response. Conversely, non-linear cells, named Y cells, increased their firing rate regardless of the polarity of the stimulus, i.e., at each stimulus reversal, regardless of the spatial phase of the grating.

Several studies further characterized the properties of the receptive field center<sup>77-79</sup> and their consequences on spatial integration<sup>5,59,80</sup>, which is not limited to the center, but also include the surround. The surround part of the receptive field of retinal ganglion cells has received an increasing attention<sup>48,81,82</sup>. The simple model of the center-surround organization as linear filtering do not always capture the modulation induced by the surround part of the receptive field as some stimuli activate the surround in a highly-nonlinear manner<sup>81</sup>. The surround part indeed, besides

providing a term of reference for the center, is involved in specialized tasks, such as regulating the sensibility to center signals while objects are moving in the surround<sup>83</sup> and, hence, in the detection of local versus global motion<sup>64,84</sup>. Interestingly, remote stimulation, i.e., visual stimulation applied considerably far away from the receptive field of retinal ganglion cells, influence the spiking activity of retinal ganglion cells in several manners. In the cat retina, a widely and historically used animal model for retinal studies, gratings shifting in the remote periphery of a selected ganglion cells induce vigorous and time-locked with the grating shift responses<sup>85–87</sup> that cannot be explained by the classical organization of their receptive field<sup>88</sup>. This phenomenon, termed ‘peripheral’ or ‘shift’ effect, has been observed in retina of several species including cats<sup>88</sup>, monkeys<sup>89</sup>, rabbit<sup>90</sup> and salamander<sup>91</sup>.

Historically, several experimental works reported examples of long-range lateral flows of information, termed periphery effect, within the retina. For instance, the presence of a stimulus far outside the classical notion of the receptive field could modulate the sensitivity and in turn the spiking activity of monkey retinal ganglion cells<sup>89</sup>. The continuous motion of grating located far away from the receptive field of a ganglion cell gave rise to an increase in the firing of the cell<sup>85</sup> or a decrease<sup>92</sup>, while sudden remote motions induced a transient response consisting in a burst of spikes<sup>86,93</sup>. The increase or decrease in the retinal ganglion cell spiking activity has been associated with the spatiotemporal features of the remote stimulus pattern, thus suggesting the activation of both excitatory and inhibitory pathways<sup>88</sup>. The stimulation of the receptive field surround of retinal ganglion cells in salamander retinas, indeed, revealed a complex nonlinear spatial integration of the stimulus<sup>81</sup> that resulted from a sub-unit organization of the receptive field surround, where each sub-unit was characterized by a center-surround architecture. The simultaneous monitoring of the retinal output provided by the full exploitation of multi-electrode arrays, indeed, revealed also that a moving object determined the pre-activation of the ganglion cells to anticipate the future location of the object, thus minimizing the latency of response for downstream processing<sup>38</sup>.

Conversely, the sudden reversal of motion direction determined the synchronous firing of a large population of retinal ganglion cells, which possibly encoded the radical reversal at the population level<sup>94</sup>. The mechanism underlying this phenomenon was proven to occur at the level of bipolar cells, with a negligible contribution of amacrine cells. Additionally, when an object is moving, such as when stimulating the remote periphery with a randomly moving dark bar, several OFF retinal ganglion cells synchronize their spiking activity<sup>95</sup>. Peripheral inhibition also shapes the activity of ganglion cells devoted to object motion to minimize predictable input induced by fixational movements, thus enhancing the detection of objects differentially moving respect to the background<sup>64</sup>.

Stimulation in the remote periphery is not limited to modulation of the spiking activity of ganglion cells<sup>96</sup> but also has consequences on the neural coding of local stimuli<sup>82</sup>. Specifically, remote stimulation enhance retinal ganglion cell responses to local stimulation up to 1 mm increasing the sensibility to a broader range of contrasts suggesting a built-in mechanism of attention<sup>91</sup>.

Given the highly organized retinal anatomy<sup>13</sup>, the possible pathways of horizontal communication are represented by horizontal and amacrine cells<sup>12</sup>. However, while the first class

of cells is mostly devoted to the local regulation of the input, amacrine cells can have functional roles both locally or at long ranges depending on their sub-types, their morphology and horizontal extension. Furthermore, amacrine cells can form extensive networks among each other and tend to correlate the spiking activity of their target retinal ganglion cells<sup>22,47</sup>. Wide-field amacrine cells can innervate the inner plexiform layer with dendrites extending for millimeters<sup>3</sup>. Hence, their morphology suggests that long-range interaction within the retina might be more crucial in shaping the response of retinal ganglion cells than what was recognized so far. Additionally, inhibitory amacrine cells are known to spread laterally visual information inducing an excitatory effect on retinal ganglion cells as a consequence of synaptic disinhibition<sup>88</sup>. Amacrine cells are also involved in temporal processing providing the necessary inhibition to sharpen transient responses<sup>36</sup>.

Overall, the functional relevance of long-range horizontal interactions within the retina, however, remains still unclear and deserves further studies.



## Bibliography

---

1. Purves, D. Vision. in *Handbook of Neuroscience for the Behavioral Sciences* (John Wiley & Sons, Inc., 2009). doi:10.1002/9780470478509.neubb001012
2. Masland, R. H. Neuronal diversity in the retina. *Curr. Opin. Neurobiol.* **11**, 431–436 (2001).
3. Wässle, H. Parallel processing in the mammalian retina. *Nat. Rev. Neurosci.* **5**, 747–757 (2004).
4. Demb, J. B. & Singer, J. H. Functional Circuitry of the Retina. *Annu. Rev. Vis. Sci.* **1**, 263–289 (2015).
5. Gollisch, T. & Meister, M. Eye Smarter than Scientists Believed: Neural Computations in Circuits of the Retina. *Neuron* **65**, 150–164 (2010).
6. Gollisch, T. Features and functions of nonlinear spatial integration by retinal ganglion cells. *J. Physiol. Paris* **107**, 338–348 (2013).
7. Litke, A. & Meister, M. The retinal readout array. *Nucl. Inst. Methods Phys. Res. A* **310**, 389–394 (1991).
8. Li, P. H. *et al.* Anatomical Identification of Extracellularly Recorded Cells in Large-Scale Multielectrode Recordings. *J. Neurosci.* **35**, 4663–4675 (2015).
9. Perry, V. H. & Cowey, A. The ganglion cell and cone distributions in the monkey's retina: Implications for central magnification factors. *Vision Res.* **25**, 1795–1810 (1985).
10. Jeon, C. J., Strettoi, E. & Masland, R. H. The major cell populations of the mouse retina. *J. Neurosci.* **18**, 8936–8946 (1998).
11. Huberman, A. D. & Niell, C. M. What can mice tell us about how vision works? *Trends Neurosci.* **34**, 464–473 (2011).
12. Masland, R. H. The Neuronal Organization of the Retina. *Neuron* **76**, 266–280 (2012).
13. Kandel, E. R., James H. Schwartz & Thomas M. Jessell. *Principles of Neural Science. Neurology* **3**, (2000).
14. Masland, R. H. Neuronal diversity in the retina. *Curr. Opin. Neurobiol.* **11**, 431–436 (2001).
15. Carter-Dawson, L. D. & Lavail, M. M. Rods and cones in the mouse retina. I. Structural analysis using light and electron microscopy. *J. Comp. Neurol.* **188**, 245–262 (1979).
16. Fu, Y. & Yau, K. W. Phototransduction in mouse rods and cones. *Pflugers Arch. Eur. J. Physiol.* **454**, 805–819 (2007).
17. SUGITA, Y. & TASAKI, K. The activation of cones in scotopic and rods in photopic vision. *Tohoku J. Exp. Med.* **156**, 311–317 (1988).
18. Okawa, H. & Sampath, A. P. Optimization of Single-Photon Response Transmission at the Rod-to-Rod Bipolar Synapse. *Physiology* **22**, 279–286 (2007).
19. Baylor, B. Y. D. A., Lamb, T. D. & Yau, K. Responses of Retinal Rods To Single Photons. *J. Physiol.* **288**, 613–634 (1979).
20. Kaneko, A. Physiological and morphological identification of horizontal, bipolar and amacrine cells in goldfish retina. *J. Physiol.* **207**, 623–633 (1970).
21. Kamermans, M., Kraaij, D. & Spekrijse, H. The dynamic characteristics of the feedback signal from horizontal cells to cones in the goldfish retina. *J. Physiol.* **534**, 489–500 (2001).
22. Azeredo da Silveira, R. & Roska, B. Cell Types, Circuits, Computation. *Current Opinion in Neurobiology* **21**, 664–671 (2011).
23. Masland, R. H. The fundamental plan of the retina. *Nat. Neurosci.* **4**, 877–886 (2001).
24. Bloomfield, S. A. & Dacheux, R. F. Rod vision: Pathways and processing in the mammalian retina. *Prog. Retin. Eye Res.* **20**, 351–384 (2001).
25. Awatramani, G. B. and M. M. S. Origin of Transient and Sustained Responses in Ganglion Cells of the Retina. *J. Neurosci.* **20**, 7087–7095 (2000).
26. MASLAND, R. H. The tasks of amacrine cells. *Vis. Neurosci.* **29**, 3–9 (2012).
27. Franke, K. & Baden, T. General features of inhibition in the inner retina. *J. Physiol.* **595**, 5507–5515 (2017).
28. Balasubramanian, R. & Gan, L. Development of Retinal Amacrine Cells and Their Dendritic Stratification. *Curr. Ophthalmol. Rep.* **2**, 100–106 (2014).
29. Marc, R. E., Anderson, J. R., Jones, B. W., Sigulinsky, C. L. & Lauritzen, J. S. The All amacrine cell

- connectome: a dense network hub. *Front. Neural Circuits* **8**, 104 (2014).
30. Kolb, H. *Roles of Amacrine Cells. Webvision The Organization of the Retina and Visual System* (2005).
  31. Franke, K. *et al.* Balanced excitation and inhibition decorrelates visual feature representation in the mammalian inner retina. *bioRxiv* **542**, 40642 (2016).
  32. Euler, T., Haverkamp, S., Schubert, T. & Baden, T. Retinal bipolar cells: Elementary building blocks of vision. *Nat. Rev. Neurosci.* **15**, 507–519 (2014).
  33. Field, G. D. & Chichilnisky, E. J. Information Processing in the Primate Retina: Circuitry and Coding. *Annu. Rev. Neurosci.* **30**, 1–30 (2007).
  34. Zucker, C. L. & Dowling, J. E. Centrifugal fibres synapse on dopaminergic interplexiform cells in the teleost retina. *Nature* **330**, 166–8 (1987).
  35. Meister, M. & Berry, M. J. The neural code of the retina. *Neuron* **22**, 435–450 (1999).
  36. Nirenberg, S. & Meister, M. The light response of retinal ganglion cells is truncated by a displaced amacrine circuit. *Neuron* **18**, 637–650 (1997).
  37. Garvert, M. M. & Gollisch, T. Local and global contrast adaptation in retinal ganglion cells. *Neuron* **77**, 915–928 (2013).
  38. Berry, M. J., Brivanlou, I. H., Jordan, T. A. & Meister, M. Anticipation of moving stimuli by the retina. *Nature* **398**, 334–338 (1999).
  39. Chichilnisky, E. J. & Kalmar, R. S. Functional asymmetries in ON and OFF ganglion cells of primate retina. *J. Neurosci.* **22**, 2737–2747 (2002).
  40. Harley, C. M., Rossi, M., Cienfuegos, J. & Wagenaar, D. Discontinuous locomotion and prey sensing in the leech. *J. Exp. Biol.* **216**, 1890–1897 (2013).
  41. Barlow, H. B. Summation and inhibition in the frog’s retina. *J. Physiol.* **119**, 69–88 (1953).
  42. Hosoya, T., Baccus, S. A. & Meister, M. Dynamic predictive coding by the retina. *Nature* **436**, 71–77 (2005).
  43. Gallego, G. *et al.* Event-based, 6-DOF Camera Tracking for High-Speed Applications. (2016).
  44. Berry, M. J., Warland, D. K. & Meister, M. The structure and precision of retinal spike trains. *Proc. Natl. Acad. Sci.* **94**, 5411–5416 (1997).
  45. Portelli, G. *et al.* Rank Order Coding: a Retinal Information Decoding Strategy Revealed by Large-Scale Multielectrode Array Retinal Recordings. *eNeuro* **3**, (2016).
  46. Meister, M. Multineuronal codes in retinal signaling. *Proc. Natl. Acad. Sci.* **93**, 609–614 (1996).
  47. Brivanlou, I.H., D.K. Warland and M. Meister. Mechanisms of concerted signalling among retinal ganglion cells. *Neuron* **20**, 527–539 (1998).
  48. Pitkow, X. & Meister, M. Decorrelation and efficient coding by retinal ganglion cells. *Nat. Neurosci.* **15**, 628–635 (2012).
  49. Onken, A. *et al.* Using Matrix and Tensor Factorizations for the Single-Trial Analysis of Population Spike Trains. *PLoS Comput. Biol.* **12**, e1005189 (2016).
  50. Gollisch, T. & Meister, M. Rapid Neural Coding in the Retina with Relative Spike Latencies. *Science* (80-. ). **319**, 1108–1111 (2008).
  51. Gütig, R., Gollisch, T., Sompolinsky, H. & Meister, M. Computing Complex Visual Features with Retinal Spike Times. *PLoS One* **8**, e53063 (2013).
  52. Puchalla, J. L., Schneidman, E., Harris, R. A. & Berry, M. J. Redundancy in the population code of the retina. *Neuron* **46**, 493–504 (2005).
  53. Hosoya, T., Baccus, S. A. & Meister, M. Dynamic predictive coding by the retina. *Nature* **436**, 71–77 (2005).
  54. Segev, R. Functional Organization of Ganglion Cells in the Salamander Retina. *J. Neurophysiol.* **95**, 2277–2292 (2005).
  55. Meister, M., Pine, J. & Baylor, D. A. Multi-neuronal signals from the retina: acquisition and analysis. *J. Neurosci. Methods* **51**, 95–106 (1994).
  56. Masland, R. H. Processing and encoding of visual information in the retina. *Curr. Opin. Neurobiol.* **6**, 467–474 (1996).
  57. Fiscella, M. *et al.* Recording from defined populations of retinal ganglion cells using a high-density CMOS-integrated microelectrode array with real-time switchable electrode selection. *J. Neurosci.*

- Methods* **211**, 103–113 (2012).
58. Marre, O. *et al.* Mapping a Complete Neural Population in the Retina. *J. Neurosci.* **32**, 14859–14873 (2012).
  59. Bölinger, D. & Gollisch, T. Closed-Loop Measurements of Iso-Response Stimuli Reveal Dynamic Nonlinear Stimulus Integration in the Retina. *Neuron* **73**, 333–346 (2012).
  60. Chichilnisky, E. J. A simple white noise analysis of neuronal light responses. *Netw. Comput. Neural Syst.* **12**, 199–213 (2001).
  61. Shlens, J. *et al.* The Structure of Large-Scale Synchronized Firing in Primate Retina. *J. Neurosci.* **29**, 5022–5031 (2009).
  62. Schwartz, G., Harris, R., Shrom, D. & Berry, M. J. Detection and prediction of periodic patterns by the retina. *Nat. Neurosci.* **10**, 552–554 (2007).
  63. Maccione, A. *et al.* Following the ontogeny of retinal waves: pan-retinal recordings of population dynamics in the neonatal mouse. *J. Physiol.* **592**, 1545–1563 (2014).
  64. Ölveczky, B. P., Baccus, S. A. & Meister, M. Segregation of object and background motion in the retina. *Nature* **423**, 401–408 (2003).
  65. Krishnamoorthy, V., Weick, M. & Gollisch, T. Sensitivity to image recurrence across eye-movement-like image transitions through local serial inhibition in the retina. *Elife* **6**, E2391-2398 (2017).
  66. Segev, R., Goodhouse, J., Puchalla, J. & Berry, M. J. Recording spikes from a large fraction of the ganglion cells in a retinal patch. *Nat. Neurosci.* **7**, 1154–1161 (2004).
  67. Shlens, J. *et al.* The Structure of Multi-Neuron Firing Patterns in Primate Retina. *J. Neurosci.* **26**, 8254–8266 (2006).
  68. Obien, M. E. J., Deligkaris, K., Bullmann, T., Bakkum, D. J. & Frey, U. *Revealing neuronal function through microelectrode array recordings.* *Frontiers in Neuroscience* **9**, 423 (2015).
  69. Berdondini, L. *et al.* Active pixel sensor array for high spatio-temporal resolution electrophysiological recordings from single cell to large scale neuronal networks. *Lab Chip* **9**, 2644 (2009).
  70. Hilgen, G. *et al.* Unsupervised Spike Sorting for Large-Scale, High-Density Multielectrode Arrays. *Cell Rep.* **18**, 2521–2532 (2017).
  71. Yger, P., Spampinato, G. L. B. & Esposito, E. Fast and accurate spike sorting in vitro and in vivo for up to thousands of electrodes. *bioRxiv* 1–21 (2016). doi:10.1101/067843
  72. Lefebvre, B., Yger, P. & Marre, O. Recent progress in multi-electrode spike sorting methods. *J. Physiol. Paris* **110**, 327–335 (2016).
  73. Freed, M. a & Sterling, P. The ON-alpha ganglion cell of the cat retina and its presynaptic cell types. *J. Neurosci.* **8**, 2303–2320 (1988).
  74. Hartline, H. *The response of single optic nerve fibers of the vertebrate eye to illumination of the retina.* *American Journal of Physiology* **121**, (American Physiological Society, 1938).
  75. A, T. & Gadzella, B. *American Journal of. American Journal of Physiology -- Legacy Content* **2**, (American Physiological Society, 2006).
  76. Enroth-Cugell, C. & Robson, J. G. The contrast sensitivity of retinal ganglion cells of the cat. *J. Physiol.* **187**, 517–552 (1966).
  77. Enroth-Cugell, C. & Freeman, A. W. The receptive-field spatial structure of cat retinal Y cells. *J. Physiol.* **384**, 49–79 (1987).
  78. Hochstein, S. & Shapley, R. M. Linear and nonlinear spatial subunits in Y cat retinal ganglion cells. *J. Physiol.* **262**, 265–284 (1976).
  79. Victor, J. D. & Shapley, R. M. The nonlinear pathway of Y ganglion cells in the cat retina. *J. Gen. Physiol.* **74**, 671–689 (1979).
  80. Schwartz, G. & Rieke, F. Nonlinear spatial encoding by retinal ganglion cells: when  $1 + 1 \neq 2$ . *J. Gen. Physiol.* **138**, 283–290 (2011).
  81. Takeshita, D. & Gollisch, T. Nonlinear Spatial Integration in the Receptive Field Surround of Retinal Ganglion Cells. *J. Neurosci.* **34**, 7548–7561 (2014).
  82. Passaglia, C. L., Freeman, D. K. & Troy, J. B. Effects of Remote Stimulation on the Modulated Activity of Cat Retinal Ganglion Cells. *J. Neurosci.* **29**, 2467–2476 (2009).
  83. Roska, B. & Werblin, F. Rapid global shifts in natural scenes block spiking in specific ganglion cell

- types. *Nat. Neurosci.* **6**, 600–608 (2003).
84. Kuhn, N. K. & Gollisch, T. Joint Encoding of Object Motion and Motion Direction in the Salamander Retina. *J. Neurosci.* **36**, 12203–12216 (2016).
  85. Fischer, B., Kruger, J. & Droll, W. *Quantitative aspects of the shift-effect in cat retinal ganglion cells.* *Brain Res* **83**, 391–403 (1975).
  86. Derrington, A. M., Lennie, P. & Wright, M. J. The mechanism of peripherally evoked responses in retinal ganglion cells. *J. Physiol.* **289**, 299–310 (1979).
  87. McIlwain, J. T. Receptive fields of optic tract axons and lateral geniculate cells Peripheral extend and barbiturate sensitivity. *J. Neurophysiol.* **27**, 1154–1173 (1964).
  88. Barlow, H. B., Derrington, A. M., Harris, L. R. & Lennie, P. The effects of remote retinal stimulation on the responses of cat retinal ganglion cells. *J. Physiol.* **269**, 177–194 (1977).
  89. Krüger, J., Fischer, B. & Barth, R. The shift-effect in retinal ganglion cells of the rhesus monkey. *Exp. Brain Res.* **23**, 443–446 (1975).
  90. Watanabe, J. & Tasaki, K. Shift-effect in the rabbit retinal ganglion cells. *Brain Res.* **181**, 198–201 (1980).
  91. Jazdzinsky, P. D. & Baccus, S. A. Synchronized amplification of local information transmission by peripheral retinal input. *Elife* **4**, (2015).
  92. Enroth-Cugell, C. & Jakiela, H. G. Suppression of cat retinal ganglion cell responses by moving patterns. *J. Physiol.* **302**, 49–72 (1980).
  93. Barlow, H. B., Derrington, A. M., Harris, L. R. & Lennie, P. The effects of remote retinal stimulation on the responses of cat retinal ganglion cells. *J. Physiol.* **269**, 177–194 (1977).
  94. Schwartz, G., Taylor, S., Fisher, C., Harris, R. & Berry, M. J. Synchronized Firing among Retinal Ganglion Cells Signals Motion Reversal. *Neuron* **55**, 958–969 (2007).
  95. Deny, S. *et al.* Multiplexed computations in retinal ganglion cells of a single type. *bioRxiv* (2016). doi:10.1101/080135
  96. Passaglia, C. L., Freeman, D. K. & Troy, J. B. Effects of Remote Stimulation on the Modulated Activity of Cat Retinal Ganglion Cells. *J. Neurosci.* **29**, 2467–2476 (2009).

# ***Chapter IV - Development and application of data analysis tools for large-scale retinal ganglion cells recordings on CMOS-MEAs***

The analysis of the spiking activity recorded from a large number of retinal ganglion cells (RGCs) that can be obtained with high-resolution CMOS-MEAs imposes an important computational effort. This includes the pre-processing of the raw data that consists in the detection of spikes, the sorting of the spikes to allocate them to single-units, the identification of functional types of retinal ganglion cells (RGCs) and of their receptive fields. To overcome the significant effort of human supervision determined by the usage of algorithms non-optimized for large-scale recordings, in this part of my work I have integrated an automated chain of analysis capable of pre-processing the 4096-electrode's raw data. This development was crucial to accelerate the analysis and to proceed faster in the experimental investigation of data acquired from multiple retinas. The implemented suite of computational tools allowed reducing the analysis time from approximately, a week of continuous supervision (for a single retina) to 24h of unsupervised analysis with algorithms running in parallel on a small multicore cluster (48 CPUs) available in our laboratory.

## ***Experimental platform***

---

To perform experiments with visual stimulation of ex-vivo mice retina and high-resolution CMOS-MEA recordings, we used a setup that was developed in my laboratory during the RENVISION EC-funded project<sup>1</sup>. The experimental setup<sup>1-4</sup> records the extracellular spiking activity of retinal ganglion cells while stimulating the photoreceptor layer through the presentation of visual images, see Fig 4.1A. To fulfill this task, it integrates three principal components: a digital light projector (DLP LightCrafter Evaluation Module<sup>5</sup>, Texas Instruments), the optical pathway and the CMOS-MEA recording system (a custom Biocam prototype developed using 3Brain components). Visual stimuli are image sequences that are projected on the retina using the DLP projector and that are collimated by the optical pathway on a retina lying on the electrode array of our recording system, see Fig 4.1B. The optical pathway was designed to correct light aberrations and to focus images of 664x664 pixels on the retina. Each pixel approximately spans a  $4 \times 4 \mu\text{m}^2$  square. All the mentioned parts are fully adjustable through micromanipulators to correct the collimation and alignment of the visual stimuli. Additionally, an external camera integrated into the optical pathway using a dichroic mirror allows the monitoring of the visual stimulation during the experiment. Fig 4.1C shows a picture of the experimental setup described so far.

In addition, the light provided by the projector was attenuated through a series of neutral density filters (ND 6) to obtain a final luminance of  $0.11 \text{ cd/m}^2$ , which is in the range of mesopic light levels<sup>6–8</sup>. Under this luminance condition, which represents a physiological condition for mice, information about the visual scene is sensed in the retina by both rods and the cones<sup>9–11</sup>. The luminance contrast was quantified through the Michelson contrast convention. Specifically, we defined the contrast of the stimulus as  $100 \cdot (I_{\max} - I_{\min}) / (I_{\max} + I_{\min})$ , where  $I_{\max}$  and  $I_{\min}$  are respectively the maximum and minimum luminance of the darker/brighter luminance and 100 is a constant multiplier used to obtain values in the range (0-100). In the following sections of this work, we will refer to the luminance contrast of the stimuli as CT, followed by the value obtained in the formula above (e.g., CT25, CT50, CT75, and CT100 as used in our experiments).

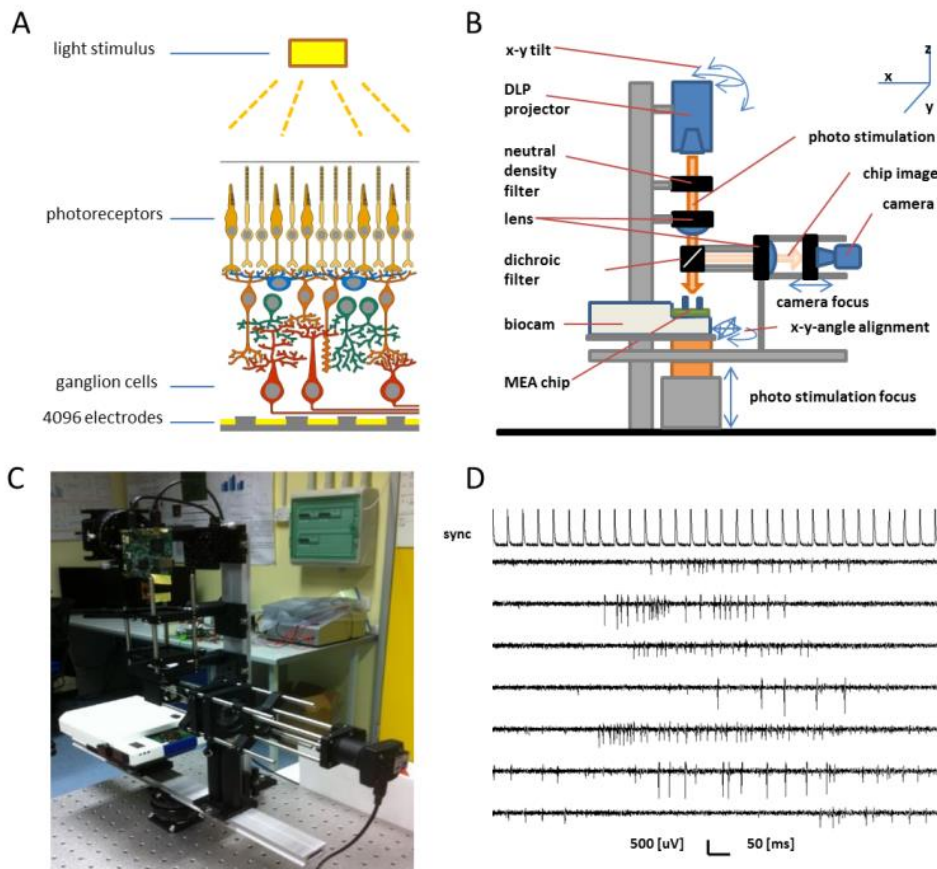


**Fig 4.1: Description of the experimental setup.** (A) The photoreceptors are stimulated by a light source (in our case a DLP projector), and the extracellular potential variations induced by the spiking activity of retinal ganglion cells are recorded by a CMOS-MEA featuring 4096 electrodes. (B) The images generated by the projector are collimated on the retina by a series of lenses that focus and correct for aberration the visual stimulus. An external camera, integrated into the optical pathway allows the monitoring of the stimulus projected onto the retina. The optical pathway and the different parts of the setup are equipped with micromanipulator to adjust and calibrate the visual projecting system. (C) A representative picture of the setup sketched in (B). (D) An illustrative raw data recorded showing several spikes in different units and the sync channel, which carries the information to align the visual stimulation to the raw data: every time a new image is presented, a positive trigger signal is recorded by the BioCam system (sync channel). Image credit: Alessandro Maccione and Stefano Di Marco.

Importantly, in order to analyze light-evoked responses we had to develop a solution to record the time stamps of the projected images with the RGCs activity. In order to synchronize at a sub-millisecond resolution the presentation of the images and recordings of the activity, we used a custom built device that reads the image stream from the display output and that generates a trigger every time a new image is projected (in the example of Fig 4.1D, one trigger every 33ms).

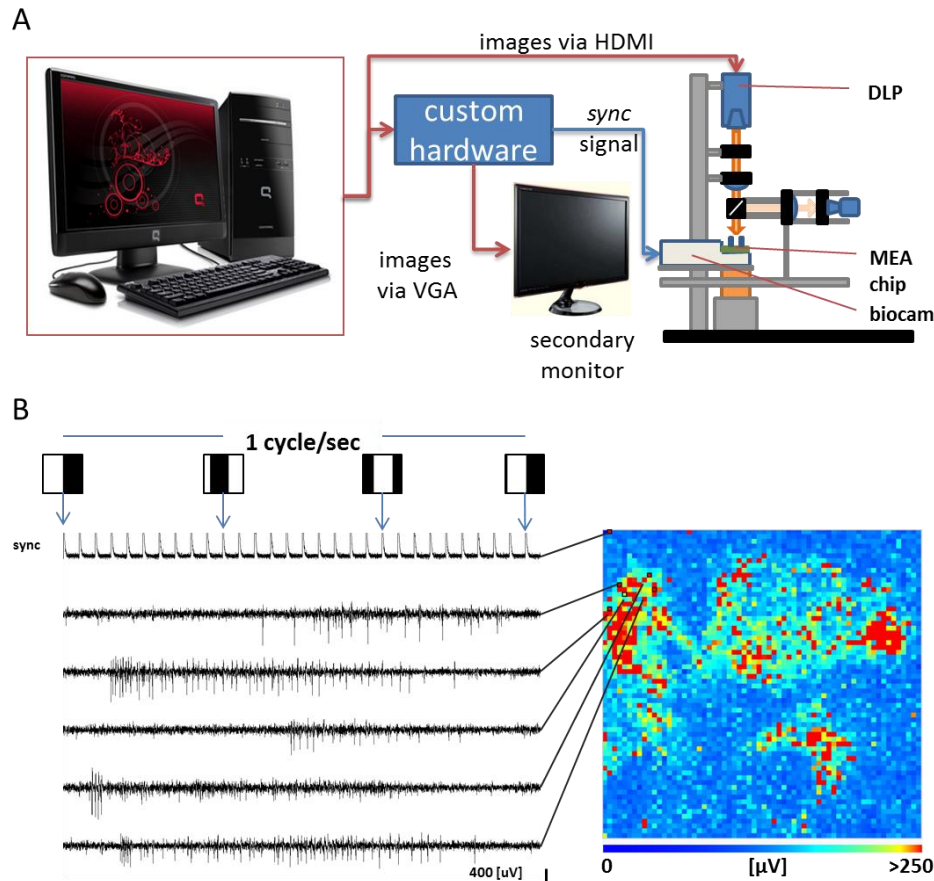


**Fig 4.2: Alignment of visual stimuli and raw data of light-evoked RGCs responses.** (A) The HDMI output of the computer generating visual stimuli splits into two pathways. The first one feeds the DLP projector whereas the second one is processed by custom hardware to generate a trigger that is sent to the Biocam system and can be read as an electrode channel. (B) After the realignment of the images with the recorded time-stamps, it is possible to correlate the extracellular activity recorded by the CMOS-MEA electrodes and the stimulus. In this illustrative example, bars drifting at the temporal frequency of 1Hz elicited responses of retinal ganglion cells with different onset timings based on the RGCs location and preferred stimulus of the cells. Image credit: Alessandro Maccione and Stefano Di Marco.

These time-stamps of the projected images are then recorded by the BioCam system and are sampled on an auxiliary electrode channel together with the extracellular signals recorded on the other electrodes, see

Fig 4.2A. In this way, at the end of each experiment, the information about the visual stimuli (i.e., which stimulus was presented and when) and the recorded activity are available for analysis. The off-line alignment of the visual images allows appreciating the spiking activity elicited by different

stimuli, as shown in Fig 4.2B. In the latter example, the presentation of square-wave bars drifting at the temporal frequency of 1Hz induced the firing of several ganglion cells whose onset depended on their spatial position on the MEA and on their preferential stimulus.

Importantly the offline procedure developed to realign the stimulation triggers with the projected images is time-consuming since it also requires verifying and correcting possible errors and mismatches between the triggers and the sequence of projected images. Hence, in my initial work, I implemented a tool to handle this realignment and to reduce the need for human intervention. Unexpectedly, as it will be described later, this implementation was also very helpful to identify a few artifacts that were induced by the visual stimulator and that were not identified in previous tests when the system was developed. Rather, the high sensitivity of the retina and the algorithms used in our analysis allowed us to detect these artifacts and to contribute to further improving the experimental setup.



## ***Integrated analysis chain of light-evoked retinal ganglion cells responses***

---

The objective of this part of my work was to integrate a computationally light and unsupervised analysis chain capable to automatically detect and sort spikes, to assign each action potential to a single and cell-type specific RGC based on their light-evoked responses.

The developed chain of analysis comprises a first stage that uses a recently published spike-detection and spike-sorting algorithm<sup>3</sup> that was developed within the RENVISION EC-funded project. Briefly, this algorithm was designed to exploit the high-resolution of our CMOS-MEAs by taking advantage of the spatial and temporal correlations of extracellular signals from the same neuron recorded by neighboring closely spaced electrodes. It allows to detect spikes and to assign them to a single unit and it also provides an estimation of the unit position in between the electrode sites. Following the event detection, I have developed custom algorithms to realign the spiking activity of each cell, the cell's position and the spatial and temporal information of the projected light-stimuli. This was obtained by processing the electrophysiological data, the images used for the visual stimulation and the time-stamps acquired from the visual stimuli during the experiments. After this step, all relevant information regarding the experimental protocol was merged into a single Hdf5 file generated for each experimental phase and data were then ready for further spike-trains analysis. The developed tool only asks for human intervention to verify (and eventually correct) the alignment of the time-stamps of the visual stimuli with the recorded spiking activity. To do so, it also generates a set of report plots that the user can verify.

Upon these first steps aimed at preparing the experimental data for further analysis, a custom suite of algorithms performs the analysis of the spike trains by exploiting the different types of visual stimuli implemented in our protocols. This includes full-field black and white flashes to identify the polarity of retinal ganglion cells and moving bars of different spatial gratings to rapidly estimate their receptive field properties (see later for further details and comparison of this method with Spike Triggered Average). In particular, the classification of RGCs was restricted to three main functional types (ON, OFF, ON-OFF), the computation of the time lag and peak of response to flash stimuli for each population, the estimation of receptive fields, the quantification of the peak and lag of responses for full-field flashes and the quantification of the Fourier coefficient at the temporal frequency of moving bars. These algorithms also provide images of comparison among different experimental conditions, such as “masked” and “full-field” stimuli (see the experimental study reported later) or “drug-treated” and “untreated” conditions. All these analyses are automatically selected or unselected by the analysis tool itself that I developed in Python. Briefly, an unsupervised algorithm tries to understand the rationale of each experimental phase using the information extracted in the first part of the analysis process (e.g., the type of visual stimuli for each phase, the annotation tags that the experimentalist included). In this way, also a not expert user can run the analysis and rapidly evaluate the outcome of the experiments. In the next paragraphs, I will shortly describe the computational methods that I developed and used to classify retinal ganglion cells and to estimate their receptive fields.

## ***Selection and classification of retinal ganglion cells based on light-evoked responses***

In all our analysis, we adopted a conservative approach and restricted our study on a subset of selected RGCs. In order to define a selection criterion, we restricted our analysis to only those cells whose interspike-interval (ISI) distribution for static iso-luminant gray stimuli and white/black flashes at maximum contrast differed significantly (Kolmogorov-Smirnov test). This straightforward criterion to filter out RGCs was derived from a similar implementation that I have performed for the analysis of spike trains in neuronal cultures (in collaboration with my colleague H. Amin) and that was previously used to study a culture model of Alzheimer disease<sup>12</sup>. In our retina experiments, out of all recorded RGCs, typically about 40-50% did not satisfy this criterion and were not included in our conservative analysis. Nevertheless, it has to be highlighted that given the large number of recording electrodes in our system, we typically considered in our analysis a total of 500-1500 of single RGCs for each retina.

To functionally classify each recorded unit as either ON, ON-OFF or OFF type RGCs I developed a greedy template matching approach<sup>13</sup>. The implemented method assigns a label to each RGC depending on the shape of the cumulative distribution of the spike trains in response to alternating flashes from light to dark and repeated 20 times at maximum contrast. This classification is based on the cumulative distributions of the spike trains rather than on specific features of single RGC responses. Indeed, we found that, given the large set of possible responses, very often it was not straightforward to assign a label using hard thresholding on specific response features. Interestingly, the measure that I have used to distinguish between the different distributions does not require any binning and it reflects the way a human observer would use to discriminate between functional types by looking at the evoked responses.

This measure named as “the earth mover's distance”<sup>14</sup>, quantifies the distance between two distributions. Specifically, if one interprets the two distributions as a certain amount of sand distributed over the same region, this measure quantifies the total work needed to move the sand from one distribution to the other as it would be needed to match the two distributions. In our case, this idea was used to compute the “cost” of turning the experimentally measured spike train distribution into the expected distributions for ideal ON, OFF or ON-OFF RGC responses. Once the earth's mover distance between the cell response and each template was computed, we assigned a label to the RGC by considering the template that better approximated the experimentally recorded distribution. The drawback of this approach is the need to define proper templates. To do so, I used an unsupervised clustering method, named Laio's clustering from the author who proposed the approach<sup>15</sup>. Briefly, this clustering algorithm first computes the local density of responses of any given retinal ganglion cell, namely how many other retinal ganglion cells exhibit a similar response based on a hard threshold on the distance measure (in our case the earth's mover distance).

The choice of this threshold, although arbitrarily, does not affect the results of the clustering as it serves only as a local descriptor for similarity. We chose this distance such that less than 1% of cells had a local density of 1, as suggested by the authors of the method. The core idea of the method is that if there is a cluster of similar responses, then at least one cell exhibits a maximal

local density, which summarizes the properties of the group. To select the proper response template, it is enough to look at the distance between the candidate cell and all the other cells that exhibit a higher local density. Indeed, by plotting the local density against the minimum distance respect to all other higher density points, it is possible to select the representative responses of the cluster by looking at the outliers of the distribution, see Fig 4.3A. Indeed, these outliers represent cells whose responses are locally similar to the others, hence representative, and at the same time, far apart from any other representative response. For further details regarding this clustering method see<sup>15</sup>.

This clustering approach is exemplified in Fig 4.3, where the typical responses of ON, ON-OFF and OFF cells to white and black alternating stimuli have been simulated by sampling their time stamps of response from the average spike-train response distribution of visually identified ON, ON-OFF and OFF cells. This choice for the functional classification of RGCs type is particularly suitable for large-scale recordings for the following reasons:

1. The response of retinal ganglion cells to white and black alternating stimuli is not sharply defined as ON or OFF responses but exhibits a continuous interval of responses bridging markedly ON and markedly OFF responses. Consequently, the concept of distance and density among cells via the earth's mover distance is well-defined.
2. The classification takes into account the whole dynamics of the response of each cell instead of relying on a subset of response features (such as the peak or the lag of response to the onset of brighter/darker plain stimuli).
3. It does not require the decision of any hard thresholding to classify cells. Specifically, by interpreting the spike trains as distributions, we are intrinsically normalizing all the cells with respect to a number of elicited spikes. Hence, it is straightforward to compare low firing and high firing cells because the method is only sensitive to how the spikes are distributed in time rather than their amount.
4. It can be extended to classify cells based on a larger set of templates (for instance when including sustained vs. transient responses).
5. Once the templates are assigned by grouping a subset of experiments, the clustering is not anymore required and the templates that were identified can be used as ground truth for the next experiments.
6. The entire procedure does not require binning the spike trains, thus preventing from deciding a priori the bin size or from using smoothing functions that might affect the overall analysis.
7. By looking at the whole spike train distribution, this method also takes into account silent intervals of the cell's activity.

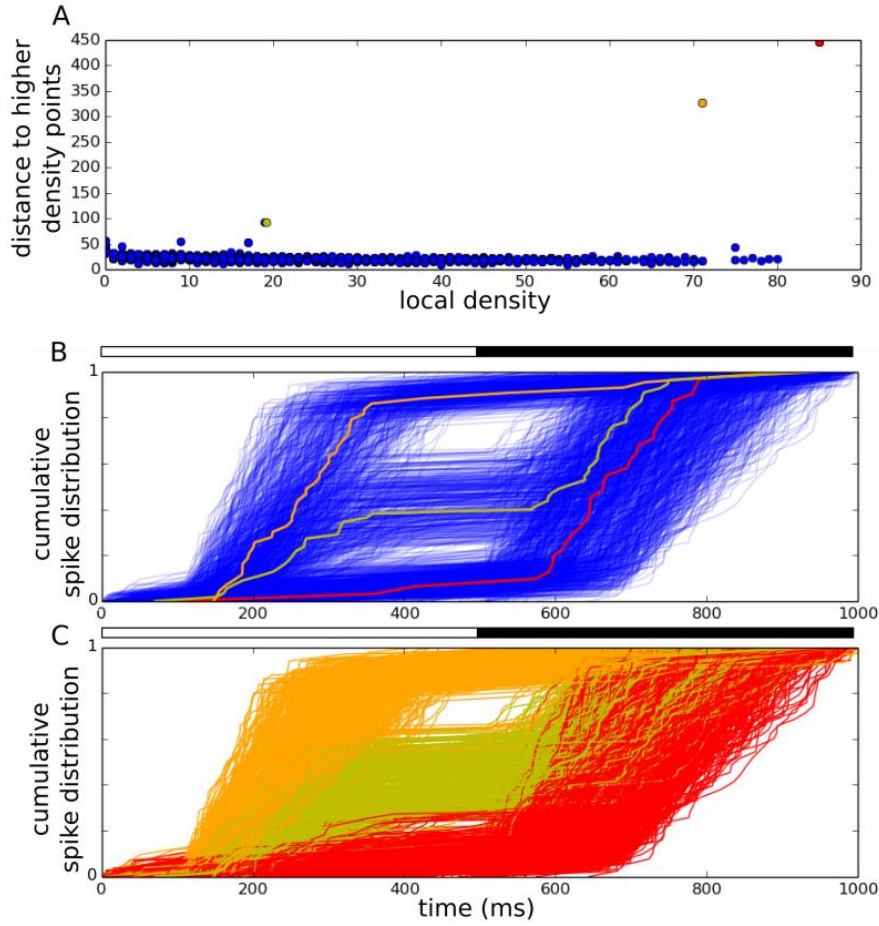


**Fig 4.3: Illustrative example of clustering simulated ON, ON-OFF and OFF cell's responses using the Laio's clustering approach adopted in my work. (A) The outcome of Laio's clustering determines a few outliers that represent the cell-type specific templates and that can be used for classification. (B) Cumulative distribution of simulated retinal ganglion cell responses (each cell is a blue line). Colored traces represent the templates selected in (A). (C) Color coding of the cumulative responses shown in (B) according to the selected template (red: 1000 OFF-cells, orange: 1000 ON-cells, green: 1000 ON-OFF cells).**

This data-driven classification method, together with the selection of RGCs based on their ISI distribution, provides a conservative approach for analyzing our dataset acquired from different retinas. Importantly, this is possible because all the classified responses were selected based on a unique set of templates. Furthermore, this method ensured that the analysis of peak and lag response to full-field alternating stimuli was not biased by an arbitrary threshold, which was inherently data-driven in this approach. However, the choice of using full-field stimuli to classify the polarity of the cells, although widely used, might not be the more appropriate. Indeed, it was reported that in full-field stimulation of mouse retina, a subclass of OFF retinal ganglion cells could exhibit an ON-OFF response if the stimulus is applied in full-field condition<sup>16</sup>. Consequently, to handle this issue in our analysis, we have filtered out this subclass of cells and we investigated the response of purely ON and purely OFF retinal ganglion cells exposed to full-field stimulation, thus excluding (at this stage of implementation) ON-OFF responses for this type of stimuli.

### Fast receptive fields (RF) estimation

To estimate the receptive field (RF) properties of the recorded RGCs, we adopted a computationally fast approach. Rather than using an approach based on Spike Triggered Average (STA), our approach is based on the analysis of the light-evoked responses of RGCs to bar stimuli of different spatial gratings and moving in a single direction at the temporal frequency of 1Hz. The rationale underlying this approach is that the response of the RGCs should be maximal for a preferred size of the moving bar stimuli. Thus, by assuming that the receptive field can be approximated with a difference of Gaussian, and by exploiting our high-resolution CMOS-MEAs recordings, we can provide a rough estimation of the receptive field properties by fitting the DoG model<sup>17</sup> to the response of the cell elicited by stimuli at different spatial gratings. It has to be noted that here we used bar stimuli moving in a single direction as a first approximation of the receptive fields. However, the same approach can be easily refined by considering moving bars in different directions. Interestingly, a similar approach was recently proposed to quantify the receptive field size of neurons in the visual cortex<sup>18</sup>.

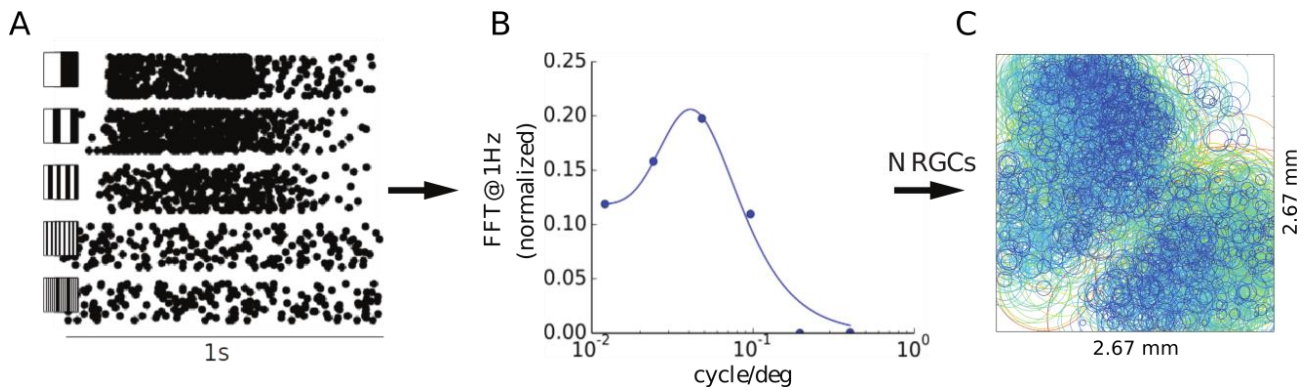


**Fig 4.4: Fast receptive fields estimation based on the analysis of RGCs responses to bar-stimuli at different spatial frequencies and moving at the temporal frequency of 1Hz.** (A) An exemplary raster of a retinal ganglion cell responses to bar stimuli for different spatial grating (0.011-0.17 cycle/deg). In this example, five different gratings were projected at full-field and repeated twenty times (each row depicts the response for each repetition and for each grating). (B) The Fourier transform of the light-evoked spike trains of each RGC is computed for each grating and the coefficient associated to the temporal frequency of the moving bars (1 Hz) is used to quantify the tuning curve of the cell. The measured points are fitted to a difference of Gaussian model to estimate the relevant parameter of the receptive field (solid line). (C) Plot of the receptive field center and size estimated for all the retinal ganglion cells recorded in an experiment. The color of the circle codes for their size. The mean diameter of the receptive field center obtained was  $314 \pm 105 \mu\text{m}$  whereas  $605 \pm 243 \mu\text{m}$  for the surround.

In our experiments we used moving bars of different spatial gratings in the range 0.011-0.35 cycle/deg (corresponding to linear bar widths of 1344-42  $\mu\text{m}$ , Fig 4.4A) and the Fast Fourier Transform (FFT) component at the same frequency of the bar motion of 1Hz as a measure of the response, see Fig 4.4B.

As shown in Fig 4.4B, while low spatial frequencies maximize the activation of the surround inhibition, the increase of spatial frequency determines the decrease of the inhibition with respect to the center excitation, until the match between the width of the bar and the size of the center of the receptive field. Further increasing the spatial frequency of the grating determines a sudden decrease of the firing of the cell as it is not able anymore to resolve finer and finer details. As illustrated in Fig 4.4C for one retina, we performed this computation for all recorded RGCs over a field of view provided by CMOS-MEAs of  $2.67 \times 2.67 \text{ mm}^2$ .

In order to assess the results obtained with this method, we cross-validated our results with the receptive fields estimation obtained with the Shifted White Noise (SWN) approach<sup>19</sup> that was developed in the RENVISION project. The latter method is a modified version of the Spike Triggered Average (STA) approach in which the randomly flickering checkerboard stimuli also include grid jitters to obtain more accurate estimations of the receptive fields by exploiting concepts from super-resolution<sup>19</sup>. The quantification of the estimation errors (Fig 4.5A) of our method with respect to the SWN revealed that our approach provides a reasonable approximation of the RGCs receptive fields. Indeed, most of the receptive fields were estimated almost correctly, with an error below 25%. Furthermore, the distribution of the differences between the two estimation approaches has a Gaussian shape profile centered in zero, thus indicating that the estimation of the receptive field is not biased towards underestimations or overestimations, see Fig 4.5B. In addition, although the estimation of the receptive fields is much more accurate with the SWN approach, our approach is suitable for fast screening. Indeed, it is computationally cheap and it requires a short experimental time of just 3 min, compared to the 30 min required for SWN. Bar stimuli moving in different directions can definitely improve the accuracy of this approach, and we are currently planning to apply the core ideas underlying this method to propose a fast, reliable and as accurate as possible real-time screening for estimating the size of receptive fields.

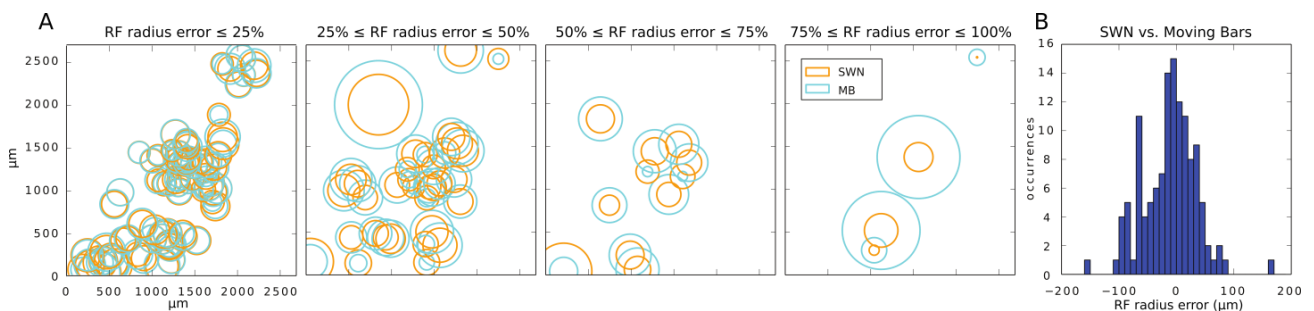


**Fig 4.5: Measured receptive fields estimation error of our method based on moving bars (MB) with respect to the method of shifted white noise (SWN).** Shifted white noise and moving bars stimuli were applied to the same retina. (A) Comparison between the receptive field estimation obtained with the SWN (orange circles) and with the moving bars (MB, blue circle) and for different intervals of the estimation error. The majority of the cells are correctly estimated with an error  $\leq 25\%$ . (B) The estimation error between the MB and SWN approach is distributed as a Gaussian centered in zero, thus indicating that the MB estimation is not consistently over/underestimating the receptive field sizes.

## Identification of visual stimulation artifacts through the analysis of RGCs light-evoked responses

The light-evoked spike-trains of RGCs acquired with our setup are extremely informative of the stimulus that was presented and allowed me to identify some artifacts introduced by the light projector that were not detected by the optical characterization of the system. By analyzing these data, I discovered that our visual stimulator was not reliably projecting the stimulus, but rather projected a slightly modified version of it. In particular, it introduced weak modulations of the light intensity that were not perceived by our eyes but that were correctly encoded by the RGCs in their spike trains. The retina indeed is very sensitive to these small amplitude variations and converted them into changes in spiking activity in a robust and reliable fashion.

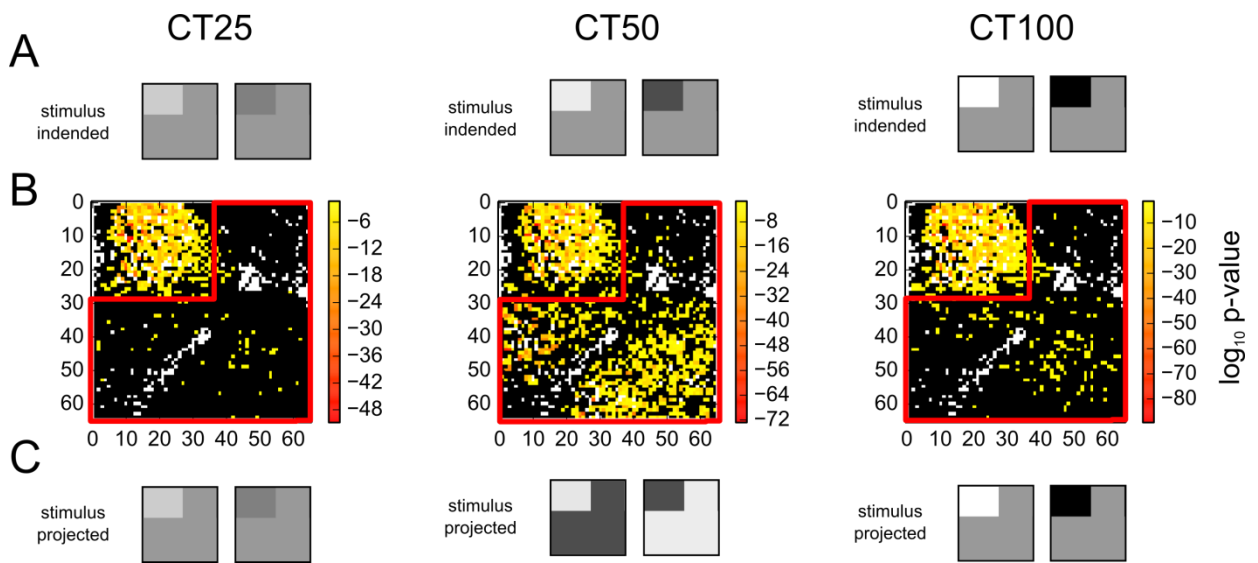


**Fig 4.6: Detection of stimulation artifacts.** (A) Alternating dim and bright stimuli of three different contrasts (CT25, CT50, CT100) has been presented in the upper corner of the retina while leaving an iso-luminant gray in the remaining part of the retina (masked area). (B) Activation map of the retinal ganglion cells upon stimulation. For each RGCs the change in its ISI distribution between stimulation phase and baseline has been quantified through the p-value of the Kolmogorov-Smirnov test. Solid red lines highlight the borders of the mask (A). At low and high contrast (CT25 and CT100), the activation of RGCs is confined in the non-masked area of the stimulus. At CT50, the activation map reveals that both masked and unmasked RGCs are actively responding to the stimulation. (C) After a careful analysis we discovered that, although the stimulus sent to the projector was correct (A), internal optimization routines of the projector modified it at CT50.

Specifically, we encountered these artifacts while stimulating with white and black alternating flashes in the presence of an iso-luminant gray mask on the stimulus, as shown in Fig 4.6A. In the illustrative example of Fig 4.7A, we presented on the stimulated area a sequence of alternating white and black flashes at CT25, CT50, CT100 respect to the iso-luminant gray that covers the masked region of the retina. The analysis of changes in the interspike interval (ISI) distribution between the stimulation phase and the baseline condition (a full field iso-luminant gray stimulus)



revealed a tight correspondence between the activated cells and the position of the stimulus, as shown in the activation map of Fig 4.6B where the p-value of the test has been color-coded to highlight the change in the ISI distribution upon stimulation. However, at CT50 respect to the iso-luminant gray, the map of response (Fig 4.6B, middle panel) is significantly different. Indeed, for this specific stimulus, a relevant fraction of the RGCs exposed to the iso-luminant gray stimulus changed their interspike interval distribution respect to their baseline.

The quantification of the population response for ON and OFF RGCs that are exposed or not to the stimulus (Fig 4.6B, middle panel), revealed a reliable and significant response of the RGCs under the mask, which were not expected to change their spiking activity as they were not directly experiencing the visual stimulation. I found that this change in the spiking activity was due to the projector that was modulating luminance of the gray mask, in counter-phase with respect to the stimulus projected in the stimulated region of the retina, see Fig 4.6C. In the masking condition, we observed this artifact for an interval of contrasts ranging from CT30 to CT67. However, we also found that this effect also depended on the size, position, and shape of the mask. Indeed, very often we observed that different masks applied to the same stimulus determined opposite behaviors of the projector. A second artifact was discovered upon measuring the light intensity with an optical power meter and it is a long-lasting adaptation (3 to 5s) of the overall luminance of the stimulus at the end of a stimulation sequence.

In order to fix these issues we empirically found a counter-measure. Specifically, we modified the software that sends the images to the projector to constantly display a sequence of blocks of different grays over a region that is not projected on the retina. So far, constraining the projector to constantly displaying a range of blocks spanning the whole range of contrasts (CT25-CT50-CT75-CT100) has completely abolished the insurgence of the mentioned artifacts. To further ensure that the stimuli presented were exactly as designed, we cross-validated the visual stimulation with an optical power meter (PM 130, Thorlabs<sup>20</sup>). Indeed, the set of stimuli used in this work were simple enough to measure the luminance of the masked and not masked regions directly. These unwanted effects were not observed for full-field stimuli and were removed for the masked stimuli after having adopted the proposed fix.

### ***Investigating the effects of the spatial extension of visual stimuli on local RGCs responses***

---

The large-scale recording capabilities of high-density multi-electrode arrays together with the visual stimulation performances of our setup (sub-millisecond time precision,  $4 \times 4 \mu\text{m}^2$  light-pixel resolution) and the data analysis tools developed in my work allowed us to start investigating possible effects of long-range interactions in shaping the light-evoked responses of RGCs. In particular, we designed a stimulation protocol with the aim to study whether the extent of the stimulated area of the retina might affect light-evoked spiking activity responses of RGCs.

To this end, the protocol (Fig 4.7) consisted in projecting on the retina a set of simple stimuli consisting of black and white flashes (Fig 4.7A) and moving bars (Fig 4.7B) of different spatial gratings, under two different conditions. The first condition consisted in applying these visual stimuli over the entire retina (“full-field” condition). The second consisted in applying the same



stimuli by confining them onto a small area of the retinal area (“masked” condition). Under this condition, the remaining part of the retina was exposed with an iso-luminant gray. In addition, we recorded RGCs responses under these two conditions using stimuli with different contrasts (25%, 50%, 75%, 100%, Fig 4.7C), both for flashes and moving bars. The location of the exposed area under the masked stimulation condition (referred next as non-masked area) was selected during the experiment based on the achieved retina-to-chip coupling. For the analysis, we evaluated the response profiles of the ON and OFF main classes of RGCs responding to such stimuli and that were located in the area that was always exposed to the patterned stimuli under the two conditions. In the next paragraphs, we will refer to these RGCs as “always exposed RGCs” or aeRGCs.

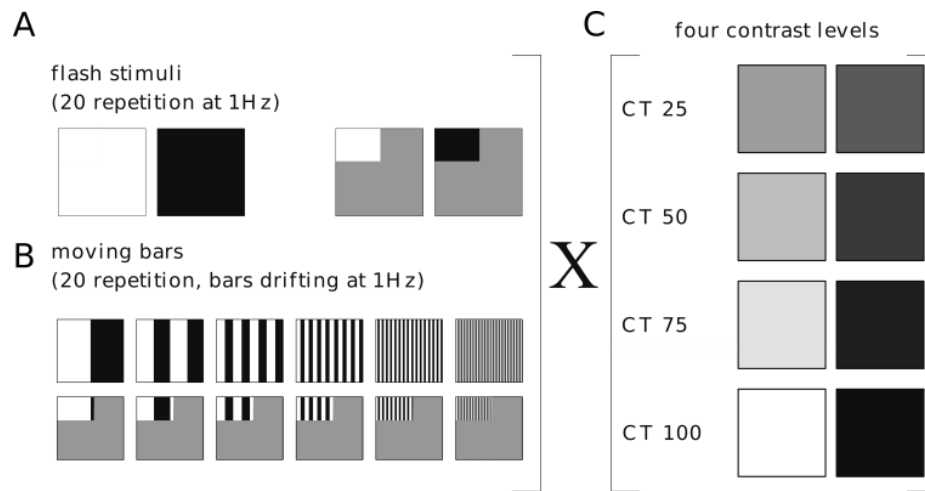


**Fig 4.7: Experimental protocol of “full-field” and “masked stimuli” used to investigate the effects of long-range interactions on RGCs light-responses.** (A) Black and white alternating flashes and (B) moving bars at different gratings were projected on the retina, either in full-field or masked conditions. (C) The stimuli in (A-B) have been tested at four different contrast levels. This allowed evaluating how the extent of the stimulated area might affect the light-evoked spiking activity of RGCs that are always exposed to the stimulus (aeRGCs).

#### *Timeline of the visual stimulation protocol*

The experimental protocol used for visual stimulation is organized as shown in Fig 4.8A and has a total duration of approximately 100 minutes for each retina. The total duration is inline with previous experimental investigations that have indicated a stable and reliable response of the ex-vivo tissue for experiments lasting less than 150-200 minutes. Each trial for a set of visual stimuli includes both full-field and masked conditions and has a duration of 25 minutes. Finally, each set of visual stimuli includes five different stimuli: Flash CTALL, Bars CT25, Bars CT50, Bars CT75 and Bars CT100. All these visual stimuli were projected considering three main phases:

Phase I, or “Initial baseline”: at the beginning of each protocol 60s of iso-luminant gray are presented to the retina

Phase II, or “Stimulation phase”: after the initial baseline, a different set of images, depending on the visual stimulation protocol, is presented to the retina

Phase III, or “In-between baseline”: at the end of the stimulation phase, the retina is readapted to the isoluminant gray

Phase II and Phase III are then iterated to build up every single protocol of stimulation that lasts 260s. The sequence of these protocols of stimulation is organized as shown in Fig 4.8B:

**1. Flash CTALL: White and black alternating flashes of increasing contrast**

Phase II is a sequence of 40 images switching every 500ms that consisted of alternating dim and bright uniform images while Phase III lasts 30s.

After Phase I, both Phase II and Phase III are repeated by changing to CT25, CT50, CT75 and CT100 the contrast of the dim and bright images presented Phase II.

**2. Bars CT25: Moving bars in a single direction at the temporal frequency of 1Hz at CT25**

Phase II consists of a sequence of images displaying dim and bright bars at CT25 that periodically move at the temporal frequency of 1Hz in a single direction. Phase II lasts 20s, while Phase III is always set to 10s, except for the last repetition that lasts 30s.

After Phase I, both Phase II and Phase III are repeated by changing the spatial frequency of the bars displayed during Phase II to 0.750, 0.090, 0.045, 0.365, 0.180 and 0.022 cycle/deg, respectively.

**3. Bars CT50: Moving bars in a single direction at the temporal frequency of 1Hz at CT50**

Identical to protocol 2 (Bars CT25), except for the increased contrast (CT50) between dim and bright bars.

**4. Bars CT75: Moving bars in a single direction at the temporal frequency of 1Hz at CT75**

Identical to protocol 2 and 3 (Bars CT25, Bars CT50), except for the increased contrast (CT75) between dim and bright bars.

**5. Bars CT100: Moving bars in a single direction at the temporal frequency of 1Hz at CT100**

Identical to protocol 2,3 and 4 (Bars CT25, Bars CT50, Bars CT75), except for the increased contrast (CT100) between dim and bright bars.

Before starting the experiment and during the time intervals between different stimuli, an isoluminant gray stimulus, identical to the one presented during Phase III of each protocol of stimulation, is applied to the retina.

Protocols 1-5 are firstly presented in full-field condition and afterward in masked stimuli conditions.

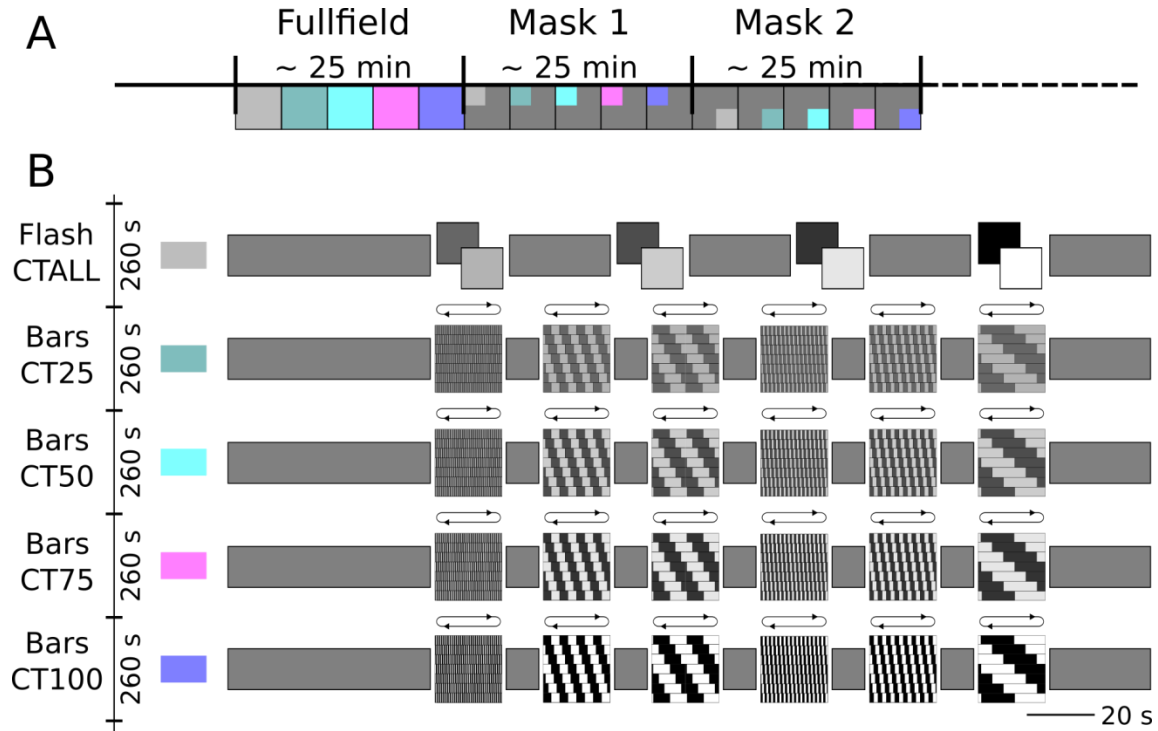


**Fig 4.8: Time course of the visual stimuli used for the full-field-masking protocol. (A)** The visual stimulation begins in full-field condition (i.e., the stimuli are presented to the whole retina) and subsequently, the masks are superimposed to the stimuli (e.g., Mask 1, Mask 2 and Mask 3). Each stimulation condition lasts approximately 25 minutes during which five different visual stimuli are presented: alternating flashes of four different contrasts (Flash CTALL, gray), moving bars in a single direction at different contrasts, namely CT25 (Bars CT25, light blue), CT50 (Bars CT50, cyan), CT75 (Bars CT55, magenta) and CT100 (Bars CT100, blue) contrast. **(B)** The Flash CTALL starts with 60s of iso-luminant gray, 20s of dim and bright alternating flashes at CT25 switching every 500ms, 30s of iso-luminant gray, 20s of dim and bright alternating flashes at CT25, CT50, CT75, CT100 switching every 500ms interleaved with 30s of iso-luminant gray. The moving bars stimuli consists of bars of different spatial gratings moving in a single direction at the temporal frequency of 1Hz. Each of these stimuli (Bars CT25, CT50, CT75, CT100) differ in their contrasts between dim and bright bars. They start with 60s of iso-luminant gray. After the initial baseline, 20s of moving bars at 0.750, 0.090, 0.045, 0.365, 0.180, 0.022 cycle/deg in spatial frequency are interleaved with 10s of iso-luminant gray.

#### *Assessing the visual stimulation confinement capability of the setup*

As a first step, we assessed the capability of our visual stimulator to spatially confine the light stimuli on the retina as required to implement the masked stimulation condition. As shown in Fig 4.9A,B, the application of the masked stimuli yielded a nearly negligible scattering effect that induced a change in only in a few cells (<2%) of the ISI distribution between the baseline activity recorded with an iso-luminant gray stimulus and the spiking activity recorded during the visual stimulation. These changes might have been originated by causes other than light-scattering, such as, for instance, a changing coupling between RGCs and the electrodes, an incidental variation of the firing rate or a false positive RGC included in the dataset. Consequently, given the aim of this work, these effects were accounted as part of the intrinsic heterogeneity of the tissue and of our recordings.

On the other hand, the confined stimulus activated aeRGCs similarly than in the full-field stimulation condition. Importantly, the p-value map shown in Fig 4.9B reveals sharp boundaries between responsive and silent RGCs. These boundaries tightly overlap with the borders of the applied mask (solid cyan box). Furthermore, under the masked stimulation condition the array-wide spike count for either ON, ON-OFF, and OFF RGCs that were exposed to the iso-luminant gray did not exhibit any stimulus-dependent response (gray line, Fig 4.9C) as, on the contrary, it occurred for aeRGCs (colored lines, Fig 4.9C). All in all these observations indicated that our setup could spatially confine the visual stimuli in the region of interest (non-masked area).

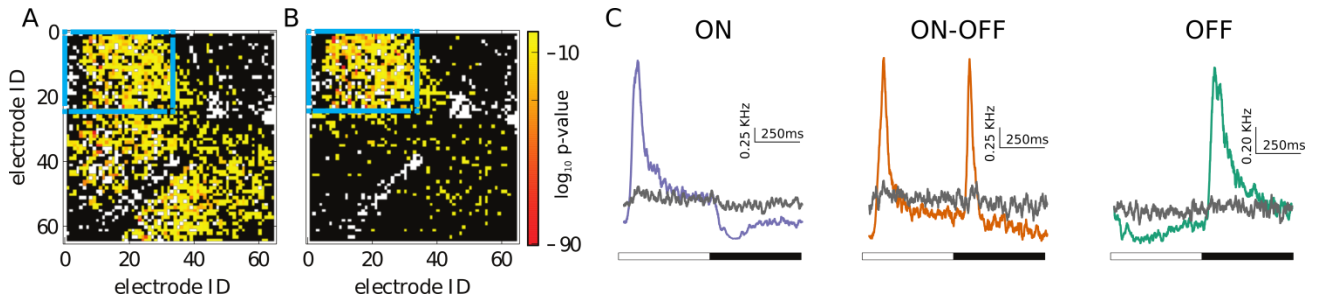


**Fig 4.9: Assessment of the stimulus confinement and localized RGCs response.** False-colour map of the p-value associated with the change in the ISI distribution for each active electrode side of the array, upon full-field (A) and masked visual stimulations (B). The cyan square area highlights the always exposed RGCs (aeRGCs), namely those cells that experience the same stimulus in both full-field and masked stimuli condition. (C) Population response of ON, ON-OFF and OFF cells to alternating white and black flashes for aeRGCs (colored lines) and RGCs under the mask (gray lines), thus revealing that the stimulus is spatially confined to the imposed non-masked area.

### *Simulated and recorded effects on RGCs responses to a confined visual stimulation*

After having assessed the capability to spatially confine our visual stimuli we investigated whether the responses of aeRGCs (RGCs that are always exposed to the stimulus under both masked and full-field conditions) for each retina were affected by the masked stimuli with respect to the full-field stimuli. For the analysis, we selected and classified the aeRGCs into ON and OFF cells (Fig 4.10A). We quantified two biophysical indexes for each cell: the maximum firing rate of a cell elicited by the stimulus presentation (peak) and the time required to reach the peak value (lag), see Fig 4.10B. Note that the peak value of response can be associated with the strength of the RGC response, whereas the lag denotes the inertia (or responsiveness) of the cell upon presentation of the preferred stimulus. In order to quantify these indexes, we smoothed the instantaneous firing rate of each cell (computed by binning the spike trains at each millisecond) using an averaging time-window of 25 ms. Successively, we averaged the stimulation trials for each aeRGC to compute their peak response as the maximum value of the smoothed curve in the light phase of the stimulus for ON cells and, respectively, the dark phase of the stimulus for OFF cells. The corresponding lag of response was computed as the time interval from onset of the visual stimulus (light or dark phase) and the corresponding peak of the response. The statistical significance of differences between full-field and masked conditions was evaluated using a paired t-test (two-tailed) at 0.05 level. The peak and lag<sup>21</sup> computed for a single representative ON aeRGCs under the two stimulation conditions (white flash at the minimum contrast CT25) are shown in Fig 4.10B. As shown, the two stimulation conditions gave rise to a different peak and lag values.

In order to interpret the experimental data we also simulated the expected peak and lag responses of ON and OFF aeRGCs. The classical idea of receptive fields predicts that the aeRGCs peak of response should equal or increase its magnitude upon application of the masked stimuli, see Fig 4.11. Indeed, the visual stimulus covering the receptive field center of these cells is precisely the same by construction. Consequently, the responses of aeRGCs in full-field or masked stimulation conditions should be nearly indistinguishable (or slightly increased) because the mask can cut part of the inhibitory domain of the receptive field surround of these cells.

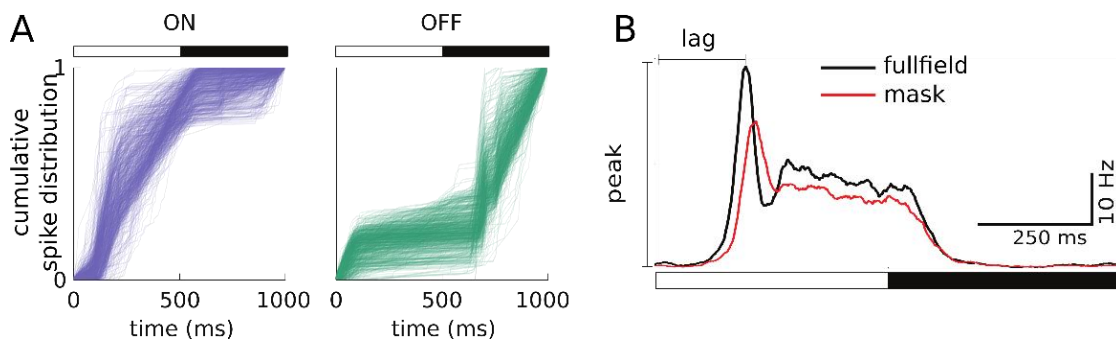


**Fig 4.10: Quantification of retinal ganglion cells responses to flash stimulation. (A)** Cumulative spike train distribution to alternating white and black flashes (20 repetitions) for both OFF and ON aeRGCs (each line represent a single cell). **(B)** The peak of response is the maximum firing rate of the aeRGC elicited in response to its preferred stimulus, whereas the lag of response quantify the time interval between the stimulus onset and the peak amplitude of the firing rate.

However, as shown in Fig 4.10B, the exemplary ON aeRGC behaved differently than predicted by the model. Specifically, in full-field stimulation condition, the peak firing rate of the cell rapidly reached the peak value of  $\approx 85$  Hz after a typical lag of  $\approx 210$  ms (Fig 4.10B, black line). In contrast to the prediction of the classical receptive field model, under the masked stimulation condition, the peak amplitude decreased significantly to  $\approx 65$  Hz (Fig 4.10B, red line) and the lag of the response upon mask application increased by  $\approx 30$  ms with respect to the full-field stimulation condition. Differences between the simulated and experimentally measured responses can also be appreciated in Fig 4.10B that reports results for all the measured RGCs of an entire retina.

Such an attenuated response observed in our experiments with the masked stimulation condition might be consistent with a partial overlap between the receptive field center and the stimulus. However, this phenomenon can occur only in those cells that experienced a different overlap between the stimulus and the center part of the receptive field. This argument does not apply to aeRGCs, whose receptive field center, by definition, is within the non-masked area. Also, note that aeRGCs were selected with a conservative approach and in a spatial window consisting in an area that was 4 electrodes far from the border to the mask ( $\approx 160$   $\mu\text{m}$ ). Therefore, our results suggest that the portion of the retina that is not directly stimulated in the masked stimulation condition mitigates the inhibitory contribution on the receptive field of aeRGCs observed in the full-field condition. As reported in the false-color map of Fig 4.11B, most of the aeRGCs decreased their peak of response in the masked condition with respect to the full-field. In the next sections, we report the results of the analysis for the peak and lag of the responses performed on different retinas and for specific ON and OFF RGCs populations.

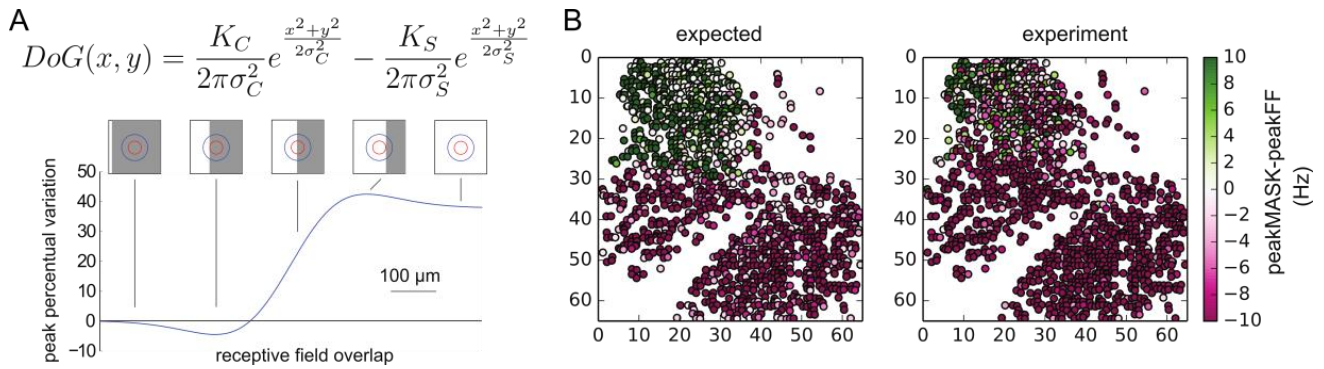


**Fig 4.11: Simulated and experimentally measured change in response peak according to the classical receptive field model and experimental data.** (A) Classical receptive field model. As a function of the overlap, a cell responds by increasing its firing rate (center part of the graph). Once the mask goes beyond the boundaries of the receptive field center, the cell decreases its firing rate as a consequence of the inhibitory surround (right part of the graph). (B) False-color map of the change in the peak response for simulated and experimental data of an entire retina.

### *Masked stimuli reduce the peak response for both ON and OFF exposed RGCs populations*

In order to test whether the effect reported above was specific for a particular population of RGCs, we divided the aeRGCs as ON and OFF cells according to their spike train distribution. For each cell in the population, we computed its peak and lag of response. This was used to assess if the effect observed in the exemplary single ON aeRGC shown in Fig 4.10C holds true for both ON and OFF populations, as reported in Fig 4.12. We pooled data from 2023 ON aeRGCs and 1141 OFF aeRGCs recorded from four different retinas and using three different masks for each retina.

The quantification of the peak difference across this large set of cells revealed interesting properties, see Fig 4.12A. First of all, although the result obtained is not significantly different for all the contrasts (e.g., in OFF aeRGCs  $p=0.32$  and  $p=0.13$  for CT25 and CT75, while in ON aeRGCs  $p=0.16$  for CT75), our analysis shows that the reduction of the peak firing rate is robust across retinas and mask's locations. Second, the reduction seems to affect more the ON population than the OFF population (-21% vs. 12% average decrease), thus suggesting a higher sensitivity to the presence of the mask for ON aeRGCs compared to OFF aeRGCs. It should also be noted that in full-field condition OFF cells increment almost linearly their responses depending on the contrast of the stimulus. The same trend is preserved in the masked condition. On the other hand, the peak of response for ON RGCs in full-field condition reaches a saturated response at 75% contrast with respect to the iso-luminant gray. However, also in this case, the curve obtained for the masked condition mimics the one obtained for the full-field except an almost constant offset.

Consequently, our results show that the masked condition (addition of a mask of uniform iso-luminant gray) lowered the peak response curve for both ON and OFF aeRGCs without changing the envelope.

### *Masked stimuli reduce the lag of response for ON and OFF exposed RGCs populations*

Under masked stimulation condition, our results show that the latency of ON aeRGCs increased significantly and independently from the applied contrast, see Fig 4.12B. Instead, the latency of OFF aeRGCs was significantly increased by  $41\pm12$  ms compared to the full-field condition only for low contrast stimuli and it was nearly the same for contrast stimuli  $\geq$  CT50, see Fig 4.12B.

This analysis reveals that the effect of the masked stimulation condition on the light-evoked response of aeRGCs is not limited to a reduction of their peak firing rate, but it also affected the responsiveness of aeRGCs. However, this effect is more significant for ON than OFF aeRGCs. Specifically, as shown in Fig 4.12B, the OFF population delayed the response to the masked stimulation only at low contrast (CT25) while the lag difference for higher contrast stimuli was almost negligible ( $169\pm46$  vs.  $173\pm41$  ms). On the other hand, the ON aeRGCs significantly delayed the response for all contrasts except for CT50, resulting in a  $21\pm36$  ms average increase of the lag. Similarly to the peak response curves, the ON aeRGCs lag response curve in masked stimuli condition closely followed the trend of the full-field stimulation one. Conversely, the lag response curve of OFF cells in masked stimulation condition was not only shifted with respect to the full-field one but also displayed a substantial difference, in particular at CT25.



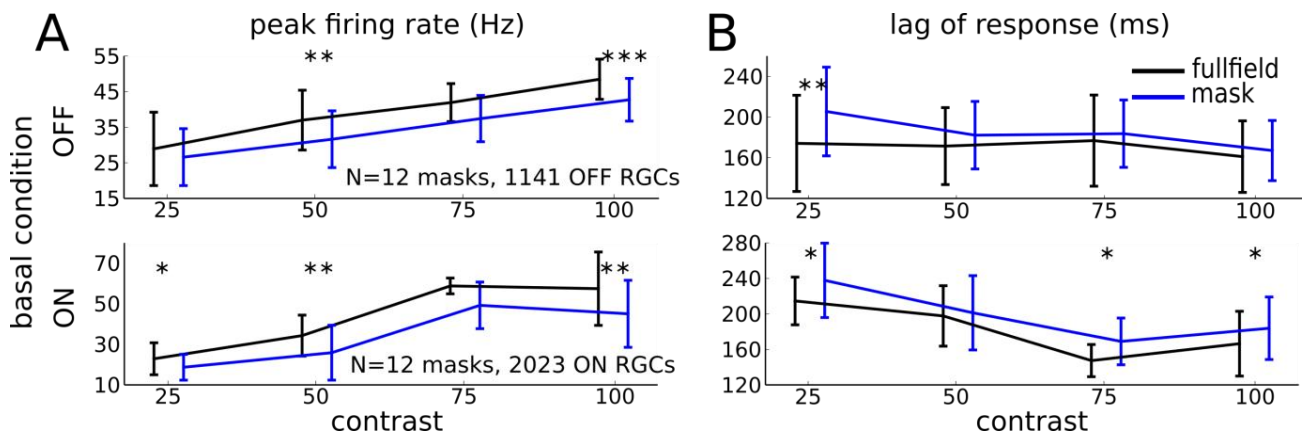


**Fig 4.12: Population responses to full-field (black) and masked (blue) black and white alternating flashing stimuli as a function of the contrast, for ON and OFF always exposed RGCs (aeRGCs).** Compared to the full-field condition, the masked condition decreased the peak amplitude of both ON and OFF populations (A) while the responsiveness of the ON population was significantly more delayed than OFF aeRGCs (B) by the mask application. Asterisks mark a significant difference  $p=0.05$ . The data represent the pooling of three different masks for each retina and a total of 4 retinæ (2023 ON aeRGCs, 1141 OFF aeRGCs). Paired t-test \* $p<0.05$ , \*\* $p<0.01$ , \*\*\* $p<0.001$ .

#### *GABA<sub>A</sub>-blockade partially recovers population response differences between masked and full-field conditions*

As previously shown, the reduced amplitude of the response peak is somehow counterintuitive to explain based on the classical notion of receptive field. Hence, as a first attempt to dissect the potential mechanism underlying our observations we selectively blocked the inhibitory transmission mediated by GABA<sub>A</sub> through application of 30 $\mu$ M of bicuculline (N=2 retinas, 3 masks per retina, 464 OFF aeRGCs and 636 ON aeRGCs). The rationale behind this choice was to impair the medium/long-range inhibitory transmission that is mostly, although not entirely, mediated by GABA<sub>A</sub><sup>22</sup>. However, it is important to highlight that this pharmacological manipulation is not specific, since GABA<sub>A</sub>ergic transmission is not solely mediating long-range interactions through amacrine cells, but also the horizontal processing occurring at the level of horizontal cells<sup>23</sup>. With this caveat in mind, we compared the response to full-field and masked stimuli upon administration of bicuculline to evaluate whether GABA<sub>A</sub>ergic transmission contributes to the observed differences between full-field and masked stimulation conditions.

Our results show that upon bicuculline administration the peak of response resulted in an almost linear dependence on the contrast, see Fig 4.13A. However, independently on the contrast, the peak of response was significantly reduced in the masked stimulation condition respect to full-field stimulation, for both ON and OFF aeRGCs. On the other hand, the administration of bicuculline drastically reduced the differences in the lag of response to full-field and masked stimulation conditions. Precisely, the OFF aeRGCs lag response curves practically overlapped for the two stimulation conditions, while the ON aeRGCs still exhibited a delayed but not significant response in masked stimuli condition respect to full-field stimulation (Fig 4.13B).



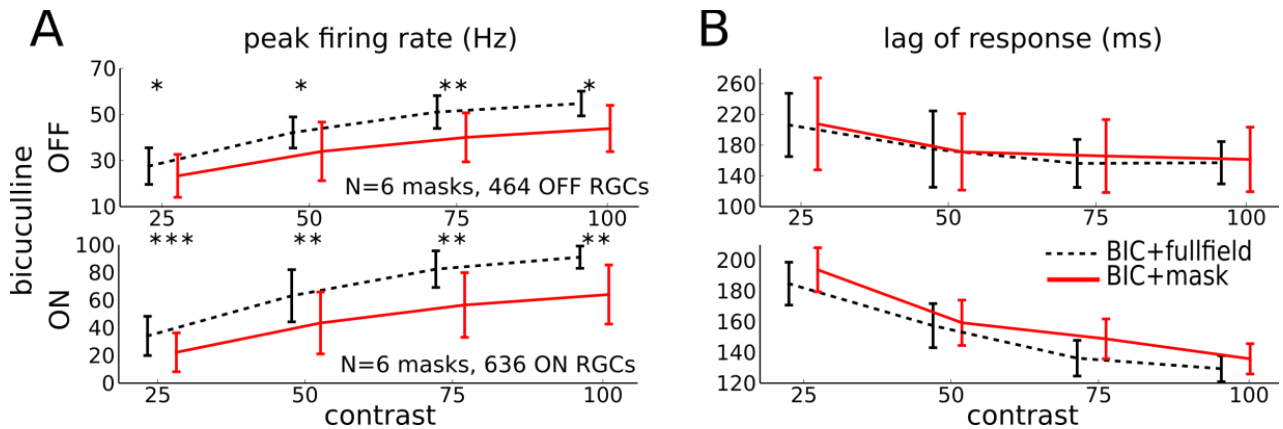


**Fig 4.13 Responses to full-field (dashed black) and masked (solid red) black and white alternating flashing stimuli as a function of the contrast upon administration of 30  $\mu$ M of bicuculline, for ON and OFF always exposed RGCs (aeRGCs). (A) The administration of bicuculline further increases the gap between the peak amplitude between the masked stimulation condition and full-field in both populations. (B) Compared to full-field stimulation, the blockage of GABAergic transmission significantly reduced the delayed response of both ON and OFF aeRGCs in masked stimulation condition respect to full-field. (N=2 retinas, 3 masks per retina, 464 OFF aeRGCs and 636 ON aeRGCs). Paired t-test \* $p < 0.05$ , \*\* $p < 0.01$ , \*\*\* $p < 0.001$ .**

These results, and in particular those on the lag, indicate that GABAergic transmission is more likely involved in shaping the different aeRGCs responses between the two stimulation conditions. However, the administration of bicuculline determined an even more pronounced difference in the peak of response than the one observed in basal condition. To gain a better understanding of the modulation of the peak response induced by the masked stimulation condition we compared the response peak in full-field condition without bicuculline and the peak of response in masked stimulation condition in the presence of the bicuculline, see Fig 4.14. Interestingly, we found that the peak curves of both ON and OFF aeRGCs were nearly indistinguishable between the two stimulation condition, except for a slightly higher variability in the mask and bicuculline condition. This analysis might suggest that population responses to a full-field stimulus are equivalent to a masked stimulus when the GABAergic transmission is disrupted. However, to support this claim, further experiments are needed as it will be discussed later.

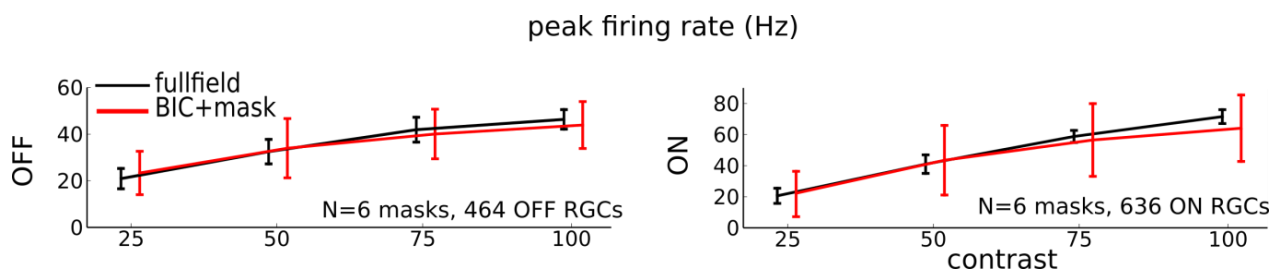


**Fig 4.14: Similar peak of response between full-field and masked stimuli condition without GABAergic transmission. The amplitude of the peak response in masked stimulation condition with the administration of bicuculline equals the one observed in full-field stimulation in untreated condition for both ON and OFF aeRGCs. (N=2 retinas, 3 masks per retina, 464 OFF aeRGCs and 636 ON aeRGCs). Paired t-test \* $p < 0.05$ , \*\* $p < 0.01$ , \*\*\* $p < 0.001$ .**

### *Effects on the asymmetric response of ON and OFF exposed RGCs to moving bars*

The response of ON and OFF aeRGCs to black and white bars moving in a single direction and at the temporal frequency of 1Hz was characterized in the two stimulation conditions (full-field and masked). Six different spatial frequencies were used to evaluate the preferred size of the stimulus<sup>24</sup> for any given aeRGC. The tuning curves for the different stimuli were quantified by considering the coefficient of the Fast Fourier Transform (FFT) of the spike trains related to the 1Hz component (N=4 retina, 3 masks per retina, 1047 OFF and 1769 ON aeRGCs).

Results obtained in the full-field stimulation condition show that ON and OFF aeRGCs populations have a poor tuning to a particular bar width for medium-high contrasts, as indicated by the steadily decreasing tuning curves shown in Fig 4.15. For low contrast stimuli (CT25), the response curve for both ON and OFF population reached a plateau for 0.01 cycle/deg spatial frequency bars, instead of steadily increasing until 0.02 cycle/deg. Although the amplitude of response is significantly lower than the one to higher contrasts; this might indicate a slight tuning to medium-sized bars at low contrast. This intuition will be discussed later through the quantification of the suppressive index (see Discussion). Notably, ON and OFF aeRGCs exhibited a different sensitivity to contrast variation. Indeed, the ON population had a much higher range of amplitudes of response that was roughly proportional to the contrast of the stimulus. Conversely, the OFF population suddenly saturated its response as quantified by the Fast Fourier Transform component at 1Hz, switching from  $\approx 0.02$  directly to the maximum observed value  $\approx 0.09$ .

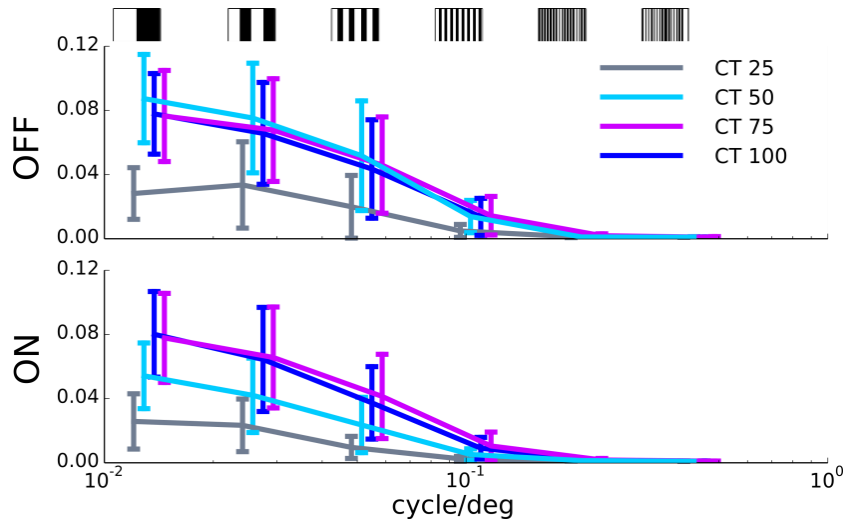


**Fig 4.15: Population response to moving bar stimuli of different spatial grating presented in full-field for different contrasts quantified by the Fast Fourier Transform. While the OFF population rapidly saturates the response as a function of the contrast, ON cells have a more abundant dynamical range. This indicates a more accurate sensibility to contrast of ON cells than OFF cells. The CT25 curve resulted significantly different from all the others for both ON and OFF populations. The curve CT50 resulted significantly different from the others only for the ON population. The statistical significance is assessed at the level  $p=0.05$ . (N=4 retina, 3 masks per retina, 1047 OFF and 1769 ON aeRGCs)**

Similarly to other studies<sup>25</sup>, such asymmetry suggests that the ON and OFF pathways contribute differently to the transduction of visual stimuli across contrasts. In particular, this result indicates that both ON and OFF cells encode and sense visual features for low contrast stimuli whereas the ON circuitry sense contrast variations in a much finer fashion at medium-high contrast levels.

Results obtained by masking the same stimuli (Fig 4.16) showed the masked stimulation condition reduced the magnitude of response in both populations (N=4 retina, 12 masks, 1021 OFF and 1185 ON aeRGCs). Specifically, responses to low spatial frequencies were particularly affected by the masked stimulation condition. Moreover, the masking effect affects to a more considerable extent the responses of ON rather than OFF aeRGCs, see Fig 4.16. This observation combined with the asymmetric perception of contrast mentioned earlier suggests that at high contrasts, OFF aeRGCs encode properties of the stimulus such as the bar width, whereas ON aeRGCs might be more involved in the encoding of contrast variations of the stimulus.

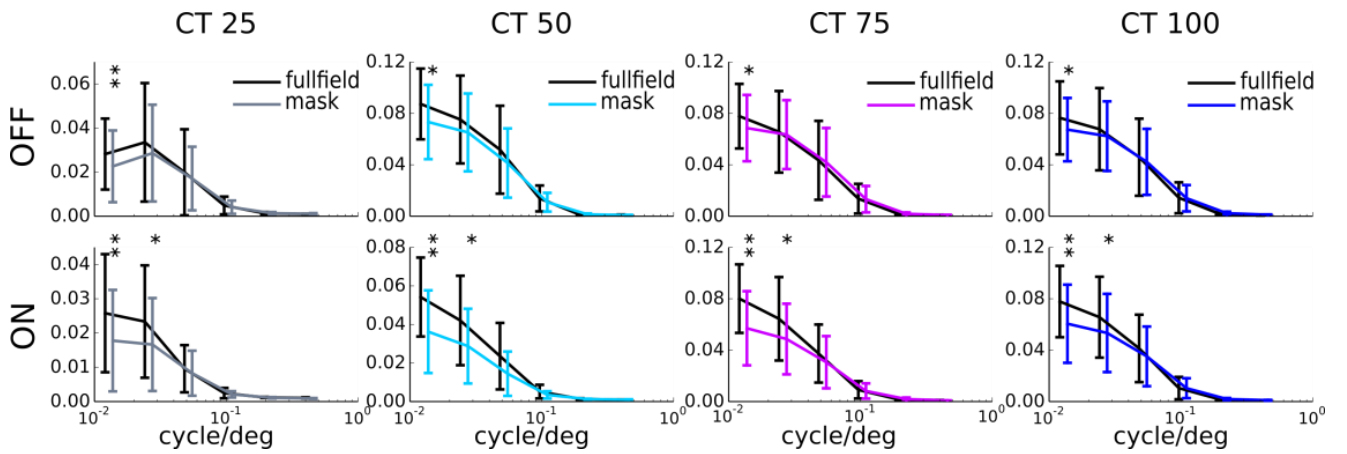


**Fig 4.16: Population response of ON and OFF cells to moving bars of the different spatial grating in full-field and masked stimulation condition.** For all contrast tested, both populations exhibit a reduced tuning to the low spatial frequency of the bars in masked condition (colored lines) respect to full-field (black lines). (N=4 retina, 3 masks per retina, 1021 OFF and 1185 ON aeRGCs). Paired t-test \* $p < 0.05$ , \*\* $p < 0.01$ , \*\*\* $p < 0.001$ .

#### *Effects on model-fitted estimated receptive field parameters of confined visual stimulation*

The previous section has revealed differences in terms of the peak and lag of the populations' responses to masked and full-field stimulation conditions using moving bars and alternating white and black flashes stimuli. Here, we investigate differences in these stimulation conditions using the previously introduced model of receptive fields. To do so, we fitted the parameters of the Gaussian model of the receptive fields with the acquired data for all aeRGCs, regardless of their polarity (N=4 retina, 3 masks per retina, 2176 aeRGCs), and we compared results on data acquired under full-field and masked stimulation conditions. As illustrated in Fig 4.17A, we evaluated the following fitted parameters of the model:  $K_c$ , the amplitude of the center;  $K_s$ , the amplitude of the surround;  $D_c$ , the diameter of the center and  $D_s$ ; the diameter of the surround.

In full-field stimulation conditions, our estimation of the receptive fields using moving bars indicated that the absolute strengths of both the center ( $K_c$ ) and the surround ( $K_s$ ) part of the receptive field are stable across contrasts, see Fig 4.17B. This is different from our previous result (flash and moving bars protocols) in which we showed an explicit dependence on the contrast in the response of aERGcs to moving bars. Interestingly, this difference can be explained by looking at the strength difference between the center and the surround.

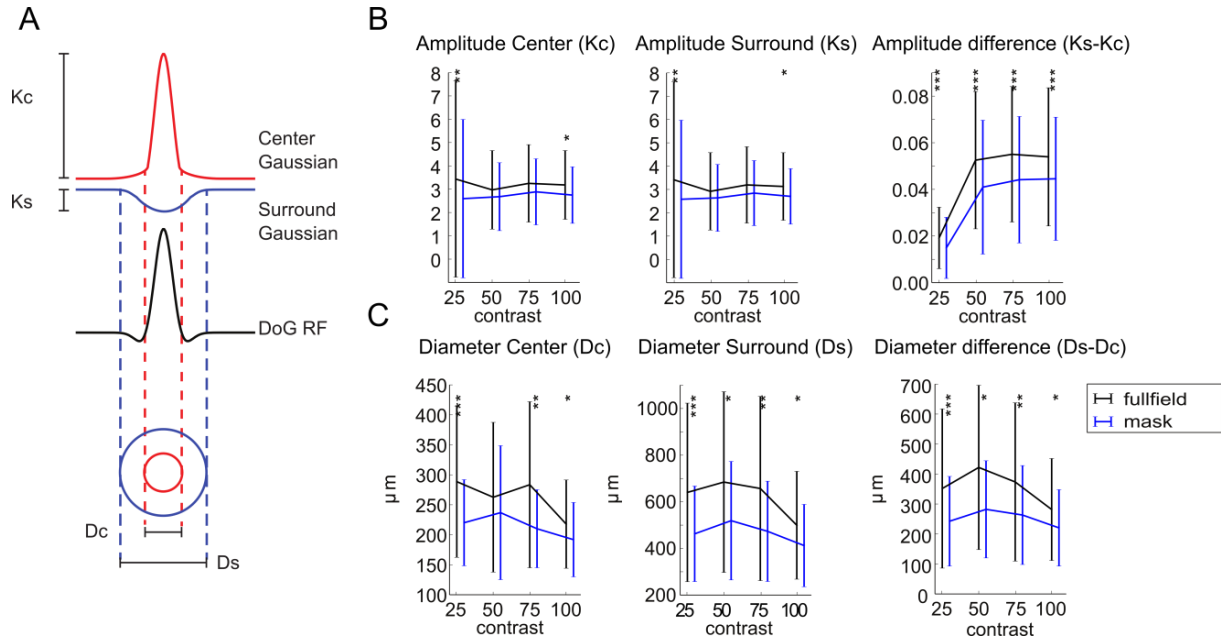


**Fig 4.17: Estimation of receptive field model parameters in full-field (black) and masked (blue) stimulation conditions.** (A) Qualitative representation of the “Difference of Gaussian” model of the receptive field.  $K_c$  and  $K_s$  represent the amplitudes of the concentric excitatory (center) and inhibitory (surround) Gaussians, respectively.  $D_c$  and  $D_s$  represent the size of the receptive field center and surround, respectively. (B) Amplitude of both the center ( $K_c$ ) and the surround ( $K_s$ ) are reduced in masked stimuli condition with respect to the full-field stimulation condition. Similarly to what was observed in the stimulation with white and black alternating flashes in full-field and masked conditions (Fig 4.12), the difference between the center and surround amplitude ( $K_c-K_s$ ), i.e., the expected response to an infinite stimulus covering both the center and the surround, was significantly reduced in masked condition respect to full-field, Paired t-test  $*p<0.05$ ,  $**p<0.01$ ,  $***p<0.001$ . (C) The size of both the center and the surround sizes are reduced in masked condition, thus suggesting a higher tuning to smaller spatial gratings or a loss of tuning for large spatial gratings. Similarly to the relative amplitude between the center and surround of the receptive field, the difference between the size of the surround and the center of the receptive field ( $D_s-D_c$ ) was reduced in masked stimuli condition respect to full-field stimuli.

Specifically, this difference rapidly increased after CT25 (from  $0.022\pm0.09$  to  $0.051\pm0.013$ , a.u. in full-field stimuli conditions), thus indicating a higher contribution of the excitatory center respect to the surround. In other words, while at low contrast the difference of the strength was almost negligible, as the contrast increased the tuning of the RGCs sharpened. Additionally, the difference in strength curve stabilized for CT75 and CT100 ( $0.050\pm0.012$  and  $0.048\pm0.011$ , a.u. respectively),

thus ensuring the convergence of our estimation method. On the other hand, the diameter of the center and the surround exhibited different trends in full-field stimulation, see Fig 4.17C. Specifically, while the diameter did not exhibit a well-defined trend as a function of the contrast, the diameter of the surround steadily decreased at CT75 and CT100 by  $\approx 6\%$  and  $\approx 18\%$  compared to CT50, possibly indicating that at the higher contrast possible the contribution of inhibition sharpened the tuning of RGCs. Indeed, the smaller difference between the center and the surround diameter was observed for stimuli at maximum contrast.

Interestingly enough, the masked stimuli condition revealed changes in the receptive field parameters similar to the ones previously observed with alternating white and black flashes stimuli. First of all, we found that the strength of both the center and the surround of the receptive field were reduced by more than 15% for any of the tested contrasts. Additionally, the difference between the strength of the center and the surround resulted significantly lower (an average reduction of  $187 \pm 52 \mu\text{m}$  among all the contrasts tested) in masked stimulation condition compared to the full-field stimulation. This suggests that for all contrast the response of an aeRGC was indeed reduced in masked stimuli condition respect to full-field stimulation as we directly measured. The same dependence on the contrast was observed between full-field and masked stimuli except for a constant offset term. Unexpectedly, we found that the estimation of the diameter of the receptive field center and surround were greatly reduced in masked condition, with an average two-fold decrease of their amplitude. Indeed, we were expecting to observe less tuned cells, similarly as what we found for a decreased responsiveness to the moving bars. The two-fold reduction of the surround and the center diameter suggests that, in masked stimulation conditions, the retinal ganglion cells experienced an increased amount of inhibition compared to full-field stimulation. This result is inherited from what we have observed with the moving bars of the different spatial grating and where the responses to large bars were significantly reduced.

## ***Discussion***

---

In this section, I discuss our results and experimental conditions with respect to four important points that might have influenced our results and their interpretation. These points are effects that might have been induced by changes in the luminance levels, by a drop-down of the retina responsiveness due to lows of tissue viability during the long duration of our experiments, an adaptation of the retina responses to the stimuli, or to the mesoscopic light stimulation regime used in our experiments. Finally, I provide a possible interpretation of our data and I discuss future experiments that should be performed in order to disentangle the mechanisms at the origin of the observed responses in full-field and masked stimulation conditions.

The first important point to take into account relates to the average luminance level of the presented stimuli. Several experimental works already highlighted the importance of the luminance of the stimulus in modulating the response of RGCs<sup>26</sup>. Specifically, changes in the ambient luminance determine significant qualitative and quantitative changes in the RGCs responses, including the appearance and disappearance of ON responses in OFF cells and vice-versa<sup>26,27</sup>. Thus, a different luminance between the masked and full-field stimulation conditions could explain some of the phenomena we observed with respect to the classical properties of

receptive fields<sup>28,29</sup>. Indeed, it is widely accepted<sup>30,31</sup> that full-field stimulation consistently decreases the peak response of ON and OFF RGCs with respect to large and optimal size spots aligned within the center of the receptive field<sup>32,33</sup>. In our flash protocol, the overall luminance of the stimuli presented to the retina is not spatially uniform over the tissue because of the alternation of dim and bright full-field phases in the exposed area (i.e., not masked). On the other hand, the presence of the mask can modulate the overall luminance as the dim and dark phases of the stimuli in the full field condition are replaced by an iso-luminant gray in the area underneath the mask. Hence, aeRGCs might reduce their peak response to masked stimuli as a consequence of the weaker luminance than experienced in the full-field condition. However, while this argument can explain the reduction in the peak amplitude found for ON and OFF aeRGCs in the masked condition compared to full-field, it is, in my opinion, a weak justification for the reduced FFT amplitude that we observed for masked stimuli. Indeed, in full field stimulation condition, the presence of bright and dark bar gratings ensures that the average spatial level of luminance equals the one applied to the masked area. Furthermore, we also verified whether our recordings are artifact-free for changes in luminance. To do so, we measured using an optical power meter (PM130, Thorlabs<sup>20</sup>) the average luminance in the un-masked region for both full-field and masked stimuli conditions. These tests performed using only the light projector have shown that the luminance in the un-masked region was replicating the same time course during both full-field and masked stimuli condition. Therefore, the observed differences in RGCs responses for the two stimulation conditions are in my opinion unlikely to occur due to luminance differences between the two conditions.

The second important point to raise relates to the viability of the ex-vivo retinas during our experiments. Indeed, degeneration over time of the explanted brain tissue and the limited amount of resources in the photoreceptors may substantially bias our results. The mentioned degenerative phenomena, indeed, might explain our results, especially given the order of the visual stimulation sequence (first full-field and secondly masked stimuli condition). However, in previous experimental investigations performed to validate the experimental platform and conditions, it has been observed that the retinal tissue was reliably and robustly responding for visual stimulations lasting more than two hours and a half, with non-significant attenuations of the peak firing rate in response to alternating dim and bright flashes. To ensure that tissue degeneration is not significantly biasing our results, in all our experiments we performed a full-field flash protocol at the end of masked stimuli condition phase.

	CT 25	CT 50	CT 75	CT 100
OFF RGCs	6.94±24.61 Hz	5.9±21.40 Hz	5.32±24.30 Hz	5.71±23.61 Hz
ON RGCs	3.32±18.93 Hz	3.06±20.59 Hz	3.07±19.29 Hz	3.22±20.11 Hz

**Table 4.1** Difference in peak firing rate in response to alternating flashes of four different contrasts between the beginning and the end of a typical experiment. The pool of cells consists of 617 and 635 OFF and ON retinal ganglion cells recorded during six experiments. The quantification revealed a slight increase of the peak firing rate at the end of the experiment, possibly due to an increased coupling of the tissue with the MEA, which might increase along the duration of the experiment.

As shown in Fig 4.18 the peak firing rate of both ON and OFF aeRGCs is not significantly decreasing (see Table 4.1) during experiments, but exhibit a slight increase possibly due to a slightly improving coupling of the tissue to the CMOS-MEA along with the duration of our experiments (note that before starting an experiment we always wait at least 30 minutes in order to ensure a good and stable coupling).

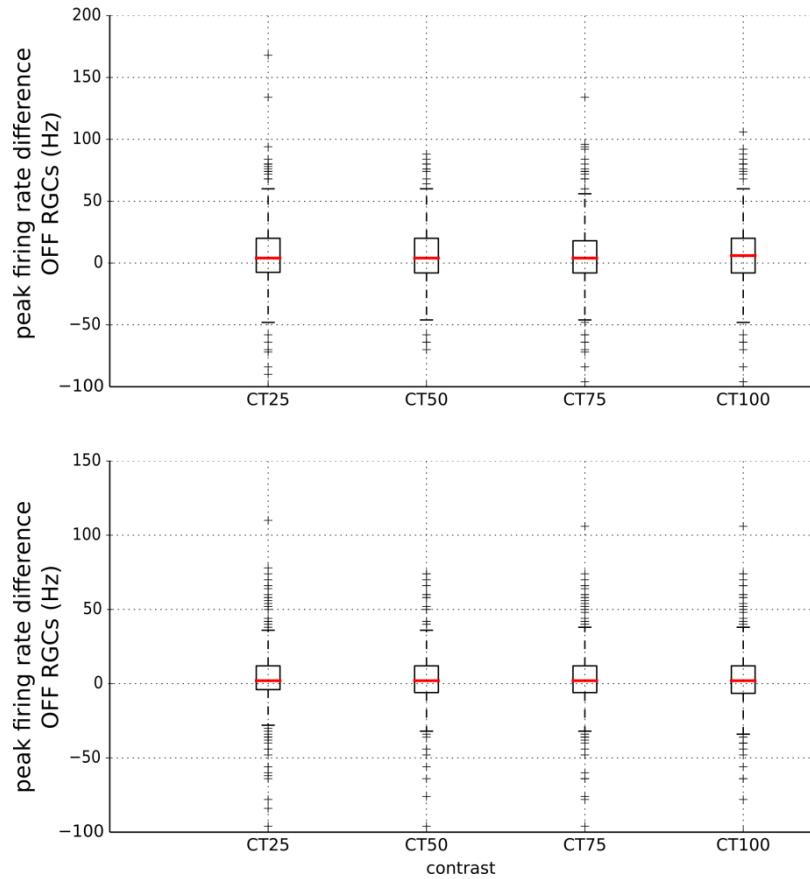


**Fig 4.18: Peak firing rate difference of OFF and ON aeRGCs between a full-field stimulus presented at the beginning and at the very end of a typical experiment and used to assess the stability of retina responses during our long (ca. 100 minutes) stimulation protocols. The peak response of both OFF and ON aeRGC population probed in four distinct areas of the retina does not significantly decrease during the experiment supporting a marginal contribution of the tissue degeneration in explaining the results obtained. Data were collected from 617 and 635 OFF and ON retinal ganglion cells in response to Flash CTALL protocols at the beginning and at the end of 6 experiments. A paired t-test reported nonsignificant decrease for all the contrast tested at  $p=0.05$  level.**

The third potential caveat in our interpretation concerns the potential adaptation of the retina to the stimuli. An adaptation can contribute in modulating the spiking response of retinal ganglion cells during the time course of our experiments. Specifically, the retinal network was shown to be able to adapt its processing from low-contrast stimuli to high-contrast stimuli and vice-versa to efficiently resolve details of the visual scene<sup>34,35</sup>. The retinal ganglion cells response, indeed, is not

solely modulated by the average level of ambient luminance, but also by second order statistics of the light intensity, such as the image contrast. In our experiments aimed at evaluating the response of retinal ganglion cells in full-field and masked stimuli conditions with different ranges of contrast, we took into account this potential risk during the design of the stimulation protocols. In particular, we included intervals with iso-luminant gray uniform images and lasting at least 30s before any change in the stimulus contrast (as the one occurring during the Flash CTALL protocol in between CT25, CT50, CT75 and CT100). This is aimed at restoring the circuit to the baseline and minimize effects of adaptation. Furthermore, at the end of each stimulation condition (i.e., full-field or masked), the retina experienced some minutes of iso-luminant gray, which is the time required for setting up the subsequent protocol of visual stimulation. It also has to be noted that in this study we focused on the mean response of retinal ganglion cells. Consequently, we averaged out the parameters in the 20s time interval of the periodic repetition of the visual stimuli. By doing so, however, the effect of retinal adaptation are masked. Indeed, we experienced adaptation of retinal ganglion cells peak response at the onset of a new sequence of flashes, for both full-field and masked stimuli condition, which affected the first dim and light flash (i.e., approximately 1s). Consequently, in next experiments we are planning to investigate whether the masking of the stimulus (and the size of the masking area) can be potentially associated with a different adaptation time constant of the retinal processing.

The fourth point that has to be considered to interpret our results relates to the mesopic regime of light stimulation used in our experiments. The mesopic luminance used in our experiments (i.e.,  $0.11 \text{ cd/m}^2$ ) seats in the middle between the two extreme scotopic and photopic regimes. Hence, we expect that the response of RGCs should mix the information collected through rods (used for scotopic vision) and the cones (used for photopic vision) pathways. In a study similar to ours<sup>27</sup> (in terms of experimental paradigm and animal model, although measured in-vivo), a set of square-wave alternating dim/bright spots of increasing size (up to full field condition) were presented to the animal, while leaving in constant luminance condition (the average luminance between the dim and bright phase of the stimulus) the portion of the visual scene outside of the spot. In this study, the peak response of RGCs to alternating dim and bright stimuli resulted to be a function of the illuminated area exhibiting the typical center-surround organization. The disagreement between the mentioned work and our results can be disentangled by observing that all our stimuli were presented in mesopic ambient luminance, while the mentioned study was carried out in the photopic regime. Hence, it is possible that the combination of rod and cone signaling pathways characterizing the mesopic regime might both contribute to RGCs responses and might explain our results. Additionally, studies performed in scotopic ambient luminance, or low ambient light levels in mice<sup>36,37</sup> and other animal models<sup>26,38</sup>, found that the antagonistic effect induced by the receptive field surround was either absent or significantly reduced. Indeed, it has to be reminded that in this regime the activation of the surround of ganglion cells requires a higher level of maintained background illumination with respect to the surround antagonism<sup>39,40</sup>. Furthermore, in the scotopic range of luminance, center responses in cat retinal ganglion cells have also been observed by presenting a small spot of light displaced  $450\mu\text{m}$  away from the center of their receptive field, but the same stimulation was shown to turn into antagonistic surround response at photopic levels<sup>38</sup>. Therefore, while in



photopic regime the retinal ganglion cells spiking activity exhibits a clear center-surround organization, in the scotopic regime, the inhibitory contribution that shapes their receptive field is significantly reduced.

Overall, these observations on the mesopic stimulation regime lead us to hypothesize a possible explanation of our results that strictly relates to the interplay in this regime between the center and the surround of the RGCs receptive fields. Theoretically, our results can be easily derived from the absence of an inhibitory surround or with a substantially reduced contribution of inhibition in shaping the center response. Specifically, in the limiting scenario of RGCs without an antagonistic surround, the higher is the extension of the stimulus, the higher the response will be. The latter consideration can indeed explain the reduced peak of response to masked stimuli with respect to full-field. For moving bars stimuli the same argument can explain why the difference in the coefficient of the FFT is statistically significant only for low spatial frequencies. Indeed, while at the medium-high spatial frequencies the alternating dim and bright gratings approximate the projected iso-luminant gray and determine a minor difference between full-field and masked stimuli condition, at low-spatial frequencies the mask significantly reduces the overlap between a stimulus and a large receptive field excitatory center, thus determining a weaker response. In this scenario, the decrease of both the receptive field center and surround for masked stimuli is the result of the reduced extension of the stimulus and of the portion that is impinging the center.

However, the later interpretation raises a series of additional questions. First, is it possible to observe retinal ganglion cells that do not exhibit a clear center-surround organization? Second, if these cells exist, how many of them are present in our recordings? These questions are interesting and can be addressed with our data due to the recording capabilities of high-density CMOS-MEAs. A lack of suppressive signaling to the center of the receptive field can be estimated by the tuning of RGCs to the spatial frequency of the moving bars. This information was hidden in our previous analysis as all the four parameters reported in Fig 4.17 collectively contributed to the RGCs tuning. To quantify the tuning of RGCs with a single parameter, we quantified the suppressive index<sup>41</sup>, which is defined as :

$$100 \cdot \left(1 - \frac{R_{\infty}}{R_{max}}\right)$$

where  $R_{\infty}$  is the response to the largest bars presented and  $R_{max}$  is the maximum response across all the presented spatial frequencies (in this quantification the response is intended as the Fourier coefficient at the temporal frequency of the applied stimuli, i.e., 1Hz). A null suppressive index would mean that the RGCs are poorly tuned, i.e., their maximum response equals the response to the largest presented bar (i.e., 1344  $\mu\text{m}$  in our case). Instead, a value approaching 100 would indicate that RGCs have a small (or no response at all) to the lowest spatial frequencies. At the same time it reveals that the cell is tuned to a single or a range of higher spatial frequencies. The latter scenario would indicate a significant contribution of the surround in shaping the center response. Thus, if our hypothesis on the reduction of the inhibitory contribution induced by the masked condition would be correct, we should expect a considerable number of RGCs with a suppressive index approaching the value of zero.

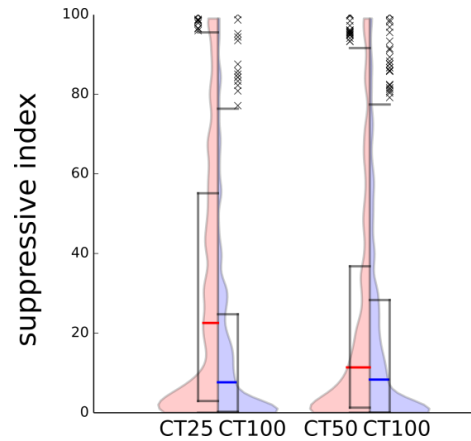


**Fig 4.19: Quantification of the Suppressive Index (SI) of aeRGCs.** The suppressive index, i.e., the tuning to high spatial frequency gratings was quantified for contrasts of CT25, CT50 and CT100 using full-field stimuli. The suppressive index reveals a poor tuning of aeRGCs (N=2176 cells) that slightly improves for low contrast stimuli (CT25).

By running this analysis, we found that a large fraction of aeRGCs was extremely poorly tuned. Specifically, more than 25% of RGCs had a suppressive index of 0 while only 10 % had a suppressive index >50. As shown in Fig 4.19, the tuning of aeRGCs also depended on the contrast and showed a slightly better tuning of the entire population at low contrast levels. Therefore, these results support the hypothesis of a reduced contribution of the inhibitory surround in shaping the response of RGCs at mesopic luminance levels and it can potentially explain why our result differs from the ones reported for photopic stimulation conditions<sup>27</sup>.

Importantly, the lack of tuning observed in our condition is compatible with an intermediate behavior between scotopic and photopic vision<sup>7</sup>. Specifically, stimulation with full-field sine-wave modulated gratings at different spatial frequency determines a strong shift from low spatial frequency to mid-spatial frequencies in the tuning of mouse RGCs for conditions from scotopic to photopic regimes<sup>36</sup>. In scotopic regimes the tuning curves in response to different spatial gratings were found to be constantly increasing with the decrease of the spatial frequency, thus corresponding to a null tuning. However, in photopic conditions, the tuning curves of the same RGCs reached a maximum at 0.017 cycle/deg (corresponding to 1632 $\mu$ m bar width) and a reduced response to lower spatial frequencies<sup>36</sup>. Similarly, the shift from low to high spatial frequency responses observed when shifting from low to high luminance ambient levels has also been observed in behavioral tests in mice<sup>42</sup>. These results are also consistent with the evidence that, in the photopic regime mouse RGCs markedly exhibit the features of center-surround organization. In this case, stimulation in the periphery of the receptive field center with the preferred stimulus determines a weaker response of the cells<sup>16</sup>.

Consequently, we estimate that under mesopic luminance condition both rods and cones pathways are conveying information to RGCs. This consideration is particularly appealing in our case since, differently than bipolar cone cells, bipolar rod cells lack a center-surround organization<sup>37</sup> and their activity is mediated by wide-field amacrine cells that in turn can provide an inhibitory feedback inhibition onto the terminals of bipolar cells<sup>43</sup>. This inhibitory feedback was shown to be GABA mediated<sup>44</sup>. The peculiar connectivity and the morphology of this type of

amacrine cells that can span for millimeter distances<sup>43</sup> represent therefore a good candidate for further studies on this horizontal signal transmission in the retina. In our study, we have attempted to disentangle a potential neuronal circuitry through preliminary experiments using pharmacological manipulation (administration of bicuculline). However, the administration of bicuculline blocked several other inhibitory pathways because the GABAergic transmission is ubiquitary in the retina (see for instance horizontal cells and amacrine cells)<sup>45</sup>. Although this important issue in our bicuculline experiments, our results revealed interesting phenomena. While bicuculline recovered the difference in the lag of response between masked and full-field stimuli condition, it further increased the gap in the peak response of aeRGCs. At the current stage, we do not have an explanation for this unexpected result. Specifically, while the reduction in the lag of response was somehow expected by the release of the inhibitory contribution on the retinal temporal processing, the significant decrease of the peak of response in the masked regions is not straightforward to understand. Finally, it has to be highlighted that several other potential targets should be considered in addition to a potential contribution of wide-field amacrine cells. These targets include the population of displaced amacrine cells<sup>46</sup>, the activation of melanopsin ganglion cells (that contact starburst), All amacrine cells that ultimately regulate the crossover between rods and cones pathways<sup>47</sup> and the dopaminergic circuit<sup>48,49</sup> which modulate the rod pathway. Conversely, we tend to exclude a possible cross-talk at the horizontal cell level because the gap junctions established among these cells have a minor influence in shifting the sensitivity to high spatial gratings when moving from scotopic to photopic regimes<sup>36</sup>.

Altogether, the results of our study raise additional questions that need to be experimentally addressed in future work. In particular, we are planning to further classify RGCs according to their tuning to provide a clearer picture of our results. To this aim, we plan to check the goodness of fit between a single excitatory Gaussian and the combination of an excitatory and inhibitory one. Given that the polarity of RGCs can change as a function of the ambient luminance<sup>26</sup>, the overlap between the center-surround organization and the stimulus<sup>16</sup>, we want to explore whether aeRGCs in our recordings do change their polarity towards ON-OFF responses. At the same time, we aim at performing a set of experiments to target the amacrine population. While methods to selectively perturb the amacrine population needs to be established, in the short term we will investigate the masked and full-field responses upon administration of a cocktail of bicuculline and strychnine, in order to remove the inhibition mediated by GABA<sub>A</sub> and the glycine<sup>50</sup>. The expected outcome of this experiment is that aeRGCs responses under full field and masked conditions should be nearly indistinguishable after the pharmaceutical treatment.

### *Functional implications of our results for vision*

Our result suggests that differently than in photopic vision, in the mesopic regime and at the luminance level that we tested, the strategy for the visual information encoding used by the retina might be substantially different and it resemble more a scotopic than a photopic type of vision. Specifically, a full-field change in luminance seems to convey much more information (in terms of number of spikes and latency to the peak response) than a confined stimulus. Importantly, since mice are nocturnal animals they most likely exploit the vision in mesopic conditions, and

consequently, the coding strategy of their retina should be adapted to maximize the efficiency and effectiveness of the visual stream. The poor tuning of retinal ganglion cells that we observed, however, suggests that in mesopic conditions low spatial frequency largely dominates over details. Thus, differently than in photopic vision, a larger area of the visual scene modulates the center response of RGCs as a consequence of a reduced lateral inhibition. Nevertheless, our data showed a good confinement of the activity induced by the mask application.

The latter observation has important implications for mesopic vision. How can mice discriminate edges with such a poor spatial resolution and in dim conditions? We suggest that border detection might be performed by downstream circuits that compare in a differential manner the output of large population of RGCs. On the other hand, in the full-field condition, the whole visual scene is rapidly changing unexpectedly. Hence, the increased peak firing rate and the diminished temporal lag might represent a signal of alert for downstream circuits. Conversely, in the photopic range, the increased spatial acuity gained by the contribution of the surround inhibition, might provide a higher resolution content of the visual scene than in mesopic condition. Consequently, RGCs are already conveying an accurate piece of information and consequently broad modulations of the retinal output related to low spatial frequencies can be filtered out.

## Bibliography

---

1. Portelli, G. *et al.* Rank Order Coding: a Retinal Information Decoding Strategy Revealed by Large-Scale Multielectrode Array Retinal Recordings. *eNeuro* **3**, (2016).
2. Maccione, A. *et al.* Following the ontogeny of retinal waves: pan-retinal recordings of population dynamics in the neonatal mouse. *J. Physiol.* **592**, 1545–1563 (2014).
3. Hilgen, G. *et al.* Unsupervised Spike Sorting for Large-Scale, High-Density Multielectrode Arrays. *Cell Rep.* **18**, 2521–2532 (2017).
4. Hilgen, G. *et al.* Pan-retinal characterisation of Light Responses from Ganglion Cells in the Developing Mouse Retina. *Sci. Rep.* **7**, 42330 (2017).
5. DLPLIGHTCRAFTER DLP® LightCrafter™ Evaluation Module | TI.com. Available at: <http://www.ti.com/tool/DLPLIGHTCRAFTER>. (Accessed: 20th November 2017)
6. Nathan, J. *et al.* Scotopic and Photopic Visual Thresholds and Spatial and Temporal Discrimination Evaluated by Behavior of Mice in a Water Maze†. *Photochem. Photobiol.* **82**, 1489 (2006).
7. Dedek, K. *et al.* Ganglion cell adaptability: Does the coupling of horizontal cells play a role? *PLoS One* **3**, 22–5 (2008).
8. Williams, G. a, Daigle, K. a & Jacobs, G. H. Rod and cone function in coneless mice. *Vis. Neurosci.* **22**, 807–16 (2005).
9. Joesch, M. & Meister, M. A neuronal circuit for colour vision based on rod-cone opponency. *Nature* **532**, 236–239 (2016).
10. Volgyi, B. Convergence and Segregation of the Multiple Rod Pathways in Mammalian Retina. *J. Neurosci.* **24**, 11182–11192 (2004).
11. Asteriti, S., Gargini, C. & Cangiano, L. Mouse rods signal through gap junctions with cones. *Elife* **2014**, e01386 (2014).
12. Amin, H., Nieu, T., Lonardoni, D., Maccione, A. & Berdondini, L. High-resolution bioelectrical imaging of Aβ-induced network dysfunction on CMOS-MEAs for neurotoxicity and rescue studies. *Sci. Rep.* **7**, 2460 (2017).
13. Brunelli, R. *Template matching techniques in computer vision: theory and practice. Theory and Practice* (Wiley, 2009). doi:10.1002/9780470744055
14. Hitchcock, F. L. The Distribution of a Product from Several Sources to Numerous Localities. *J. Math Phys.* **20**, 224–230 (1941).
15. Rodriguez, A. & Laio, A. Clustering by fast search and find of density peaks. *Science (80-. ).* **344**, 1492–1496 (2014).
16. Sagdullaev, B. T. & McCall, M. a. Stimulus size and intensity alter fundamental receptive-field properties of mouse retinal ganglion cells in vivo. *Vis. Neurosci.* **22**, 649–59 (2005).
17. Rodieck, R. W. Quantitative analysis of cat retinal ganglion cell response to visual stimuli. *Vision Res.* **5**, 583–601 (1965).
18. Fiorani, M., Azzi, J. C. B., Soares, J. G. M. & Gattass, R. Automatic mapping of visual cortex receptive fields: A fast and precise algorithm. *J. Neurosci. Methods* **221**, 112–126 (2014).
19. Pamplona, D., Hilgen, G., Cessac, B., Sernagor, E. & Kornprobst, P. A super-resolution approach for receptive fields estimation of neuronal ensembles. *BMC Neurosci.* **16**, P130 (2015).
20. Thorlabs - PM130 Digital Power Meter w/Slim Sensor S130A , 5nW-5mW/500nW-500mW, 400-1100nm. Available at: <https://www.thorlabs.com/thorproduct.cfm?partnumber=PM130>. (Accessed: 20th November 2017)
21. Carcieri, S. M. Classification of Retinal Ganglion Cells: A Statistical Approach. *J. Neurophysiol.* **90**, 1704–1713 (2003).
22. Franke, K. & Baden, T. General features of inhibition in the inner retina. *J. Physiol.* **595**, 5507–5515 (2017).
23. Gollisch, T. Features and functions of nonlinear spatial integration by retinal ganglion cells. *J. Physiol. Paris* **107**, 338–348 (2013).
24. Barlow, H. B., Derrington, A. M., Harris, L. R. & Lennie, P. The effects of remote retinal stimulation on the responses of cat retinal ganglion cells. *J. Physiol.* **269**, 177–194 (1977).

25. Jiang, Y., Purushothaman, G. & Casagrande, V. A. The Functional Asymmetry of ON and OFF Channels in the Perception of Contrast. *J. Neurophysiol.* **114**, jn.00560.2015 (2015).
26. Tikidji-Hamburyan, A. *et al.* Retinal output changes qualitatively with every change in ambient illuminance. *Nat. Neurosci.* **18**, 66–74 (2015).
27. Sagdullaev, B. T. & McCall, M. a. Stimulus size and intensity alter fundamental receptive-field properties of mouse retinal ganglion cells in vivo. *Vis. Neurosci.* **22**, 649–59 (2005).
28. Enroth-Cugell, C. & Freeman, A. W. The receptive-field spatial structure of cat retinal Y cells. *J. Physiol.* **384**, 49–79 (1987).
29. Koch, K. *et al.* How Much the Eye Tells the Brain. *Curr. Biol.* **16**, 1428–1434 (2006).
30. Kandel, E. R., James H. Schwartz & Thomas M. Jessell. *Principles of Neural Science. Neurology* **3**, (2000).
31. Purves, D. Vision. in *Handbook of Neuroscience for the Behavioral Sciences* (John Wiley & Sons, Inc., 2009). doi:10.1002/9780470478509.neubb001012
32. HEINE, W. F. & PASSAGLIA, C. L. Spatial receptive field properties of rat retinal ganglion cells. *Vis. Neurosci.* **28**, 403–417 (2011).
33. Cook, P. B. & McReynolds, J. S. Lateral inhibition in the inner retina is important for spatial tuning of ganglion cells. *Nat. Neurosci.* **1**, 714–719 (1998).
34. Smirnakis, S. M., Berry, M. J., Warland, D. K., Bialek, W. & Meister, M. Adaptation of retinal processing to image contrast and spatial scale. *Nature* **386**, 69–73 (1997).
35. Baccus, S. A. & Meister, M. Fast and Slow Contrast Adaptation in Retinal Circuitry. *Neuron* **36**, 909–919 (2002).
36. Dedek, K. *et al.* Ganglion cell adaptability: Does the coupling of horizontal cells play a role? *PLoS One* **3**, e1714 (2008).
37. Bloomfield, S. A. & Dacheux, R. F. Rod vision: Pathways and processing in the mammalian retina. *Prog. Retin. Eye Res.* **20**, 351–384 (2001).
38. Müller, J. F., Dacheux, R. F., Muller, J. F. & Dacheux, R. F. Alpha ganglion cells of the rabbit retina lose antagonistic surround responses under dark adaptation. *Vis. Neurosci.* **14**, 395–401 (1997).
39. Hammond, P. Receptive field mechanisms of sustained and transient retinal ganglion cells in the cat. *Exp. Brain Res.* **23**, 113–128 (1975).
40. Barlow, H. B. & Levick, W. R. Changes in the maintained discharge with adaptation level in the cat retina. *J. Physiol.* **202**, 699–718 (1969).
41. Marco, S. D., Protti, D. A. & Solomon, S. G. Excitatory and inhibitory contributions to receptive fields of alpha-like retinal ganglion cells in mouse. *J. Neurophysiol.* **110**, 1426–1440 (2013).
42. Umino, Y., Solessio, E. & Barlow, R. B. Speed, Spatial, and Temporal Tuning of Rod and Cone Vision in Mouse. *J. Neurosci.* **28**, 189–198 (2008).
43. Lin, B. & Masland, R. H. Populations of wide-field amacrine cells in the mouse retina. *J Comp Neurol* **499**, 797–809 (2006).
44. MASLAND, R. H. The tasks of amacrine cells. *Vis. Neurosci.* **29**, 3–9 (2012).
45. Jeon, C. J., Strettoi, E. & Masland, R. H. The major cell populations of the mouse retina. *J Neurosci* **18**, 8936–8946 (1998).
46. Pé, L., De Sevilla, R., Ller, M., Shelley, J. & Weiler, R. Displaced Amacrine Cells of the Mouse Retina. *J. Comp. Neurol* **505**, 177–189 (2007).
47. Kolb, H. *Roles of Amacrine Cells. Webvision The Organization of the Retina and Visual System* (2005).
48. Krizaj, D., Gábel, R., Owen, W. G. & Witkovsky, P. NIH Public Access. *J Comp Neurol.* **398**, 529–538 (1998).
49. Herrmann, R. *et al.* Rod Vision Is Controlled by Dopamine-Dependent Sensitization of Rod Bipolar Cells by GABA. *Neuron* **72**, 101–110 (2011).
50. Flores-Herr, N., Protti, D. A. & Wassle, H. Synaptic currents generating the inhibitory surround of ganglion cells in the mammalian retina. *J Neurosci* **21**, 4852–4863 (2001).

# Chapter V - Dissemination and attended schools

This section reports the dissemination results of my work achieved during the three years of my Ph.D. This includes publications in peer-reviewed journals, oral and poster presentations at international conferences or seminars. Finally, I also report here the schools I have attended during my Ph.D.

## ***Peer-reviewed contributions***

---

Valente, P., Romei, A., Fadda, M., Sterlini, B., Lonardoni, D., Fruscione, F., Castroflorio, E., Michetti, C., Valtorta, F., Tsai, J., Zara, F., Nieuws, T., Corradi, A., Fassio, A., Baldelli, P. & Benfenati F., Constitutive inactivation of the PRRT2 gene alters short-term synaptic plasticity and promotes network hyperexcitability in hippocampal neurons. *Cerebral Cortex*, under revision.

Aletti, G., Lonardoni, L., Naldi, G. & Nieuws T., From dynamics to links: a sparse reconstruction of the topology of a neural network. *Communications in Applied and Industrial Mathematics*, (2017), in press.

Lonardoni, D., Amin, H., Di Marco, S., Maccione, A., Berdondini, L., & Nieuws, T. Recurrently connected and localized neuronal communities initiate coordinated spontaneous activity in neuronal networks. *PLOS Computational Biology* **13**, e1005672 (2017).

Amin, H., Nieuws, T., Lonardoni, D., Maccione, A., & Berdondini, L. High-resolution bioelectrical imaging of A $\beta$ -induced network dysfunction on CMOS-MEAs for neurotoxicity and rescue studies. *Sci. Rep.* **7**, 2460 (2017).

Lonardoni, D., Di Marco, S., Amin, H., Maccione, A., Berdondini, L. & Nieuws, T., High-density MEA recordings unveil the dynamics of bursting events in Cell Cultures. *Engineering in Medicine and Biology Society (EMBC), 2015 37th Annual International Conference of the IEEE*. (2015).

Bosi, S., Rauti, R., Laishram, J., Turco, A., Lonardoni, D., Nieuws, T., Prato, M., Scaini, D. & Ballerini, L., From 2D to 3D: Novel nanostructured scaffolds to investigate signaling in reconstructed neuronal networks. *Sci. Rep.* **5**, 9562 (2015).

## ***Manuscript in preparation***

Lonardoni, D., et al. Combining high dense MEA retina recording with precise spatiotemporal visual stimulation to investigate long-range horizontal interactions.

## ***Oral presentations***

---

Talk entitled: “High-density MEA recordings unveil the dynamics of bursting events in Cell Cultures.” at 37th Annual International Conference of the IEEE Engineering in Medicine and Biology Society (EMBC) on 27/08/2015.

Talk entitled: “Determinants of spontaneous synchronized network activity in primary neuronal cultures: a computational approach” in “Reading Group Seminar-Workshop” organized by Mathematics Department of University of Milan on 23/05/2016.

## ***Poster presentations***

---

### ***Computational Neuroscience Conference 2015, Prague***

“A computational model of cell culture dynamics: the role of connectivity and synaptic receptors in the appearance of synchronized bursting events”, authors: Lonardoni D., Amin H., Di Marco S., Maccione A., Berdondini L., Nieuws, T.  
Date: 20/07/2015; Poster Board Number: P177

### ***Bernstein conference 2015, Heidelberg***

“A computational model of neuronal network dynamics: the role of synaptic receptors in modulating synchronized bursting events”, authors: Lonardoni D., Amin H., Di Marco S., Maccione A., Berdondini L., Nieuws, T.  
Date: 16/09/2015; Poster Board Number: W47

### ***Society for Neuroscience Conference 2016, San Diego***

“Determinants of spontaneous synchronized network activity in primary neuronal cultures: A computational approach”. Authors: Lonardoni D., Amin H., Di Marco S., Maccione A., Nieuws, T., Berdondini L.  
Date: 15/11/2016; Poster Board Number: NNN31

### ***26th Annual Computational Neuroscience Meeting 2017, Antwerp***

“Insurgence of network bursting events in formed neural culture networks: a computational approach”. Authors: Lonardoni D., Amin H., Di Marco S., Maccione A., Nieuws, T., Berdondini L.  
Date: 16/07/2017; Poster Board Number: 14  
“Investigating the effects of horizontal interactions on RGCs responses in the mice retina with high-resolution pan-retinal recordings”. Authors: Lonardoni D., Boi F., Di Marco S., Maccione A., Berdondini L.  
Date: 17/07/2017; Poster Board Number: 187



## ***Schools attended***

---

### ***GPWS 2015***

Gaussian Process Winter School 2015, Genova, Italy: January, 19-22, 2015

Instructor: Prof. Dr. Neil Lawrence and Prof. Dr. Lorenzo Rosasco

### ***Information Processing in Neural Systems: From Single Neurons to Large-Scale Models of Cognition***

Osnabrück, Germany: May 2-10, 2015

Instructors:

Prof. Dr. Nicolas Brunel, Prof. Dr. Gustavo Deco, Dr. Marc-Oliver Gewaltig, Prof. Dr. Frank Jäkel, Prof. Dr. Herbert Jäger, Prof. Dr. Peter König and Prof. Dr. Gordon Pipa



# ***Annex I - Neuronal cultures protocol, model implementation and analysis***

## ***Ethics Statement***

All procedures involving experimental animals were approved by the institutional IIT Ethic Committee and by the Italian Ministry of Health and Animal Care (Authorization number 110/2014-PR, December 19, 2014).

## ***Large-scale recording of neuronal spiking activity in cultured networks***

---

### *Cell cultures and high-resolution CMOS-MEA recordings*

Primary hippocampal neurons from rat embryos (at embryonic day 18, E18) were dissociated following procedures as described in <sup>1,2</sup> and plated on CMOS multi-electrode arrays (CMOS-MEAs, Biochip 4096E, from 3Brain GmbH). Chips were previously sterilized with 70% ethanol, conditioned overnight in an incubator with cell culture media and coated with adhesion-promoting molecules, i.e., a double layer of 0.1 mg/ml poly-L-lysine (Sigma P-6407) and 0.1 mg/ml laminin (Sigma L-2020). A few hours after plating at a nominal cellular density of approximately 3000 cell/mm<sup>2</sup>, the cell culture reservoir of each device was filled with 1.5 mL of Neurobasal cell culture media (Thermo Fisher, #21103049) supplemented with B-27 (Thermo Fisher, #17504044) and placed in a humidified incubator (5% CO<sub>2</sub>) at 37 °C. Cell cultures were grown on a chip for 19-21 days *in vitro*, an age where sustained spontaneous electrical activity characterized by single spikes and short bursts propagating through the network is observed.

The extracellular activity of the cultures was recorded from 4096 electrodes for 10 minutes using a custom recording system similar to the BioCam platform commercially distributed by 3Brain AG, Switzerland. The electrode array provides 4096 square electrodes (21 x 21 µm<sup>2</sup>, 82 µm electrode pitch) covering an active area of approximately 5 x 5 mm<sup>2</sup>. Pharmacologically manipulated activity with bicuculline (BIC) at 30 µM or (2R)-amino-5-phosphonovaleric acid (APV) at 50 µM was also recorded for some cultures after adding the compound to the cell culture media. All the raw data were stored as .brw files (BrainWave, 3Brain AG, Switzerland) and then exported to Python (Python Software Foundation, Python Language Reference, version 2.7) for further analysis (c.f. “Data analysis of experimental and simulated data”).

### *Computational network model*

The computational network model is composed of a set of excitatory and inhibitory spiking neuronal models implemented in NEURON <sup>3</sup>. We used the Adaptive Exponential Integrate and Fire (AdExp) neuron model described in <sup>4</sup>, which, similar to the Izhikevich model <sup>5</sup>, represents a good compromise between computational costs and the capability of mimicking the variety of firing

patterns exhibited by real neurons. The differential equations governing the AdExp dynamics are as follows:

$$\begin{cases} C \frac{dV}{dt} = -g_L(V - E_L) + g_L \Delta T e^{\left(\frac{V - V_T}{\Delta T}\right)} - w + \sum I_{syn} + I_{bg} \\ \tau_w \frac{dw}{dt} = a(V - E_L) - w \end{cases}$$

The variable  $V$  represents the membrane potential, and  $w$  is an internal state variable responsible for any adaptive phenomena. The voltage  $V$  is governed by a leak current (conductance  $g_L$ , reversal potential  $E_L$ ), a  $Na^+$ -like current involved in the upswing of the action potential given by the exponential term, an adaptive current  $w$ , the synaptic currents  $I_{syn}$  and a background noise  $I_{bg}$  current. The adaptive current  $w$  is modulated by the voltage and relaxes back to its equilibrium with the adaptation time constant  $\tau_w$ . Regarding the spiking mechanisms, whenever the voltage crosses the threshold of 0 mV, a spike is emitted, and the state variables are reset ( $V \rightarrow V_{reset}$ ,  $w \rightarrow w + b$ ). In our model, the parameter settings of the AdExp were adapted from <sup>6</sup>. Because neurons do not fire isolated bursts at the mature stage of cell culture <sup>7</sup>, we assumed standard spiking models for the excitatory and inhibitory neurons <sup>8</sup> with the same 4:1 ratio. Excitatory neurons were modelled as characteristic adaptive firing neurons, and inhibitory neurons mimicked the firing of fast-spiking interneurons. Then, to consider the heterogeneity of cells in neural cultures and to ensure that network synchronization was not a consequence of identical properties of single cells <sup>9,10</sup>, the parameters of the modelled neurons were drawn from a normal distribution (see Table 2 for values).

### Synaptic communication

Previous studies highlighted that the coordinated activities in cell cultures are determined by the chemical synapses and not by gap junctions or extracellular substances <sup>11</sup>. Therefore, we modeled the dynamics of excitatory AMPA and NMDA and inhibitory GABA chemical synapses. Synaptic transmission was delayed by a fixed time (0.5 ms) to account for synapse activation and a variable delay (maximum 1.5 ms) to account for the propagation of the pre-synaptic spike. Each type of synapse contributed with a current  $I_{syn}$  modelled as follows:

$$\begin{cases} I_{syn} = g_{syn}(v - E_{rev}) \\ \tau_{syn} \frac{dg_{syn}}{dt} = -g_{syn} \end{cases}$$

where  $g_{syn}$  is the synaptic conductance and  $E_{rev}$  is its reversal potential. The synaptic conductance has a bi-exponential profile (parameters in Table 3):

$$\begin{cases} \tau_{syn} \frac{dg_{syn}}{dt} = -g_{syn} \\ \tau_{rise} \frac{dg_{rise}}{dt} = -g_{rise} \\ I_{syn} = (g_{syn} - g_{rise})(v - E_{rev}) \end{cases}$$

Each time an action potential is delivered to a target neuron (i.e., a time  $t_{sp}$ ), the conductance parameters  $g_{syn}$  and  $g_{rise}$  are increased by  $\bar{g} \times y$ , where  $\bar{g}$  is the maximum value for the synaptic

conductance and  $y$  is the fraction of the active resources (i.e., released neurotransmitters). The synaptic current exhibits short-term depression modelled under the assumption of finite synaptic resources<sup>12</sup> as shown:

$$\begin{cases} \frac{dx}{dt} = \frac{z}{\tau_{rec}} - u \cdot x \cdot \delta(t - t_{sp}) \\ \frac{dy}{dt} = -\frac{y}{\tau_1} + u \cdot x \cdot \delta(t - t_{sp}) \\ \frac{dz}{dt} = \frac{y}{\tau_1} - \frac{z}{\tau_{rec}} \end{cases}$$

where  $x$ ,  $y$  and  $z$  represent the fraction of available, active and recovered resources, respectively. The time constant  $\tau_1$  regulates the transition between the available and active state, and  $\tau_{rec}$  is the recovery time constant.

The NMDA current was modeled similarly to the AMPA and GABA currents, with an additional magnesium block mechanism<sup>13</sup>:

$$I_{NMDA} = g_{NMDA} \cdot (v - E_{rev}) \cdot 1 / (1 + \exp(-(v - v_0)/k_0))$$

where  $k_0=6$  mV (steepness of voltage dependence) and  $v_0=-40$  mV (half-activation potential). The maximum NMDA conductance ( $\bar{g}_{NMDA}$ ) is written in terms of the AMPA conductance:  $\bar{g}_{NMDA} = K_{NMDA} \cdot \bar{g}_{AMPA}$  such that in basal/standard conditions  $K_{NMDA} = 0.09$  (i.e.,  $\bar{g}_{NMDA}=4.32$  nS), and while under APV application, an NMDA antagonist,  $K_{NMDA} = 0$ . All parameter values are reported in Table 3. To mimic the effects of the NMDA and GABA synaptic blockers (APV and BIC), the conductance of the target receptor was set to zero. Networks with only the AMPA and GABA synapses are called AG-networks in the text, and networks with in addition the NMDA current are called AGN-networks.

### Background activity of the network

From its earliest days *in vitro*, cultured neuronal networks display random spontaneous spiking activity. In the model, this activity was mimicked by injecting sub-threshold synaptic noise (i.e., miniature events<sup>11</sup>) modeled as independent Poisson processes at a mean frequency of 25 Hz. The summation of the synaptic noise occasionally brought the neurons to fire in the uncoupled network and determined a background spiking activity of  $0.010 \pm 0.007$  Hz (close to the value found in experiments when AMPA receptors are blocked with CNQX<sup>14</sup>).

### Network topology

Although network topology has been recognized to play an important role in determining network activity, many works have neglected the spatial constraints derived from the location of neurons in the network<sup>15,16</sup>. To be comparable with our experimental recordings, 4096 neurons were uniformly distributed on a unit square, and the connectivity probability among the neurons depended on the distance according to a radial Gaussian function. The distance-based connectivity rule allowed for the creation of biologically inspired networks whose graph properties (i.e., clustering coefficient or the presence of shortcuts) were not imposed but were rather inherited from the imposed spatial organization of neurons. Only graphs without any isolated component

were used in the simulations. It is important to highlight that the random arrangement of neurons, the distance-based connectivity rule and the sparseness of the connections used to establish the network topology give rise to an in-homogeneously connected network that includes clusters of nodes with denser connections. As a consequence, although the node degree is quite comparable between the Gauss and random graph, the clustering coefficient of the former is significantly higher than in the latter one.

The directionality of the synaptic connections among pairs of neurons was assigned with equal probability. Although bidirectional connections are quite common in the brain, computer simulations have shown that networks with only depressing synapses (as assumed in this work) tend to evolve unidirectional connections<sup>17</sup>. Regarding the connectivity of the network, in 2D cell cultures, each neuron receives somewhere from 150 to 400 synapses<sup>18</sup>. Because each neuron is contacted by eight synapses from the same neuron on average<sup>19</sup>, the actual effective synapses in the model were decreased to  $41.6 \pm 6.4$  synapses per neuron. Table 1 summarizes the graph properties (e.g., clustering coefficient, mean path length, degree<sup>20</sup>) of the simulated network. Note that neurons at the border of the domain were treated exactly like the other nodes and were consequently connected to a smaller number of neurons.

#### *Data analysis of experimental and simulated data*

To facilitate the comparison with the experimental data, the simulated spike trains were subjected to the same filtering criteria used in the experiments. Thus, only neurons whose firing rate (i.e., average number of spikes per unit time) fell in the interval [0.1-15] Hz were considered.

### ***Detection and quantification of spontaneous activity in neuronal cultures***

---

#### *Spike detection and spike-based quantification*

We quantified the spiking network activity by using standard activity parameters<sup>14,21</sup> such as the mean firing rate of the network (MFR) and the interspike interval (ISI) distribution. The MFR is the average of the firing rates of all of the active neurons of the network, and the ISI is the first order difference of the spike times. Additionally, to characterize the network burst regime, we quantified canonical parameters such as the mean bursting rate (MBR), the mean firing intra burst (MFIB) and the mean burst duration (MBD), as in<sup>22</sup>. Finally, as most of the neurons in these networks participate in NBs with a burst of spikes, we defined an indirect measure of asynchronous network activity (Random Spikes), as the percentage of spikes that are not part of a burst (a sequence of 5 or more spikes separated by less than 100 ms). Bursting events (NBs) are stereotyped network activities characterized by a large fraction of neurons simultaneously active for  $\approx 100\text{ms}$ , and thus, these events could be detected by setting a hard threshold on the instantaneous MFR<sup>23,24</sup>. This algorithm works well on simulated data, but on real experimental data, the detection of NBs can be hindered by noise (e.g., false-positive spikes). We have therefore designed an alternative algorithm (NB-graph) based on a graph theory approach that overcomes this limitation. A detailed description of the algorithm and a comparison with the standard procedure used to detect NBs is reported in<sup>25</sup>.

### *Spatial and temporal profile of the network bursts*

The temporal and spatial resolution of our data allowed for the faithful investigation of the dynamics of the network bursts, particularly how NBs occur over time and if they share some similarity that could be explained from the underlying organization of the network. To this end, we computed the NB correlation matrix to study groups of neurons with similar firing patterns. The entries  $\bar{C}_{n,m}$  of the NB correlation matrix<sup>26</sup> were given by the following equation:

$$\bar{C}_{n,m} = \max_{\tau} \left( \sum_{i=1}^N C_{n,m}^i(\tau) \right)$$

where the sum runs over the neurons, and the maximum is taken on the time window of the event (e.g.,  $0 < \tau < 150ms$ ). The term  $C_{n,m}^i(\tau)$  represents the cross-correlation between the NBs  $m$  and  $n$  of neuron  $i$ . Such entries are then reordered using a standard hierarchical clustering algorithm aimed at highlighting the presence of similar NBs. The optimal cut point of the dendrogram was obtained by maximizing the Silhouette score. In addition, the spatial propagation of the spiking activity during an NB was also represented in terms of its centre-of-activity trajectory (CAT<sup>27,28</sup>).

The CAT collapses the overall network activity to its center of mass (i.e., regions of the network with more activity have a higher weight), allowing for the representation of how the activity in the network evolves over time with just two coordinates and the clustering of NBs with similar propagation trajectories. In our analysis, at each time point, the CAT was computed over 20-ms time bins with a sliding of 1 ms. To cluster CATs with different durations (e.g., when inhibition is blocked), the NBs were realigned to a common time interval.

### *Network dynamic analysis*

Emergent network activity can be explained to a large extent by the anatomical connectivity<sup>29</sup>. However, such activity can also be determined by the particular dynamical state of the network. Thus, an analysis of the statistical relationships between firing neurons can be informative of the information flow in the network. To determine the strength of the functional connections in the network, we performed a cross-correlation analysis<sup>8</sup>. Functional links were selected to meet two requirements. First, we considered the pairs of neurons whose cross-correlation peak was above the 95<sup>th</sup> percentile of all the computed cross-correlation values. Second, for each selected pair, we assigned a functional link every time that their cross-correlation peak was ranked in the top of the ten strongest correlation peak values for both neurons, thus determining a bi-directional relationship. The first condition avoids the inclusion of spurious functional connections in the analysis. The second condition reveals potential structural network motifs that determine synchronous activities in the network. The bi-directional functional connections clearly do not correspond to structural ones (that are unidirectional, see Annex I - Network topology for further details). Indeed, the functional graphs shared only  $4.9 \pm 1.8\%$  of connections with the anatomical graph. However, these conditions allow for the determination of pathways of activity of neuronal pairs that receive similar inputs, either direct or indirect, from common firing neurons. The functional links with the longest connection (longer than 0.2, which roughly corresponds to 550  $\mu m$  on the CMOS-MEA) were filtered from the analysis.

### *Detection of ignition sites*

An additional measure was used to analyze subgraphs characterized by a strong level of internal connectivity (also referred to as community structures<sup>30</sup>). Ideally, the network is divided into groups of nodes with a maximally possible number of within-group links and a minimally possible number of between-group links<sup>30</sup>. We estimated communities through the Infomap approach<sup>31</sup>, which determines subgraphs in a given network by minimizing the expected length of random walks over possible network partitions. To test the reliability of the procedure, we validated our results by varying the topologies (i.e., random, radius and Gauss graphs) as well as by changing the neuronal connectivity within the network ( $n=10$ ).

The overlap between the ignition sites (ISs) and the fCOMs was quantified as follows. First, we defined the area covered by an fCOM as the concave hull defined by the set of neurons of the fCOM. Second, to address border effect problems (i.e., assign the events that start close to the border of an fCOM to that fCOM), we extended the confines of the fCOMs by a factor of 5%. To assess if the ISs significantly overlapped with the fCOMs, we randomly reassigned (500 times) the detected fCOMs to another position in the network and quantified the overlap.

### *Quantification of structural connectivity motifs*

To quantify the occurrence of small template subgraphs, i.e., structural motifs, in a given region of the network, we proceeded as follow. First, we considered all possible connected graphs of less than six nodes and built a list of motifs to test. Second, for each motif, we determined the number of isomorphic subgraphs in the target graph<sup>32</sup>. Finally, those numbers were normalized to the total motifs found in the target graph. Due to computational limitations for this extensive research, graphs had to be turned into their undirected counterpart. To assess significant differences in the motif composition of a given subgraph (fCOM), we defined three different null models (sCOMs, rCOMs, and rndCOMs) with the same number of nodes as that of the original subgraph. The sCOM was generated following a two-step procedure. At first, we applied the Infomap algorithm to a portion of the structural network that excluded the nodes of the fCOMs. The Infomap algorithm<sup>30</sup> allows for the partitioning of the complementary network into structural communities for which the information flow within the community is maximized and the information transmission towards the remaining neurons of the network is minimized. To faithfully compare an sCOM to an fCOM, the size of the sCOMs was constrained to be the same as that of the fCOMs. This down-sampling was performed by removing nodes from the sCOM and maximizing the spatial density of the remaining nodes of the subgraph. The latter step was intended to avoid poorly connected regions of the network. The rCOM subgraphs were obtained as follows. First, a node in the complementary network was randomly chosen, and the closest  $K-1$  nodes were aggregated ( $K$  is the size of the compared graph). Finally, the rndCOM subgraphs were obtained by turning the original fCOM into a random graph, i.e., preserving the number of nodes and edges but randomly reassigning the links.

Even though the sCOMs and rCOMs have a different number of edges than the fCOMs, they are useful to compare equivalent regions of the network that do not elicit NBs. However, the rndCOMs have the same number of edges as the structural graph and can be used as a null model to investigate the relevance of the topology. The significant difference in the motif composition was



assessed through paired t-tests (fCOMs compared to null models) at level  $p=0.05$ .

#### Detection and clustering of pre-NB spiking activity

To relate the spiking activity preceding a spontaneous burst event (pre-NBs) to the subsequent propagating event, we took advantage of the NB-graph algorithm<sup>25</sup> (with parameters  $\tau_{NB} = 10$  ms,  $d_{NB} = 1/8$ ). With the aim of determining whether pre-NB spikes shared similar spatiotemporal structures (i.e., temporal motifs), all pre-NB spikes falling in the 100 ms preceding the starting point of an NB were analyzed. This was done by considering the largest connected component (i.e.,  $\alpha_L$ ,  $\beta_L$ ) of the induced NB-graphs (i.e.,  $\alpha_G$ ,  $\beta_G$ ). Two pre-NB motifs that share a common subgraph of at least  $M=6$  spikes (6-motif) are declared as similar. Importantly, the parameters  $\tau_{NB}$ , and  $d_{NB}$  allow for the declaration of two spike patterns as being similar even if they are not identical. That is, shared temporal patterns can be regarded as jittered versions of the same spike pattern, and the similarity measure is robust to these variants.

The similarity of the network motifs was computed in terms of the matrix:  $SM(X, Y) = \sum_x \sum_y K(x, y) / N$ , where  $x, y$  are NB events of the clusters  $X, Y$  and the sums run over the  $x, y$  elements of the clusters  $X, Y$ .  $K(x, y)$  is the Kronecker distance (equal to 1 if  $x$  is similar to  $y$ , 0 otherwise), and  $N$  is a normalization factor given by  $N = \sum_y SM(X, y) \cdot \sum_x SM(x, Y)$ . To compare the pre-NB spiking sequences for all NBs, a similarity index was introduced and defined as follows:

$$S = \frac{\sum_X SM(X, X)}{\sum_{X, Y} SM(X, Y)}$$

To quantify the similarity among NBs, we defined the ‘per-cluster’ measure as a weighted average with respect to the cluster size and the ‘ALL’ measure, defined on all trajectories irrespective of the cluster’s size. To further characterize how the number of shared pre-NB spikes influences the measure of similarity, shown in, we reported the cumulative similarity curve from  $M=6$  to  $M=66$ . The similarity was also computed for pairs of pre-NB activities belonging to the same NB cluster (IN) or among pre-NB activities belonging to distinct NB clusters (ACROSS).

#### Tables of parameters

Table: Average values for graph properties ( $n=10$  graph realizations).

$N$	$\sigma^2$	$degree$	$SPL$	$CC$
4096	0.005	$41.6 \pm 6.4$	$6.54 \pm 0.48$	$0.24 \pm 0.03$

Table: Parameters of AdExp for the two neuronal population of the model.

Neuronal population	$a$ ( $\mu S$ )	$b$ ( $nA$ )	$C$ ( $pF$ )	$g_L$ ( $\mu S$ )	$E_L$ ( $mV$ )	$V_T$ ( $mV$ )	$\Delta_T$ ( $mV$ )	$\tau_w$ ( $ms$ )	$V_{reset}$ ( $mV$ )	$I_{bg}$ ( $nA$ )
Inhibitory	$2 \pm 0.005$	$0 \pm 0$	$200 \pm 0.497$	$10 \pm 0.024$	$-70 \pm 0.173$	$-50 \pm 0.123$	$2 \pm 0.005$	$30 \pm 0.073$	$-58 \pm 0.145$	$175 \pm 0$
Excitatory	$2 \pm 0.005$	$60 \pm 0.150$	$281 \pm 0.711$	$12 \pm 0.025$	$-70 \pm 0.175$	$-50 \pm 0.124$	$2 \pm 0.005$	$300 \pm 0.759$	$-58 \pm 0.147$	$175 \pm 0$

Table: Parameters of the modelled synapses.

Synapse type	$\tau_{syn}$ ( $ms$ )	$E_{rev}$ ( $mV$ )	$\tau_{rise}$ ( $ms$ )	$g_{max}$ ( $nS$ )	$\tau_{in}$ ( $ms$ )	$\tau_{rec}$ ( $ms$ )	$u$
AMPA	3	0	1	48	1	100	0.5
GABA	8	-70	1	48	1	100	0.5
NMDA	280	0	5.5	4.8	1	100	0.5



## Bibliography

---

1. Maccione, A. *et al.*, Experimental investigation on spontaneously active hippocampal cultures recorded by means of high-density MEAs: analysis of the spatial resolution effects. *Front Neuroeng* **3**, 4 (2010).
2. Banker, G. & Goslin, K., *Culturing Nerve Cells, Cellular and Molecular Neuroscience* (MIT Press, Cambridge, 1998).
3. Carnevale, N. T. & Hines, M. L., *The NEURON Book* (Cambridge University Press, 2006).
4. Brette, R. & Gerstner, W., Adaptive exponential integrate-and-fire model as an effective description of neuronal activity. *J Neurophysiol* **94**, 3637-3642 (2005).
5. Izhikevich, E. M., Simple model of spiking neurons. *IEEE Trans Neural Netw* **14**, 1569-1572 (2003).
6. Naud, R., Marcille, N., Clopath, C. & Gerstner, W., Firing patterns in the adaptive exponential integrate-and-fire model. *Biol Cybern* **99**, 335-347 (2008).
7. Baltz, T., Herzog, A. & Voigt, T., Slow oscillating population activity in developing cortical networks: models and experimental results. *J Neurophysiol* **106**, 1500-1514 (2011).
8. Garofalo, M., Nieuws, T., Massobrio, P. & Martinoia, S., Evaluation of the performance of information theory-based methods and cross-correlation to estimate the functional connectivity in cortical networks. *PLoS One* **4**, e6482 (2009).
9. Thivierge, J.-P. & Cisek, P., Nonperiodic synchronization in heterogeneous networks of spiking neurons. *J Neurosci* **28**, 7968-7978 (2008).
10. Persi, E., Horn, D., Volman, V., Segev, R. & Ben-Jacob, E., Modeling of synchronized bursting events: the importance on inhomogeneity. *Neural Comput* **16**, 2577-2595 (2004).
11. Maeda, E., Robinson, H. P. & Kawana, A., The mechanisms of generation and propagation of synchronized bursting in developing networks of cortical neurons. *J Neurosci* **15**, 6834-6845 (1995).
12. Markram, H., Wang, Y. & Tsodyks, M., Differential signaling via the same axon of neocortical pyramidal neurons. *Proc Natl Acad Sci U S A* **95**, 5323-5328 (1998).
13. Nieuws, T. *et al.*, LTP regulates burst initiation and frequency at mossy fiber--granule cell synapses of rat cerebellum: experimental observations and theoretical predictions. *J Neurophysiol* **95**, 686-699 (2006).
14. Chiappalone, M., Bove, M., Vato, A., Tedesco, M. & Martinoia, S., Dissociated cortical networks show spontaneously correlated activity patterns during in vitro development. *Brain Res* **1093**, 41-53 (2006).
15. Kitano, K. & Fukai, T., Variability v.s. synchronicity of neuronal activity in local cortical network models with different wiring topologies. *J Comput Neurosci* **23**, 237-250 (2007).
16. Grinstein, G. & Linsker, R., Synchronous neural activity in scale-free network models versus random network models. *Proc Natl Acad Sci U S A* **102**, 9948-9953 (2005).
17. Vasilaki, E. & Giugliano, M., Emergence of connectivity motifs in networks of model neurons with short- and long-term plastic synapses. *PLoS One* **9**, e84626 (2014).
18. Cullen, D. K., Gilroy, M. E., Irons, H. R. & Laplaca, M. C., Synapse-to-neuron ratio is inversely related to neuronal density in mature neuronal cultures. *Brain Res* **1359**, 44-55 (2010).
19. Wierenga, C. J., Ibata, K. & Turrigiano, G. G., Postsynaptic expression of homeostatic plasticity at neocortical synapses. *J Neurosci* **25**, 2895-2905 (2005).
20. Rubinov, M. & Sporns, O., Complex network measures of brain connectivity: uses and interpretations. *Neuroimage* **52**, 1059-1069 (2010).
21. Bologna, L. L. *et al.*, Low-frequency stimulation enhances burst activity in cortical cultures during

- development. *Neuroscience* **165**, 692-704 (2010).
22. Lonardoni, D. *et al.*, High-density MEA recordings unveil the dynamics of bursting events in Cell Cultures. *Engineering in Medicine and Biology Society (EMBC), 2015 37th Annual International Conference of the IEEE.* (2015).
  23. Masquelier, T. & Deco, G., Network bursting dynamics in excitatory cortical neuron cultures results from the combination of different adaptive mechanisms. *PLoS One* **8**, e75824 (2013).
  24. Vedunova, M. *et al.*, Seizure-like activity in hyaluronidase-treated dissociated hippocampal cultures. *Front Cell Neurosci* **7**, 149 (2013).
  25. Lonardoni, D. *et al.*, Recurrently connected and localized neuronal communities initiate coordinated spontaneous activity in neuronal networks. *PLOS Computational Biology* **13**, e1005672 (2017).
  26. Baruchi, I. & Ben-Jacob, E., Towards neuro-memory-chip: Imprinting multiple memories in cultured neural networks. *Phys Rev E Stat Nonlin Soft Matter Phys* **75**, 050901 (2007).
  27. Chao, Z. C., Bakkum, D. J. & Potter, S. M., Region-specific network plasticity in simulated and living cortical networks: comparison of the center of activity trajectory (CAT) with other statistics. *J Neural Eng* **4**, 294-308 (2007).
  28. Gandolfo, M., Maccione, A., Tedesco, M., Martinoia, S. & Berdondini, L., Tracking burst patterns in hippocampal cultures with high-density CMOS-MEAs. *J Neural Eng* **7**, 056001 (2010).
  29. Bullmore, E. & Sporns, O., Complex brain networks: graph theoretical analysis of structural and functional systems. *Nat Rev Neurosci* **10**, 186-198 (2009).
  30. Girvan, M. & Newman, M. E. J., Community structure in social and biological networks. *Proc Natl Acad Sci U S A* **99**, 7821-7826 (2002).
  31. Rosvall, M. & Bergstrom, C. T., Maps of random walks on complex networks reveal community structure. *Proc Natl Acad Sci U S A* **105**, 1118-1123 (2008).
  32. Cordella, L. P., Foggia, P., Sansone, C. & Vento, M., A (sub) graph isomorphism algorithm for matching large graphs. *IEEE Trans Pattern Anal Mach Intell* **26**, 1367-1372 (2004).

# ***Annex II - Preparation of mouse retina whole-mounts on CMOS-MEAs***

## ***Ethics Statement***

All the experiments were performed in accordance with the guidelines established by the European Community Council (Directive 2010/63/EU of 22 September 2010). All procedures involving experimental animals were approved by the institutional IIT Ethic Committee and by the Italian Ministry of Health and Animal Care (Authorization number 110/2014-PR, December 19, 2014).

## ***Retina preparation for high-resolution CMOS-MEA recordings***

---

Twelve hours dark-adapted male mice (6 weeks old C57BL/6) were barely anesthetized with CO<sub>2</sub> and subsequently killed by cervical dislocation. After eyeballs enucleation retina was extracted by accurately removing all the surrounding tissues as cornea, crystalline, sclera and vitreous. Once isolated, the retina was faced down onto a pre-conditioned MEA (its reservoir was filled with Neurobasal for 2 hours at 37°) putting the retinal ganglion layer in contact with its surface and leaving the photoreceptor layer exposed. On top of this latter was placed a polyester membrane filter (Sterlitech Corp., Kent, WA, USA) held in turn by a circular anchor. A perfusion line, supplied by a peristaltic pump (~1 ml/min), ensured a constant flow of a media composed by AMES's medium (Sigma - Merck KGaA, Darmstadt, Germany) with 1.9g/L of sodium bicarbonate equilibrated with carboxigen (95% O<sub>2</sub> and 5% CO<sub>2</sub>).



## ***Annex III - Evaluation reports and reviews***

I sincerely thank Dr. Tim Gollisch and Dr. Michele Giugliano for their evaluation of the preliminary draft of my dissertation. Here, I report a summary of the changes that I have made during the revision by taking into consideration all the specific points raised by Dr. Tim Gollisch.

- Foremost, the thesis should benefit from a thorough proofreading to reduce the number of grammatical errors and typos.

*I apologize to the reviewer for the lack of English quality of the first manuscript. I have deeply revised the text of the manuscript to improve its readability and to remove grammatical errors and typos.*

- Second, some small errors should be corrected:
  - 1) Page 24. Galvani's experiments were not in 1971 but in the 18th century.
  - 2) Page 82. There seems to be confusion between the "inner" and "outer" side; typically inner refers to the layers towards the center of the eye, so horizontal cells are considered to be in the outer, not inner retina, and ON bipolar cells have their axonal arbors in the inner part of the inner plexiform layer, OFF bipolar cells in the outer part, not vice versa.
  - 3) Page 88. The number of types of ON-OFF direction-selective cells is given as eight, but should be four.
  - 4) Page 117, "to ensure that this happened as consequence of spurious correlations". Is this supposed to mean "...that this did not happen..."?
  - 5) Page 124, "a value approaching 1100". This should probably be "100".

*I am grateful to the reviewer for pointing these mistakes out that I had not noticed. I have corrected all of them in the present version and specifically I have modified:*

*1) Galvani's performed his experiments in 1791 rather than 1971*

*2) On the distinction between outer and inner part of the retina, the text now reads:*

"These cells, whose soma is located in the inner nuclear layer<sup>20</sup>, mainly integrate the output of multiple photoreceptors horizontally and provide negative feedbacks to the photoreceptors and bipolar cells in the outer plexiform layer<sup>4</sup> (see below). Consequently, they are considered part of the outer retina from their functional role.

(...)

ON and OFF bipolar cells form synaptic contacts with retinal ganglion cells in specific locations of the inner plexiform layer: ON bipolar cells form synapses in the inner part of the inner plexiform layer whereas OFF bipolar cells in the outer one<sup>3</sup>. Furthermore, while the communication with photoreceptor is mediated by ionotropic receptors in OFF bipolar cells, ON bipolar cells integrate the signal through metabotropic receptors<sup>12</sup>."

3) *The reviewer is right and the number “eight” instead of “four” was a mistake. I know that there are four populations, but in the rush of editing the manuscript, I wrote eight instead.*

4) *The reviewer understood the sentence correctly, despite his complexity. The text has been corrected as suggested to improve its readability.*

5) *The reviewer is right, the number (Suppressive Index value) is “100” instead of “110” and it has been corrected.*

- Third, a potential caveat regarding the interpretation of response differences under full-field and masked stimulation is that something like this could be the result of run-down of the experimental preparation or slow adaptation effects across the course of the experiments. This is difficult to assess because the thesis provides little information about the order and duration of the different stimuli or whether the stimulation alternated between full-field and masked stimuli. It might be appropriate to at least discuss briefly the potential influence of run-down or adaptation of the retina.

*I am grateful to the evaluator for raising this point that was not sufficiently explored in the draft of the dissertation. To address these relevant concerns, I firstly included a more precise and detailed description of the protocol used in our experiments on retina whole-mounts (see Section xx). As it is now described, a typical full-field/masking experiment lasts about 100 minutes for each retina. With respect to the concern on the run-down of the responses, previous investigations and setup validations, which have been confirmed also with our full-field/masking protocol (Section added in Discussion), indicate a not significant decay of the peak response of retinal ganglion cells between the beginning and the end of the experiment. Under these experimental conditions, the recording of retinal ganglion cells exhibits a stable response up to 120-150 minutes.*

*With respect to the concern on adaptation during our experiments, it has to be noted that in the designed protocol the retina is actively stimulated only for approximately 40 minutes, while the remaining time is used to project an iso-luminant gray uniform image to avoid adaptation of the retina to the different stimuli and trials. In particular, we interleaved visual stimulations of different contrasts with at least 30s of iso-luminant gray to restore the retinal processing to the reference baseline before evaluating its performance with other types of stimuli. By doing so, we expected to provide a fair quantification of the retinal response to full-field and masked stimuli condition. However, as also highlighted by the reviewer, a promising direction to investigate is whether the adaptation time scale between full-field and masked stimuli condition differs as a consequence of the spatial extent of the stimulus. I now discuss the potential implications of this second consideration in the discussion section of the dissertation (see page 119-120).*

- Fourth, some small, local aspects:
  - 1) Page 118. I do not see, as claimed that ON and OFF aeRGCs showed higher sensitivity to large bars at CT25; maybe explain. Also, what are the units of the response measures .02 and .09 given below?



- 2) Page 124. I don't think that a suppressive index near 100 means that RGCs would be highly tuned to a particular spatial frequency; it just means that they don't respond well to large bars, but could be broadly tuned for others.
- 3) Page 126. Bicuculline is not sufficient to completely remove GABAergic inhibition, as it only blocks GABA-A receptors and not, for example, GABA-C receptors.

*I thank the reviewer for raising these points. I have inserted in the text additional clarifications to improve the accuracy of our statements.*

*1) The statement at page 114 was too strong and poorly explained. Upon re-editing, it now reads:*

*"For low contrasts stimuli (CT25), the response curve for both ON and OFF population reached a plateau for 0.01 cycle/deg spatial frequency bars, instead of steadily increasing until 0.02 cycle/deg. Although the amplitude of response is significantly lower than the one to higher contrasts; this might indicate a slight tuning to medium-sized bars at low contrast. This intuition will be discussed later through the quantification of the suppressive index (see Discussion)."*

*2) The statement that a suppressive index near 100 implies a tuning to a unique particular frequency can be misinterpreted. Indeed, a counter-example would be the case of a cell that has a low response to large bars but an equally higher response for a broad range of higher spatial frequency bars. We now clarify that the Suppressive Index, in our context, was used as a simple measure to quantify whether cells are tuned or untuned. Specifically, we expected that low spatial frequency bars would evoke a lower response compared to high spatial frequencies due to the surround antagonism of the receptive field. Our results reveal an opposite trend, thus suggesting that for most of the retinal ganglion cells, the larger is the stimulus, the higher the response will be. Consequently, to provide a more precise description to the reader, the text now reads:*

*"A null suppressive index would mean that the RGCs are poorly tuned, i.e., their maximum response equals the response to the largest presented bar (i.e., 1344  $\mu$ m in our case). Instead, a value approaching 100 would indicate that RGCs have a small (or no response at all) to the lowest spatial frequencies. At the same time it reveals that the cell is tuned to a single or a range of higher spatial frequencies."*

*3) With respect to page 121, the reviewer is right and the text has been modified accordingly:*

*"While methods to selectively perturb the amacrine population needs to be established, in the short term we will investigate the masked and full-field responses upon administration of a cocktail of bicuculline and strychnine, in order to remove the inhibition mediated by GABA<sub>A</sub> and the glycine<sup>50</sup>."*

- Fifth, overall the main text is relatively light on quantitative or statistical evaluations. Sometimes, these can be found in the figures, but this is not always easy to connect. Thus, as an optional suggestion, I would like to recommend checking whether more quantitative statements can be inserted into the text. Some examples include

- 1) the central finding that the “GAUSS” model, in contrast to other tested models, reproduces the time scales and firing rate distributions of the network bursts (page 47),
- 2) the finding that there are “well-segregated regions where the density of links was higher than the average level of the network” (page 60),
- 3) the evaluation of the graph architecture of pre-NB activity (page 65).

*I am grateful to the reviewer for this comment and support to improve the comprehension of my results. As highlighted by the reviewer, many quantifications were previously inserted in the figures but not in the main text. Others were not included in the previous version of the dissertation. As suggested I have now included some quantitative statements within the text to support the reported findings, both in the mentioned parts of the dissertation (points 1,2,3 raised by the reviewer) as well as in the rest of the text to uniform the style of the dissertation.*

Prof. Dr. Tim Gollisch, University Medical Center Göttingen,  
Waldweg 33, D – 37073 Göttingen, Germany

Office of the PhD Course in Neuroscience  
XXX Cycle  
Istituto Italiano di Tecnologia  
Genova, Italy

**Sensory Processing in the Retina**  
**Department of Ophthalmology**

Email: [tim.gollisch@med.uni-goettingen.de](mailto:tim.gollisch@med.uni-goettingen.de)  
Tel: +49 (0)551 39 13542  
Fax: +49 (0)551 39 13541

December 22, 2017

## Evaluation of Doctoral Thesis of Davide Lonardoni

I have read the dissertation thesis of Davide Lonardoni with much interest. In a combination of experimental data analysis and computational modeling, the thesis investigates how large-scale recordings with CMOS-based multielectrode arrays can be applied to study the signaling in neuronal networks. In the two major parts of the thesis, the examples of hippocampal cultures and of whole-mount retinas under visual stimulation are considered. In particular, the first part of the thesis manages to show how recorded data can be used to aid the construction and evaluation of models of recurrent networks so that hypotheses of the generation of network bursts can be tested. The second part of the thesis, on the other hand, provides important groundwork for the analysis of large-scale multielectrode recordings from the retina and suggests that long-range interactions shape the light response properties of retinal ganglion cells.

The thesis is extensive with thought-provoking results in both parts, nice illustrations of the findings and appropriate presentation of background and discussion. I therefore approve of this thesis to allow Davide Lonardoni access to the final dissertation.

Yet, I do have a few comments and suggestions for revisions, which could improve the thesis. Foremost, the thesis should benefit from a thorough proofreading to reduce the number of grammatical errors and typos. Second, some small errors should be corrected: 1) Page 24. Galvani's experiments were not in 1971, but in the 18th century. 2) Page 82. There seems to be confusion between the "inner" and "outer" side; typically inner refers to the layers towards the center of the eye, so horizontal cells are considered to be in the outer, not inner retina, and ON bipolar cells have their axonal arbors in the inner part of the inner plexiform layer, OFF bipolar cells in the outer part, not vice versa. 3) Page 88. The number of types of ON-OFF direction-selective cells is given as eight, but should be four. 4) Page 117, "to ensure that this happened as consequence of spurious correlations". Is this supposed to mean "...that this did not happen..."? 5) Page 124, "a value approaching 1100". This should probably be "100".

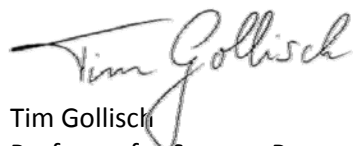
Third, a potential caveat regarding the interpretation of response differences under full-field and masked stimulation is that something like this could be the result of run-down of the experimental preparation or slow adaptation effects across the course of the experiments. This is difficult to

assess because the thesis provides little information about the order and duration of the different stimuli or whether the stimulation alternated between full-field and masked stimuli. It might be appropriate to at least discuss briefly the potential influence of run-down or adaptation of the retina.

Fourth, some small, local aspects: 1) Page 118. I do not see, as claimed that ON and OFF aeRGCs showed higher sensitivity to large bars at CT25; maybe explain. Also, what are the units of the response measures .02 and .09 given below? 2) Page 124. I don't think that a suppressive index near 100 means that RGCs would be highly tuned to a particular spatial frequency; it just means that they don't respond well to large bars, but could be broadly tuned for others. 3) Page 126. Bicuculline is not sufficient to completely remove GABAergic inhibition, as it only blocks GABA-A receptors and not, for example, GABA-C receptors.

Fifth, overall the main text is relatively light on quantitative or statistical evaluations. Sometimes, these can be found in the figures, but this is not always easy to connect. Thus, as an optional suggestion, I would like to recommend checking whether more quantitative statements can be inserted into the text. Some examples include 1) the central finding that the "GAUSS" model, in contrast to other tested models, reproduces the time scales and firing rate distributions of the network bursts (page 47), 2) the finding that there are "well-segregated regions where the density of links was higher than the average level of the network" (page 60), and 3) the evaluation of similarity of the graph architecture of pre-NB activity (page 65).

Sincerely,



Tim Gollisch  
Professor for Sensory Processing in the Retina

**THEORETICAL NEUROBIOLOGY LABORATORY  
DEPARTMENT OF BIOMEDICAL SCIENCES**

Prof. Dr. Michele Giugliano      Voice:      +32 3 820 24 88  
University of Antwerp      Fax :      +32 3 820 26 69  
Campus Drie Eiken - D.T.121      GSM :      +32 493 1294 04  
Universiteitsplein 1      Skype :      meekeee  
B-2610 Wilrijk (Belgium)      E-mail :      michele.giugliano@ua.ac.be  
WWWWeb :      www.giugliano.info



To the  
Doctoral School  
Italian Institute of Technology  
Genova, Italy

Antwerp, January 10<sup>th</sup> 2018

**Subject: Evaluation of the PhD thesis manuscripts by Mr Alessandro Soloperto and of Mr Davide Lonardoni in partial fulfilment of the European PhD title award**

Dear Madam or Sir,

in response to your request to be part of the evaluation committee for the evaluation of Soloperto's and Lonardoni's PhD theses, this letter constitutes my positive assessment of the eligibility of their submitted manuscripts for the final oral defense and - if successful - for receiving the European PhD title award. This is based on the direct evaluation of the theses manuscripts received in December 2017.

I am definitely impressed by the high quality of both Soloperto's and Lonardoni's PhD theses and their overall scientific results, which are of relevance particularly for the domains of Neuroengineering and fundamental Neuroscience. I have read with great personal scientific interest the results reported and I overall value the candidates among the top 15% of graduate students I supervised or otherwise had direct experience of, while being staff member at the Univ. of Bern (2001-2005), at the Swiss Federal Institute of Technology of Lausanne (2005-2008), and at the Univ. of Antwerp (2008-present).

In the view of the scientific quality of the submitted manuscripts, their excellent publication and dissemination, the participation as presenters of the two candidates to international conferences and workshops, I have no hesitation to provide you with a positive evaluation for both Soloperto's and Lonardoni's eligibility to defend orally their work and - if successful - to receive the European PhD titles award.

In conclusion, I am pleased to provide a positive review of the works by Mr Alessandro Soloperto and of Mr Davide Lonardoni, and I recommend no major changes to the manuscripts.

Yours faithfully,

Prof. Dr. Michele Giugliano